



# SYNTHESIS AND EVALUATION OF NOVEL FORMATS IN MOLECULAR IMPRINTING

Dem Fachbereich Chemie der Universität Dortmund zur  
Erlangung des akademischen Grades eines  
Doktor der Naturwissenschaften  
(Dr. rer. nat.)  
vorgelegte Dissertation

von:

Dipl.-Chem. Maria-Magdalena Titirici  
geboren am 24.03.1977  
in Bucharest, Romania

Betreuer: Priv. Doz. Dr. Börje Sellergren

Koreferrent: Univ.-Prof. Dr. Rainer Haag

Universität Dortmund, Institut für Umweltforschung

Januar 2005

*„Felix qui potuit rerum conoscere causas“*

*Lucretius*

*“There are ancient cathedrals which, apart from their consecrated purpose, inspire solemnity and awe. Science has its cathedrals, built by the efforts of few architects and of many workers.....”*

*G.N. Lewis*

*“In archaic and traditional societies, the surrounding world is conceived as a microcosmos. At the limits of this closed world begins the domain of the unknown, of the formless. On this side there is order - because of inhabited and organised - space; on the other, outside this familiar space, there is the unknown.....”*

*Mircea Eliade*

*La steaua care-a răsărit  
E-o cale-atât de lungă,  
Că mii de ani i-au trebuit  
Luminii să ne-ajungă.*

*Poate de mult s-a stins în drum  
În depărtări albastre,  
Iar raza ei abia acum  
Luci vederii noastre.*

*Mihai Eminescu*

*For my father*

---

## ACKNOWLEDGMENTS

➤ I would like to thank my supervisor, Dr. Börje Sellergren for giving me the opportunity to work in this interesting field and for support with new ideas and advises during my research.

➤ I acknowledge to Prof. Dr. Michael Spiteller for the prospect of working in the Institut für Umweltforschung at the University of Dortmund.

➤ I also thank all my colleagues that moved with me from Mainz to Dortmund; Panos, Andy, Ravindra and Francesca, for the general nice atmosphere in the lab and for professional and moral support. Also to the newcomers: Filipe, Carla and Issam for bringing some Mediterranean breeze in the group and for some very enjoyable nights. Special thanks to Carla for helping me with experiments in the last months while writing my thesis.

➤ And speaking of Mediterranean breeze, I would like to thank Fernando, our guest researcher from Spain, who together with the Portuguese duo, made the cold rainy autumn in Dortmund far more pleasant. Many thanks also to Susana for the nice time at the “Weihnachtsmarkt” in Dortmund and the even nicer time in Spain.

➤ Thanks to Andy who helped at the beginning a lost student from Romania to find her way in the synthetic lab, for lots of going out to avoid the “wonderful” ESG room as much as possible and for the “original” presentation in Illstrop, Sweden. Thanks also for language support, my English has definitely enriched in expressions.

➤ Thanks to Panos, my “Balkanic” neighbour, first of all for helping me find the way through the complicated world of computers and teaching me some useful tricks associated with the Microsoft Office package, but also for the nice birthday parties we made together, including the most fun part of cooking together and some other

activities, *e.g.* the most wicked trip Mainz-Copenhagen-Lund-Ilstrop-Lund-Rostock-Mainz. We proved that travelling without any planning really works.

➤ Thanks to Francesca for revealing to me the secrets of analytical chemistry and for assistance in my “first contact” with an HPLC equipment. Thanks also for the so-necessary cafés after lunch, where conversations about science are strictly forbidden to certain persons. (no names provided!)

➤ Lots of thanks to Marco, our only German colleague in AK-Sellergren Dortmund, for solving so many “burocratic” issues and for useful advice concerning the synthetic aspects of my work.

➤ Thanks to our Indian expert in ellipsometry Ravindra for some very funny late evenings at work and for throwing the solvent waste in my place.

➤ Thanks to Eric and Cristiana for the nice time I had in the Glasgow trip.

➤ Thanks also to the research team in Mainz, Claudia, Beate, Tom, Brian, Zöfre, Andreas, Carmine, Romas and Sandra, for so many nice going-out and “beach” activities and also to Prof. Klaus Unger for the nice Christmas parties, the wonderful wine and fish and for the very nice workshop in Ilstrop, Sweden.

➤ Thanks to Prof. Markus Antonietti from the MPI für Kolloid- und Grenzflächenforschung in Golm for giving me the opportunity to spend two weeks in his research team, where I could perform the last measurements for my thesis and enhanced my knowledge concerning hierarchical structures. I would specially like to thank Dr. Jürgen Hartmann for the SEM and TEM measurements and Matthijs Groenewolt for helping me to use the available facilities in Golm, *e.g.* TG measurements.

➤ I would also like to thank to the people working in the AquaMIP EU Project for some enjoyable (after)project meetings, *e.g.* Mainz, Dortmund or Glasgow. In this direction I would especially like to thank to Cristina and Ersilia from the University of Pavia, Italy and to Amaia, Elisabeth and Peter from the University of Strathclyde, Glasgow. Special thanks to Elisabeth for accommodating me in Glasgow.

➤ Thanks to Georgios Theodoridis (George) from the University of Thessaloniki for teaching me some chromatography history and for his very nice idea concerning the application of hierarchical imprinting to produce artificial receptors for Alzheimer's disease. Thanks also for all the kebabs and baklavas we had together in Germany and for the ούζο and πετσίνα, from Greece. And thank you for sending Michalis to Dortmund, it was so much fun....

➤ Thanks again (although some mentioned before) to all the research guests in Dortmund for learning a little bit more from each of them and for a very nice time in the evenings. Thank you Fernando, Cristina, Elisabeth, George, Zoe, Heiko, Stephan, Erban, Florance, Axel, and Ece.

➤ Special thanks to the "Romanian Mafia" from Mainz, Gabi, Andrea and Madalina and the "Ruhr-Gebiet" Mariana, Monica, Valentina, Cornel, Bogdan, Sorin, Ciprian, Marius, Ionut, Dan, Onoriu and Radu for making me feel like home from time to time.

➤ I would like to thank my schoolteacher in chemistry, Gabriela Savu, for failing me two trimesters in Chemistry, thus obliging me to actually start studying the subject and finding it so interesting that I ended-up doing my PhD in it.

(Aș dori să mulțumesc în mod special profesoarei mele de liceu, Gabriela Savu, pentru faptul că m-a lăsat corijentă două trimestre consecutive, obligându-ma în acest fel să încep să studiez chimia și să o găsec așa de interesantă încat să sfârșesc prin a-mi face doctoratul în ea.)

➤Loads of thanks to my family for financial and moral support during all my studies. Thanks to my grandfather, my aunt Tic, my dad and most of all to my mum, for being close and helping every time I needed. Unique thoughts of gratitude go to my wonderful grandmother Maria. I wish you were still here with me!

(Mii de mulțumiri familiei mele pentru suport moral și financiar pe tot parcusul studiilor. Mulțumesc bunicului meu, mătușii mele Tic, tatălui meu și în primul rând mamei mele pentru faptul că au fost mereu aproape și m-au ajutat de fiecare dată când am avut nevoie. Gânduri de profundă recunoștința se îndreaptă spre bunica mea care m-a crescut. Cât aș da să mai fi încă cu mine!)

➤Last but not least, I would like to thank my boyfriend Cedric for being so patient during the last three years, for supporting and trying to understand me and make me feel happier in difficult moments.

➤I would like to thank Gunnar Glasser (MPI für Polymerforschung, Mainz), Monika Meuris (University of Dortmund) and Dr. Jürgen Hartmann (MPI für Kolloid- und Grenzflächenforschung) for recording the SEM and TEM micrographs, Prof. Klaus Unger and Zöfre Bayram-Hahn (University of Mainz) for nitrogen sorption measurements, Willi Dindorf (University of Mainz) for the elemental analysis measurements, Bernd Matiasch (University of Mainz) for some FT-IR measurements and Matthijs Groenewolt (MPI für Kolloid- und Grenzflächenforschung) for the TGA. Dr. Dieter Lubda (Merk, Darmstadt) for providing the silica gel used in the grafting experiments, Dr. Cedric du Fresne for providing the silica gel used in the hierarchical imprinting, Fernando Tamayo and Filipe Vilela for help with the RAFT agent synthesis and Carla Aureliano for help with the IR-measurements and batch-rebinding experiments. Special thanks go to Uli Schoppe, the most efficient and talented “Shopper” in the whole of Germany.

➤Financial support from the Deutsche Forschungsgemeinschaft (DFG) under the projects Se777/5-1 and Se777/5-2 is gratefully acknowledged.

---

<b>1</b>	<b>SUMMARY</b> .....	<b>1</b>
<b>2</b>	<b>INTRODUCTION</b> .....	<b>4</b>
<b>3</b>	<b>MOLECULAR IMPRINTING-STATE OF ART</b> .....	<b>10</b>
3.1	INTRODUCTION TO MOLECULAR IMPRINTING .....	10
3.2	AN HISTORICAL PERSPECTIVE OF THE DEVELOPMENT OF MOLECULAR IMPRINTING .....	11
3.2.1	Molecular Imprinting in Silica .....	11
3.2.2	Molecular Imprinting in Organic Polymers .....	13
3.3	METHODS FOR PREPARATION OF SPHERICAL MIP BEADS .....	20
3.4	OTHER MIP FORMATS .....	25
3.5	GRAFTING TECHNIQUES .....	27
3.5.1	The “Grafting To” Approach .....	28
3.5.2	The “Grafting From” Approach .....	30
3.6	SURFACE OR INTERFACIAL IMPRINTING .....	34
3.7	APPLICATIONS OF MOLECULARLY IMPRINTED POLYMERS .....	42
3.7.1	Chiral Separations (MICSP) .....	42
3.7.2	Peptides and Proteins Recognition .....	45
3.7.3	Solid Phase Extractions .....	50
3.7.4	Biosensors .....	51
3.7.5	Catalysis .....	51
3.8	CONCLUSIONS .....	52
<b>4</b>	<b>RESULTS AND DISCUSSION (I): HIERARCHICAL IMPRINTING</b> .....	<b>54</b>
4.1	IMPRINTING USING IMMOBILISED NUCLEOTIDES .....	55
4.1.1	Template Immobilisation .....	56
4.1.2	Characterisation of the Resulting Intermediates .....	60
4.1.3	Preparation of the Imprinted Polymers .....	65
4.1.4	Characterisation of the Imprinted Polymers .....	67
4.1.5	Evaluation of the Imprinted Polymers as Stationary Phases in HPLC .....	74
4.1.5.1	<i>Evaluation of Adenine Imprinted Polymer Prepared using GPS</i> .....	74
4.1.5.2	<i>Evaluation of Adenine Imprinted Polymers Prepared using CPS</i> .....	76



4.1.5.3	<i>Evaluation of 9-ethyadenine and Triaminopyrimidine Imprinted Polymers Prepared using APS</i>	77
4.1.5.4	<i>Comparison between Different Silane Approaches</i>	79
4.1.5.5	<i>Binding Measurements in Aqueous Media</i>	81
4.1.5.6	<i>Recognition of Larger Molecules</i>	84
4.1.5.7	<i>Comparison between Hierarchical and Bulk Polymers</i>	85
4.1.6	Conclusions	87
4.2	IMPRINTING USING IMMOBILISED PEPTIDES	89
4.2.1	Solid Phase Synthesis; Template Immobilisation	90
4.2.2	Characterisation of the Solid Phase Synthesis Products	95
4.2.3	Preparation of the Imprinted Polymers	97
4.2.4	Characterisation of the Imprinted Polymers	99
4.2.5	Assessment of the Imprinted Polymers as Stationary Phases in HPLC	106
4.2.5.1	<i>Influence of Covalent Template Immobilisation</i>	106
4.2.5.2	<i>Selectivity of Mono- and Di-Amino Acids Epitope Imprinted Polymers towards Small Amino Acid Derivatives</i>	108
4.2.5.3	<i>Selectivity of Mono- and Di-Amino Acids Epitope Imprinted Polymers towards Larger Peptides</i>	110
4.2.5.4	<i>The Effect of Epitope Size on Retention towards Larger Peptides</i>	112
4.2.6	Conclusions	115
4.3	IMPORTANCE AND OUTLOOK	116
<b>5</b>	<b>RESULTS AND DISCUSSION (II): THIN FILM MIP-COMPOSITES</b>	<b>119</b>
5.1.	LIVING RADICAL POLYMERISATION	120
5.2	GRAFTING OF MIPs VIA A SURFACE BOUND AZO-INITIATOR USING RAFT POLYMERISATION	129
5.2.1	Surface attachment of free radical initiator	129
5.2.2	Grafting Step	130
5.2.3	Characterisation of Grafted Polymer Layers	133
5.2.4	Characterisation of the Materials in the Chromatographic Mode	140
5.2.5	Conclusions and Outlook	144
5.3	GRAFTING OF MOLECULARLY IMPRINTED POLYMERS VIA A SURFACE BOUND INIFERTER INITIATOR	145
5.3.1	Iniferter Coupling and Characterisation	145
5.3.2	Polymer Grafting and Composite Characterisation	146
5.3.3	Evaluation of the Composites as Stationary Phases in HPLC	153

---

5.3.4.	Conclusions.....	157
5.4	THIN-WALLED IMPRINTED POLYMERS GENERATED FROM INIFERTER-BASED COMPOSITES.....	159
5.4.1	Synthesis and Characterisation.....	160
5.4.2	Enantioselectivity of Thin-Walled MIPs and Corresponding Composites.....	169
5.4.3	Importance and Outlook.....	180
<b>6</b>	<b>EXPERIMENTAL SECTION.....</b>	<b>182</b>
6.1	HIERARCHICAL IMPRINTING USING IMMOBILISED NUCLEOTIDES.....	182
6.1.1	Silica Surface Activation.....	182
6.1.2	Silica Surface Silanisation.....	182
6.1.3	End-Capping using Hexamethyldisilazane (HMDS).....	183
6.1.4	Immobilisation of Adenine onto the GPS-Modified Silica Surface.....	183
6.1.5	Immobilisation of Adenine onto the CPS-Modified Silica Surface.....	183
6.1.6	Immobilisation of Adenine onto the APS-Modified Silica Surface.....	184
6.1.7	Immobilisation of Pyrimidine onto the APS-Modified Silica Surface.....	184
6.1.8	Polymerisation in the Template-Modified Silica Pores.....	185
6.1.9	Silica Dissolution from the Resulting Composites.....	185
6.1.10	Coupling of Fluorescent Label.....	186
6.2	HIERARCHICAL IMPRINTING USING IMMOBILISED PEPTIDES.....	186
6.2.1	Immobilisation of <i>FMOC</i> -Gly-OH onto the APS-Modified Silica Surface.....	186
6.2.2	Deprotection of <i>FMOC</i> -Gly-Si.....	187
6.2.3	Coupling reaction between <i>FMOC</i> -Phe-OH and H-Gly-Si.....	187
6.2.4	Deprotection of <i>FMOC</i> -Phe-Gly-Si.....	188
6.3	THIN LAYER MIP-COMPOSITES VIA A SURFACE BOUND AZO- INITIATOR AND RAFT POLYMERISATION.....	188
6.3.1	Attachment of Azo bis(cyanopentanoic acid) to the Silica Surface.....	188
6.3.2	RAFT Agent Synthesis.....	190
6.3.3	Template Synthesis.....	190
6.3.3.1	<i>Synthesis of BOC-L/D-Phenylalanine anilide</i> .....	191

---

6.3.3.2	<i>Synthesis of L/D-Phenylalanine anilide</i> .....	191
6.3.4	Polymerisation.....	192
6.4	THIN LAYER MIP-COMPOSITES VIA A SURFACE BOUND INIFERTER-INITIATOR.....	193
6.4.1	Silanisation of silica surface with p-(chloromethyl) phenyl trimethoxysilane.....	193
6.4.2	Immobilisation of benzyl <i>N, N</i> -diethyldithiocarbamate iniferter.....	193
6.4.3	Polymerisation.....	194
6.4.4	Generation of Thin-Walled MIPs.....	194
6.4.5	Synthesis of benzyl- <i>N,N</i> -diethyldithiocarbamate iniferter in solution.....	194
6.4.6.	Treatment of benzyl- <i>N,N</i> -diethyldithiocarbamate with ammonium hydrogen difluoride.....	195
6.5	CHARACTERISATION TECHNIQUES AND THEORY.....	195
6.5.1	Elemental Analysis.....	195
6.5.2	FT-IR Spectroscopy.....	195
6.5.3	Fluorescence Microscopy.....	196
6.5.4.	Thermogravimetric Analysis.....	196
6.5.5	Scanning Electron Microscopy.....	196
6.5.6.	Transmission Electron Microscopy.....	197
6.5.7.	Energy Dispersive X-Ray Analysis.....	197
6.5.8.	Swelling Experiments.....	197
6.5.9	Nitrogen Adsorption Measurements.....	198
6.5.10	HPLC Measurements.....	200
6.5.11	Rebinding Tests.....	201
6.5.12	Kinetic Experiments.....	203
6.6	CHEMICALS.....	204
6.6.1	Chemicals for Synthesis.....	204
6.6.2	Chemicals for Analysis.....	206
6.6.3	HPLC Solvents and Chemicals.....	206
7	REFERENCES.....	207

---

**List of Abbreviations**

3-AQ	3-Aminoquinoline
9EA	9-Ethyladenine
A	Adenine
ACN	Acetonitrile
ACPA	4,4'-Azo-bis-(4-cyanopentanoic acid)
AD	Alzheimer's Disease
AFM	Atomic Force Microscopy
AIBN	Azo- <i>N,N'</i> -bis isobutyronitrile
AIDA	2,2'-Azo-bis-( <i>N, N'</i> -dimethyleneisobutyramidine)
APS	3- Aminopropyltriethoxysilane
APT	Amyloid Precursor Protein
ATRP	Atom Transfer Radical Polymerisation
Bp	Back Pressure
C	Composite
C	Cytosine
CDAP	2-Chloro 4,6-diaminopyrimidine
CEC	Capillary Electrochromatography
COMP	Composites
CPS	Chloropropyltrimethoxysilane
CRP	Controlled Radical Polymerisation
CSP	Chiral Stationary Phases
CT	Chain transfer
CTA	Chain transfer agent
DAP	2,4-Diaminopyrimidine
DCC	Dicyclohexylcarbodiimide
DCM	Dichloromethane
DMF	Dimethylformamide
DMSO	Dimethylsulphoxide
D <sub>s</sub>	Area Density
DVB	Divinyl benzene
EDMA	Ethylene glycol dimethacrylate
EDX	Energy Dispersive X-Ray Analysis
FOL	Folic acid
GPS	Glycidoxypropyltrimethoxysilane
HEMA	2-Hydroxyethylmethacrylate
HMDS	Hexamethyldisilazane
HOBt	1-Hydroxybenzotriazole

---

HPLC	High Performance Liquid Chromatography
IF	Imprinting factor
LFRP	Living Free Radical Polymerisation
MAA	Methacrylic acid
MeOH	Methanol
MIP	Molecularly Imprinted Polymer
MTX	Methotrexate
N	Plate number
NIP	Non-Imprinted Polymer
PA	Phenylalanine anilide
PA-pNO <sub>2</sub>	Phenylalanine p-nitroanilide
PDMS	Poly(dimethylsiloxane)
PMC	Perfluoro-(1,3-dimethylcyclohexane)
PR	Primary termination
PU	Polyurethane
QCM	Quartz Crystal Microbalance
RAFT	Reversible Addition Fragmentation Transfer
ROMP	Ring-Opening Metathesis Polymerisation
SEM	Scanning Electron Microscopy
SFRP	Stable Free Radical Polymerisation
SPE	Solid Phase Extraction
T	Thymine
TAP	2,4,6-Triaminopyrimidine
TEM	Transmission Electron Microscopy
TGA	Thermogravimetric Analysis
THF	Tetrahydrofuran
TRIM	Trimethylolpropane trimethacrylate
TSA	Transition State Analogue
TW	Thin-Walls
U	Uracyl

## ZUSAMMENFASSUNG

Die vorliegende Arbeit befasst sich mit der Entwicklung neuer synthetischer Methoden zur Optimierung von molekular geprägten Polymeren, die als stationäre Phasen in Trennungsprozessen wie etwa der Hochleistungsflüssigchromatographie (HPLC) Anwendung finden.

Im ersten Teil der Arbeit wird das Konzept der "Hierarchischen Prägung" vorgestellt, das zu neuartigen mesoporösen Polymeren mit selektiven, oberflächenlokalisierten Bindungsstellen führte. Diese Materialien wurden als stationäre Phasen in der Trennung von Nukleotidbasen und großen Peptidmolekülen in wässrigen Medien eingesetzt. Durch Immobilisierung eines Templatmoleküls an die Oberfläche einer sphärischen mesoporösen Kieselgels, anschließende Befüllung der Poren mit einer Präpolymerlösung, Polymerisation innerhalb der Poren, und Entfernung des Kieselgelskeletts resultierten Polymere mit Bindungsstellen, die sich ausschließlich an der Oberfläche des polymeren Abdrucks befanden. Als Beweis konnte die molekulare Erkennung von größeren Molekülen, die die immobilisierte Unterstruktur trugen, gezeigt werden.

Im zweiten Teil der Arbeit beschreibe ich die Herstellung molekular geprägter Komposite mit geringen Schichtdicken, die durch die "grafting-from"-Methode an mesoporösen Kieselgelträgern aufgebaut wurden. Diese Komposite wurden durch zwei verschiedene Verfahren, RAFT (Reversible Addition Fragmentation Polymerisation) und lebende radikalische Polymerisation mit Initiator des Iniferter-Typs, hergestellt. Beide Techniken erlaubten die Herstellung geprägter homogener Schichten und die Unterdrückung unerwünschter Polymerisation in Lösung. Die Polymermaterialien wurden erfolgreich als chirale stationäre Phasen in der HPLC angewendet. Auf diesen Kompositen basierend, wurden neuartige molekular geprägte Polymere mit nanometer-dünnen Wänden generiert. Diese freistehenden Filme besitzen eine erhöhte Enantioselektivität, schnellere Sorptionkinetik sowie homogenere Bindungsstellen im Vergleich zu den Ausgangskompositen.

## 1 SUMMARY

This thesis describes the development of novel methods for producing molecularly imprinted polymeric materials with improved properties for analytical applications.

In chapter four I present a new method for synthesising MIPs containing surface-accessible binding sites. This procedure, named "hierarchical imprinting", consists in the immobilisation of a template on the surface of a mesoporous silica mold, polymerisation within the mold and subsequent dissolution of the mold. This resulted in polymeric materials that possess a "mirror image" pore system containing binding sites residing uniquely at the surface. In this way, templated sites were obtained with maintained control of the original particle and pore morphology.

In our first report [1], the synthesis of these hierarchically imprinted polymers was optimised for the imprinting of nucleotide bases, thus developing the first chromatographic application using this type of materials. The particles were prepared using three different methods to immobilise the template. All the resulting polymers exhibited a clear selectivity for the template and its analogues. The chromatographic parameters (plate numbers, peak shape, back-pressure) were improved in comparison to those associated with traditional imprinting materials. The retention properties were also investigated as a function of pH. Furthermore, due to the surface-located binding sites, the materials were able to retain larger molecules with similar substructures, when assessed as stationary phases in HPLC.

Exploiting the benefits of confining the sites to the pore wall surface, the concept of hierarchical imprinting was also used for the development of affinity phases in order to separate biological macromolecules, *e.g.* peptides and proteins [2,3]. In this regard the format allowed a more efficient exploitation of the epitope approach introduced by Rachkov and Minoura [4]. There, a smaller peptide corresponding to a unique amino acid sequence of a target protein was used as template in order to generate a site that can subsequently, selectively bind the larger target molecule. This required that the site is associated with the accessible surface of larger pores capable of accommodating the larger protein. The crude products resulting from solid phase

peptide synthesis satisfied these criteria and served as epitope templates to generate surface confined-sites for larger peptides and proteins. I demonstrated this concept by first synthesising the peptide epitope on the surface of a porous silica support and using the immobilised peptide for the generation of a hierarchically imprinted material. Furthermore, the benefit of this approach over a non-confinement approach, where the peptide is dissolved in the monomer mixture, is also presented. The target molecule was a heptadecapeptide, Nociceptin, an androgenous opioid analogue. Components of the N-terminal sequence of this peptide were immobilised on the surface of the mesoporous silica support using standard Merrifield chemistry. After template attachment, the pores of the immobilised templates were filled with a mixture of MAA, EDMA and an azo-initiator (AIBN). This mixture was then thermally cured at 60°C. Dissolution of the silica mold by treatment with a solution of aqueous  $\text{NH}_4\text{HF}_2$  resulted in organic polymer beads with size and morphology reflecting that of the original silica mold.

These materials were applied in HPLC and exhibited recognition for the immobilised peptidic templates, as well as for the larger target Nociceptin in water-containing mobile phases. The retention and selectivity for Nociceptin increased with increasing the size of the immobilized epitope. This has led to new recognition elements for biological macromolecules that can include, besides the peptide phases described here, nucleic acids and oligosaccharides. The retention behaviour was also maintained in aqueous environments, proving the general applicability of this method for biological samples.

All the intermediates and final products involved in the hierarchical imprinting were carefully characterised by elemental microanalysis, FT-IR spectroscopy, thermogravimetry (TGA), fluorescence microscopy, EDX, electron microscopy (SEM, TEM) and nitrogen sorption.

In chapter five the preparation of thin film molecularly imprinted composites for chiral separations in HPLC is described. MIP-composites were prepared using either azo [5] or iniferter-type initiators covalently bound to the surface of mesoporous silica particles. When azo-initiators were employed, the polymerisation was controlled through the use of Reversible Addition Fragmentation chain Transfer



agents (RAFT) [6]. The use of a chain transfer agent (CTA) during polymerisation offered good structural control and many advantages over the conventional grafting process: polymerisation in solution was suppressed, therefore allowing the use of higher densities of immobilised initiators which led to thicker and more homogeneously grafted layers. The polymerisation reaction could be easily up-scaled.

Living radical polymerization using benzyl-*N,N*-diethyldithiocarbamate iniferter species prevented solution polymerization due to the presence of a non-active radical in solution upon decomposition [7]. Furthermore, the living properties of this system could be used to graft several different polymer layers consecutively [8].

The materials were prepared in a short time and exhibited superior mass transfer properties and saturation capacities compared to the traditional imprinted monoliths or materials prepared without the polymerisation control through CTAs. All the materials were characterised using elemental microanalysis, FT-IR, nitrogen adsorption, fluorescence microscopy, TGA, SEM, TEM, and EDX. The layer thicknesses of the grafted polymers were estimated from three different experimental methods and the materials were applied in HPLC as CPSs. The composites prepared using RAFT showed very good racemic resolution and higher efficiency compared to those prepared using iniferter initiators. The iniferter-based composites offered no racemic resolution but enantioselective retention when the two antipodes were injected separately in HPLC. In batch rebinding experiments, the enantioselectivity was more pronounced, presumably due to the static equilibrium conditions where analyte adsorption to the enantioselective sites was under thermodynamic control.

Portions of the composite materials were subjected to a chemical etching process via suspension in aqueous  $\text{NH}_4\text{HF}_2$  resulting in the dissolution of the silica to give a new type of MIPs with nanometre thin walls. The materials possessed gel-like properties and were assessed in batch rebinding experiments for their ability to discriminate between the two antipodes of the template. The enantioselectivity was clearly enhanced as compared with the parent composites due to a better accessibility to the binding sites upon removal of the silica matrix and the binding sites are more homogeneous.

## 2 INTRODUCTION

The remarkable examples in nature of molecular recognition have inspired chemists to embark on the design and construction of synthetic receptors which can mimic biological systems in terms of selective interactions with ligands, structural reorganization and self-assembly into supramolecular architectures. In practical terms, this involves the preparation of low molecular weight “building blocks” designed to interact either with a template or with each other *via* complementary surfaces. Similarly, the assembly of a recognition site around a template molecule can be achieved within highly cross-linked polymeric matrices using molecularly imprinted techniques where the complementary functionality is introduced in the form of polymerisable monomers. Furthermore, the ability to control the structure and composition of materials at nanometre scale is the key to a number of advanced functions in diverse areas, such as drug delivery, diagnostics and sensing, molecular electronics, catalysis, separations and mimicry of biological systems. While nature has mastered this task, several synthetic, so-called “bio-inspired” approaches have appeared, leading to materials mimicking various morphologies found in nature, such as molecules or particles with a core-shell structure, membranes and vesicles. Robust synthetic approaches to design materials with a good level of structural control are an important goal in materials science.

The work presented in this thesis knits both concepts: molecular recognition (function) and structural control (meso).

Mesoporous materials with controlled porosity, well-defined textures and morphologies are expected to function as improved-performance stationary phases in separation processes [9,10,11]. Because of the ability to template porosity at the mesoscale, *e.g.* in a variety of inorganic materials, polymers, and carbon compounds, a unique opportunity presents itself to create a new generation of materials that may be cast as films for thin-layer chromatography or as separation membranes, as spheres for traditional chromatographic columns, as monoliths for high speed chromatographic columns and as micron-scale elements for lab-on-a-chip analysis systems. The appeal of templated porous materials with regular structures that span

multiple length scales is that they can be synthesised straightforwardly with particular pore sizes, tailored surface properties and designed morphology. These features can be rationally tuned through chemistry to provide optimum molecule adsorption and diffusion behaviour that is reproducible from sample to sample, the goal being to maximise the resolution of the chemical components in mixture.

On the other hand, the technique of molecular imprinting has become an established technique to prepare robust molecular recognition elements toward a wide variety of target molecules [12,13,14]. The relative ease of preparing the molecularly imprinted polymers (MIPs) has led to their assessment as substitutes for antibodies or enzymes in chemical sensors, catalysis and in separation.

Presently the techniques used to prepare MIPs most often result in materials exhibiting high affinity and selectivity, but low capacity and poor site accessibility for the target molecule(s). This leads to long response times when the materials are assessed as recognition elements in chemical sensors and broad, asymmetric peaks when they are assessed as stationary phases in the chromatographic mode.

Traditionally, MIPs are obtained as monoliths and useful particles can only be obtained after crushing and sieving cycles, leading to a high loss of material and heterogeneous binding sites. As a consequence, these materials are assessed mainly as molecular recognition elements for analytical quantifications, *e.g.* as materials for solid-phase extraction, and thus are in formats which are not dependent on high sample load capacity, chromatographic efficiency or large quantities of material.

To advance into preparative scale applications or high efficiency separations, new MIP morphologies and manufacturing techniques need to be developed. A robust manufacturing technique should result in a high yield of uniform particles, with particle and pore size distributions controlled independently from the monomers, templates and solvents used in the synthesis of the MIP. Structural control at the length scales is of particular importance for larger template molecules, which can only access the surface of larger mesopores or macropores. Therefore, approaches to confine the binding sites to highly accessible domains of the polymer matrix need to be developed.

In this thesis, a combination of two approaches is described: *Mesostructured Materials* and *Molecular Recognition*. The purpose is the improvement of MIP properties and morphologies, bringing them closer to a number of advanced functions which are required in science today. This refers to the need for stable materials able to mimic the recognition properties of biological structures, such that they are useful for the separation and analysis of a vast variety of biologically active or harmful substances in industry, health services and in environmental monitoring or to high efficiency chiral separations of pharmaceutically active compounds.

Imprinted materials in beaded form have so far been produced by suspension or emulsion polymerisation [15,16,17] and dispersion or precipitation polymerisation [18,19,20]. The downside to these techniques is that the morphology of the resulting products is very sensitive to small changes of the synthesis conditions. Even under strictly controlled conditions, a simple change of template may require a complete re-optimisation of the conditions in order to achieve a given morphology. Furthermore, most of these procedures are limited with respect to the types of monomer(s) and solvent(s) that can be used for the polymerisation.

The work described herein comprises new methods for the synthesis and development of novel MIP formats to be used in separation science. The application of these new types of materials could be further extended to other areas such as drug delivery, diagnostics and sensing, molecular electronics or catalysis.

Molecular imprinting has been mainly applied to small molecules, with the templating of larger entities still posing a technical challenge due to the multitude of functionalities and the size of these target molecules. Especially biomolecules represent difficult targets as such molecules do not show tolerance to typical polymerisation conditions (organic solvents, increased temperatures, *etc.*). Thus, very limited work has so far been performed for the imprinting of large peptides and proteins, despite the advantageous features these MIPs could offer.

However, the field of bio-separation science requires novel, knowledge-based functional materials capable of recognising larger biomolecules (peptide, proteins, and nucleotides). In the light of the post-genome era, research on the human proteome asks for tailor-made media with tailor-made interactions and bio-

molecular recognition. This can involve the fractionation of proteins and peptides into groups of common functionality, common structure or other common features in order to simplify their analysis, *e.g.* by mass spectroscopy.

Conventional separation techniques (chromatography) or immunoassays suffer from high costs, poor stability and low selectivity. Furthermore, such methods are cumbersome, offer low reproducibility and require excessive human effort and expensive instrumentation. Hierarchical imprinting, the technique I have developed proved to be a suitable method to recognise large biomolecules in aqueous media and might satisfy the criteria mentioned above for the fractionation of the biomolecules in the future.

For guest molecules to access the host binding site, they need to penetrate pores whose size is difficult to control independently from the generation of the imprinted site using conventional imprinting protocols. One way to decouple these processes is to immobilise the template on the surface of mesoporous disposable solids that act as molds to create a desired porosity [1,2,3]. Thus, regardless of the conditions used to generate the imprinted sites, the pore system is determined by the solid mold. In addition, all imprinted sites are confined to the pore wall surface of the resulting material. In this way, access to these sites can be controlled by the porosity of the solid mold, which may in turn allow substructures of larger target molecules to be recognised by the surface-exposed sites. The benefits of confining the binding sites to the pore wall surface have been clearly demonstrated and the concept has been used for the development of affinity phases for the separation of biological macromolecules.

These new hierarchically imprinted materials designed for molecular recognition of nucleotide bases, large peptides and proteins may find use as separation media (chromatography, extraction) or as sensors for diagnostic purposes. In this regard, but also to serve other perspectives (purification, preparative separation), methods that facilitate selective analyte isolation are of great importance.

Besides the development of the hierarchically imprinted materials, another aspect of my research dealt with the synthesis and development of thin film molecularly imprinted composites to be used as chiral stationary phases in separation science.

Chiral separations are of great importance in the pharmaceutical industry. One relevant example is the drug "*Contergan*", used in the early 1960s when chiral separations were still in their incipient stage. "*Contergan*" showed how important it is for the active component of a drug to be in a pure enantiomeric form. While the R-enantiomer of thalidomide, presumably the only component of this drug, had a calming, relaxing effect on pregnant women, the S-form led to severe malformations of the newly born children.

Since then, enantioseparation has developed continuously and today we are dealing with new chiral stationary phases (CSPs) which comprise either natural polymers (polysaccharides, proteins) or synthetic polymers, such as polyacrylates containing chiral groups, polyamides, cyclodextrins bound to silica phases or helical polymer phases. These CSPs show high density of active sites and can be used in preparative separations with very good efficiencies. One problem associated with such conventional stationary phases is the order of elution. It is not known from the beginning which enantiomer will be eluted first. Therefore, before developing the analytical method, the library of these stationary phases needs to be screened in order to establish the elution sequence. This is time-consuming and the pharmaceutical and environmental industries of today require new, rapid and efficient analytical methods of chiral separation.

An alternative to the conventional CSPs comprise molecularly imprinted polymers, tailored for the separation of a specific compound or class of compounds. So far, most applications of MIPs as CSP in chromatography have been based on conventional imprinting [21,22]. Such MIPs are able to separate the enantiomers with good separation factors but, unfortunately, the separation efficiency, as seen in the corresponding resolution factors and plate numbers are typically rather low (1000-3000 plates per m). This is often due to severe peak broadening and tailing, especially of the more retained enantiomer, which in turn can be attributed to the heterogeneous population of binding sites, with respect to their affinities and accessibilities, as well as to a low functional capacity of the material.

Numerous attempts have been made to improve the performance of MIPs and to avoid the problems mentioned above. This involved the optimisation of the

separation protocol including temperature, mobile phase, addition of competitors and the use of gradient elution protocols [23] to improve peak shapes.

More promising approaches appear to be those in which efforts are made to synthesise better imprinted materials in the first place. In this thesis, I will present three alternative synthetic procedures resulting in imprinted materials with improved mass transfer properties.

### 3 MOLECULAR IMPRINTING - STATE OF ART

#### 3.1 INTRODUCTION TO MOLECULAR IMPRINTING

Molecular recognition is integral to biologic processes such as the immuno response, ligand-receptor interactions and enzyme catalysis. The ability of biological hosts to bind strongly and specifically to a particular molecular structure is a key factor in the biological machinery. Well known examples are the sensitivity of the immune response, where antibodies are generated in response to minute amounts of a foreign antigen and the energy saved by enzymes due to their ability to stabilise the transition state of the reaction to be catalysed. With biological examples as models, chemists hope to be able to mimic these properties for various applications.

One technique that has been increasingly adopted for the generation of artificial macromolecular receptors is molecular imprinting in synthetic polymers [12,13,14].

It is a process whereby functional and cross-linking polymers are co-polymerised in the presence of template molecules, which may be small molecules, biological macromolecules, micro-organisms or whole crystals. The functional monomers initially form a complex with the template molecule and following polymerisation, their functional groups are held in position by the highly cross-linked polymeric structure. Subsequent removal of the imprint molecule reveals binding sites that are complementary in size and shape to the template or to an analogous structure (Figure 3-1).

The advantages of molecularly imprinted polymers, as compared to biological receptors, include their mechanical and chemical stability, low cost of preparation and wide range of operating conditions. However, they suffer from some drawbacks in certain applications, such as the heterogeneous distribution of binding sites, low capacity and selectivity and poor site accessibility. The development of suitable methods for overcoming these problems will open the door to considerably more diverse application opportunities than are available right now. This thesis is focused on the development of such new methodologies for producing imprinted materials exhibiting uniform structures and high affinity to the target molecules.



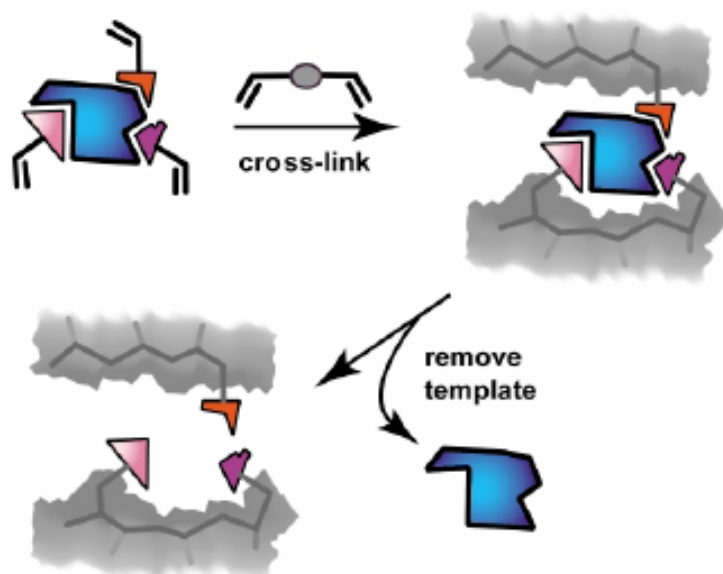


**Figure 3-1:** Schematic representation of the molecular imprinting process showing one binding site within the polymer matrix.

## 3.2 AN HISTORICAL PERSPECTIVE OF THE DEVELOPMENT OF MOLECULAR IMPRINTING

### 3.2.1 Molecular Imprinting in Silica

An important area of investigation in the early part of the 20<sup>th</sup> century was focused on biochemical processes and the structures of biomolecules. Linus Pauling was an important contributor to the area as in 1940, he proposed the “instructional theory” for the formation of antibodies [24]. In Pauling’s theory, antibodies were thought to adopt a specific three-dimensional complementary structure toward the antigen upon contact with it, as illustrated schematically in Figure 3-2. This theory was proposed before several landmarks of biochemistry, such as the implicit connection between the genetic code, the subsequent peptide-chain and the final three-dimensional structure of the resulting antibody, were established.

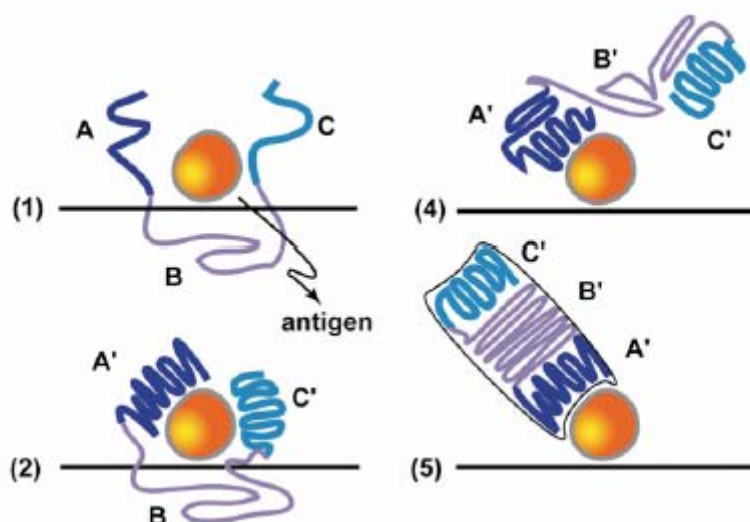


**Figure 3-2:** Scheme showing four steps of Pauling's mechanism by which an antigen imprints structural information into an antibody molecule.

Although the concept proved incorrect in describing how antibodies develop in the immune system, it gave inspiration and stimulus towards the development of artificial receptor molecules, as illustrated by the work of Dickey [25]. Dickey prepared silica gels "by procedures analogous to the formation of antibodies". The method involved polymerisation of sodium silicate in the presence of a dye. Four different dyes were used, namely methyl, ethyl, *n*-propyl and *n*-butyl orange. As much as possible of the dye was subsequently removed and in rebinding experiments, it was found that the silica prepared in the presence of any of these "pattern molecules" would bind the pattern molecule in preference to the other three dyes.

Molecularly imprinted silicas have been intensively tested in separation science serving as stationary phases in HPLC columns and thin layer chromatography. Dickey presented the idea that specific catalysis, analogous to enzymes, was a possible application for silicas imprinted against selected reactants or products [25]. Structure elucidation was another application, as reported in 1957 by the group of Beckett [26] who adsorbed stereoisomers of unknown configurations onto silica imprinted by a single stereoisomer of a related compound of known configuration.

After a steady flow of publications for a period of over 15 years, the interest in imprinted silica experienced a decline. The main limitations relate to the poor stability and poor reproducibility of the imprinted silica materials.

### 3.2.2 Molecular Imprinting in Organic Polymers

In 1972 the groups of Wulff and Klotz presented independently the first examples of molecular imprinting in synthetic organic polymers. The first report of Wulff and Sarhan described “a controlled distance method” involving the co-polymerisation of D-glyceric-(p-vinylanilide)-2,3-o-p-vinylphenylboronate and divinylbenzene. Subsequent hydrolysis of the glycerate moiety disclosed imprints exhibiting chiral recognition of D-glyceric acid [27] (Figure 3-3). In addition to boronic esters, ketals, and Schiff bases, other covalent linkages have also been exploited for covalent imprinting [28]. This method have come to be called “covalent imprinting” and offers the possibility of defined template-monomer constructs, thus allowing control of the stoichiometry of the imprinting mixture; this generally results in binding sites that are more homogeneous than those obtained using other techniques (see later). However, a limitation of this technique is the lack of readily reversible covalent linkages which may be utilised. Further, the “on-off” kinetics of template recognition is rather slow.

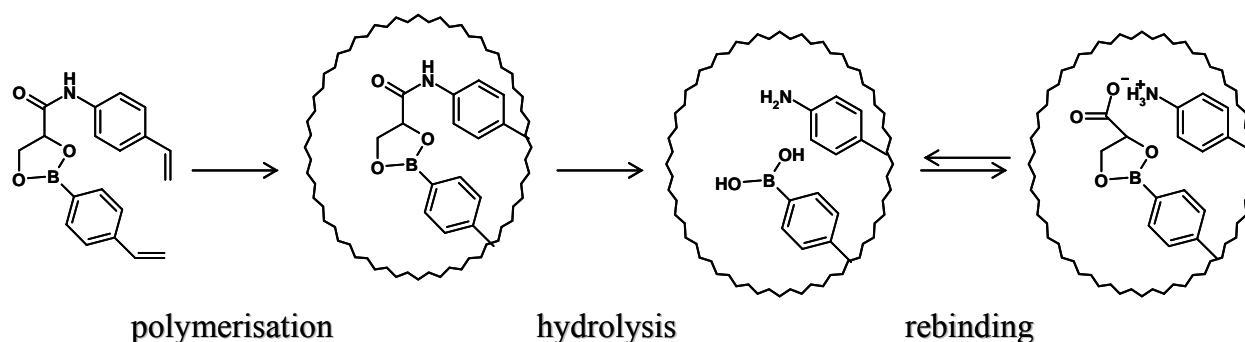


**Figure 3-3:** The covalent approach to molecular imprinting in organic polymers, as introduced by the group of Wulff, exemplified by the D-glyceraldehyde MIP.

A very important development in the history of molecular imprinting in organic polymers was introduced by the group of Mosbach in the early 1980s [29,30]. This important contribution named “non-covalent imprinting” broadened the scope of molecular imprinting significantly by using non-covalent interactions between the target molecule and the functional monomers. The first paper on non-covalent imprinting reports a “*host-guest polymerisation*” technique for the imprinting of rhodamine blue and safranin [29] (Figure 3-4).

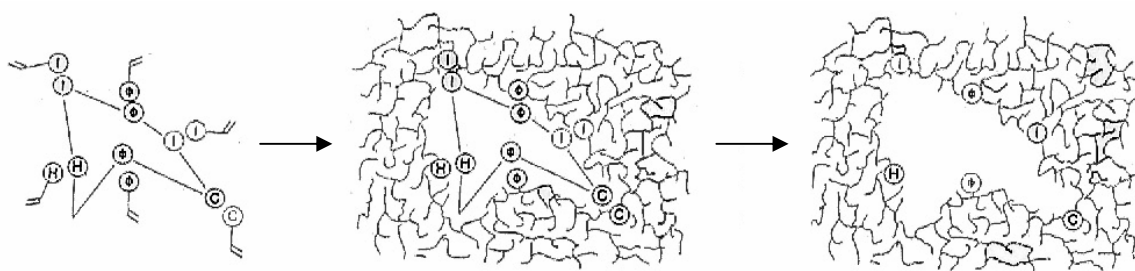


**Figure 3-4:** *The first non-covalent approach to molecular imprinting in organic polymers, as introduced by the group of Mosbach, exemplified by the rhodamine blue MIP.*

Non-covalent imprinting is more straightforward and flexible than covalent imprinting. Here, monomer(s) and template are dissolved in a suitable solvent and self-association occurs to give template-monomer complexes. On copolymerisation with an excess of cross-linking monomer(s), these complexes are envisaged to be “locked in” to the 3D-polymeric matrix. Template removal may be achieved simply by solvent extraction. A wide variety of monomers exists, with functionalities that are complementary with most template molecules. Some popular functional monomers used in non-covalent imprinting are shown in Figure 3-5.

The correct arrangement of functional monomers around the target molecule is one of the most important aspects of this technique. When designing an imprinting procedure, the choice of functional monomers is usually based on complementarity. For example, if the target molecule is a basic compound, the functional monomers should be acidic or if the target is a hydrogen bond donor, the functional monomer should be a hydrogen bond acceptor.

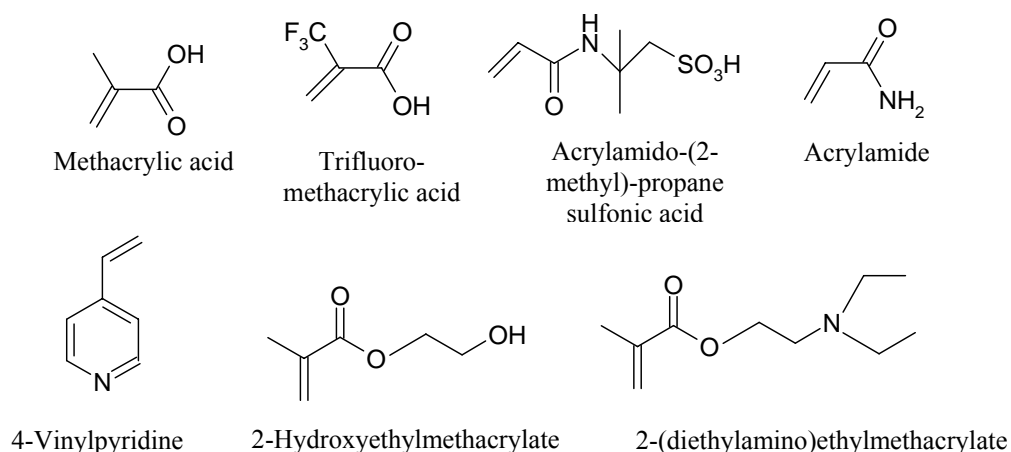


**Figure 3-5:** Selection of common functional monomers used in molecular imprinting protocols.

So far, the most successful non-covalent imprinting systems using commercially available monomers are those based on acrylic or methacrylic monomers, such as methacrylic acid (MAA), cross-linked with ethyleneglycol dimethacrylate (EDMA).

Initially model systems were investigated in order to understand and elucidate the recognition process based on non-covalent interactions in synthetic polymers.

First, derivatives of amino acid enantiomers were used as templates for the preparation of imprinted stationary phases for chiral separations (MICSPs), but the system has proven generally applicable to the imprinting of templates which are capable of allowing hydrogen bonding or electrostatic interactions to develop with MAA [31]. One of the most investigated model system is based on the imprinting of L-phenylalanine anilide (L-PA). In the first step, the template (L-PA), the functional monomer (MAA) and the cross-linking monomer (EDMA) are dissolved in an aprotic solvent of low to medium polarity. The free radical polymerisation is then initiated with an azo initiator, commonly 2,2'-azo-bis-isobutyronitrile (AIBN), either by photochemical homolysis below room temperature [31] or thermochemically at 60°C or higher [32]. Lower thermochemical initiation temperatures down to 40 or 30 °C may be employed, using *e.g.* 2,2-azo-bis-(2,4-dimethyl-valeronitrile) (ABDV).

In the final step, the resultant polymer monolith is crushed by mortar and pestle or ball mill, extracted using a Soxhlet apparatus, and sieved to a particle size suitable for chromatographic (25-30  $\mu\text{m}$ ) or batch (150-250  $\mu\text{m}$ ) applications. The recognition

properties of the polymers are then assessed in batch rebinding experiments, by measuring the amount of template taken up by the polymers at equilibrium, or in chromatography, by comparing the retention time or retention factor ( $k$ ) of the template with that of structurally related analogues when using the imprinted and control polymers as stationary phases.

In the elucidation of retention mechanism, an advantage using enantiomers as model templates is that non-specific binding, which affects both enantiomers equally, will cancel out. Therefore the separation factor ( $\alpha$ ) uniquely reflects the contribution to binding from the enantioselectively imprinted sites. As an additional comparison, the retention of the imprinted phase is compared with the retention on a non-imprinted reference phase.

Many studies have been performed using L-PA imprinted monolith polymers as a model system. These involved the study of chromatographic band broadening [33], effect of the porogen [34], ion exchange retention model [31], photo-*versus*-thermal polymerisation [32], protonation states [31], effect of thermal annealing [35], factors affecting the chromatographic response [36,37], monomer-template interaction [32] model of a binding site [32], study of the adsorption isotherms [36], *etc.*

$^1\text{H-NMR}$  spectroscopy and chromatography were used to study the association between MAA and L-PA in solution as a mimic of the pre-polymerisation mixture [32]. The  $^1\text{H-NMR}$  chemical shifts of either the template or the monomer versus the amount of added MAA, as well as the chromatographic retention of L/D-PA versus the amount of acid in the mobile phase, varied in accordance with the formation of multimolecular complexes between the template and the monomer in the mobile phase. A 1:2 template-monomer complex was proposed to exist prior to polymerisation. Based on these results, hydrogen bond theory and the assumption that the solution structure was preserved after polymerisation, a structure for the polymeric binding was proposed (Figure 3-6).

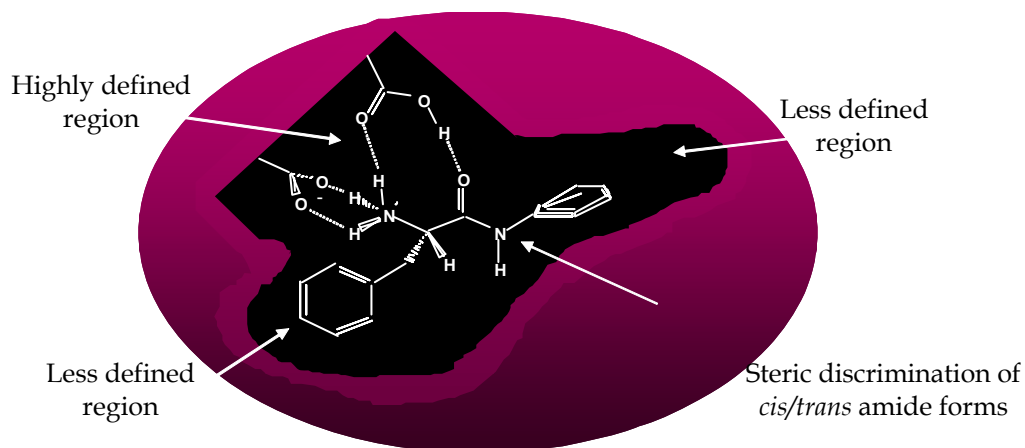


**Figure 3-6:** Model of L-PA binding site based on NMR and chromatographic data adapted (with permission) from [32].

After an intensive study of model systems in non-covalent molecular imprinting technology, efforts are currently directed towards the optimisation of these synthetic receptors.

In order to obtain an optimised polymer for a given target analyte, combinatorial approaches to MIP synthesis have been used. Here, the ingredients of the imprinting recipe, in particular the kind and molar ratio of the functional and cross-linking monomers are varied. This may be done using automated procedures. Our group has reported recently on such techniques, allowing the high-throughput synthesis and evaluation of adsorbents imprinted with the local anaesthetic Bupivacaine on a reduced scale (mini-MIPs). The materials were optimised for use in purely aqueous environments [38].

Another approach which aims at selecting the best functional monomer(s) for a given template is the use of computational techniques based on molecular modelling [39].

MIPs with an enhanced capacity can also be obtained via non-covalent imprinting by taking elements from supramolecular chemistry in order to design novel functional monomers that will interact more strongly with a given target molecule than the commonly used monomers. Our group recently reported the one step synthesis of a novel *bis*-urea functional monomer and its application in the imprinting of N-Z-L-glutamic acid. The ability of this new designed functional monomer to form strong intermolecular hydrogen bonds to 1,5-dicarboxy anions in a competitive medium

(DMSO- $d_6$ ) was quantified and the ability of the MIP to recognise the template N-Z-L-Glu over N-Z-L-Asp and N-Z-Gly, in the chromatographic mode, was proven [40]. Another alternative to built recognition sites in organic polymers was introduced by Whitcombe *et al.* [41]. Figure 3-7 illustrates the first published example of this “*semi-covalent*” imprinting procedure that can be viewed as a hybrid of the above two methods. Here the template cholesterol was esterified with 4-vinylphenol to give a 4-vinylphenyl carbonate ester. After co-polymerisation of the template construct with excess of cross-linker, the carbonate-bond was cleaved, releasing the template and a small, sacrificial molecule, carbonic acid. Following extraction of the template, the imprinted recognition site bore a phenolic residue oriented in a manner that allows specific rebinding via non-covalent interaction with the hydroxyl group of cholesterol.

The authors claimed that the polymer rebound cholesterol with a single dissociation constant, thus displaying binding characteristics similar to biological entities.

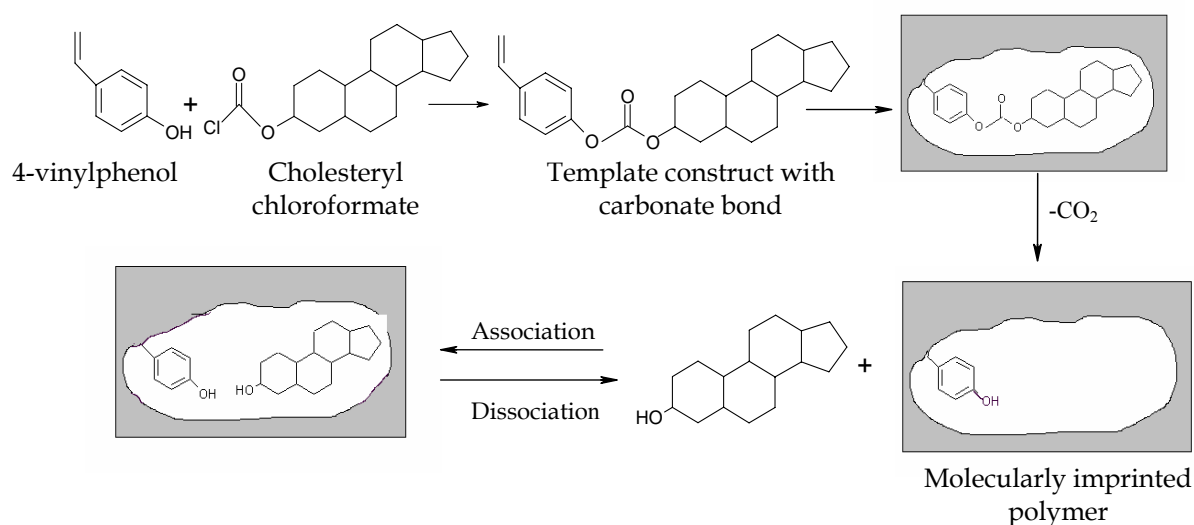


**Figure 3-7:** The first semi-covalent approach to molecular imprinting in organic polymers, as introduced by the group of Whitcombe, exemplified by the cholesterol MIP.



Metal-coordination interactions can be used as well for preparing molecularly imprinted polymers. The first exemplification of this concept was reported by Belkon and co-workers [42]. Using bis [N-(5-methacryloylamino) salicylidene-S-norsalinate] Co (III) complexes as the metal-complexing monomers, cross-linking template polymerisation was carried out using *N,N'*-methylenebisacrylamide as the cross-linking agent. This produced rigid polymer matrices with stabilised octahedral  $\text{Co}^{3+}$  chiral complexes (Figure 3-8). Deuterium exchange studies with the polymeric complex proceeded with full retention of the configuration of the amino acid, thus suggesting that the initial conformation of the complex was retained in the polymer matrix.

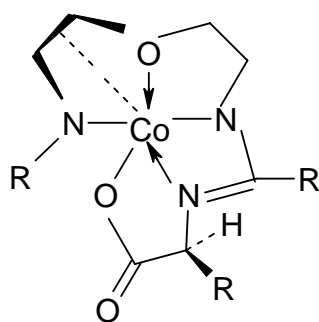


**Figure 3-8:** The first approach to molecular imprinting using metal-complexes monomers as introduced by the group of Belkon.

An important contribution to the development of metal-coordination interaction based MIPs was brought by Arnold and co-workers. In the first attempt to demonstrate the advantage of this binding interaction, the strong coordination between the iminodiacetic (IDA)- $\text{Cu}^{2+}$  complex and imidazole was utilised to prepare MIPs [43]. Near quantitative desorption and reloading of the metal ions and substrates with these polymers suggested the high accessibility of the binding sites in these polymers.

In conclusion, the history of molecular imprinting is longer than generally perceived and comprises several different and independently developed approaches.

### 3.3 METHODS FOR PREPARATION OF SPHERICAL MIP BEADS

Traditionally, MIPs have been and continue to be prepared by thermal or photo copolymerisation of a concentrated homogenous solution of functional monomer(s) and the cross-linker in the presence of the target molecule. The resulting polymers are formed as monoliths and they must be crushed with mortar and pestle or a ball mill before use. After sieving, the particles are sorted into the correct size for a particular application. The template is extracted with solvent using a Soxhlet apparatus. Although the traditional MIPs prepared via this rather inelegant method still find a wide range of applications, there are some associated problems that need to be overcome.

First, the work-up of the materials is tedious, unhealthy and leads to a high loss of materials (> 50%) in the form of fine particles, thus leading to reduced yields of useful material. Further, a portion of the template molecule often cannot be extracted from these bulk polymers because they are deeply buried within the cross-linked matrix. Even if the entire template is extracted, a portion of the sites are likely to have very low accessibility and are therefore lost for use in many applications. The resulting particles are also irregularly shaped (Figure 3-9) and, due to flow disturbances and diffusion limitations, this causes a poor efficiency in chromatography, making these particles unsuitable for such applications.

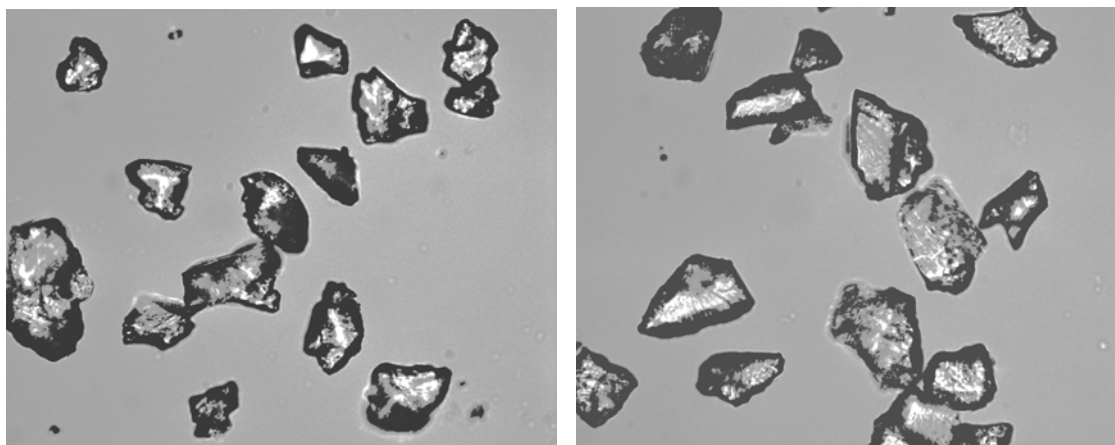


**Figure 3-9:** Irregularly shaped particles resulting from mechanical grinding of a “traditional” molecularly imprinted polymer.

Since molecular imprinting is now maturing towards the point where it can be usefully integrated into real-world applications, the need to produce materials cheaply, efficiently and reproducibly in beaded form, thin films, membranes, gels or other new formats is becoming much more pressing. During the past few years, three aspects have mainly been addressed: (i) the synthesis of small, spherical particles of micrometer or nanometre size, (ii) the synthesis of thin layers and (iii) the creation of surface imprints. The aim in the first of these areas is to synthesise uniformly sized and shaped particles with narrow particle size distributions and improved mass-transfer properties, resulting in MIPs with better quality binding sites. Some alternatives for accomplishing these issues are described below.

Suspension polymerisation with water as the continuous phase is a very well established method for preparing organic polymer beads. The process is relatively easy to perform and has been used to make imprinted beads when rather stable covalently bonded adducts, such as carboxylate esters [44] or metal chelates [45] were used as templates. Whitcombe *et al.* have reported cholesterol-imprinted beaded polymers made using aqueous suspension polymerisation [46]. Little work has been done to date with imprinting in aqueous conditions, as water is incompatible with most of the interactions used in non-covalent procedures.

Methods for suspension polymerisation in two different non-aqueous media, i.e. silicon oil and liquid perfluorocarbon have been reported. The latter method was first described by Mayes and Mosbach [47] and is a fast and reliable methodology to synthesise MIPs particles by UV irradiation in less than 2h. The beads obtained have a diameter that can vary between 5 and 50  $\mu\text{m}$ , depending on the stirring speed and the amount of surfactant used. This technique employs a perfluorocarbon solvent (perfluoro-(1,3-dimethylcyclohexane) (PMC)) as the continuous phase, which allows the establishment of the same interactions that occur in traditionally “bulk” polymers (each particle acts like a mini bulk reactor). The fluorocarbon suspending medium can be easily recycled by distillation. The method has as drawbacks the fact that it is necessary to synthesize perfluorinated surfactants and not only one surfactant can be used in all protocols. In addition perfluorocarbon is an expensive material.

Recently, Kempe *et al.* developed a new technique for synthesising spherical MIP beads by suspension polymerisation in mineral oil [15]. The method was applied to a MIP library imprinted with Propanolol for the purpose of optimising the MIP formulation.

MIPs in the bead format have also been prepared by a multi-step swelling procedure. This method was first applied for producing MIPs by Hosoya *et al.* [48]. It requires several swelling steps of the initial polymer particles with the imprinting mixture before polymerisation proceeds. In this case, the continuous phase of the polymerisation medium is water. This method produces monodisperse particles in the micron range (2-50  $\mu\text{m}$ ) with good control of the final size and number of particles.

Emulsion polymerisation is another technique that allows the production of spherical nano-sized imprinted beads. One example is the synthesis of core-shell imprinted particles [16,17]. They have a structured morphology that allows the incorporation of any added property into the core of the particle without interfering with the imprinted shell. The continuous medium during the polymerisation is water. Particles obtained *via* this method are monodisperse and can be produced in a colloidal size range of 0.05-2  $\mu\text{m}$ .

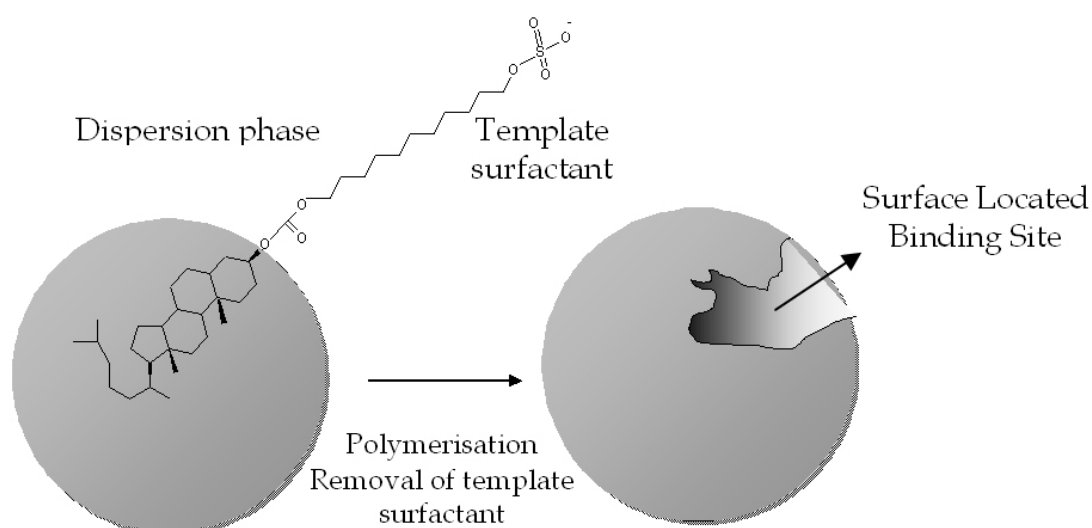


**Figure 3-10:** Synthesis of cholesterol-imprinted nanospheres by emulsion polymerisation using a template surfactant.

An interesting example of this imprinting procedure is the preparation of small beads in an oil-in-water biphasic system stabilised by a surfactant. The particularity of the protocol is that the imprint molecule (cholesterol) is part of the surfactant, i.e. pyridinium 12-(cholesteryloxy-carbonyloxy) dodecane sulfate [16]. Thus, the resulting binding sites are all situated at the particle surface (Figure 3-10). This was demonstrated by flocculation experiments using PEG-bis-cholesterol.

Imprinting by surface rearrangement of latex particles was first introduced in 1992 [49] and has been the subject of other studies since then. While this approach to surface imprinting is attractive, to date it has only been demonstrated for metal ion imprinting. If the technique could be extended to small organic molecules then it would have a greater impact and would have particular relevance to agglutination type assays and the targeting of macromolecules, where access to surface-localised binding sites is crucial, as will be shown in Chapter 4 which is dedicated to my own developed method, namely hierarchical imprinting.

Precipitation polymerisation is performed with similar pre-polymerisation mixtures as for traditional MIPs, except that the relative amount of solvent present in the mixture is much higher. When polymerisation progresses, imprinted nano- or microspheres precipitate instead of polymerising together to form a polymer monolith. The method has the drawback that, because of the dilution factor, larger amounts of imprint molecule are needed, although this may be compensated by the typically higher yields. Also the method needs re-optimisation of the polymerisation conditions and monomer stoichiometry for every different template. Still, in the last few years, this method of synthesising MIP spherical beads has been increasingly investigated.

For example, this method was successfully used by Ye *et al.* to prepare imprinted particles for binding assays [18] and it has been proven that in some applications, these particles performed better than those particles obtained by the grinding of monoliths.

Spherical MIPs were recently prepared using precipitation polymerisation and used for the controlled delivery of Sulfazine [50].

Tamayo *et al.* synthesised spherical imprinted beads against fenuron, a phenylurea herbicide. From rebinding experiments it was claimed that the imprinted polymer prepared using methacrylic acid possessed a homogenous binding site distribution and permitted quantitative recoveries over a wide concentration range during SPE processes [19].

The group of Cormack has successfully developed a precipitation polymerisation method for producing theophylline imprinted polymer beads for HPLC and SPE applications using DVB as cross-linker and MAA as functional monomer [20]. These particles were spherical and uniformly sized, with a diameter of about 5  $\mu\text{m}$  and high surface areas of up to 600  $\text{m}^2/\text{g}$  (Figure 3-11).

Overall, the precipitation polymerisation approach offers an effective solution to bead production in many situations. Particles with the desired size, morphology, porosity and a better accessibility of binding sites can be easily produced by appropriately tuning the imprinting procedure.

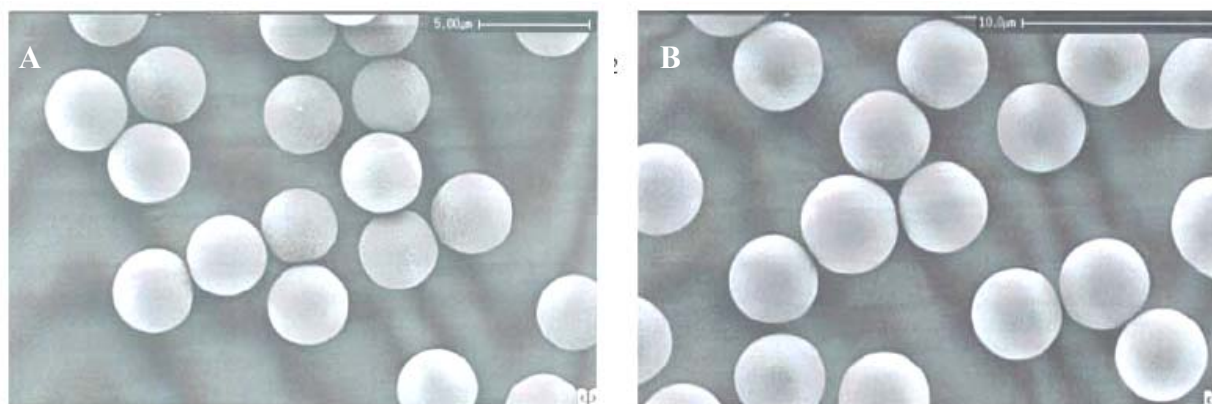


**Figure 3-11:** Scanning electron micrographs of theophylline imprinted (A) and non-imprinted (B) microspheres prepared via precipitation polymerisation adapted with permission from Wang *et al.* [20].

Wulff's group has used an approach somewhat similar to the precipitation polymerisation mentioned above [51]. However, instead of precipitated particles, soluble polymer microgels were produced. These had a molecular weight of *ca.*  $10^6$   $\text{g mol}^{-1}$ , *i.e.* in the same order of magnitude as proteins, and possessed a small number of binding sites per molecule. Although microgels were readily obtained with

optimised protocols, obtaining selective, imprinted materials proved more difficult using this technique, even though a covalent imprinting complex was used.

### 3.4 OTHER NOVEL MIP FORMATS

The group of Zimmermann has recently published some reports on molecular imprinting in dendrimers [52]. This method involves the covalent attachment of dendrons to a porphyrin (the template) core, cross-linking of the end-groups of the dendrons, followed by removal of the porphyrin template by hydrolysis. This approach ensures nearly homogeneous binding sites, quantitative template removal, and the presence of only one binding site per molecule and solubility in common organic solvents. Whether it is broadly applicable to a wide range of target molecules still remains to be proven. There are a number of examples in the literature where thin layers of MIPs have been chemically or physically anchored on various surfaces. One novel simple method, reported recently, involves spin-coating of MIP films of controlled thickness and porosity [53]. This is the first report on *in situ* synthesis of films, *via* the polymerisation of vinyl-based monomers, and comprises spreading a MIP pre-polymerisation mixture containing a novel porogenic solvent of low volatility onto a substrate followed by UV curing of the obtained films. The films were imprinted with a chiral template and the selectivity was proven.

Sol-gel technique is also used to prepare sol-gel molecularly imprinted thin films. This may offer potential advantages over the organic-polymer thin films including a simple preparation at room temperature, rapid condensation followed by rapid solvent evaporation during the coating process and the availability of a large library of functional trialkoxy-silanes needed for successful imprinting. Recently a comparison between two thin film polymeric systems, organic (acrylic) and metal oxide (inorganic SiO<sub>2</sub>) for imprinting of racemic Propanolol showed that the inorganic film offers higher affinity to the imprinting molecule, higher selectivity and faster kinetics of adsorption [48].

Silica has been used as the imprinting matrix for the imprinting of inorganic ions [54] and organic molecules [55,56,57,58]. Here, either the bulk material can be imprinted by the sol-gel method, thus creating microporous materials with specifically

arranged functional groups [54,55,56] or an imprinted polysiloxane layer may be deposited onto a silica surface [57,58]. Another material that has been imprinted using sol-gel techniques is titanium oxide [59,60,61,62].

Several attempts were made using the imprinting approach to develop new stable affinity membranes for separation and sensor technology. Unlike a particle-based stationary phase in a column or cartridge, a membrane can be easily operated in continuous processes and is therefore highly advantageous from an industrial point of view. One of the first examples of the preparation of imprinted membranes was the use of the so-called phase-inversion precipitation method presented by Kobayashi *et al.* [63]. The method is based on linear polymers and makes use of the fact that the polymer is soluble in one solvent but coagulates in another.

MIPs can be elegantly combined with a pre-formed membrane to give a composite material. This unites the mechanical integrity of the base membrane with the selectivity of the imprinted polymer. The majority of MIP-composite membranes have been prepared by simply immersing the support membrane in a pre-polymerisation imprinting mixture. Various materials have been investigated as base-membranes, including glass filters [64], alumina-based support membranes [65] and porous poly(propylene) membranes [66]. Finally, the imprinted polymer can be firmly anchored to base-membranes by grafting procedures, in order to obtain thin films that are confined to the vicinity of the support membrane. Since the films are thin, high permeabilities are ensured. Grafting has been accomplished via functionalisation of support membranes with a photoinitiator and the support membranes used in this approach were based on polyacrylonitrile [67], polypropylene [68] and polyvinylidene [69,70]. Grafting on membranes will be described in detail in the following section.



### 3.5 GRAFTING TECHNIQUES

Grafting of polymer films “from” and “to” preformed surfaces of solids is a well-established technique for their modification and functionalisation. Grafted polymer layers can dramatically affect the surface properties of substrates such as wettability, friction, adhesion, lubrication and biocompatibility.

Generally, grafting of polymers is accomplished through three general procedures: physisorption, spin-coating (for flat surfaces) or covalent coupling of polymers to the surface of preformed materials.

Physisorption of polymers on solid supports takes place through van der Waals or hydrogen bond interactions between the polymer and the surface. These interactions are very weak and, therefore, the resulting composite materials are not very stable. Desorption of the polymer from the surface can easily occur by simple use of solvents or thermal treatments.

Polymer films attached to surfaces of solids through covalent coupling are far more robust and stable. Polymer chains are typically covalently attached to a substrate surface by means of either “grafting to” or “grafting from” techniques. Preformed polymer chains are reacted with a surface in the “grafting to” method. In the “grafting from” technique, initiator species immobilised on substrate surfaces are used to initiate polymerisation upon exposure to a monomer under appropriate conditions.

In the literature, there are many examples using grafting methodologies to redesign and reengineer surfaces of various solids, but I will focus here on the examples that combine polymer grafting with molecular imprinting.

Using grafting techniques, MIPs can be grown on preformed support materials of known morphologies. This may lead to specific adsorbents layered around a core bead that can be used for example as stationary phases in chromatography or SPE. MIPs have been also prepared as grafted coatings on silica supports [71,72], on organic polymer supports [73,74] and on the walls of fused silica capillaries [75,76]. MIPs were also grafted on membranes for affinity filtration [59], on flat surfaces such as glass [53], gold [77,78], or the gold surface of a Quartz-Crystal-Microbalance (QCM) resonator [79] to produce chemical sensors.

### 3.5.1 The “Grafting To” Approach

Most of MIP coatings have been prepared by grafting polymers to the various surfaces. The “grafting to” method implies the existence of polymerisable double bonds on the surface one wishes to graft onto. Thus, these double bonds can add to the growing polymer chain in solution and link them to the surface.

One such example is the coating of methacrylate-modified silica with an imprinted organic polymer, as reported by Norrlöw *et al.* [64] and illustrated in Figure 3-12. Polymerisable acrylate groups on the surface of porous support beads enable the coating of the pore-surface with a thin molecularly imprinted film. The imprinted material coated on silica was suitable for immediate use as a stationary phase in chromatography.

Wulff *et al.* reported a similar approach in which methacrylate modified porous silica was used and a layer of imprinted polymer was grafted onto the pore walls. Imprinting was performed here employing covalent imprinting methods and materials for use in enantioseparation were synthesised [72].

Another example using the “grafting to” technique to imprint a protein was reported by Minoura *et al.* [80]. A polymer layer was grafted around silica beads containing vinyl groups. The layer was composed of acrylamide, acrylic acid and cross-linkers using glucose oxidase (GOD) as a template. The composite was able to recognise GOD in a mixture of proteins.

“Grafting to” has also been used in combination with metal-chelating monomers. Thus, in a paper by Arnold *et al.*, propylmethacrylate-activated silica particles were coated by copolymerisation with the metal-complex monomer  $\text{Cu}^{2+}$ -[N-(4-vinylbenzyl)-imino] diacetic acid, a metal-coordinating template (imidazole), and EDMA [73].

In a report from Glad *et al.*, pre-formed, porous, spherical poly (TRIM) beads were utilised. These beads contained residual polymerisable groups on the surface within their porous structure. By carefully filling the pores of the beads with a standard MIP pre-polymerisation mixture, a “TRIM-MIP” composite was obtained. The composite material was spherical and suitable for immediate use in HPLC [74]

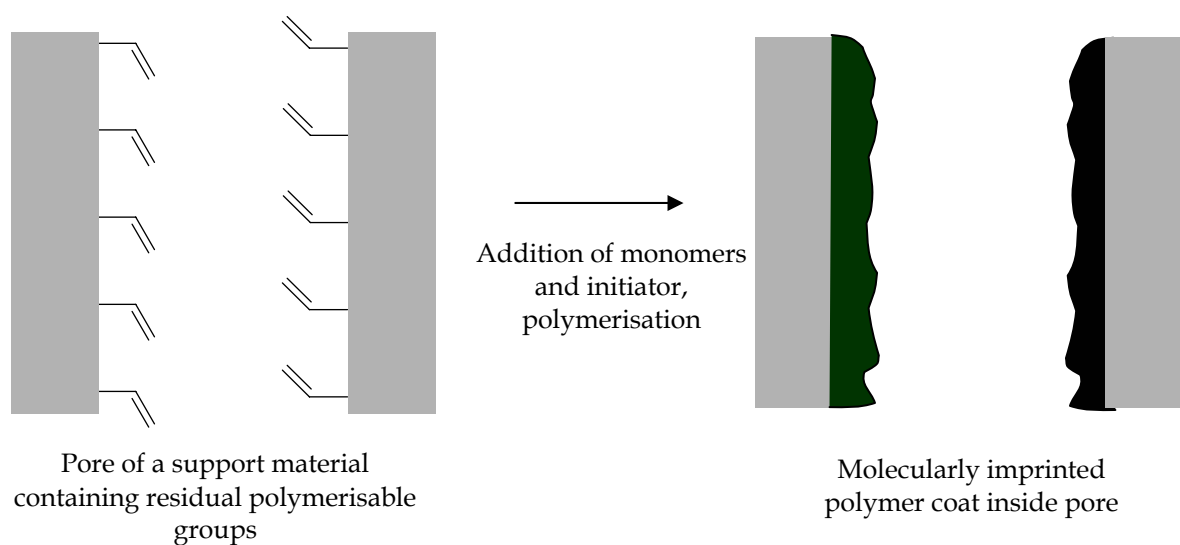


**Figure 3-12:** Schematic representation of “the grafting to” process of a thin MIP layer onto a porous support.

One problem with the “grafting to” technique is the presence of initiator in solution, requiring the monomer mixture to be applied as a liquid thin film on the surface prior to polymerisation. Thus, the exact amount of monomers that will coat the available surface with a thin liquid film is dissolved together with the initiator in an excess of solvent. Thereafter the modified support is added and the solvent evaporated to leave the monomer film and initiator on the surface. Polymerisation is then usually carried out at elevated temperatures. With this procedure the thickness of the polymer layer is difficult to control and capillary forces upon evaporation of solvent may cause incomplete wetting of the surface. Moreover, the maximum density of grafted polymer chains is here limited due to kinetic and sterical factors. Therefore, the formation of surface-bound polymer monolayers by such a “grafting to” technique is limited to low graft densities and low film thicknesses. As an alternative, surface initiated polymerisation has been employed using a variety of monomers in order to modify the surfaces of solid substrates.

### 3.5.2 The “Grafting From” Approach

A more promising approach for the preparation of covalently attached polymer layers is presented by the use of immobilised initiators for the *in situ* generation of the grafted polymers. This is known in literature as the “grafting from” method. By confining the initiator to the surface one ensures that the propagation step of the polymerisation occurs only at the support surface and that a higher density of grafted polymer chains can be achieved.

In the systems described so far in literature, azo-compounds were mostly used as initiators for the conventional grafting using radical chain polymerisation of various monomers [81,82,83]. Grafting using classic free-radical initiators with azo moieties shows poor control over chain length and terminal chain functionality.

Growth of polymers at surfaces using azo-initiators has been previously studied [84,85]. In all cases strong differences between polymer molecules grown at surfaces and polymer generated in solution are predicted. The first study demonstrates that the polydispersity of the polymer grafted on the surface is much higher compared with the same reaction occurring in solution. This is due to the fact that long chains are more efficient at adding additional monomer than short chains, which are consequently growing slower.

To achieve some degree of control of the polymerisation with surface attached initiators, it is essential to know to what extent the mechanism of polymer growth is affected by the immobilisation of the growing chains at the solid surface. In contrast to a conventional solution polymerisation where all the chains are evenly distributed throughout the solution, the covalent bond between the growing chains and the surface of the substrate prevents free diffusion and restricts all (active and already terminated) polymer chains to a small volume in close proximity to the surface.

Rühe *et al.* studied the kinetics and the mechanism of radical chain polymerisation with an azo initiator that has been immobilised to the surface of a silica substrate [85]. The authors concluded that initiation and growth of the polymer at low conversion of a surface-attached initiator are very comparable to polymerisation in solution. Differences in the polymerisation mechanism between surface and solution polymerisation are mostly due to differences in the termination reactions.

If the termination of surface attached chains by free chains growing in solution becomes a significant pathway of termination, the rate of termination decreases with increasing the graft density of attached chains. This is due to the fact that the free chains have to diffuse against the concentration gradient into the film in order to allow a termination reaction to occur. Another difference between solution polymerisation and surface polymerisation is that in the latter, all the transfer reactions to either solvent or monomer lead to a termination of the growth of the surface-attached chains and the film growth is completely stopped.

During past few years, new controlled “grafting from” methods have been reported. The reduced concentration of radical centres at the chain end of living radical polymerisation opens up a number of possibilities in the synthesis of complex macromolecular architectures due to the very low occurrence of side reactions such as radical-radical chain coupling.

These techniques use various type of immobilised initiators, e.g. iniferter-type initiators [86], initiators for Atom Transfer Radical Polymerisation (ATRP) such as alkyl halides [87], nitroxides mediated Living Free Radical Polymerisation (LFRP) [88], Ring-Opening Metathesis Polymerisation initiators (ROMP) [89] or conventional azo initiators using Reversible Addition Chain Transfer Fragmentation Agents (RAFT) [90].

Our group was the first to report on the grafting of thin MIP layers on porous silica particles using immobilised initiators [5]. The use of covalently coupled initiators to graft an imprinted layer using Controlled Radical Polymerisation (CRP) conditions is one of the topics of this thesis and the results will be presented in Chapter 5.

In the paper of Sulitzky *et al.* [5], an azo-initiator, 4,4'-azo-bis-(4-cyano pentanoic acid) (ACPA), was covalently immobilised on silica particles previously modified with epoxy or amino groups. Alternatively, a diamidine azo-initiator, 2,2'-azo-bis-(N, N'-dimethylene isobutyramidine), (AIDA) was physically adsorbed to similar silica particles (Figure 3-13). The grafting experiments were then performed using the chiral template L-phenylalanine anilide (L-PA), EDMA as cross-linker and MAA as functional monomer, with dichloromethane or toluene serving as porogenic solvents.

The resulting materials prepared using covalently immobilised initiators proved to be superior to those prepared using physically adsorbed initiators, where the initiator or the polymer may be displaced by acids or bases competing with the initiator for the surface adsorption sites. The obtained materials were successfully applied as chiral stationary phases in HPLC [5] and CEC [91]. The main problem associated with this grafting method is that, due to only single point attachment of the initiators, solution polymerisation and resulting gelation was difficult to avoid. Therefore, the method is poorly reproducible, and not suitable for up-scaling. This disadvantage has been solved performing the polymerisation under controlled polymerisation conditions by using RAFT agents. Homogeneous films were grafted exhibiting superior properties in LC (section 5.2).

Rückert *et al.* reported the use of an iniferter type initiator, covalently attached to silica particles or to Merrifield resins, for the grafting of thin MIP layers (Figure 3-13) [7]. The use of such initiators prevents polymerisation in solution, since one of the radicals formed upon decomposition is a very poor initiator. Taking advantage of the living properties of this system two consecutive polymer layers imprinted with two different templates or one imprinted and one non-imprinted layer in any order were grafted [8]. The use of iniferter initiators to produce molecularly imprinted composites and generate a new type of thin walled gel-like imprinted polymers will be described in section 5.3.

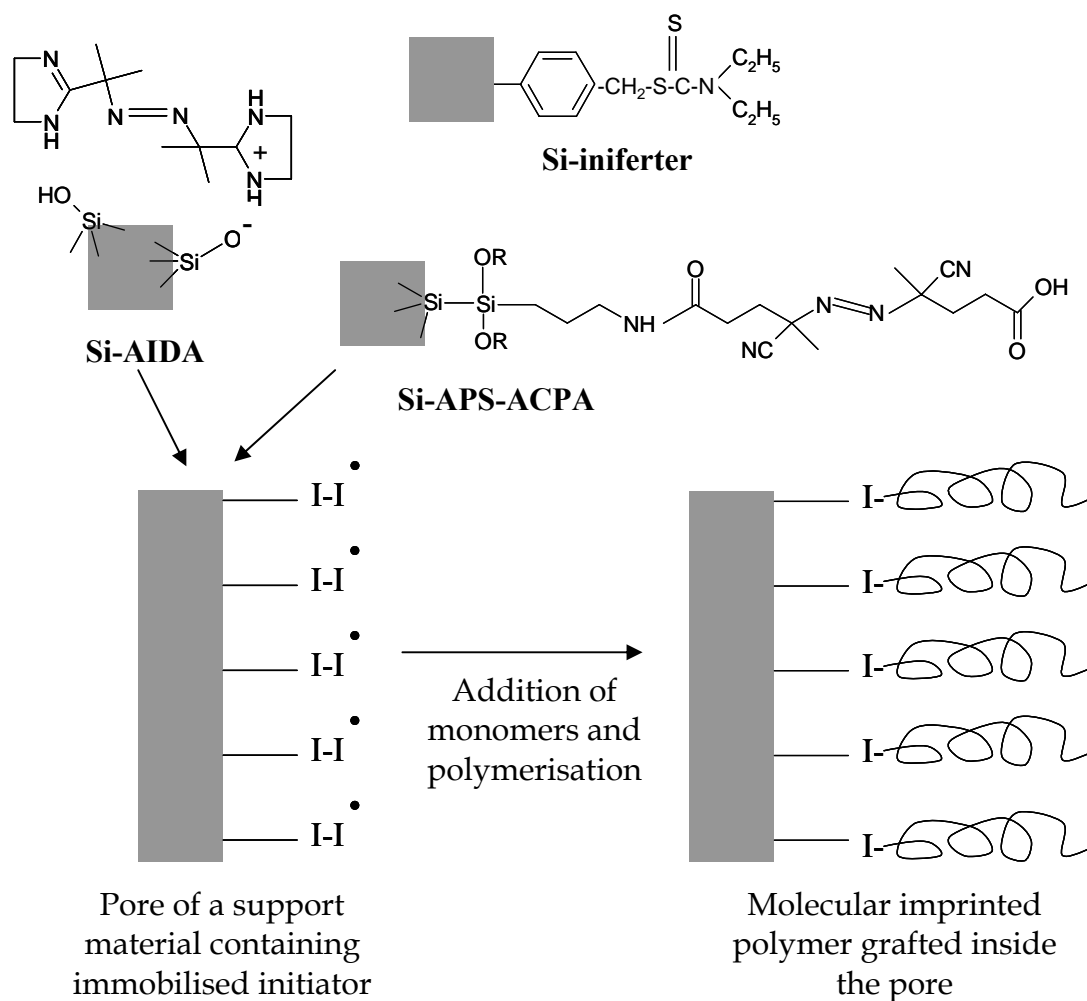


**Figure 3-13:** Schematic representation of the “grafting from” process for the formation of a thin MIP layer onto a porous support using various immobilised initiators.

Polymeric membranes with molecular imprint functionality have been also prepared using the “Grafting from” methodology. These materials are very attractive for efficient separations, including SPE.

The first association of Living Radical Polymerisation with MIPs grafting was reported by Kobayashi *et al.* [67]. A polymer layer containing binding sites for theophylline was grafted on a polyacrylonitrile membrane, which had incorporated a photosensitive dithiocarbamate group. It was found that the polymeric layer grafted on the membrane surface can recognize with high efficiency the template theophylline, while the analogue caffeine could not be effectively recognised by the imprinted sites.

The concept of heterogeneous photografting from membranes was explored by Ulbricht *et al.* [92,93]. Here, polymer membranes are coated with a photoinitiator, for example benzophenone, which after selective UV excitation *via* a hydrogen abstraction reaction creates radicals on the membrane polymer surface.

These radicals can be used as starters of a graft copolymerisation of functional monomers from the surface and thus creating a thin layer of covalently attached functional polymer covering the entire specific surface of the membrane.

Grafting methodologies allow the preparation of thin films of imprinted polymers on various support materials. Since the morphology of the resulting composite materials is determined by the underlying support, this gives fast and facile access to monodisperse, spherical imprinted beads with immediate application in separation science. Furthermore, MIPs grafting has the benefit of allowing the MIP films to be prepared using a variety of solvents and functional monomers, thus disregarding the effect of these parameters on polymer structure and morphology or the ability of these systems to yield stable suspensions. This allows the focus of the attention to be mainly on the search for conditions that result in high quality binding sites. The technique can be applied to different templates and exhibit distinct advantages over the conventional monolith procedure. Thus, the materials are obtained in a short time (1-4 h) and minimal work-up is required. Assuming that the monomer solution can be recycled, the consumption of template can be significantly reduced.

### 3.6 SURFACE OR INTERFACIAL IMPRINTING

Approaches to imprint larger target molecules show some resemblance to lithography, a technique used to prepare semi-conducting materials.

Figure 3-14 presents one possible procedure for lithography or replica molding. First, a master mold with a patterned relief structure on its surface is prepared. This is done by controlled exposure *via* a mask containing a designed pattern, *e.g.* silane-vapour that can thus be applied in a designed fashion leading to the desired relief and topology on the wafer.

Casts of patterned surfaces can be obtained by simply pouring a soft pre-polymer solution over the so-called master mold. In this way, an imprinted stamp can be



obtained which mirrors the pattern of the master mold. Thus, the imprinted stamp is a negative of the master mold and can later be used to create copies of the master by embossing the stamp into a new material.

A recent, comprehensive review discusses applications of lithography in a wide variety of fields ranging from microelectronics to biotechnology [94].

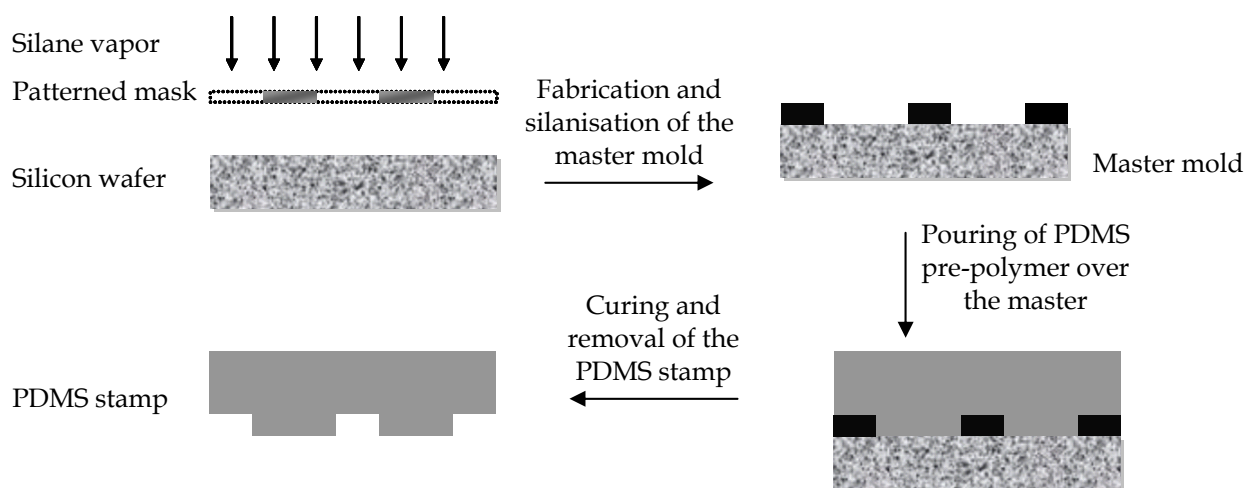


**Figure 3-14:** Schematic representation of the replica moulding process.

The imprinting of templates and structures which are placed on a solid flat surface closely resembles the process of lithography and the progression of new lithographic techniques may have an impact on molecular imprinting technology.

Related to lithography are recent advances in imprinting technology using templates fixed on solid supports. However, a significant difference from conventional lithographic processes is that both the topology of the template and the chemical characteristics at the molecular level can be reproduced. Much smaller structures can be imprinted and biological entities such as cells, proteins or other molecules can serve as patterns on a surface and can leave impressions in the polymer. Some examples of these systems are given below.

Cells are the largest structures that have been successfully imprinted to date. Compared to lithographic techniques, the size of cells ( $\mu\text{m}$ -range) is similar to the dimensions of the structures used in lithography. Work published on the theme of cell imprinting making use of a lithographic procedure was presented by the group of Vulfson [95,96]. By using the tendency of cells to assemble at the interface between

organic and aqueous layers, the reporters were able to carry out polymerisation at or around the surface of bacteria under physiological conditions of pH and temperature.

The bacteria-mediated lithographic process is schematically represented in Figure 3-15. A suspension of bacteria (green ovoids) is stirred with water-soluble monomers (shown in white) in a two-phase system (a): The organic solvent is depicted in light grey. Cell partition to the aqueous-organic interface as polyamide microcapsule walls (dark blue) form (b). Acrylic monomers in the organic phase are cross-linked photochemically to give beads with a solid core (dark grey) (c). The polymer beads are reacted with an isocyanate-functional perfluoropolyether (red); only those areas which are not covered by bacteria are blocked by the reagent (d). The cells are removed to expose imprint sites (e), and the functionality in the sites is developed by reaction with a fluorescent label or affinity ligand (yellow) as the final stage of the lithographic process (f).

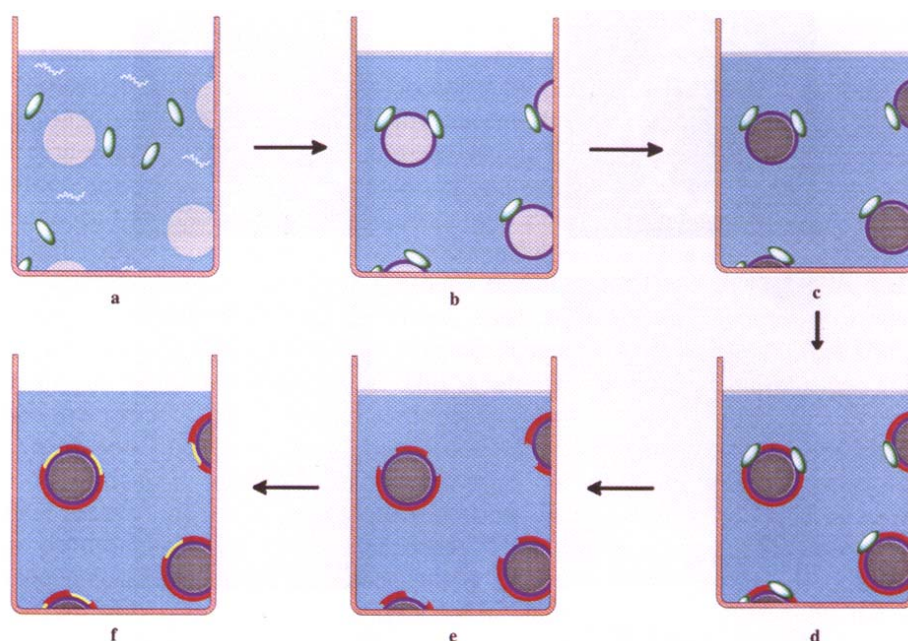


**Figure 3-15:** Schematic presentation of the bacteria-mediated lithographic process.

Later, Hayden and Dickert explored the utility of polyurethane (PU) as a polymeric matrix for imprinting processes by creating imprints from a cell in a pre-polymer of PU [97]. The polymer was imprinted with yeast cells and attached to the sensor

surface of a quartz crystal microbalance. The authors claim that both the geometrical fit and the functionalities in the formed pits contribute to the MIP surface specificity for a distinct micro organism.

The imprinting of proteins associated with solid supports was performed following the same basic steps as in lithography or in cell imprinting [98]. These smaller natural entities were adsorbed onto a surface and employed as a pattern for the formation of imprinted polymers, as exemplified by Figure 3-16.

Adsorption of the protein on a mica wafer was performed in buffer and a protective sugar layer was spin-cast to form a thin sugar over-layer. The sugar over-layer forms specific, non-covalent interactions with the underlying protein, mostly via hydrogen bond formation. A fluoropolymer layer was then deposited, a process in which the monomer is highly reactive and cross-links both with itself and with the organic sugar layer on the surface. The deposited plasma film was then mounted onto a glass slide support using an epoxy resin such that the layered composite was stabilised for the next step of removing the mica wafer and the protein.

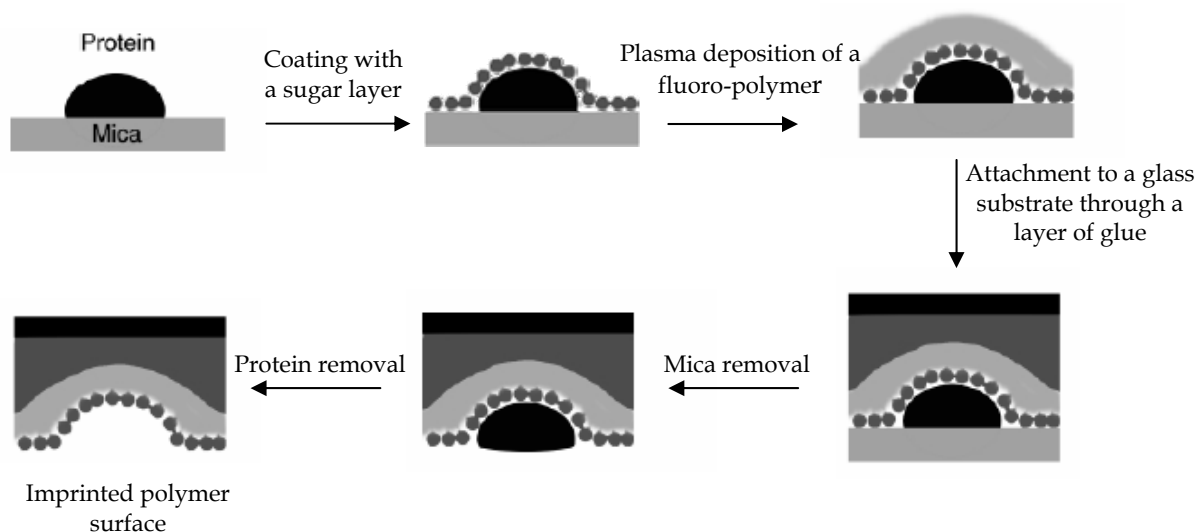


**Figure 3-16:** *Imprinting of proteins adsorbed to mica wafers.*

Tapping mode AFM images of the polymer surface confirmed that the cavities complemented the size and shape of the protein. Furthermore, competitive adsorption experiments were performed and it was observed that the imprinted surfaces selectively rebound the template protein in preference to other proteins with different sizes and shapes.

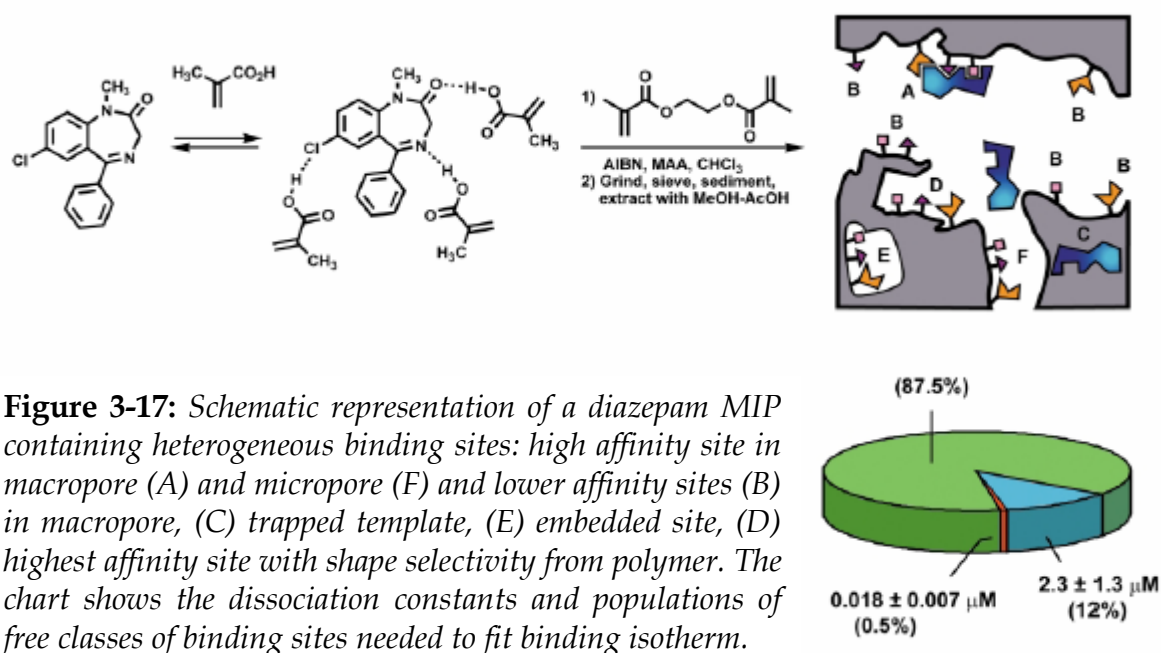
The bare surface of a solid crystal could be also imprinted using solid supports. Calcite crystals were incubated with the monomer to permit proper assembly on the crystal surface and subsequent polymerisation was initiated after addition of the cross-linker. After completion of the polymerisation, the crystals were removed with acidified solvents [99]. Re-crystallisation studies revealed that the imprinted polymer promoted the formation of calcite crystals rather than aragonite crystals, even though the conditions in the solution were more favourable for the formation of aragonite. Such MIPs can serve, for example, as biomimetic nucleation sites for the formation of biologically relevant minerals.

Immobilised molecules can be imprinted using a technique entitled “hierarchical imprinting”, “interfacial imprinting” or “surface imprinting”.

This technique is based on template synthesis. Synthesis of materials using nanostructured templates has emerged as a useful and versatile technique to generate ordered nanostructures [100]. Early work of Mallouk [101] started with the replication of zeolitic pore structures into phenol-formaldehyde type resins. Later on, Mallouk reported on production of ordered mesoporous polymer of tuneable pore size from colloidal silica templates. The interstitial pores obtained from agglomeration of silica nanoparticles were filled with DVB or EDMA or both, followed by dissolution of silica template. This led to a polycrystalline network of interconnected pores [102]. Hierarchical imprinting uses the same principle. A template molecule is immobilised at the pore walls of a silica mold, the pores are completely filled with a pre-polymerisation mixture followed by removal of the silica template to obtain an ordered porous polymeric replica with imprinted sites. (Figure 3-18).

In homogeneous imprinting systems, in which both template and monomers are free in solution, the templates are constantly moving and are in a dynamic equilibrium with the monomers. It is assumed that, this tumbling contributes to create a broad spectrum of binding strengths. This can lead to diverse groups of binding cavities, containing varying numbers of functional monomers and possessing varying binding strengths.

For example, the classic bulk imprinting of diazepam MIPs reported by Mosbach [103] illustrates the degree of heterogeneity possible, as well as its origin. The template being free in solution will lead to a polymer containing many sites formed without template or without the full complement of binding functionality (e.g. binding sites B in Figure 3-17). Some extraordinarily tight binding sites are present, but most sites have considerably lower affinity and presumably lower selectivity [104].



In order to reduce such heterogeneity, the template molecule may be fixed onto a support material and then brought into contact with interacting monomers. Because the template is immobilised at the pore walls of the support, the assembly between template and monomers, would then be ordered. Consequently, the binding sites will be confined to the surface presumably resulting in narrow site distributions (Figure 3-18). These features would bring imprinted polymers closer in characteristics to biological receptors, antibodies and enzymes, which share these features of a single binding constant, defined active arrangement and uniform site entrance accessibility.

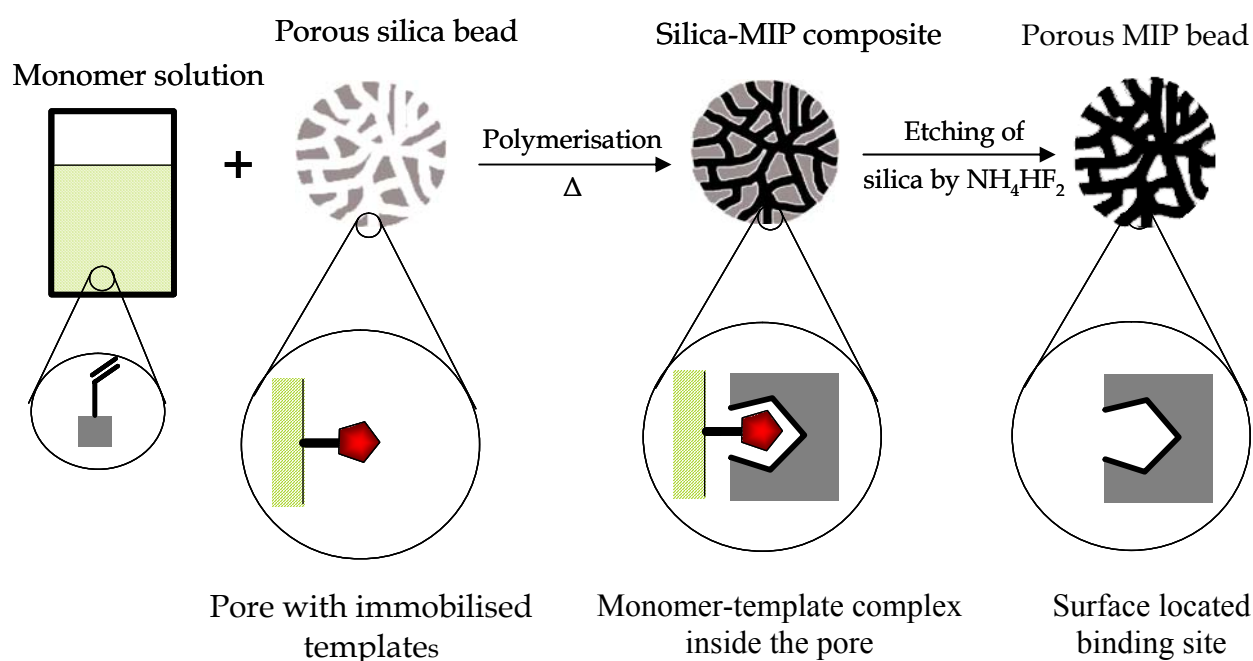


**Figure 3-18:** Schematic representation of the hierarchical imprinting process.

The first example of imprinting immobilised templates was reported by Yilmaz *et al.* [105]. The drug theophylline was used as a model target for immobilised species employed in molecular imprinting. The selectivity for the imprinted template was here checked *via* equilibrium batch rebinding assays. The imprinted polymer had a higher capacity towards theophylline than the corresponding control polymer.

Our group was the first to report the application of imprinting using immobilised templates for producing methacrylate-based mesoporous beads useful for chromatographic applications [1]. These beads featured surface-confined binding sites for adenine and triaminopyrimidine, which were also capable of recognising larger structures containing the template functionality. Later, we extended the principle to peptide imprinting [2,3].

These two independently developed approaches comprise the immobilisation of a template on the surface of a porous silica mold and polymerisation in the pores followed by dissolution of the silica matrix. This results in a “mirror image” pore system containing binding sites uniquely residing at the surface leading to hierarchically imprinted materials.

The term “hierarchical imprinting” was first associated with MIPs prepared by Dai *et al.* where metal ions were used as templates on the microporous level and micellar structures produced by self-assembly of surfactant molecules were used as templates on the mesoporous level. Removal of both metal ions and surfactant micelles resulted in imprints with different sizes within the silica matrix, each with a specific function [106,107].

Through this method uniformly sized and shaped particles with a narrow pore size distribution can be produced. Larger molecules containing the immobilised template substructure to be recognised by the surface exposed binding sites. A disadvantage of the method could be the limitation of monomers due to the incompatibility with the harsh difluoride treatment required for silica removal.

---

### 3.7 APPLICATIONS OF MOLECULARLY IMPRINTED POLYMERS

#### 3.7.1 Chiral Separations (MICSP)

Table 3-1 summarises the most important types of CSPs presently available for analytical or preparative HPLC applications together with their advantages and disadvantages.

The first application of MIPs was as stationary phases in affinity chromatography, in particular for the enantioseparation of racemic mixtures of chiral compounds, and much of the early work on MIPs was devoted to this aspect using model systems as described already in section 3.2.2. The imprinting process introduces enantioselectivity into polymers that are synthesised from (in most cases) non-chiral monomers.

The particularity of MIPs over conventional CSPs is that they are tailor-made for a specific target molecule, hence their selectivity is predetermined. For example, if a polymer is imprinted with the L-enantiomer of an aminoacid, an HPLC column packed with the MIP will retain the L-enantiomer more than the D-enantiomer, whereas a column containing an identical but non-imprinted polymer will not be able to separate the enantiomers.

The selectivities of MIPs are, in many cases, comparable to those of commercially available CSPs. Some examples of MIP-CSPs are given in Table 3-2.

The below mentioned results are impressive and suggest that good enantioseparations should be achievable. Unfortunately, reality is often rather different, as the separation efficiency, seen in the corresponding resolution factors and plate numbers are typically rather low (500-2000 plates  $m^{-1}$ ). This is due to severe peak broadening and tailing, especially of the more retained enantiomer, which in turn can be attributed to the heterogeneous population of binding sites, with respect to their affinities and accessibilities, as well as to a slow mass transfer.

In the past few years many efforts have been made to improve the efficiency of chiral separations using MIPs and to overcome the previous mentioned disadvantages.



**Table 3-1: Main types of CSPs.**

Type	Advantages	Disadvantages
<b>Pirkle <math>\pi</math>-donor/ <math>\pi</math>-acceptor CSPs</b> <i>e.g.:</i> Whelk-O ULMO Pirkle 1J Alpha-Burke Beta-Gem Phenylglycine Leucine Naphtylleucine	<ul style="list-style-type: none"> <li>Resolve a wide range variety of enantiomers in numerous compound groups</li> <li>Universal solvent compatibility</li> <li>Ability to invert elution order</li> <li>Good for preparative and analytical separations</li> <li>High density of binding sites (1-40 mg/g saturation capacity)</li> <li>Good chromatographic efficiency</li> </ul>	<ul style="list-style-type: none"> <li>Bound to silica therefore <math>2.5 &lt; \text{pH} &lt; 7.5</math></li> </ul>
<b>Modified Polysaccharides CSPs</b> <i>e.g.:</i> Cellulose Triacetate Cellulose Tribenzoate	<ul style="list-style-type: none"> <li>Resolve a wide range variety of enantiomers</li> <li>Reasonable good efficiency</li> <li>Reasonable good capacity</li> </ul>	<ul style="list-style-type: none"> <li>Poor stability/durability</li> <li>Poor solvent compatibility</li> <li>Can not invert elution</li> <li>Unpredictable structure-resolution properties</li> </ul>
<b>Cyclodextrin CSPs</b>	<ul style="list-style-type: none"> <li>High stability</li> <li>Compatible with a wide range of solvents</li> </ul>	<ul style="list-style-type: none"> <li>Limited to compounds which can enter cyclodextrin cavity</li> <li>Small changes in analyte structures causes unpredictable effects upon resolution</li> <li>Can not invert elution order</li> <li>Poor capacity</li> </ul>
<b>Poly(meth)acrylamides CSPs</b> <i>e.g. :</i> Poly [(S)-N-acryloylphenylalanine ethyl ester]	<ul style="list-style-type: none"> <li>High capacity</li> <li>Good efficiency</li> </ul>	<ul style="list-style-type: none"> <li>Limited applicability</li> <li>Poor solvent compatibility</li> <li>Can not invert elution order</li> </ul>
<b>Protein CSPs</b> <i>e.g.:</i> Bovine Serum Albumine (BSA) Cellobiohydrolase (CBH) $\alpha$ 1-acid glycoprotein (AGP)	<ul style="list-style-type: none"> <li>Broad generality in chiral recognition of diverse enantiomers</li> <li>Good efficiency</li> </ul>	<ul style="list-style-type: none"> <li>Low capacity-unsuitable for preparative applications</li> <li>Poor solvent compatibility with organic solvents</li> <li>Can not invert elution order</li> </ul>
<b>Antibodies CSPs</b>	<ul style="list-style-type: none"> <li>Tailor made</li> <li>Elution order known</li> <li>Separation under isocratic conditions</li> </ul>	<ul style="list-style-type: none"> <li>Poor solvent compatibility</li> <li>Poor stability</li> <li>Poor efficiency</li> <li>Low capacity</li> <li>Expensive</li> </ul>
<b>MIP-CSPs</b>	<ul style="list-style-type: none"> <li>Tailored made</li> <li>Elution order known</li> <li>Separation under isocratic conditions</li> <li>Robust</li> <li>Inexpensive</li> </ul>	<ul style="list-style-type: none"> <li>Poor solvent compatibility (with aqueous based mobile phases)</li> <li>Low capacity</li> <li>Poor efficiency</li> </ul>

Most of these efforts have been directed towards the design and optimisation of novel preparation methods for MIPs, mostly in a beaded form [108], membranes for separation science [66] or as thin layers grafted on flat surfaces for sensor devices [53,55]. Recently, Spivack *et al.* reported on a novel cross-linking monomer leading to enhanced enantioselectivity in MIPs [109].

**Table 3-2:** A selection of molecularly imprinted CSPs for HPLC.

Print molecule	Polymer <sup>a</sup>	$\alpha^b$	$R_s^c$	f/g <sup>d</sup>	Ref.
<b><u>Amino acids</u></b>					
H-L-Phe-OH	poly (CuVBIDA-co-EDMA)	1.45	n.d.	n.d.	[23]
H-L-Phe-NHPh	poly (MAA-co-EDMA)	13	n.d.	n.d.	[22]
H-D- <i>p</i> -NH <sub>2</sub> Phe-NHPh	poly (MAA-co-EDMA)	15	n.d.	n.d.	[22]
Ac-D-Trp-OMe	poly (MAA-co-EDMA)	3.92	2.20	1.00	[110]
Ac-L-Trp-OH	poly (AAM-co-EDMA)	3.24	2.02	n.d.	[111]
BOC-L-Trp-OH	poly (MAA-co-2VPy-co-EDMA)	4.35	1.90	1.00	[112]
FMOC-L-Phe-OH	poly (MAA-co-EDMA)	1.36	n.d.	n.d.	[113]
Z-L-Asp-OH	poly (4VPy-co-EDMA)	2.81	1.22	0.81	[114]
Z-L-Phe-OH	poly (MAA-co-TRIM)	2.29	3.14	1.00	[115]
Z-L-Tyr-OH	poly (MAA-co-PETRA)	2.86	5.47	1.00	[115]
<b><u>Peptides</u></b>					
H-L-Phe-Gly-NHPh	poly (MAA-co-EDMA)	5.1	n.d.	n.d.	[114]
BOC-L-Phe-Gly-OEt	poly (MAA-co-TRIM)	3.04	3.44	1.00	[23]
Z-L-Ala-L-Ala-OMe	poly (MAA-co-TRIM)	3.19	4.50	1.00	[23]
Ac-L-Phe-L-Trp-OMe	poly (MAA-co-EDMA)	17.8	n.d.	1.00	[114]
Z-L-Ala-Gly-L-Phe-OMe	poly (MAA-co-TRIM)	3.60	4.15	1.00	[23]
<b><u>Pharmaceuticals</u></b>					
(S)-Timolol	poly (MAA-co-EDMA)	2.9	2.0	n.d.	[116]
(S)-Naproxen	poly (4VPy-co-EDMA)	1.65	n.d.	n.d.	[117]
(S,R)-Ephedrine	poly (MAA-co-TRIM)	3.42	1.6	n.d.	[21]
(S,S)-Pseudoephedrine	poly(MAA-co-TRIM)	3.19	1.6	n.d.	[21]

<sup>a</sup>AAM = acrylamide; CuVBIDA = Cu(II)[N-(4-vinylbenzyl)iminodiacetate; 2VPy = 2-vinylpyridine; 4VPy = 4-vinylpyridine

<sup>b</sup> $\alpha = k_{\text{print molecule}} / k_{\text{optical antipode}}$ ;  $k = (t-t_0)/t_0$ ;  $t$ =retention time of the analyte ;  $t_0$ =retention time of the void marker

<sup>c</sup>The resolution factors ( $R_s$ ) were calculated according to G. Wulff *et al.*, *J. Liq. Chromatogr.* **1986**, 9, 385.

<sup>d</sup>The resolution factors ( $f/g$ ) were calculated according to V. R. Meyer, *Chromatographia*, **1987**, 24, 639

Such efforts are further presented in Chapter 5 of this thesis. Using the “grafting from” technique under CRP conditions, MIP composites with enhanced capacities and efficiencies have been prepared for use as CSPs.

CEC is also a promising chromatographic technique to be used in combination with MIPs, in particular for chiral separations. MIP-based CEC profits from the inherent separation power of this method when compared with MIP-based HPLC. MIP-based CEC show appreciable efficiencies ( $> 100,000$  plates  $m^{-1}$ ) and high separation factors. In one study, enantioseparation of the  $\beta$ -blockers Propranolol and Metoprolol was achieved with MIP-CEC. Here, the polymer was cast *in situ* in the capillary in the form of a macroporous monolith attached to the inner wall of the capillary. The racemate of Propranolol was resolved within 120 s and when non-racemic samples containing mainly the R-enantiomer were injected, very small amounts of S-enantiomer could be distinguished [118].

Other possibilities to use MIPs in combination with CEC or capillary electrophoresis are in the form of continuous polymer rods [119], particles included in a gel matrix [120] and small particles suspended in the carrier electrolyte [121].

### 3.7.2 Peptides and Proteins Recognition

Proteins are directly responsible for cellular structure and function, therefore analytical methods are required to monitor protein expression and modifications to understand cellular systems. This task is not trivial. Samples can be extremely complex, tissue homogenates may contain ten of thousands of components whose expression levels range over 6 orders of magnitude.

Proteins can be separated and purified taking advantages of their properties such as charge, size and solubility, which vary from one protein to the next. The source of a protein is generally tissue or microbial cells. The cell must be broken open and the protein must be released into a solution called a crude extract. Once the extract is ready, a variety of methods are available for separation of proteins.

Proteomics, namely the large-scale screening of proteins of a cell, organism, or biological fluid, was given the name in the mid 1990s but had actually originated

over 20 years ago when the separation of proteins from total cell extracts was accomplished.

An important set of methods is available for the separation of proteins, based on the migration of charged proteins in an electric field, process called gel electrophoresis. The advantage of this method is that proteins can be visualised as well as separated, allowing the researcher to estimate quickly the number of proteins in a mixture, or the degree of purity of a particular protein. In addition, gel electrophoresis allows determination of crucial properties of a protein such as its isoelectric point and approximate molecular weight.

Another important technique for the separation of peptides and proteins is capillary electrophoresis. This technique not only that provides an attractive alternative to conventional gel electrophoresis for protein analysis, but also meets the requirements for implementation in high-throughput analysis and automated instrumentation.

It provides fast, high efficient and automated separation and requires a minute amount of sample. A numbers of CE modes are available for separation of proteins and polypeptides. These modes include capillary zone electrophoresis (CZE), micellar electrokinetic capillary chromatography (MECC), capillary sieving electrophoresis (CSE), capillary isoelectric focusing (CIEF) and capillary electrochromatography (CEC).

Several methods for the separation of peptides and proteins using LC techniques are available.

Reversed phase chromatography of proteins and peptides is based on molecular weight and sample size, proteins being separated according to their sizes.

Ion-exchange chromatography of proteins and peptides is often a complementary technique to reversed phase chromatography. It is based on an entirely different separation mechanism and the selectivity is different. Here separation is based on net charges (pI). The advantage of ion exchange chromatography over reversed phase chromatography is that the mobile phases used are generally less denaturing toward sample protein than the solvents employed in the other case.

For chromatographic separations there is still a strong need for a tailored separation media *e.g.* for enhanced automated sample pre-treatment or for selective pre-concentration (“analyte fishing”) of biologically active macromolecules.

Affinity chromatography represents one alternative and it is based on the combination of the chromatographic process with bio-recognition mechanisms, involving the difference in binding affinity of the proteins. In this case, a ligand (antibody, enzyme, inhibitor) is covalently attached to the stationary phase in the column and a certain protein is bound to the ligand while the other proteins pass through. The protein is then released by conditions which either denature the protein, which then loses “grip” on ligand, or by competing the protein off with a ligand analogue. Extremely high selectivity for a specific protein can be obtained through interactions such as antigen-antibody reactions, enzyme-substrate/inhibitor binding and hormone-receptor binding. Unfortunately, these methods tend to be very expensive and involve labile systems. For example, in order to develop a specific antibody to a certain protein, the protein has to be first injected into an animal. After the antibody is produced and isolated, it needs to be immobilised (covalent or non-covalent) with its correct orientation onto the stationary phases (polysaccharides gels, silica).

Therefore, there is a strong need to develop inexpensive, robust and reusable replacements for these expensive and labile recognition agents. Design and synthesis of novel materials which are capable of recognising proteins and other biological assemblies, such as whole cells and viruses, have potential fundamental and practical applications. Specific applications of such materials would encompass down-stream bio-processing for the purification of biopharmaceuticals, drug delivery, diagnostics, sensors, separation of proteins (proteomics) *etc.*

In this direction, the technique of molecular imprinting appears to be attractive for the preparation of synthetic receptors able to recognise large biomolecular species such as oligopeptides and proteins. Compared with antibodies, MIPs are very robust and stable (pH, temperature), can offer predicted selectivity, do not imply tedious preparation protocols (no animals required, no purification, no hapten conjugation), there is no loose of activity due to bad immobilisation and are cheap to produce.

So far, most of the efforts in molecular imprinting have been directed in the preparation of synthetic receptors for small-organic molecules. The literature on the development of imprinted polymers for the recognition of proteins is rather poor. This is due to the fact that designing imprinted polymers for biopolymers is a difficult mission compared with small molecules. Some of the limitations include the relative complexities of protein and cell surfaces, which carry large numbers of competing binding sites. Furthermore, their sensitivity to temperature, pH, and the nature of the solvent, biocompatibility and large molecular sizes are some of the major factors which need consideration while designing molecular imprinting polymerisation processes for these substrates. This implies the necessity to develop very innovative chemistries to prepare imprinted polymers as receptors to selectively recognise and bind biological macromolecules and assemblies.

In spite of the above limitations, efforts have been made in recent years to prepare imprinted polymers for the recognition of proteins. Such efforts are presented in section 4.2 of this thesis.

The first example in the direction of protein imprinting was reported by Mosbach *et al.* [122]. They were able to prepare a thin layer of polymer coating on the surface of porous silica beads, which was selective for the glycoprotein transferrin.

Minoura *et al.* performed a similar kind of investigation to prepare protein imprinted polymers [123]. They used methacrylate modified silica particles as the carrier matrix on which imprinted sites were created. Using acrylic acid as the functional monomer and *N,N*-1,2-diethylene bisacrylamide as the cross-linker, template polymerisation was carried out in the presence of glucose oxidase. Preferential affinity of the polymer for its template after extraction, suggest the formation of substrate-selective binding sites in the polymer matrix.

Rachkov and Minoura reported on a more promising approach to recognise peptides and proteins [124] using the “epitope approach”. In this report, a short peptide that represents only a small exposed fragment of a larger protein was used as a template. In this way, the resulting imprinting polymer was able to recognise both, the template and the larger protein, in this case oxytocin.

Combining this principle with the hierarchical imprinting described in section 3.6 I have prepared imprinting polymers for Nociceptin [2]. Using this method, spherical particles containing surface located binding sites were prepared.

A column-switching system between a column packed with a MIP against (S)-ibuprofen prepared using multistep swelling polymerisation and a conventional C18-silica column was applied successfully to the assay of ibuprofen in rat plasma after oral administration [125].

Proteins have been successfully imprinted on flat surfaces. A remarkable example for surface immobilised protein imprinting on mica was described in the section 3.6 of this thesis [84].

A novel, innovative approach to prepare molecularly imprinted matrices for the selective recognition and binding of proteins was proposed by Arnold *et al.* [126].

They used metal coordination interactions to induce complementary binding between the matrix bound metal chelates, with the corresponding ligands present on the surface of proteins. Surface exposed metal coordinating residues such as histidines, exhibit high affinity for different metal ions (*e.g.* Cu(II), Zn(II), Hg(II), *etc.*). This affinity between metal chelates and proteins has been the basis for protein purification using immobilised metal affinity chromatography [127].

Using the affinity of N-terminal histidine residues for Ni(II) and a polymerisable acrylamide functionalised nitrilotriacetic ligand, Shea *et al.* provided a “handle” in the polymer to bind peptides containing N-terminal histidine residues in water [128]. Preparation of the imprinted polymers for the recognition of proteins and other biomacromolecules and assemblies may open the door to the preparation of polymer based biosensors and other diagnostics, which may present the currently dominant enzymes and antibodies with their first serious challengers as biomedical analytical tools. Unlike small molecules imprinting, implementation of template polymerisation techniques to recognise large biopolymers possessing complex surface epitopes, does present significant challenges. Surface imprinting appears a promising way around this problem. Ratner [84] was the first one to prepare template imprinted nanostructured surfaces for protein recognition on a mica surface. Our approach to use the surface imprinted sites in hierarchically imprinted polymers in order to

recognise larger polypeptides containing the imprinting epitope is a progress in the direction of protein recognition [2,3]. It might be used for example to differentiate between the C-terminal  $\beta$ -amyloid peptides providing a tool for early diagnosis of Alzheimer's disease (section 4.3).

### 3.7.3 Solid Phase Extractions

The separation technique that has been most intensively studied in the last few years with respect to the possible use of imprinted materials is solid phase extraction (SPE) [129,130,131,132,133,134]. The need for efficient methods for sample pre-concentration and clean-up in medical, food and environmental analyses is constantly increasing. The advantages of SPE over liquid-liquid extraction (LLE) are that it is faster and more reproducible, cleaner extracts are obtained, emulsion formation is not an issue, solvent consumption is reduced and smaller sample sizes are required. Moreover, SPE can be easily incorporated into automated analytical procedures. In this context, it is not surprising that much of the current research in the molecular imprinting field is concentrated on SPE, as here the advantages of MIPs, especially their low price and their stability in different environments, come into play, while some of the limitations are less important than with other separation techniques. MIPs are not only more selective than common sample pre-treatment methods using C18 or ion exchange materials, but are at the same time more stable than immunoextraction matrices [135]. Since MIPs are compatible with organic solvents, MIP-SPE can be applied directly after a solvent pre-extraction step. Further, the low resolution factors associated with MIPs in chromatography are not an issue, as SPE works in the adsorption-desorption mode. Thus, SPE seems to be one of the most promising applications for MIPs thus far and is also the application that is closest to commercialisation. This is also reflected in the comparatively large number of reports dealing with real samples. MIP-SPE has been used to extract target analytes from blood plasma and serum [129, 130], urine [131], bile [129], liver extract [132], environmental waters and sediment [133], plant tissue [134], *etc.*



### 3.7.4 Biosensors

In sensors, a chemical or physical signal is generated upon the binding of the analyte to a biological recognition element such as an antibody, a receptor or an enzyme. A transducer then translates this signal into a quantifiable output signal. The same general principle applies if a MIP is used as the recognition element instead of a biomolecule. In the simplest case, a change in one or more physicochemical parameters of the system upon analyte binding (such as mass accumulation) is used for detection [136]. The principle is widely applicable and more or less independent of the nature of the analyte. In order to increase sensitivity and the signal-to-noise ratio, reporter groups may be incorporated into the polymer that generate or enhance the sensor response. If the analyte possesses a specific property (such as fluorescence or electrochemical activity) this can also be used for the purpose of detection [137].

In terms of sensitivity, MIP-based biomimetic sensors are, with some honourable exceptions, still somewhat inferior to biosensors. This situation will certainly improve through further optimisation of the MIPs and the transducers. In particular, what one hopes to achieve is the development of MIPs that contain a more homogeneous binding site population with a higher affinity for the target analyte which can also be used in aqueous based solvents. On the other hand, the outstanding stability of MIPs, their low price, as well as the fact that they can be tailor-made for analytes for which a biological receptor cannot be found, are among properties that make them especially suitable for sensor applications.

### 3.7.5 Catalysis

One of the most intriguing challenges for the use of MIPs is their use as enzyme mimics. In parallel to the exciting work done with catalytic antibodies, attempts have been made to achieve catalytic activity exerted by the imprinted sites. Several different strategies have been pursued in this line. The most common approach has been the use of transition state analogues (TSAs) as templates in the imprinting protocol [138,139], thus establishing the reaction transition and enhancing the rate of

product formation. Special emphasis has been put on the hydrolysis of active esters, using a phosphonate TSA as print molecule. Other strategies to acquire catalytically active polymers are the use of coenzyme analogues for providing a useful pre-determined catalytic mechanism and the use of coordination compounds for mediation of catalytic reactions.

The hierarchical imprinting was used recently for the preparation of an esterolytic imprinted polymer with catalytic sites on the surface [140]. A template was prepared by immobilising a transition state analogue of an esterolytic reaction within porous silica particles.

Recently, Mosbach *et al.* reported on a MIP prepared using known bioactive templates that possesses binding sites mimicking those of the corresponding biological targets. They demonstrated that these artificial sites can be used to control synthetic reactions, so that the desired bioactive products can be enriched [141].

### 3.8 CONCLUSIONS

The current, almost exponential, growth in MIP literature published each year is an indicator of the growing interest in this technology. In addition, molecular imprinting is now maturing from a phenomenon of interest to academics to a technique of potential practical interest to the industrial chemist. This process will continue to involve fundamental research and some areas with high priority may be listed: (i) to obtain a better knowledge base for optimisation of both MIP synthesis and use, (ii) mechanistic studies of imprint formation and imprint recognition will remain an important area, (iii) extension of the types of chemistry available, especially for non-covalent imprinting, must be addressed, (iv) it is necessary to establish strategies for selection of the best recipe of monomers, cross-linkers and polymerisation conditions for a particular combination of analyte and application. This includes consideration of which is the best format of the MIP, be it a thin film, monodisperse beads or a macroporous monolith, with the optimal pore morphology. The end user of MIPs is interested in factors such as the elimination of template leakage and batch-to-batch reproducibility.

Finally, development of MIP systems useful for aqueous-based samples, such as serum, plasma, urine and ground water, continue to be a key focus.

I will show that through the studies I have performed during my doctoral research, I contributed to the further progress and development of molecular imprinting technology.

---

## 4 RESULTS AND DISCUSSION (I): HIERARCHICAL IMPRINTING

Hierarchy is a defining feature of self-assembly that has long been appreciated in biology and is now emerging as a unique opportunity to make exciting new materials in chemistry. Hierarchy involves the organisation of basic building entities in a series of parallel, self-assembly, co-assembly or direct assembly processes, whereby the process begins with the simplest construction units and assembles them into more complicated objects. Assembly continues until the highest level of structural complexity in the hierarchy is attained. As the mesoscale is, by its very nature, directly at the top of the molecular scale, it is uniquely placed in the hierarchy of materials structure and properties design considerations.

Ordered mesoporous polymers of tuneable pore size have been obtained previously by replication of colloidal silica templates [102]. The concept of “hierarchical imprinting” has a similar principle, described in section 3.6. It comprises immobilisation of the target molecule on the surface of a mesoporous inorganic material, followed by complete pore filling with the appropriate monomer mixture, polymerisation and removal of the inorganic support. The inorganic template can be chosen according to the required pore size in the final material. Thus, the silica beads used in our approach were 10  $\mu\text{m}$ , with tailored morphological properties, synthesised from poly(ethoxy)siloxane (PES) according to a procedure reported by du Fresne *et al.* [142]. This material possesses a specific surface area ( $a_s$ ) of 350  $\text{m}^2/\text{g}$ , a specific pore volume ( $V_p$ ) of 1  $\text{ml}/\text{g}$  and a mean pore diameter ( $p_d$ ) of 10  $\text{nm}$ . It should be noted that the majority of commercial HPLC packing materials have similar characteristics.

In this chapter I will describe the newly developed double template approach to produce methacrylate-based polymer replicas. The principle was first optimised for the imprinting of immobilised nucleotide bases. It was then extended to the recognition of large peptides through the so-called “epitope approach”.

---

## 4.1 IMPRINTING USING IMMOBILISED NUCLEOTIDES

There have been many examples of abiotic synthetic receptors for each of the nucleotide bases reported in literature [143,144,145,146]. These artificial, small molecule receptors exhibit binding constants with these bases in the range 11,000-120,000 M<sup>-1</sup> in chloroform. Apart from gaining a more detailed understanding of the interactions and mechanism in DNA-DNA or protein-DNA recognition, applications have been envisioned in the fields of biosensors, drug therapy, separation science and genetic engineering. Binding sites for nucleotide bases in macromolecular structures have also been successfully created using antibodies [147], synthetic macromolecules [148] and monolayers [149].

The interest in DNA-specific binding molecules prompted many research groups to apply the molecular imprinting technique to this important area.

Nucleotide bases have been imprinted mostly in the traditional format [150,151,152]. The most commonly used template has been 9-ethyladenine (9EA). Shea *et al.* showed that those MIPs can exhibit similar association constants as the previously described receptors [152]. Takeuchi *et al.* reported on a MIP-9EA receptor having a porphyrin-based recognition centre [153]. MIPs targeting 9EA have also been formed *in situ* inside a capillary for the electrochromatographic separation of nucleotide bases [154].

9EA has been widely used as a model compound to understand and to elucidate the binding phenomena in MIPs. After the introduction of non-covalent imprinting, many studies relating to the monomer-template solution complexes and determination of their association constants, adsorption isotherms to the polymers, kinetics and effect of the mobile phase have been performed using this model compound. Most of the studies have been carried out using MAA as functional monomer and EDMA as cross-linker. First proton NMR studies of interactions between butyric acid and 9EA in chloroform gave an association constant  $K_a = 160 \text{ M}^{-1}$  for 1:1 complexes [155]. This example of binding between adenine and carboxylic acid was a good indicator of its potential to pre-organize MAA in a pre-polymerisation complex for molecular imprinting. The interaction of MAA with 9EA prior to and during copolymerisation with EDMA was designed to produce an array

of carboxylic acids placed in complementary arrangement to 9EA. Formation of 9EA imprinted polymers follows the procedure shown in Figure 4.1.

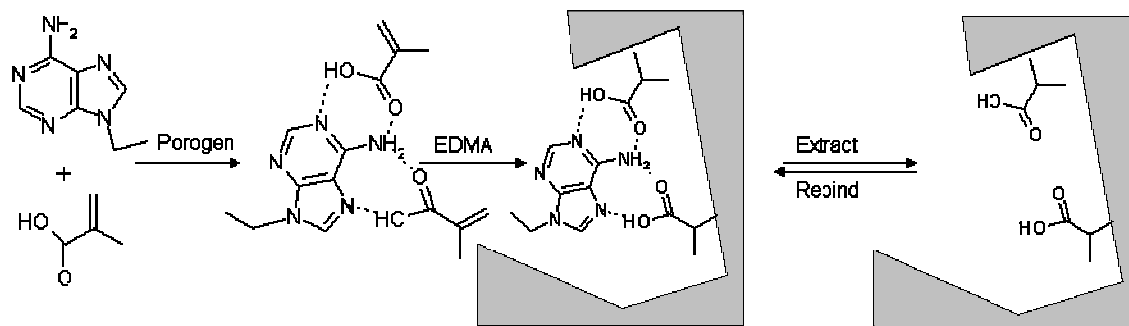


**Figure 4-1:** Template strategy for creating selective sites to 9-ethyladenine within network polymers.

Due to the detailed knowledge concerning the properties of these MIPs we chose 9EA as a model system and applied it in hierarchical imprinting. For this, we immobilised 9EA to the pore walls of our silica gel. A pyrimidine base, 2,6-diaminopyrimidine (DAP), was also employed in the hierarchical imprinting process and the results obtained with the two templates were compared.

#### 4.1.1 Template Immobilisation

The covalent immobilisation of the templates for the hierarchical imprinting of nucleotides comprised several distinct steps.

First, the silica surface was activated, by rehydroxylation, due to the loss of silanol groups in the calcination process subsequent to the silica synthesis. This was accomplished through treatment with hydrochloric acid, which converted the siloxane bonds into silanol groups according to Figure 4-2. The silanol group concentration of calcined and rehydroxylated silica was calculated from thermogravimetric analysis. The silanol group concentration after rehydroxylation reached the fully hydroxylated state ( $\alpha_{\text{OH}} \sim 8 \mu\text{mol}/\text{m}^2$ ).

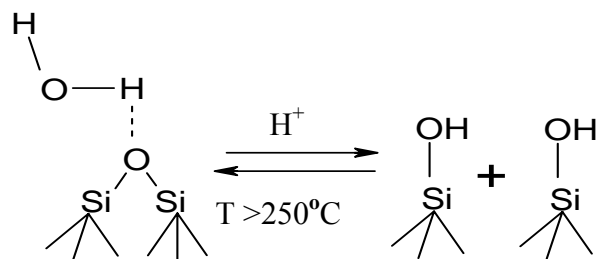


**Figure 4-2:** Rehydroxylation of siloxane groups.

After rehydroxylation, the silica surface was modified using three different types of silanes, namely glycidoxy propyltrimethoxysilane (GPS), chloropropyl trimethoxysilane (CPS) and aminopropyltrimethoxysilane (APS).

The reactions were performed according to well established literature procedures [71,72]. The silanol groups on the silica surface were converted into three different functional groups (glycidoxy, chloro and amino) through the condensation reactions shown in Figure 4-3.

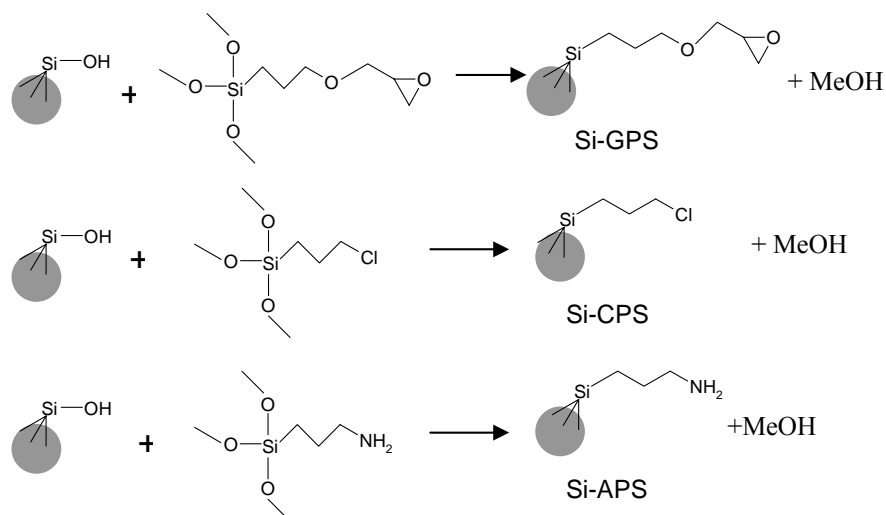


**Figure 4-3:** Functionalisation of the silica surface using GPS, CPS and APS.

The surface densities of the introduced ligands depended strongly on the reaction conditions and on reagent stoichiometry. These densities were determined from elemental analysis data (Table 4-1). Due to sterical hindrance between the introduced chains, not all the surface hydroxyl groups were available for reaction with the silane molecule. The unreacted silanol groups were end-capped in a subsequent step in order to prevent them from interfering in later reactions.

Prior to template immobilisation, all remaining free silanol groups were end-capped with hexamethyldisilazane (HMDS), well-known as a methylating and deactivating reagent. HMDS reacts readily with hydrophilic silanols, yielding very stable methylsilyl groups according to the reaction shown in Figure 4-4. Through this procedure, one ensured that all the template precursors reacted only with the functional groups at the surface. In addition, after the polymerisation process in the silica pores, the silanol group could not interfere in the chromatographic separation and recognition processes.

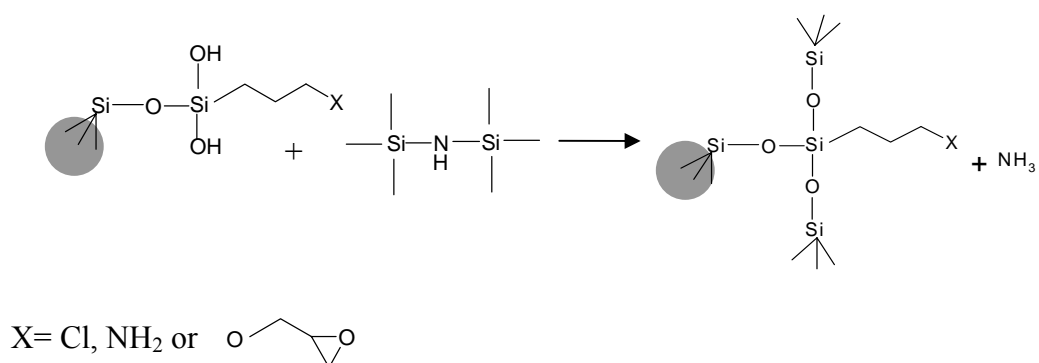
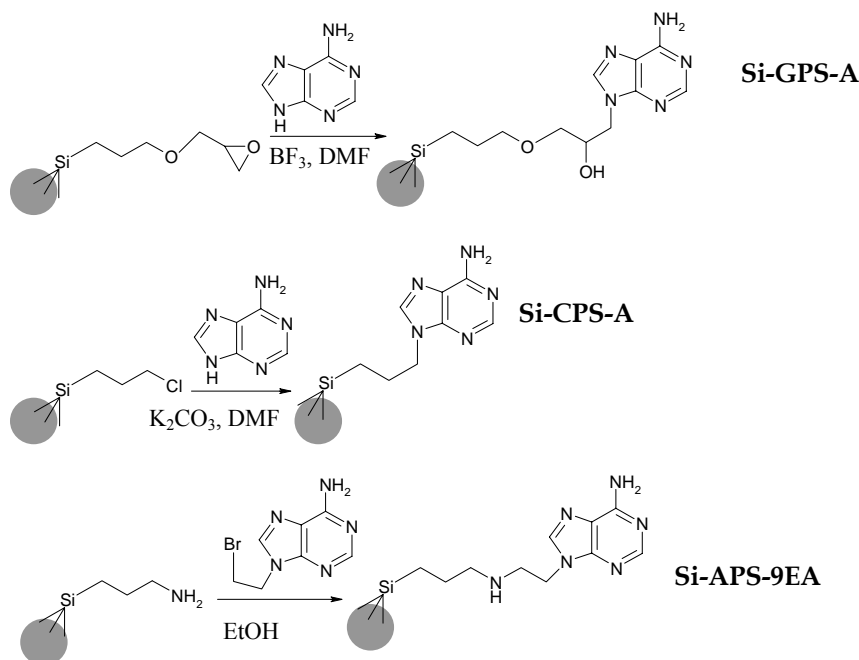


**Figure 4-4:** End-capping of the functionalised silica surface.

Two different templates were immobilised on the silica surface, one belonging to the purine bases (adenine) and the other a pyrimidine base for the recognition of the 2-aminopyrimidine containing molecules. Adenine was connected to the silica surface using all three types of functionalised silica gels whereas only the amino-modified silica (Si-APS) was employed in the pyrimidine immobilisation. The reactions leading to the covalent immobilisation of the templates are shown in Figure 4-5.



- Immobilising adenine:



- Immobilising pyrimidine:

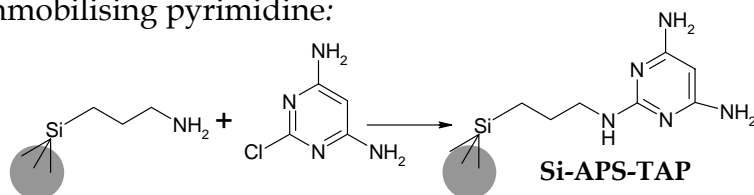


**Figure 4-5:** Template surface immobilisation of adenine and pyrimidine.

All employed reactions were simple standard coupling reactions used in organic chemistry, all following an  $\text{S}_{\text{N}}2$  mechanism. In the GPS case the reaction takes place first by opening the epoxy ring in the presence of boron trifluoride, followed by coupling to the adenine at N9, which is more reactive than the exocyclic primary amine because of the increased acidity of its proton. For the CPS modified silica, the acidic H9 proton of adenine is abstracted using potassium carbonate and the anion formed reacts with the functionalised silica. The APS case is the most straightforward where, *via* elimination of HBr, adenine is coupled to the amino-modified silica *via*  $\text{S}_{\text{N}}2$  substitution.

#### 4.1.2 Characterisation of the Resulting Intermediates

The products resulting from the previously described reactions were characterised using elemental microanalysis and FTIR spectroscopy.

From elemental microanalysis data, more precisely from the change in carbon and nitrogen contents in each step, we could estimate the amount of immobilised ligand on the silica surface. The data are presented in Table 4-1. The area density ( $D_s$ ) of immobilised ligand was calculated based on the change in carbon ( $\Delta C$ ) or nitrogen ( $\Delta N$ ) content versus the preceding step, e.g. for  $\Delta N$ :

$$D_s = \frac{m_N}{M_N \times S} \quad \text{where:} \quad m_N = \frac{\Delta N\%}{100 - \frac{\Delta N\% \times M_w}{M_N}}$$

$M_w$ =molecular weight of the coupled ligand,

$M_N$ =weight of nitrogen per mole of coupled ligand,

$S$ = surface area of the silica support (350m<sup>2</sup>/g).

**Table 4-1:** Evaluation of ligand densities of the GPS-, CPS- and APS-adenine and pyrimidine modified silica particles using elemental analysis data.

Material	%C	$\Delta C$	%N	$\Delta N$	$D_s$ ( $\mu\text{mol}/\text{m}^2$ )	
					$\Delta C$	$\Delta N$
<i>Si-GPS</i>	2.40	2.40	-	-	1.03	
<i>Si-GPS end-capped</i>	7.05	4.65	-	-	2.05	-
<i>Si-GPS-A</i>	8.2	1.15	0.70	0.70	0.50	0.30
<i>Si-CPS</i>	1.50	1.50	-	-	0.77	-
<i>Si-CPS end-capped</i>	6.67	5.17	-	-	5.70	-
<i>Si-CPS-A</i>	7.40	0.73	0.75	0.75	0.35	0.31
<i>Si-APS</i>	2.73	2.73	0.43	0.43	1.73	0.94
<i>Si-APS end-capped</i>	4.26	1.53	0.44	0.43	0.62	-
<i>Si-APS-9EA</i>	5.43	1.17	1.44	1.00	0.44	0.42
<i>Si-APS-TAP</i>	5.08	0.82	0.89	0.45	0.66	0.23

---

The initial concentration of the silanol groups on the silica surface was determined by TGA to be  $\sim 8 \mu\text{mol}/\text{m}^2$ . Therefore we considered this value as corresponding to a maximum 100% coverage of the silica surface. From Table 4-1, one can observe that the final densities of the functional groups after modifying the silica with the corresponding silanes ranged between  $0.77 \mu\text{mol}/\text{m}^2$  for GPS and  $1.73 \mu\text{mol}/\text{m}^2$  for APS. This corresponded to a conversion of 10 to 20% of the silanol groups initially present on the rehydroxylated silica surface. The maximum yield for the silane coupling is 50% according to the literature [82], meaning that two silanol groups are replaced by one organosilane molecule. The reproducibility of these modifications was very good, showing similar results for similarly employed reaction conditions. The highest density was obtained in the case of modification with aminosilane. This observation is in agreement with Revillon [82] and the explanation for this may lie in the fact that there are stronger hydrogen bonds between the amino and the silanol groups from the silica surface probably leading to the non-covalent adsorption of the silane to the silica surface.

The end-capping process was the most efficient for the case of Si-CPS ( $5.7 \mu\text{mol}/\text{m}^2$  HMDS groups). In the other cases not all the remaining silanol groups could be end-capped.

The final densities of immobilised adenine lay in the range of  $0.3\text{-}0.4 \mu\text{mol}/\text{m}^2$  for all the employed silanes. This corresponded to  $\sim 4\%$  conversion of the initial reactive silanol groups and implied that the template molecules were separated by an average distance of  $\sim 4 \text{ nm}$ , which should be sufficient for a complete separation of the templated sites. The final area densities were calculated considering both the percentage of nitrogen and carbon and showed similar values. The yield of conversion of the silane functional groups into adenine immobilised templates was  $\sim 50\%$  for all three cases, the lowest being for the Si-APS case. A possible explanation for the low density for APS might be found again in the fact that some of the amino groups were associated with the free silanol groups *via* hydrogen bonds and were thus not free to react with the adenine derivative, 9-(2-bromoethyl) adenine. For the immobilised pyrimidine the area density was in the same range of  $\sim 0.2 \mu\text{mol}/\text{m}^2$ .

The second means of characterising the immobilised nucleotides was infrared spectroscopy.

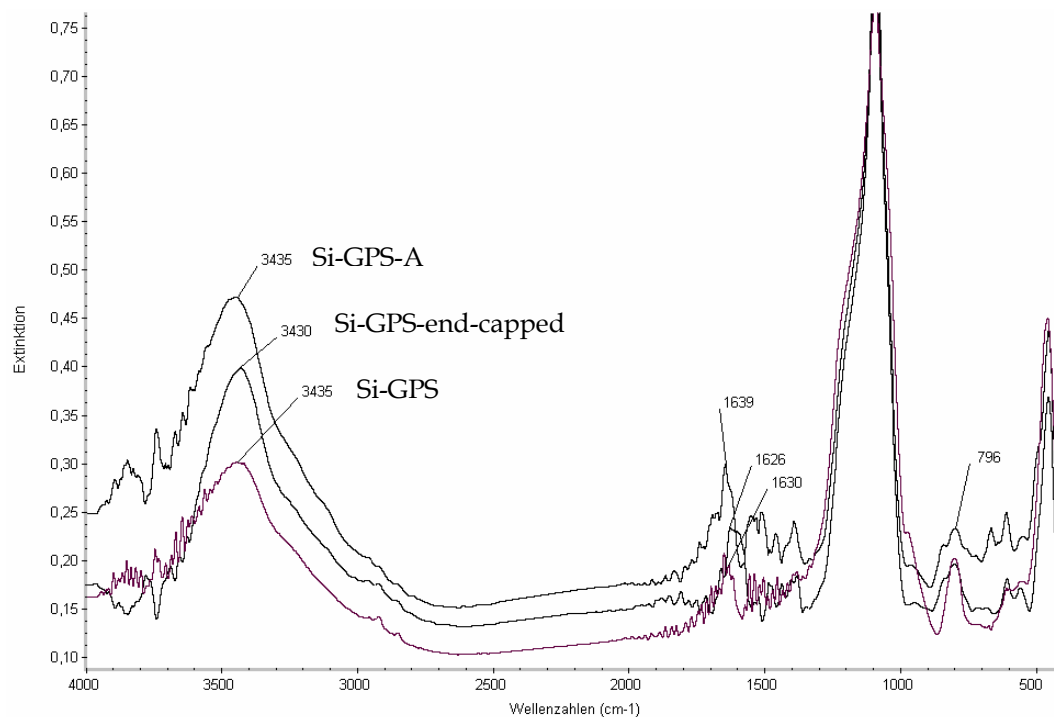


**Figure 4-6:** FT-IR spectra of the Si-GPS-A system.

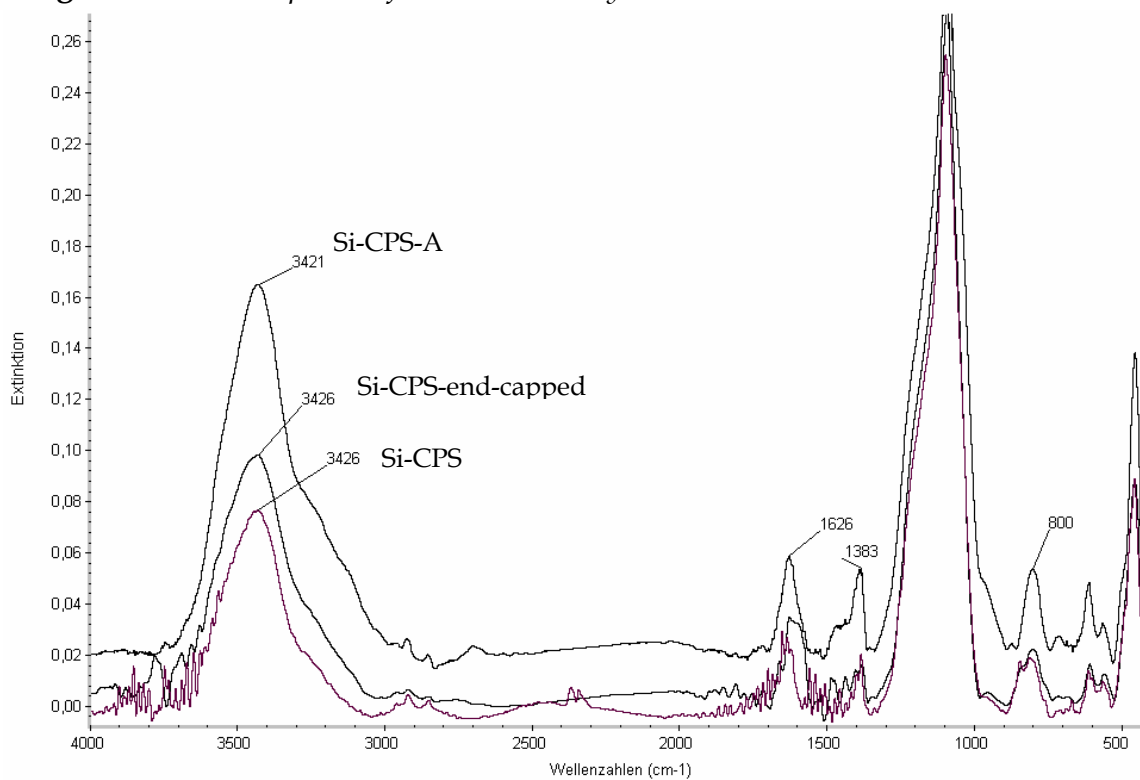


**Figure 4-7:** FT-IR spectra of the Si-CPS-A system.

---

In the first spectra corresponding to the GPS-modified silica (Figure 4-6), the concentration of the epoxy groups was too small (0.36  $\mu\text{mol}$  epoxy groups/g silica) for the band corresponding to the epoxy stretch at  $\sim 1270\text{ cm}^{-1}$  to be clearly seen.

The Si-C stretching frequencies are reported in the range of  $900\text{-}500\text{ cm}^{-1}$ . The group Si-CH<sub>2</sub>-R has a weak band near  $1410\text{ cm}^{-1}$  (CH<sub>2</sub> deformation), and a medium-intensity IR band at  $1250\text{-}1200\text{ cm}^{-1}$  (CH<sub>2</sub> wag). In all spectra, we observed bands corresponding to the Si-O-Si stretching of siloxanes, characterised by the very strong IR complex in the region  $1000\text{-}1100\text{ cm}^{-1}$ . The Si-O-H group had a strong IR band involving Si-O stretch at  $920\text{-}830\text{ cm}^{-1}$ . The OH band is like in alcohols between  $3700\text{-}3200\text{ cm}^{-1}$  for free or hydrogen-bonded OH. Very weak signals at around  $2900\text{ cm}^{-1}$  could be attributed to the CH<sub>2</sub> stretch from the alkyl chain present in the silanes. The appearance of the IR spectra did not change significantly for the end-capped modified silica. The more intense absorption band at  $3450\text{ cm}^{-1}$  might be due to the partial adsorption of the resulting ammonia to the silica surface.

Once adenine was covalently linked to the silica, new absorption bands appeared:  $1640\text{ cm}^{-1}$  corresponding to the NH<sub>2</sub> scissors bending from the amino-substituted pyrimidine ring and the semicircle stretch band from  $\sim 1480\text{ cm}^{-1}$  region. The presence of the exocyclic amino group could be clearly seen at  $3450\text{ cm}^{-1}$ .

The Si-CPS-A case (Figure 4-7) was similar with the above. The frequency of C-Cl is affected by the mass of the halogen atom and normally shows strong bands in the lower region of the infrared spectra due to the C-Cl stretching vibrations ( $760\text{-}550\text{ cm}^{-1}$ ). The weaker intensity in the peak at  $3430\text{ cm}^{-1}$  (NH<sub>2</sub> stretch) as compared to the previous case might be due to the lower concentration of adenine on the silica surface as compared to Si-GPS-A (See Table 4-1).

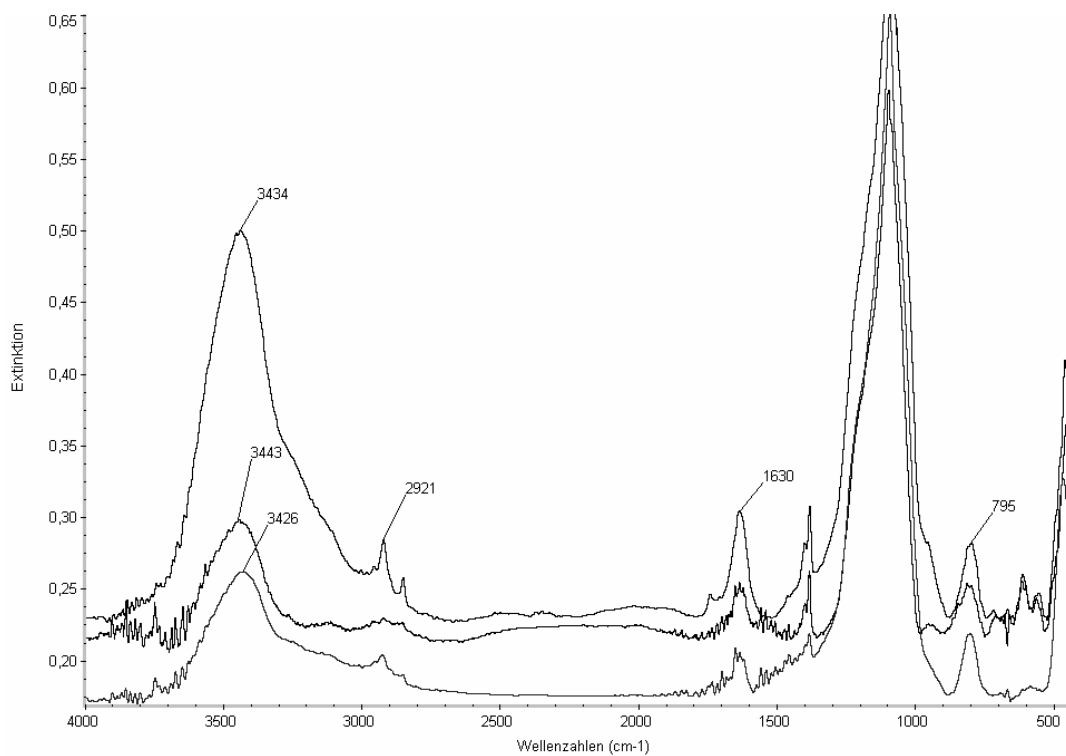


**Figure 4-8:** FT-IR for the Si-9EA system.

For the Si-APS spectra (Figure 4-8), an increase of the peak intensity at 3420 cm<sup>-1</sup>, due to the NH vibration (stretching) of the amino groups present on the surface, was observed. This made the intensity of the peak for Si-APS-9EA stronger than in the other cases, although the concentration of adenine on the silica surface was similar with the Si-GPS-A case.

### 4.1.3 Preparation of Molecularly Imprinted Polymers

The pore system of the modified silica was completely filled with a mixture of EDMA (83%) MAA (17%) and dissolved initiator by repeated vacuum-nitrogen purge cycles, as shown schematically in Figure 4-9-A. Polymerisation was then performed by heating the particles at 60°C for 24h. The silica was subsequently dissolved by treatment of the composite particles with an aqueous solution of (NH<sub>4</sub>)HF<sub>2</sub> over a period of two days. In all cases a 50% mass loss was monitored, implying that the difluoride treatment successfully removed the majority of the silica template.

The concentration of monomers was chosen according to the procedure used for 9EA model system to prepare MIP monoliths [152], using MAA as the functional monomer. A control non-imprinted polymer (NIP) was prepared under the same conditions by polymerisation in the pores of silica without any immobilised template.

In most cases when preparing a MIP, a solvent is used as a porogen. The template molecule is dissolved in a mixture containing the functional monomer, the cross-linked monomer and the porogenic solvent. Polymerisation is then performed in this concentrated solution, most commonly *via* free radical polymerisation. The term porogen should be used only in those cases where a permanently porous polymeric structure is obtained. In the hierarchical imprinting method I have developed, no porogen is required. The template is covalently immobilised to the silica pore walls and interacts with the functional monomer in the pores *via* hydrogen bonds (Figure 4-9-B). The pore structure of the obtained polymers is formed only by dissolution of the silica backbone. All the imprinted binding sites should therefore be located at the surface of the pores and, thus, greatly facilitate diffusion of the analyte to the binding sites. Through this procedure, templates that are not soluble in the pre-polymerisation mixture can be immobilised and then brought in contact with the monomers. This fact has been already demonstrated by our group for the imprinting of the N-terminal sequence of the  $\beta$ -amyloid peptides H-Asp-Ala-Glu-OH, a molecule not soluble in most commonly used porogens [156]. Furthermore, once the

inorganic mold is removed, the immobilised template is automatically removed as well. Thus, there is no need for an extraction step to eliminate the template as in the classical procedure.

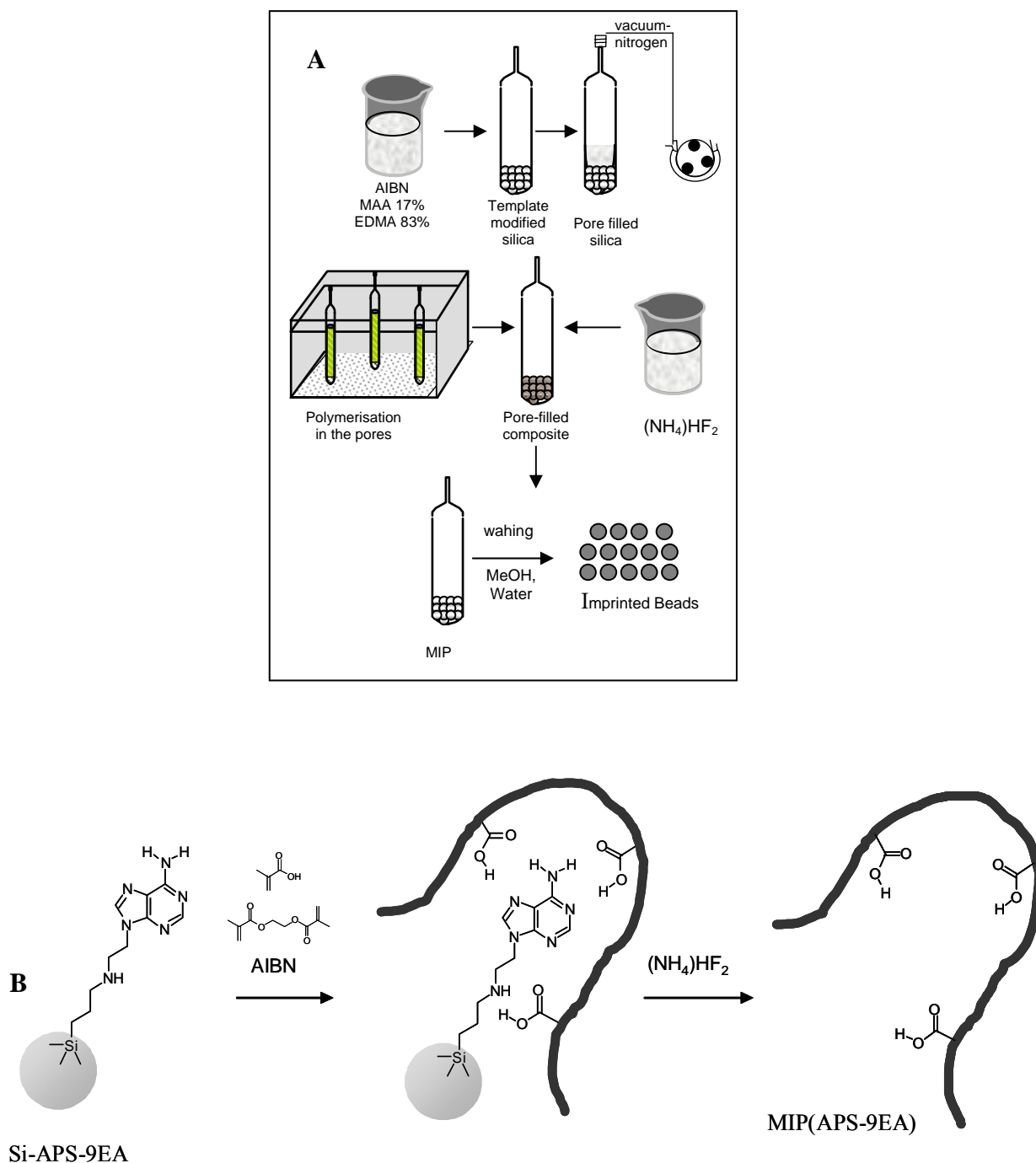


**Figure 4-9:** (A) Schematic illustration of the steps involved in hierarchical imprinting (B) Schematic illustration of the functional monomer-template interaction inside the silica pore and generation of a binding site.



#### 4.1.4 Characterisation of the Imprinted Polymers

The extent of silica removal from the composites was investigated through elemental microanalysis, FTIR spectroscopy and Energy Dispersive X-ray analysis (EDX). Particle morphology and binding site accessibility was examined using Scanning Electron Microscopy (SEM), and fluorescence microscopy respectively. Nitrogen sorption and swelling experiments were used to extract information about the porosity of the obtained polymers.

The elemental composition of the polymers indicated that almost all the inorganic matrix had been removed at the end of the hierarchical imprinting process (Table 4-2). The percentage of carbon in the obtained polymers was comparable to the theoretical value of a polymer prepared with the same monomer stoichiometry (% C = 59.95; % H = 7.23).

**Table 4-2:** Elemental composition of the polymer composites and resulting polymers.

Imprinted Composite	% C	%N	Imprinted polymer	% C	%N
Comp(GPS-A)	29.56	0.43	MIP(GPS-A)	56.85	0.23
Comp(GPS)	29.70	0.22	NIP(GPS)	59.27	0.15
Comp(CPS-A)	28.09	0.44	MIP(CPS-A)	57.36	0.22
Comp(CPS)	28.48	0.22	NIP(CPS)	57.73	0.14
Comp(APS-9EA)	28.98	0.45	MIP(APS-9EA)	57.25	0.21
Comp(APS-TAP)	29.88	0.39	MIP(APS-TAP)	57.46	0.19
Comp(APS)	28.96	0.29	NIP(APS)	54.25	0.22

In Figure 4-10 it can be observed that, after polymerisation, the composite spectrum (red) still contained the Si-O-Si stretch at  $\sim 1100\text{ cm}^{-1}$  and all the other absorption bands. Simultaneously, we found the absorption bands from C=O stretch at  $1700\text{ cm}^{-1}$  and the OH stretch from  $3500\text{ cm}^{-1}$  due to the carboxylic functional groups of the polymer composite. The -CH<sub>2</sub>- stretch from the cross-linked polymer was present around  $2900\text{ cm}^{-1}$ .

The spectrum above (black) belongs to the corresponding imprinted polymer and showed no longer any of the characteristic silica stretch bands, proving the successful removal of the silica matrix. The C-O stretch was now visible at around  $1100\text{ cm}^{-1}$ . The intensity of the C=O stretch from  $1700\text{ cm}^{-1}$  doubled in comparison to the composite material. The intensity of the peaks due to the OH stretch from  $3500\text{ cm}^{-1}$  and of CH<sub>2</sub>- stretch also increased after removal of the silica template.

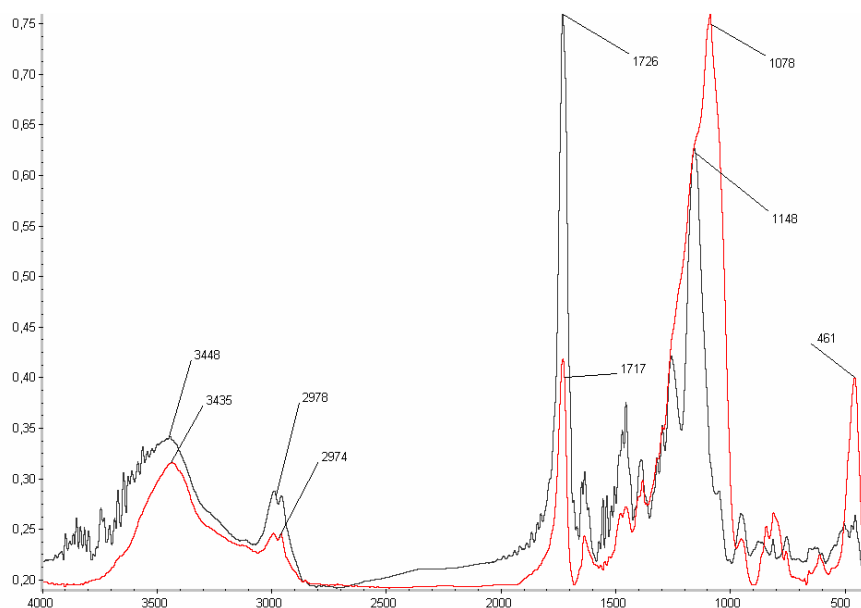


**Figure 4-10:** FT-IR spectra of a hierarchically imprinted polymer and the corresponding composite.

As can be seen from the EDX spectra in Figure 4-11, the silica was successfully removed from the matrix when preparing the hierarchical polymers. This is exemplified for MIP (APS-TAP): The peak corresponding to the silicon atom was no longer present in the spectra of the hierarchical polymer (a), when compared with the EDX spectra of the corresponding composite (b). The principle of EDX analysis is described in section 6.5.5.

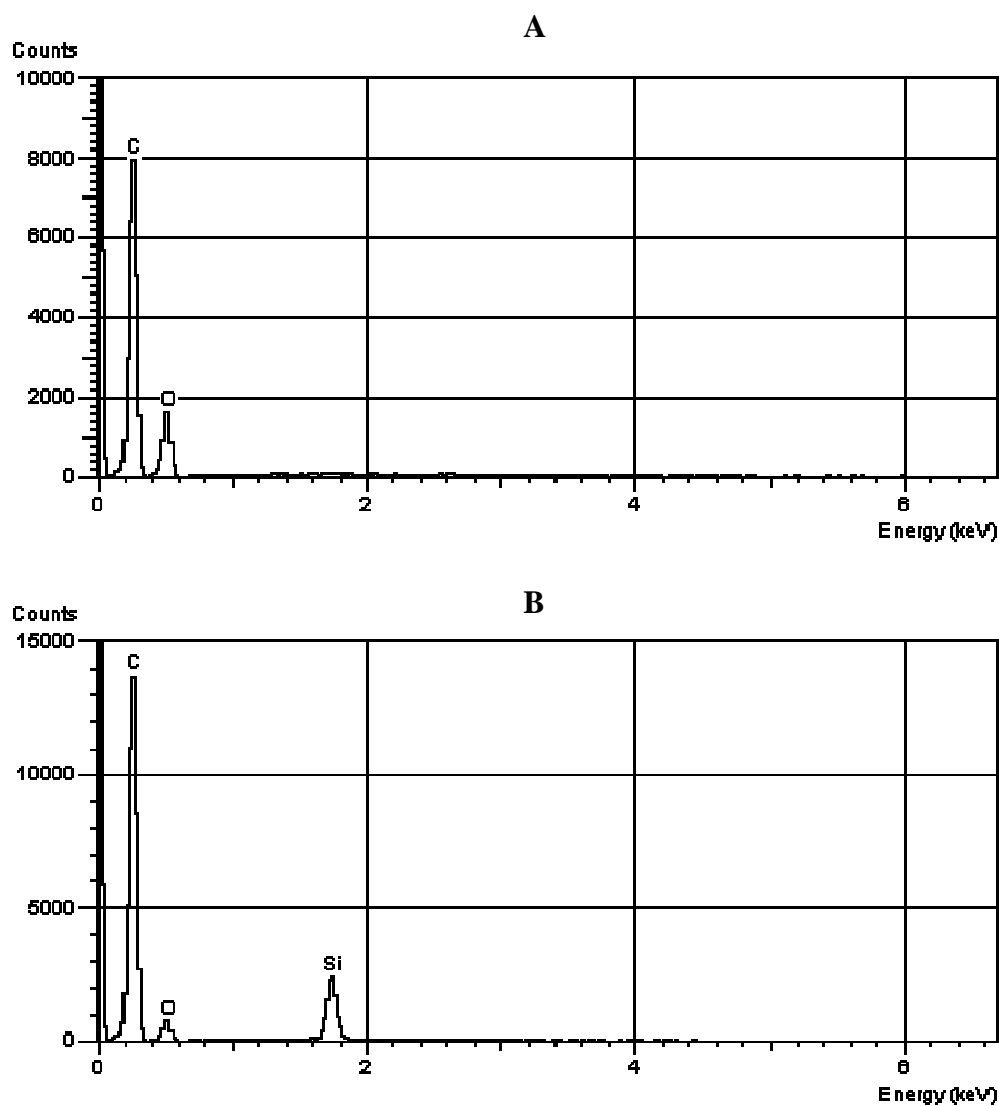


**Figure 4-11:** EDX-spectra of (A) MIP (APS-TAP) and (B) Comp (APS-TAP).

The SEM micrographs in Figure 4-12 showed spherical particles with an average diameter close to that of the original silica particles. No agglomeration took place and the rather harsh treatment for removing the silica template did not damage the polymer particles in any way.

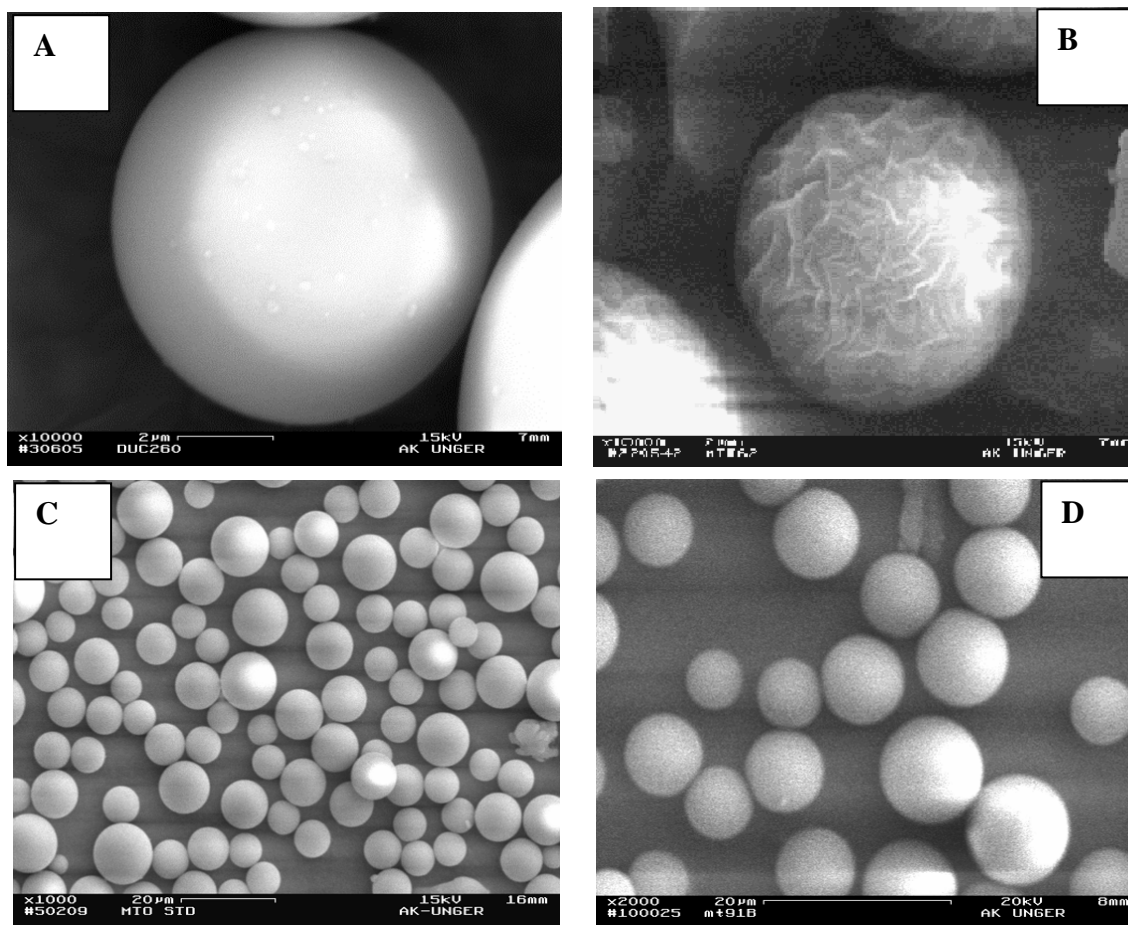


**Figure 4-12:** Scanning electron micrographs of (A),(C) starting silica, (B) P(APS-TAP), (D) P(APS-9EA). The pictures were made using a magnification of 10,000 (A,B); 1,000(C) and 2,000(D).

In order to investigate the accessibility of the carboxylic acid functional groups on the surface, fluorescence labelling by reaction with 3-aminoquinoline according to the reaction from Figure 4-13 was performed. The labelled particles were studied with respect to the distribution of the fluorescence intensity between and within the particles. Only weak intensity was observed after labelling particles still containing the silica template (Figure 4-13-A) which blocked access to the carboxylic acid groups. However, particles no longer containing the silica template exhibited a strong fluorescence, indicative of a high accessibility of the surface carboxylic acid groups (Figure 4-13-B).

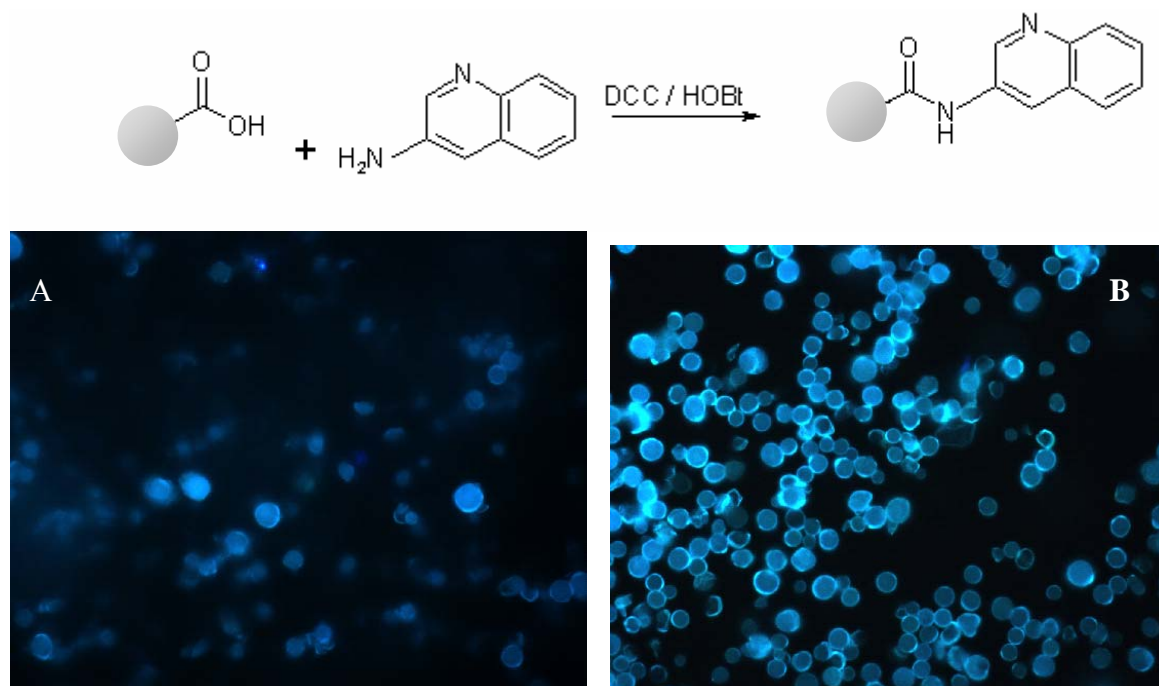


**Figure 4-13:** Fluorescence micrographs of (A) composite particles C(APS-9EA) and (B) imprinted polymer particles P(APS-9EA) after the removal of the silica cores. The pictures were taken using  $\times 40$  magnification.

**Table 4-3 :** Pore structural parameters of individual imprinted polymers determined from nitrogen sorption measurements.

Imprinted polymer	$a_s$ ( $\text{m}^2/\text{g}$ )	$V_p$ ( $\text{mL}/\text{g}$ )	$d_p$ ( $\text{nm}$ )
MIP(GPS-A)	248.7	0.51	8.25
NIP(GPS)	272.6	0.64	9.48
MIP(CPS-A)	263.2	0.56	8.53
NIP(CPS)	298.8	0.72	9.62
MIP(APS-9EA)	290.7	0.61	8.42
MIP(APS-TAP)	292.7	0.59	7.85
NIP(APS)	267.2	0.57	8.89

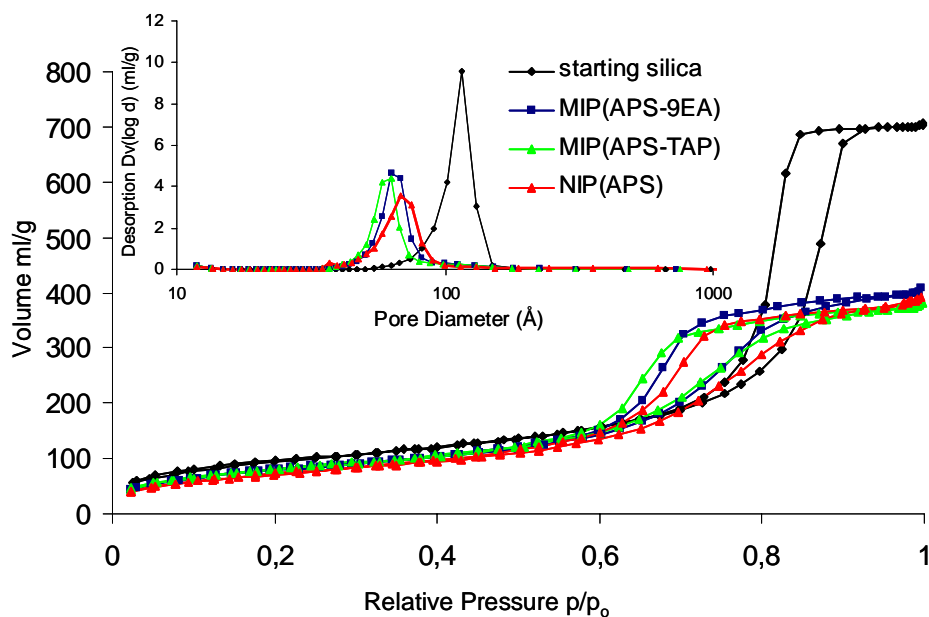
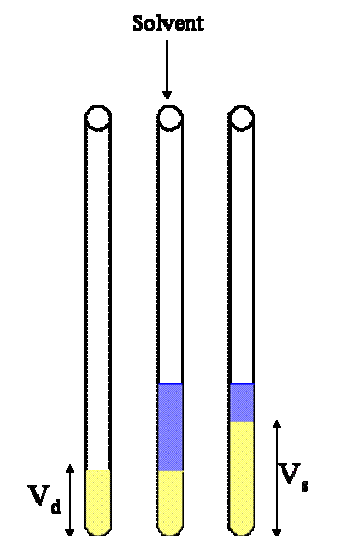


**Figure 4-14** : Nitrogen sorption isotherms and pore size distributions of the obtained MIPs.

Nitrogen sorption experiments indicated that the obtained polymers possessed surface areas and mesoporosities in the same range as the precursor silica particles. The type of the isotherms is typical for mesoporous materials (type IV) containing a hysteresis loop (Figure 4-14). Particularly striking was the narrow pore size distribution observed around 8-9 nm, which stands in stark contrast to the broad distribution observed for the conventional MIPs. In the traditional imprinting procedure, one can often observe that the surface areas and porosity are very different between the MIP and the NIP. This is usually explained by the broadness of the pore size distribution. As a result, the materials can not be exactly compared when assessed in HPLC or SPE. The pore volume decreased in all cases from 1 ml/g (original silica) to half value (Table 4-3). This may be due to the resulting mirror image structure of the starting silica. The pores of the polymers arose from the backbone of the silica. The pore size decreased as well, from 11 nm (silica) to ~ 8 nm in the polymer. This value may correspond to the original thickness of the silica pore wall (the skeleton thickness).

In order to better elucidate the difference between the dry state and the solvent-swollen state of the polymers, swelling tests were performed in acetonitrile which was further used as mobile phase in the chromatographic evaluation. The swelling is

dependent on the level of cross-linking, the higher the cross-linking the lower the swelling. Swelling was measured by allowing a known volume of dry polymer with a known particle size and weight to equilibrate in the solvent, whereafter the volume of the swollen particles was measured. The volume swelling ratio was calculated as:



$$V_s \text{ ratio} = \frac{\text{bed volume swollen part } (V_s)}{\text{bed volume dry part } (V_d)}$$

$$V_s \text{ ratio ("hierarchical MIP")} = 1.05 \text{ ml/ml}$$

$$V_s \text{ ratio ("classical MIP")} = 1.2 - 2 \text{ ml/ml}$$

All polymers obtained had low swelling factors ( $<1.15 \text{ mL/mL}$ ) in acetonitrile implying that the materials had a relatively homogeneous distribution of cross-links. This was also in contrast with the bulk imprinted counterpart.

### 4.1.5 Evaluation of the Imprinted Polymers as Stationary Phases in HPLC

The particles were slurry packed in columns and assessed in the liquid chromatographic mode for their ability to retain the templates and other analytes shown in Figure 4-15.

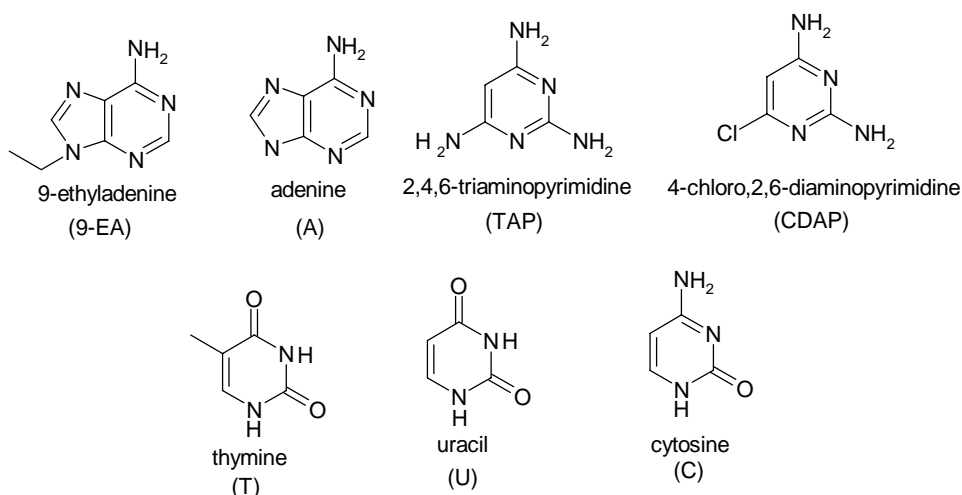


**Figure 4-15:** DNA/RNA bases and derivatives used as analytes for the polymer evaluations.

#### 4.1.5.1 Evaluation of Adenine Imprinted Polymer Prepared using Si-GPS

Using an organic based mobile phase system (acetonitrile/acetic acid: 99/1 (v/v)) the imprinted polymer exhibited a clear selectivity for the template and its analogues (Table 4-4). Thus, adenine (A) and 9EA were two times longer retained on the polymer imprinted with immobilised adenine than on the non-imprinted polymer. Cytosine was also strongly retained on the polymer imprinted with adenine. This was presumably due to its 2-aminopyrimidine substructure (Figure 4-15). The retention of TAP on the MIP may be similarly explained. CDAP was retained less than TAP, illustrating the importance of the exocyclic amino group to the recognition mechanism. By substituting one amino function with a chloro group, one interaction



was lost; therefore CDAP was equally retained on the MIP and NIP. T and U do not possess the 2-aminopyrimidine substructure and therefore exhibited little affinity. The behaviour of the bases containing the 2-aminopyrimidine substructure on the MIP is in agreement with the observations of Spivak and Shea [150] using a traditional 9EA imprinted polymer. The retention factors and the imprinted factors of the nucleotide bases were calculated according to the following formulas and are listed in Table 4-4.

$$k_{MIP} = \frac{R_{tMIP} - R_{t0}}{R_{t0}}$$

where:

$k_{MIP}$  = the retention factor on the MIP

$t_{MIP}$  = the retention time on the MIP

and

$R_{t0}$  = the retention time of the void marker (generally acetone)

IF = the imprinting factor

$$IF = k_{MIP}/k_{NIP}$$

Analyte (1mM)	$R_{tMIP(GPS-A)}$ (min)	$R_{tNIP(GPS)}$ (min)	$k_{MIP(GPS-A)}$	$k_{NIP(GPS)}$	IF
9EA	1.66	1.03	4.3	2.0	2.1
A	3.39	2.26	12.1	5.7	2.1
TAP	2.22	2.26	6.3	5.6	1.1
CDAP	0.74	0.79	1.4	1.3	1.0
T	0.42	0.45	0.3	0.3	1.0
U	0.34	0.45	0.3	0.3	0.2
C	2.64	1.09	7.5	1.9	3.8

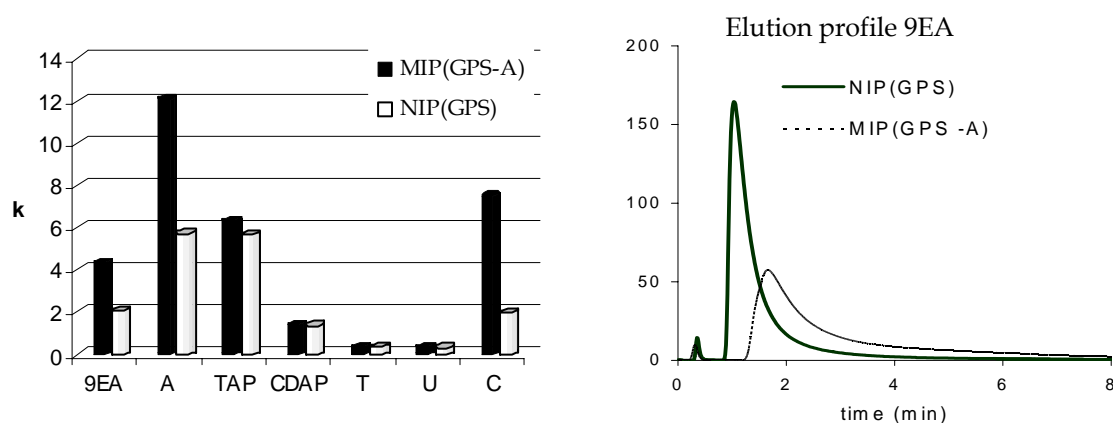


**Table 4-4 and Figure 4-16:** Retention of the nucleotide bases (10 $\mu$ l of 1mM solutions) on columns (50 x 5 mm. i.d) packed with MIP (GPS-A) and NIP (GPS).

## 4.1.5.2 Evaluation of Adenine Imprinted Polymer prepared using Si-CPS

These polymers were evaluated in the same organic mobile phase (acetonitrile/acetic acid: 99/1 (v/v)) and retention properties are listed in Table 4-5. The system exhibited a different behaviour to the GPS system. A and 9EA showed the highest imprinting factors. TAP and CDAP were stronger retained than in the GPS case.

Analyte (1mM)	R <sub>t</sub> MIP(CPS-A) (min)	R <sub>t</sub> NIP(CPS) (min)	k <sub>MIP(CPS-A)</sub>	k <sub>NIP(CPS)</sub>	IF
9EA	1.76	0.56	4.40	0.7	6.2
A	4.19	0.78	11.8	1.4	8.4
TAP	10.68	4.36	30.5	10.9	2.7
CDAP	2.14	1.00	5.50	2.0	2.6
T	1.22	0.65	2.70	0.9	2.7
U	1.74	0.95	4.30	1.9	2.2
C	3.98	2.7	10.7	6.4	4.7

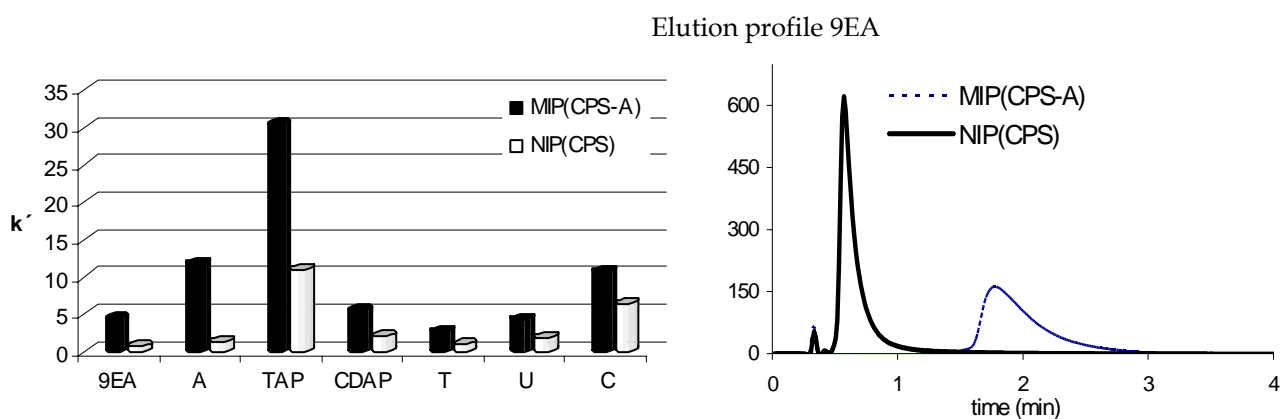


**Table 4-5 and Figure 4-17:** Retention of the nucleotide bases (10 $\mu$ l of 1mM solutions) on columns (50 x 5 mm i.d.) packed with MIP (CPS-A) and NIP (CPS) using as mobile phase acetonitrile/acetic acid: 99/1 (v/v) and a flow rate of 1.0 mL/min.

Once more, the bases with the 2-aminopyrimidine substructure were more strongly retained than those without (T and U). The imprinting factors were generally higher than in the case of the GPS. A possible explanation for the higher values of retention and imprinting factors, in comparison to the GPS system may be found in the length of the alkyl chain of the silane. For the GPS system the distance between the adenine and the anchor point at the silica walls is longer than in the CPS system, where only three carbon atoms separate the template from the silica surface. Furthermore, in the GPS system the presence of a hydroxyl group which can interact with a neighbouring silanol group, may lead to a poor orientation of the ligand for the creation of a high fidelity templated site.

#### 4.1.5.3 Evaluation of 9-ethyladenine and Triaminopyrimidine Imprinted Polymers Prepared using APS

Using the same organic-based mobile phase system, the imprinted polymers exhibited a clear selectivity for the template and its analogues (Figure 4-18, Table 4-6 and Table 4-7). Thus, 9-ethyladenine (9EA) was retained *ca.* 3.5 times more on the MIP (APS-9EA) than on the non-imprinted polymer. Likewise, triaminopyrimidine (TAP) was retained *ca.* 3 times more on the MIP (APS-TAP) than on the NIP (APS). Both the imprinted polymers selectively retained purines and pyrimidines containing exocyclic amino groups common to the template structures, whereas the non-related bases uracil and thymine were weakly retained with lower selectivity. More direct evidence for the fidelity of the binding sites was given by the cross-retentivity observed for 9EA and TAP (Figure 4-18). Thus, both templates were more retained on their complementary polymers than on the analogue imprinted polymer. Free adenine, however, was more retained on P-TAP than on P-9EA. This can be explained considering the anticipated orientation of the carboxylic acid groups in the binding sites. The predominant interactions between the immobilised templates and carboxylic acids in aprotic media, based on previously characterised homogeneous systems [157] were indicated in Figure 4-9-B. It can be seen that the carboxylic acid group interacting with the pyrimidine ring nitrogen *ortho* to the site of coupling of

TAP may offer complementary hydrogen bonding interactions to both N3 and H9 of adenine.

**Table 4-6:** Retention of the nucleotide bases (10 $\mu$ l of 1mM solutions) on columns (50 x 5mm i.d.) packed with MIP (APS-9EA) and NIP (APS) using as mobile phase acetonitrile/acetic acid:99/1 (v/v) and a flow rate of 1.0 mL/min.

Analyte (1mM)	R <sub>t</sub> MIP(APS-9EA) (min)	R <sub>t</sub> NIP(APS) (min)	k <sub>MIP(APS-9EA)</sub>	k <sub>NIP(APS)</sub>	IF
9EA	7.06	2.12	17.6	5.30	3.3
A	9.64	3.92	24.4	10.6	2.2
TAP	15.20	5.91	39.0	16.5	2.3
CDAP	2.29	1.23	5.0	2.60	1.9
T	0.81	0.59	1.1	0.70	1.4
U	0.76	0.58	1.0	0.70	1.4
C	8.65	2.55	21.8	6.50	3.3

**Table 4-7:** Retention of the nucleotide bases (10 $\mu$ l of 1mM solutions) on columns (50 x 5 mm i.d.) packed with MIP (APS-TAP) and NIP (APS) using as mobile phase acetonitrile/acetic acid:99/1 (v/v) and a flow rate of 1.0 mL/min.

Analyte (1mM)	R <sub>t</sub> MIP(APS-TAP) (min)	R <sub>t</sub> NIP(APS) (min)	k <sub>MIP(APS-TAP)</sub>	k <sub>NIP(APS)</sub>	IF
9EA	5.72	2.12	16.2	5.30	3.0
A	12.80	3.92	37.5	10.6	3.5
TAP	19.97	5.91	59.1	16.5	3.6
CDAP	1.790	1.23	4.4	2.60	1.6
T	0.79	0.59	1.4	0.70	1.8
U	0.77	0.8	1.3	0.70	1.8
C	5.99	2.55	17.0	6.60	2.6

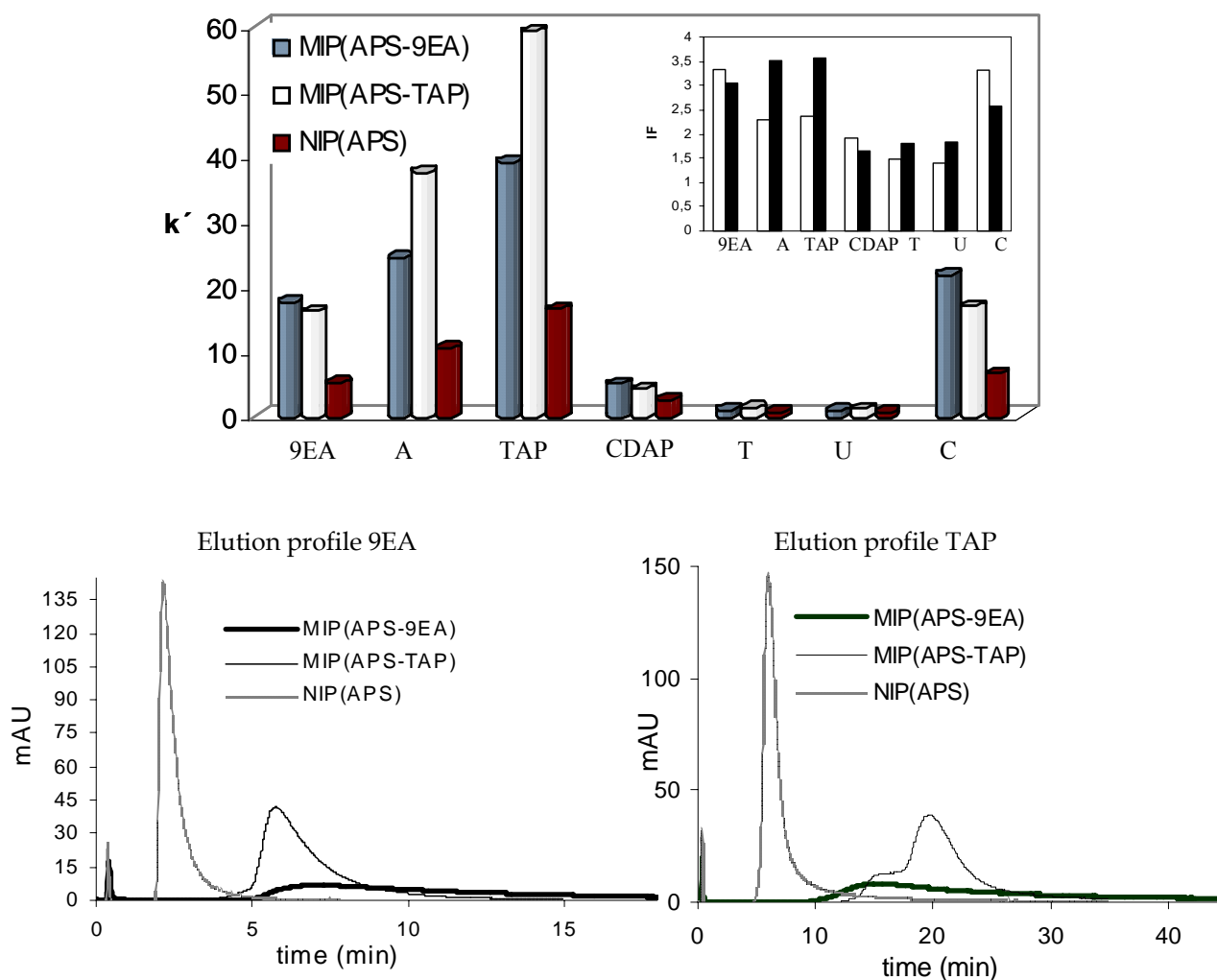


**Figure 4-18:** Retention of the nucleotide bases (10 $\mu$ l of 1mM solutions) on columns (50 x 5. mm i.d.) packed with MIP (APS-A), MIP(APS-TAP) and NIP (APS) using as mobile phase acetonitrile/acetic acid:99/1 (v/v) and a flow rate of 1.0 mL/min.

#### 4.1.5.4 Comparison between Different Silane Approaches

Figure 4-19 shows a comparison between the retention behaviours of all the adenine imprinted polymers against the injected nucleotide bases. The CPS system had, overall, the highest selectivity for its direct complements A and 9EA.

Unlike the GPS and APS, the CPS system contained no extra interfering functional groups. In the CPS case there were no possible interactions between a functional group from the connecting alkyl chain and a silanol group. These interactions might lead to a change in the ligand orientation on the silica surface.

All the imprinted polymers showed higher selectivity for their direct templates and a similar trend for all the other nucleotide bases. The 2-aminopyrimidine moiety appeared to be responsible for the good binding characteristics of molecules containing this unit with all the methacrylic acid containing polymers. Thus, C was strongly retained on all the imprinted polymers. This might be due to a two point interaction with the polymer functional groups, one through the exocyclic amino group and the other *via* the C=O exocyclic bond.

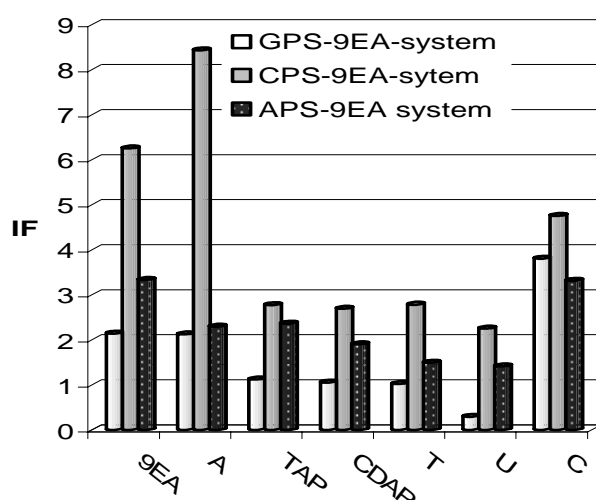


**Figure 4-19:** Selectivity versus nucleotide bases (10 $\mu$ l of 1mM solutions) on columns (50 x 5 mm i.d.) packed with MIP (GPS-A); MIP(CPS-A) and MIP (APS-9EA) using as mobile phase acetonitrile/acetic acid:99/1 (v/v) and a flow rate of 1.0 mL/min.

Although there were many trends that could be gleaned from the data presented so far, one observation must be highlighted: the substrates possessing the 2-aminopyrimidine substructure showed the highest binding to the adenine- and pyrimidine- imprinted polymers. The imprinted cavities with a shape and functionality similar to the 2-aminopyrimidine resulted in the polymers mimic the Watson-Crick binding mode of adenine with thymine [158] found in the double helix of DNA (Figure 4-20); thus the imprinting method could actually elicit major binding motifs, with prior knowledge of actual receptor design.

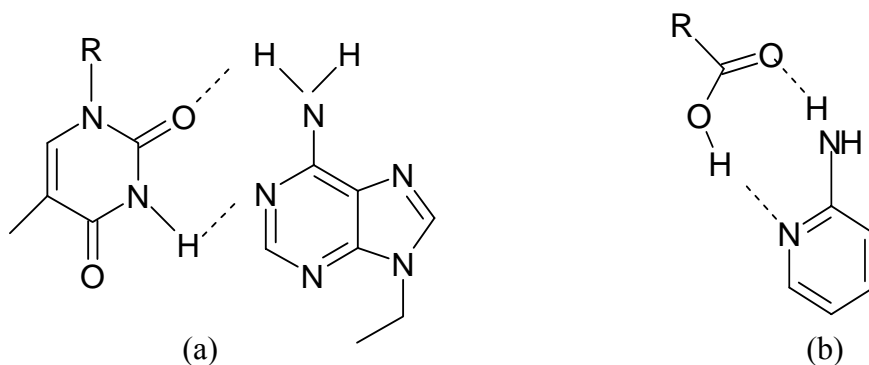


**Figure 4-20:** Watson-Crick binding mode between (a) thymine and adenine and (b) Watson-Crick-type binding between a carboxylic acid and 2-aminopyridine.

#### 4.1.5.5 Binding Measurements in Aqueous Media

Binding measurements were performed using an aqueous mobile phase. Due to the high selectivity, the APS system was chosen for further investigations. The APS system is the only case imprinted with two different immobilised templates and exhibited high fidelity for the direct complements, cross-retentivity, high binding for the 2-aminopyrimidine structured bases and poor selectivity for U and T.

Using a mobile phase consisting of  $\text{KH}_2\text{PO}_4\text{-K}_2\text{HPO}_4$  (pH=4.3) (aq)/ acetonitrile (3/7) TAP, was retained more strongly, on its complementary column MIP (APS-TAP) as were 9EA and A on MIP(APS-9EA) (Figure 4-21). The explanation could be the protonation of the N-1 nitrogen of the bases at pH 4.3, and the resulting ion-exchange process controlling the retention mechanism. Triaminopyrimidine having three electron-donating aminogroups will be, at an acidic pH, the most easy protonable base and, as a consequence, will be the strongest retained electrostatically on both its own complement and also strong retained with  $k= 3.9$  on the MIP(APS- 9EA) column. The same explanation is valid for CDAP with only two electron-donating aminogroups, strongly retained on its direct complement and also strongly retained on the MIP(APS-9EA) but weaker in comparison with TAP. Thymine, cytosine and uracil were only weakly retained in this mobile phase.

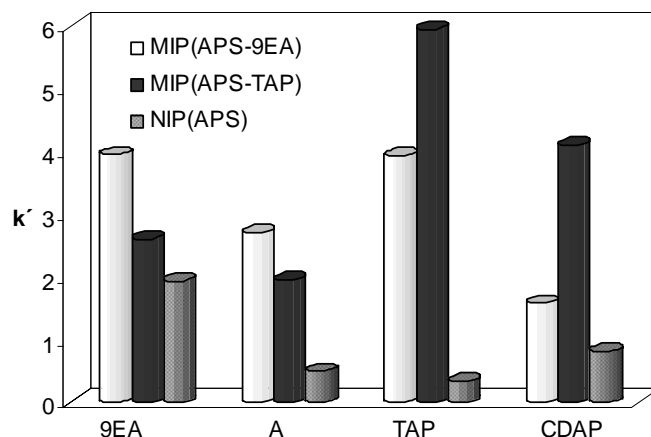


**Figure 4-21:** Retention of templates and structural analogues (10  $\mu$ L of 1mM solutions) on columns (50x 5 mm i.d.) packed with MIP(APS-9EA), MIP(APS-TAP) or NIP(APS) using a mobile phase of phosphate buffer (pH=4.3)/acetonitrile 3/7(v/v) and a flow rate of 1.0 mL/min.

As an optimum pH, 4.3 was chosen in the previous study investigating the binding dependence versus pH for the 9EA on its direct imprinted complement. The pH profile for the retention of 9EA on its own imprinted polymer MIP (APS-9EA) versus the blank polymer NIP (APS) was determined (Figure 4-22). Enhanced binding at pH= 4.3 may be accounted for by protonation of the 9EA (Figure 4-23) (the pKa was found to be 3.6 in 95/5 ACN/H<sub>2</sub>O, and 4.15 in water). This would lead to a positively charged 9EA molecule that would bind well to the carboxylate groups of the polymer.

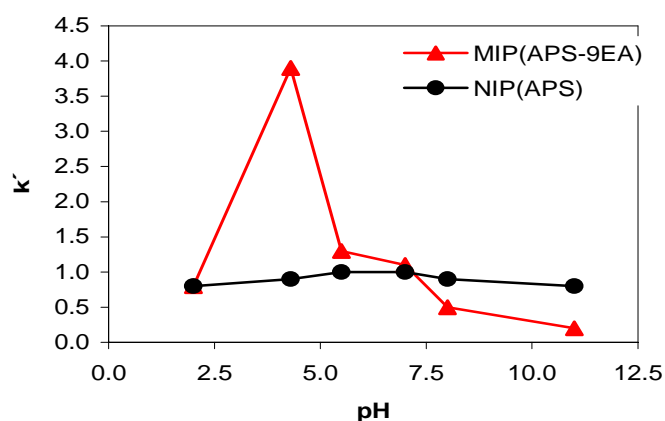


**Figure 4-22:** Retention of 9EA on MIP (APS-9EA) and NIP(APS) as function of pH.



Maximum retention occurred at pH= 4.3, a value close to the pKa of N-1 on 9EA [151], which suggested that the retention is controlled by an ion-exchange process. This is supported by a theoretical ion-exchange model, described in the literature [159] for imprinted polymers, which showed a correlation between the pKa of the solute and maximum chromatographic retention. In looking at the non-imprinted polymer in Figure 4-22, there was little dependence of retention on pH. The reason for this may be that although the optimum binding conditions of the polymer can be controlled by the pH of the mobile phase, the selectivity is controlled by the imprinting process. The selectivity of the imprinted polymers is due to the shape-selective cavity built into the polymer matrix and the pre-organisation of functional groups complementary to the template molecule. This was further substantiated by showing pH-dependent selectivity of the 9EA imprinted polymer for 9EA, A, TAP and CDAP only and not for other DNA base derivatives as T, C and U. (Figure 4-24) The strong binding of TAP and CDAP on the column imprinted with 9EA at pH=4.3 was explained by the presence of the amino groups in the molecule. Because of the strong electron-donating effects, these molecules will be protonated more easily than 9EA and A and therefore strongly retained. This demonstrates a possible link between binding and specificity in imprinted polymers. The specificity of the imprinted polymer appears to be enhanced as binding affinity increases. The specificity is determined by the complementarity of the functional groups as well as the shape of the binding cavity.

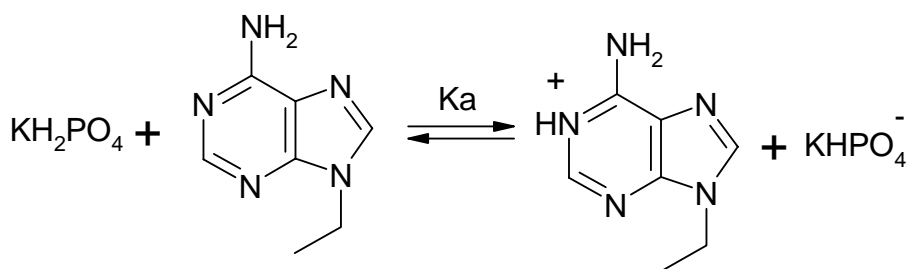


**Figure 4-23:** First protonation of 9EA.

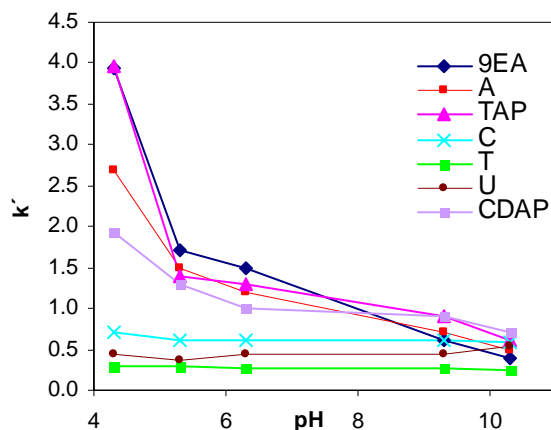
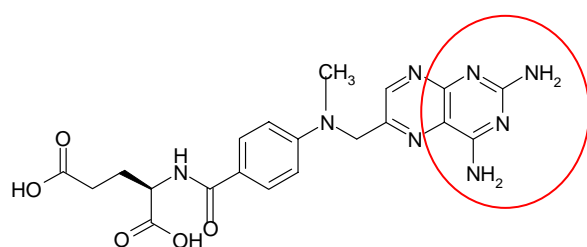


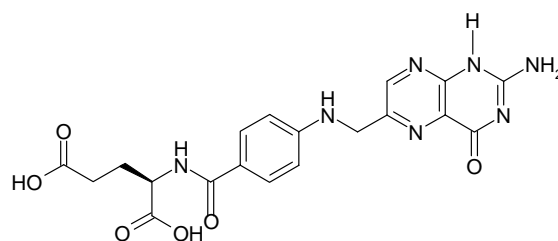
**Figure 4-24:** Comparison of retention factors for various nucleotide base derivatives on the P (APS-9EA) column at different pHs.

#### 4.1.5.6 Recognition of Larger Molecules

As proven by the fluorescence microscopy studies, the MIPs obtained *via* hierarchical imprinting contained accessible binding sites which, due to the double imprinting procedure, should be located at the surface. This implies that larger template molecules containing a similar substructure to the immobilised template may also bind to those sites. Thus, using an aqueous mobile phase (phosphate buffer, 0.1M, pH= 4.3, containing 5% acetonitrile) we investigated the retention of the 2,4-diaminopteridine containing drug methotrexate (MTX) which is used in cancer therapy. Substructure approaches to recognise this drug have previously been developed by our group [157].



Methotrexate (MTX)



Folic Acid (FOL)

---

The MIP (APS-TAP) showed an imprinting factor of 2 for the drug MTX whereas folic acid (FOL) was 1.5 times more retained on the MIP (APS-TAP) than on the NIP(APS). The retention can be explained by the fact that MAA forms complexes with the amino substituted N-heterocyclic bases stabilised by strong cyclic hydrogen bonds at two sites. MTX was slightly more strongly retained than FOL given the presence of the two exocyclic amino groups on the pyrimidine ring, similar to the TAP immobilised template. Due to the surface-located binding sites and strong association between MAA and N-heterocyclic bases, MTX and FOL could be recognised by the TAP imprinting sites.

The fact that by imprinting only a small portion of a larger and complex target molecule the target can be recognised, encouraged us to move towards the next application of hierarchical imprinting concerning the recognition of large peptides *via* imprinting of small epitopes, as will be presented in section 4.2 of this thesis.

#### *4.1.5.7 Comparison between Hierarchical and Bulk Imprinted Polymers*

The system described above serves as an excellent reference for comparison with the retention data observed with traditional imprints [150,151,152,159].

It must be mentioned that for the bulk imprinted polymers, the control polymer was not a NIP. A smaller, differently structured “generic” template was used: benzoic acid or benzylamine. Additionally, in the bulk studies, TAP was never employed as a template nor as a solute, so it is not possible to compare the TAP and CDAP retention on the adenine or pyrimidine imprinted polymers.

Overall, the hierarchically imprinted polymers exhibited lower selectivity compared to their monolithic counterparts. Whereas the MIPs for 9EA exclusively retain adenine derivatives, the hierarchical MIPs exhibited a considerably broader selectivity and lower imprinting factors. This is a reasonable consequence of the sterical effect caused by coupling of the template to the silica surface, which may prevent complementary interactions developing at this point. Further, the fluoride treatment may, to some extent degrade the templated sites, although monolithic MIPs appear to be stable to similar treatments. The results concerning the selectivity dependence versus pH of the hierarchical polymers were in good agreement with the

bulk case [151], but again lower specificity and broader selectivity was registered for the hierarchical case.

For the hierarchical imprinted polymers the chromatographic efficiency has been greatly improved. It must be kept in mind that in this case we are dealing with spherical, uniformly shaped particles with a high surface area and a narrow pore size distribution. These factors make them superior for HPLC applications in comparison to the irregularly shaped monolith particles (Figure 4-25). The binding sites were surface-located and not buried in the polymer matrix or destroyed during a crushing and sieving process. The plate numbers were considerably higher for the hierarchical materials, pointing to greater separation efficiency (Table 4-8). A brief overview of chromatography is given in section 6.5.7. The higher the plate number is, the higher the separation efficiency and the narrower the peaks. The peak shape was considerably improved for the hierarchical MIPs showing sharper and more symmetric peaks in comparison to the bulk case. However, some tailing and broadening of the peaks occurred also on the columns packed with the hierarchically materials especially for analytes corresponding to the direct complements. This may be a result of the imprinting effect.

**Table 4-8:** Comparison of the selectivity, plate number and back pressure of the columns (50x 5 mm i.d.) imprinted with a bulk imprinted polymer and the hierarchical imprinted polymers using 9EA as a substrate in acetonitrile/acetic acid: 99/1 (v/v).

Parameter	Bulk	Hierarchically Imprinted Polymers		
	P(9EA)	MIP(GPS-A)	MIP(CPS-A)	MIP(APS-9EA)
$k_{MIP}$	39.7	4.3	4.4	17.6
IF	31.4	2.14	6.25	3.3
$N (m^{-1})$	950	7602	7864	5510
Bp (Bar)	86	20	20	25

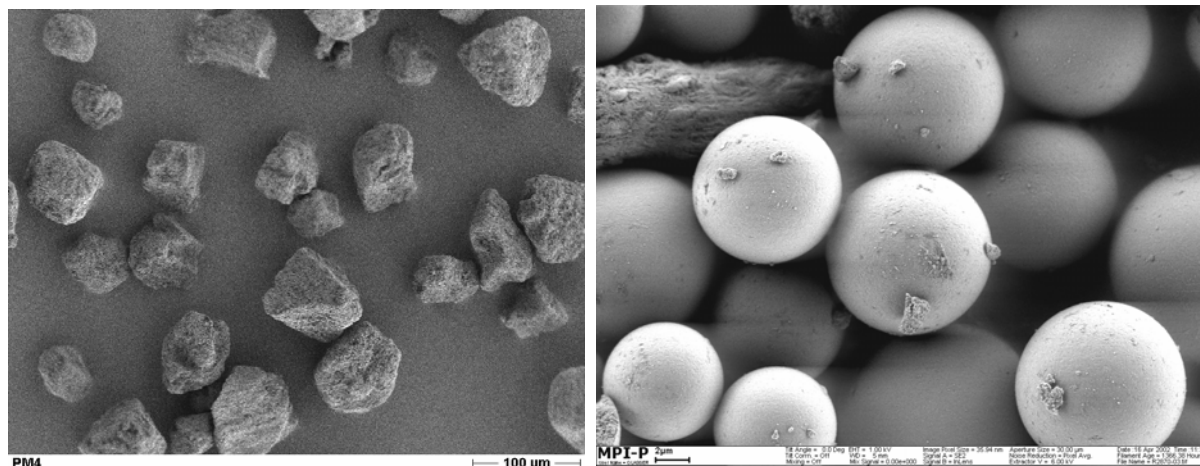


**Figure 4-25:** Comparison between: left: irregularly shaped particles obtained by traditional imprinting of 9EA; right: imprinted polymer particles obtained by hierarchically imprinting method (MIP(CPS-A)).

The results shown in Table 4-8 stress that polymers prepared by hierarchical imprinting are superior to the bulk imprinted counterparts concerning chromatographic efficiency. This study was the first HPLC application in which spherically-shaped particles, selective for a class of compounds, were produced using fully characterised preformed porous silica gel particles *via* the proposed alternative interfacial imprinting [1]. In this way, the resulting imprinted polymer particles presented a controlled and homogeneous morphology with optimum characteristics to be used as stationary phases in HPLC.

#### 4.1.6 Conclusions

The development of molecularly imprinted synthetic receptors capable of recognising nucleotide bases with enhanced chromatographic efficiency has been described in this section. The polymers were prepared using a hierarchical imprinting strategy that employed on one hand an inorganic template (silica gel), used as a sacrificial solid porogen to control the pore structure of the resulting polymers and, on the other hand, a molecular template (nucleotide base) used to create recognition binding sites in the polymer matrix. The templates were covalently immobilised on the silica surface using three different silane modifiers, followed by polymerisation inside the pores of the inorganic mold and dissolution of the silica

matrix. The resulting polymers possessed a mirror image structure related to the original silica gel and a similar morphology. Spherical imprinted polymer beads with a high surface area and a narrow pore size distribution were obtained. Fluorescence microscopy studies indicated that the polymers possessed highly accessible binding sites. The surface confinement of these binding sites was confirmed by the possibility to retain larger molecules with similar structures. Thus, using an aqueous based mobile phase the polymer imprinted with TAP was able to retain the 2,4-diaminopteridine drug methotrexate and folic acid.

All the polymers exhibited selectivity for their own templates and other analogues with similar structure. Using an organic mobile phase consisting of acetonitrile modified with 1% acetic acid, enhanced binding was found for adenine, pyrimidine and cytosine derivatives. These three bases have a 2-aminopyrimidine substructure in common, which appeared to be an important component for binding and specificity of purine and pyrimidine bases to imprinted polymers with carboxylic acid functionalities. In contrast, thymine and uracil derivatives, which do not contain the 2-aminopyrimidine substructure, were poorly retained in the same mobile phase. Finally, the retention of 9EA on its imprinted polymer was found to be pH dependent. From these results, it could be concluded that electrostatic forces played an important role in rebinding interactions of 9EA in imprinted polymers. Only the aminopyrimidine derivatives were retained on the 9EA column at the same pH conditions as adenine which was explained by the protonation of these compounds. The retention of other DNA and RNA base derivatives showed no dependence on pH. Thus, it was concluded that the origin of specificity must lie in the complementarity built into the polymer and is not just a differential binding affinity among the different bases.

---

## 4.2 IMPRINTING USING IMMOBILISED PEPTIDES

Peptide-macromolecule interactions are ubiquitous in nature. Examples include sensory neuropeptides, *e.g.* enkephalins, which play a role in signalling peptide hormones (*e.g.* corticotropin, vasopressin) and peptide antibiotics (*e.g.* gramicidins). A critical element in the above processes is the recognition of a specific peptide by a macromolecular receptor. The preparation of artificial binding sites for such peptides may provide insight into such recognition processes. In addition, these artificial receptors may facilitate screening of peptide mixtures or assist in the evaluation of peptidomimetics that can be used to either enhance or inhibit receptor responses.

Most MIPs reported to date show selectivity for low molecular mass compounds and are limited to traditional imprinting formulations. However, as targets with more biological relevance, such as peptides and oligonucleotides, are identified, these traditional formulations are no longer effective or suitable due to practical matters, *e.g.* the lack of solubility of peptides in organic media and more subtle effects such as peptide conformation. Therefore, the imprinting of oligopeptides and proteins for aqueous-based separations continues to be an important challenge as described already in section 3.2.7.

With a few remarkable exceptions, the reports involving the protein itself in the polymerisation process [160,161,162] have been characterised by low selectivity and poor reproducibility. This may be related to the use of various solvents, temperatures, pH and ionic strengths causing partial denaturation of the protein.

In order to circumvent the problems associated with the imprinting of complex biomolecules, an epitope approach may be used. Here, a smaller peptide corresponding to a unique amino acid sequence of a target protein is used as a template to generate a site that can subsequently bind the larger target molecule [4]. Expanding this concept, I used immobilised peptides as templates to generate surface-confined sites for larger peptides *via* the hierarchical imprinting methodology.

My final target was a heptadecapeptide, Nociceptin (or Orphanin FQ), a newly discovered natural antagonist of the opioid receptor-like (ORL 1) receptor, a G

protein-coupled receptor. Nociceptin has the following 17 amino acid linear sequence: H-Phe-Gly-Gly-Phe-Thr-Gly-Ala-Arg-Lys-Ser-Ala-Arg-Lys-Leu-Ala-Asn-Gln-OH. It is derived from a larger precursor, prenociceptin (PNNOc), sharing sequence homology with classical opioid peptides. Despite this sequence homology with most of the opioid peptides, Nociceptin binds to opioid receptors with very low affinities [165] and its pharmacological properties differ from those of opioids. Nociceptin has been linked with several physiological functions in the central nervous system including memory, locomotion and the processing of pain signals. Recent structure-activity relation studies of Nociceptin and an opioid peptide, dynorphin A (H-Tyr-Gly-Gly-Phe-Leu-Arg-Arg-Ile-Arg-Pro-Lys-Leu-Lys-Trp-Asp-Asn-Gln-OH), have revealed that the two Phe residues at positions 1 and 4 are important structural requirements for ORL 1 receptor binding and biological activity and also for discriminating Nociceptin activity from opioid activities [163,164,165].

In order to develop a synthetic receptor analogue for this peptide we used the crude products resulting from solid phase peptide synthesis. Through the immobilisation of increasing amino acid sequences corresponding to the N-terminus of this peptide, I generated surface-confined binding sites for larger peptides containing the immobilised epitope, including Nociceptin. Apart from its biological functions and physiological importance, Nociceptin was also chosen for the simplicity of its N-terminal sequence, H-FGGFT, in order to first demonstrate the principle.

#### **4.2.1 Solid Phase Synthesis; Template Immobilisation**

The epitopes were immobilised step-by-step on the surface of the same mesoporous silica gel, modified with amino groups as described previously. The coupling was accomplished using standard Merrifield chemistry and dicyclohexylcarbodiimide (DCC) as the coupling reagent. The neighbouring C=N bonds of this reagent are susceptible to nucleophilic attack by the carboxyl group of the amino acid forming an isourea with dehydration favouring the formation of a highly stable urea (Figure 4-26).



1-Hydroxybenzotriazole (HOBt) was also employed in the carbodiimide-mediated couplings as a catalytic auxiliary nucleophile to reduce possible side reactions, including racemisation. In addition to providing an excellent leaving group, HOBt is capable of acting as proton acceptor, aiding deprotonation of the ammonium ion intermediate and thereby greatly increasing the reaction rate. Although added in equimolar quantities to the acylating component, HOBt is catalytic and therefore remains in essentially a fixed concentration through the coupling step. This ensures that the highly activated isourea derivative is short-lived.

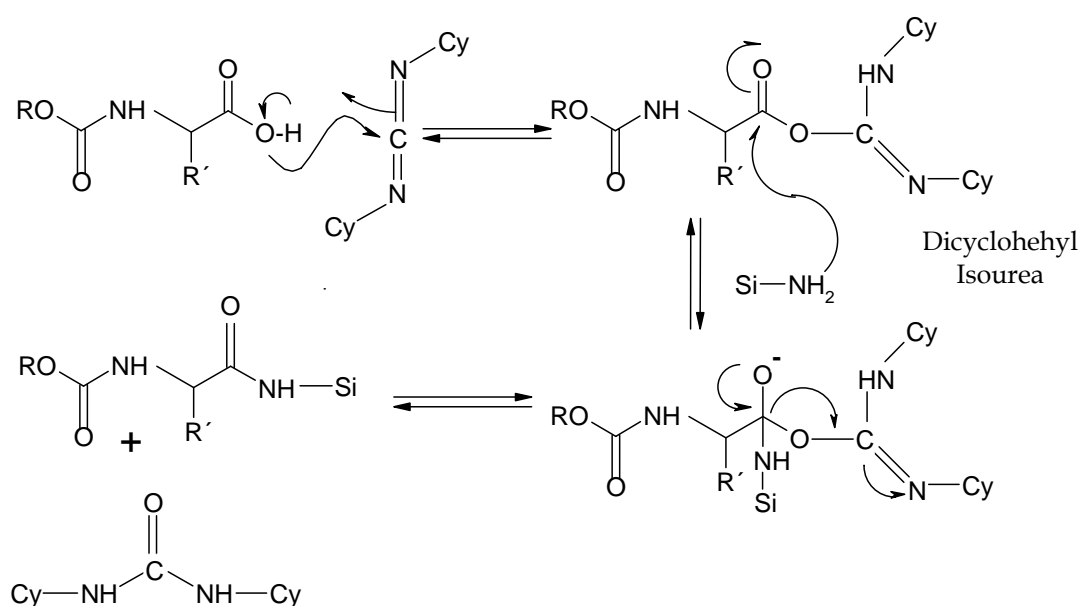


**Figure 4-26:** The mechanism of carboxyl group activation using DCC as a coupling agent.

There is a risk that the amine nucleophile itself reacts with the carbodiimide, resulting in the formation of undesired guanidine, but this reaction is sufficiently slow to be unimportant under the conditions conventionally used for solid phase peptide synthesis. The resulting dicyclohexylurea is simply washed from the solid silica support after the reaction using a high excess of DMF.

In all cases, when coupling a new amino acid to the modified silica surface, its amino group was protected with the fluorenylmethyloxycarbonyl (Fmoc) group. The Fmoc group has achieved wide acceptance due to its resistance to acidic conditions and the ease of deprotection using weak bases, particularly secondary amines. Piperidine emerged early as a popular inexpensive base causing few side reactions.

Deprotection occurs through base catalysed abstraction of the  $\beta$ -proton of the protecting group, with elimination leading to the formation of the free amine and dibenzofulvene. Piperidine forms an adduct with the dibenzofulvene released upon deprotection (Figure 4-27).

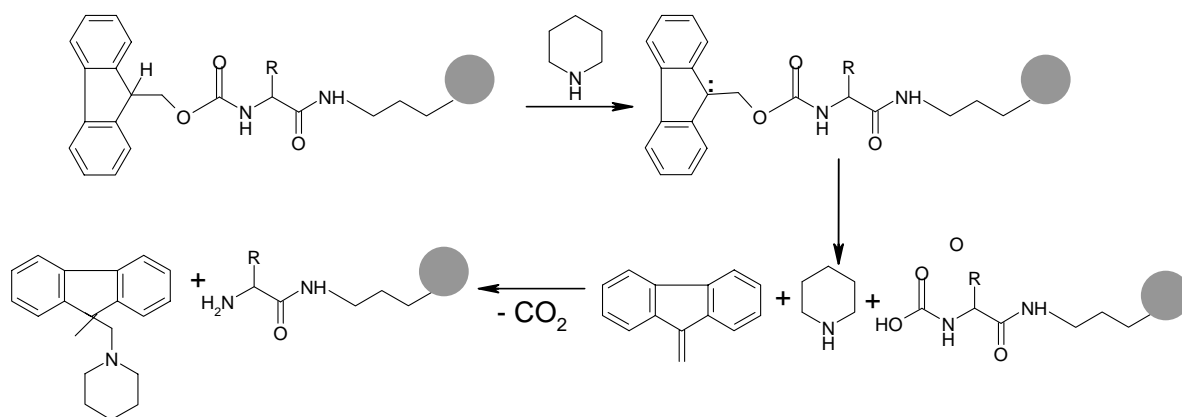


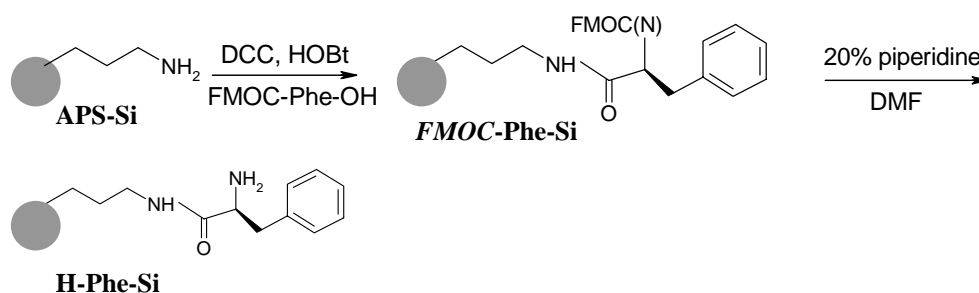
**Figure 4-27:** Mechanism of Fmoc deprotection on the silica support.

Prior to activation, the silica surface was reacted with APS and end-capped with HMDS as described in section 4.1.1, followed by the step-wise immobilisation of the first four amino acids from the N-terminal sequence of Nociceptin. Thus, in the first step *Fmoc*-Phe-OH was coupled to the amino-modified silica surface followed by *Fmoc* removal using piperidine/DMF. In the next two step reaction the dipeptide was coupled to the silica surface. Thus, *Fmoc*-Gly-OH was coupled through DCC catalysed amide bond formation. After deprotection, *Fmoc*-Phe-OH was coupled in order to obtain the N-protected or non-protected dipeptide. The immobilised tripeptide was obtained by coupling the *Fmoc*-Gly-OH to the silica surface, deprotection and further reaction with *Fmoc*-Phe-Gly-OH. Finally, the four amino acids epitope was covalently attached to the silica surface by coupling the amino groups of silica with *Fmoc*-Gly-Phe-OH, deprotection and subsequent coupling with *Fmoc*-Phe-Gly-OH. All these reactions are described in Figure 4-28.

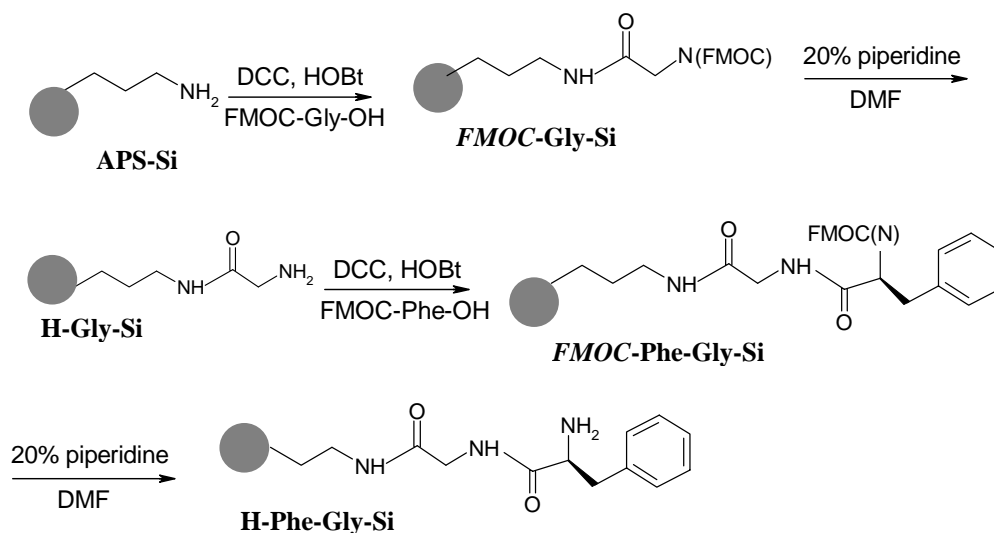
In order to create a high fidelity surface confined binding site for the N-terminal sequence of Nociceptin H-Phe-Gly-Gly-Phe-Thr-Gly-Ala-Arg-Lys-Ser-Ala-Arg-Lys-Leu-Ala-Asn-Gln-OH, the four amino acids epitope immobilisation had to be started with the phenylalanine placed before threonine followed by glycine, glycine and

again phenylalanine resulting in H-Phe-Gly-Gly-Phe-Si. Thus, when using Nociceptin as analyte, the new generated binding site should be complementary to the correct sequence of its N-terminal. The inverse of the imprinting fidelity dipeptide sequence H-Gly-Phe-Si was prepared as control. The resulting binding site should show no structural fidelity for Nociceptin or smaller H-Phe-Gly-related analogues, as will be demonstrated later.

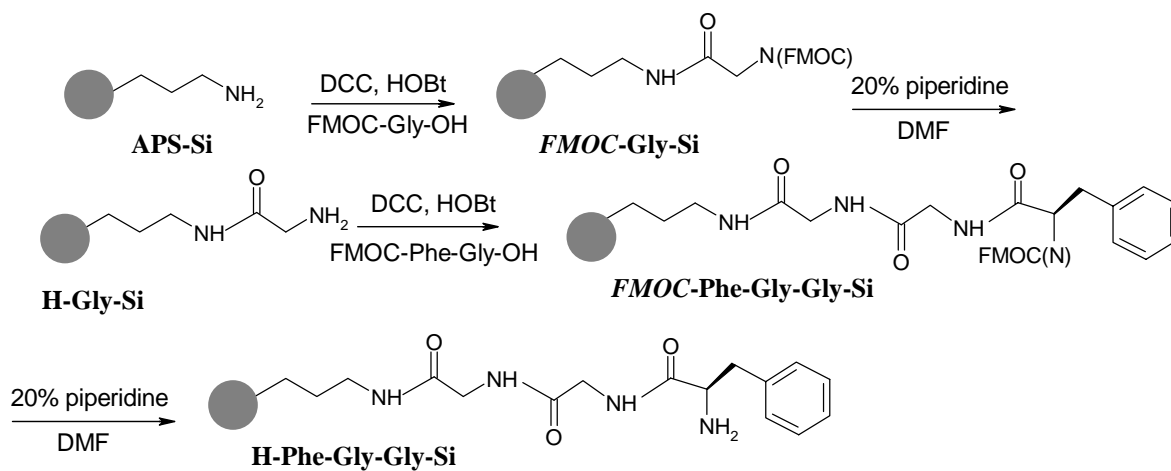
➤ First amino acid immobilisation



➤ Dipeptide immobilisation



## ➤ Tripeptide immobilisation



## ➤ Tetrapeptide immobilisation

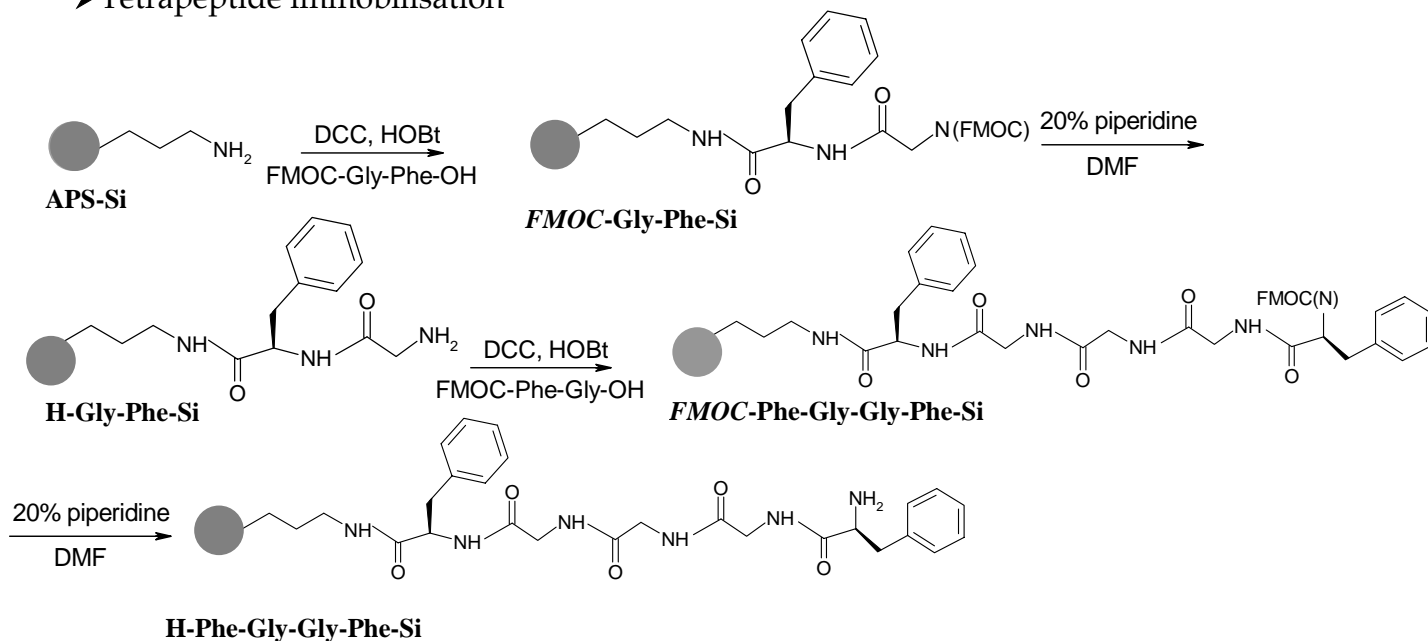


**Figure 4-28:** Peptide solid phase synthesis. Step-by-step immobilisation of N-terminal epitopes of the Nociceptin sequence.

#### 4.2.2 Characterisation of the Solid Phase Synthesis Products

Each intermediate resulting from solid phase synthesis was fully characterised by elemental microanalysis, infrared spectroscopy and fluorescent spectroscopy.

**Table 4-9:** Characterisation of the modified silica beads by elemental analysis.

Template name	Silica template					
	% C	$\Delta C$ (%)	% N	$\Delta N$ (%)	$D_s$ ( $\mu\text{mol}/\text{m}^2$ )	
					$\Delta C$	$\Delta N$
APS-Si	4.28	4.11	1.65	1.65	3.85	4.00
FMOC-Phe-Si	16.02	10.47	1.78	0.13	1.20	0.27
H-Phe-Si	9.94	4.39	1.91	0.26	1.23	0.54
FMOC-Gly-Phe-Si	13.3	9.02	2.53	0.88	0.95	1.04
H-Gly-Phe-Si	10.24	5.96	2.77	1.12	1.4	1.25
FMOC-Gly-Si	17.04	11.49	3.28	1.63	4.88	4.00
H-Gly-Si	6.24	0.69	2.21	0.56	0.84	1.17
FMOC-Phe-Gly-Si	16.44	10.25	2.93	0.72	1.17	1.81
H-Phe-Gly-Si	11.91	5.67	2.97	0.76	1.63	1.69
FMOC-Gly-Si	14.1	9.82	2.29	0.64	1.6	1.50
H-Gly-Si	6.76	2.48	2.89	1.24	0.82	1.30
FMOC-Phe-Gly-Gly-Si	19.47	12.71	4.20	1.31	1.41	1.67
H-Phe-Gly-Gly-Si	13.92	7.16	4.16	1.27	1.77	1.44
FMOC-Gly-Phe-Si	15.37	11.09	3.61	1.96	1.20	2.90
H-Gly-Phe-Si	9.86	5.58	3.05	1.40	1.30	1.60
FMOC-Phe-Gly-Gly-Phe-Si	18.07	8.21	5.09	3.69	0.85	0.90
H-Phe-Gly-Gly-Phe-Si	13.58	3.72	3.53	0.88	0.85	0.96

From the change in carbon and nitrogen content, with reference to the starting material, the area density ( $D_s$ ) of the coupled ligand could be estimated, together with the associated coupling yield (Table 4-9). Area densities ( $D_s$ ) of immobilised ligands were calculated based on the change in carbon ( $\Delta C$ ) or nitrogen ( $\Delta N$ ) content versus the preceding step, *e.g.* for  $\Delta N$ :  $D_s = m_N / (M_N S)$ ,

where  $m_N = \Delta N\% / (100 - \Delta N\% M_w / M_N)$ ,  $M_w$  = molecular weight of the coupled ligand,  $M_N$  = weight of nitrogen per mole of coupled ligand and  $S$  = surface area of the silica support ( $S = 350 \text{ m}^2/\text{g}$ ).

Assuming a maximum density of  $8 \mu\text{mol}/\text{m}^2$  on the native silica gel, APS occupied *ca.* 50% of the available sites, which was in agreement with results reported in the literature. The calculated area density of all the final coupling products was found to lie in the range of  $1\text{-}2 \mu\text{mol}/\text{m}^2$ . This relates to an average conversion of  $\sim 50\%$  of the amino groups present on silica surface which corresponds to an average distance between ligands of  $10\text{-}15 \text{ \AA}$  assuming a random ligand distribution.

The crude solid phase synthesis products were also characterised using FT-IR spectroscopy. The presence of the peptidic bonds could in all cases be clearly observed in the region  $1695\text{-}1630 \text{ cm}^{-1}$ , acting as further support for the success of the coupling reactions. In this section I present the IR spectra corresponding to the immobilisation of the two amino acid epitope, H-Phe-Gly-Si, as an example.

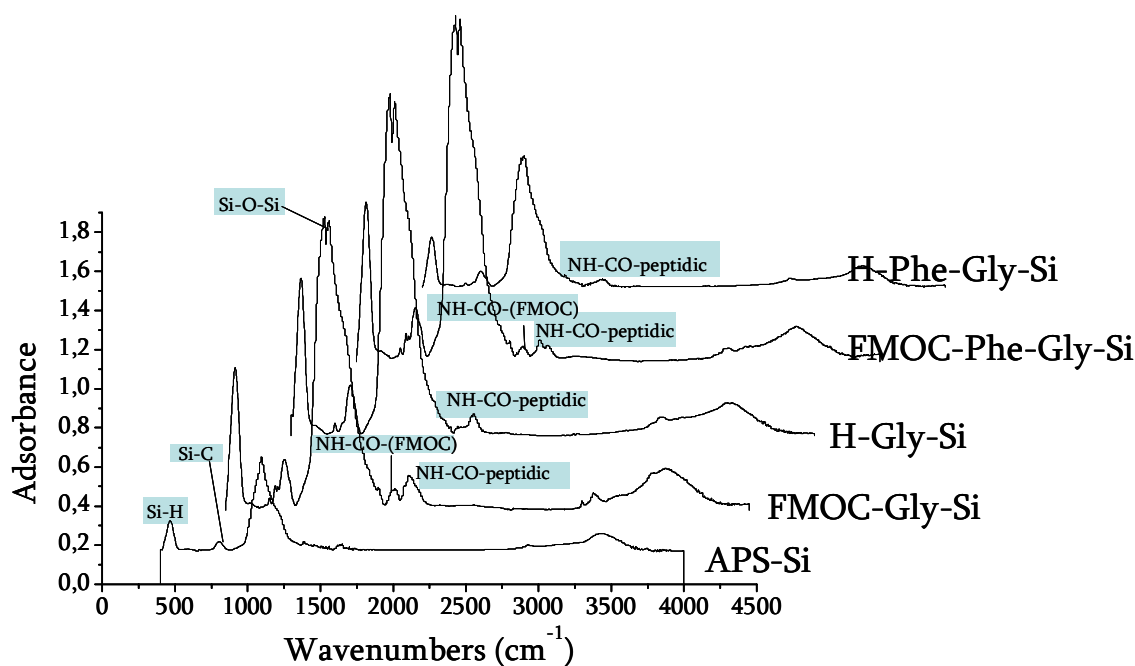


**Figure 4-29:** FT-IR spectra corresponding to the stepwise immobilisation of the amino dipeptide epitope to the silica surface.

In Figure 4-29, the bands corresponding to the peptide bonds can be clearly seen at  $\sim 1670\text{ cm}^{-1}$ . It can also be observed that all the *Fmoc* protected amino acids possessed another absorption band at a slightly higher wavelength ( $\sim 1700$ ). This was due to the carbamate group of *Fmoc* protecting group which disappeared on deprotection. N-monosubstituted amides usually exist with the NH and C=O bond in the trans-conformation. The hydrogen-bonded NH stretch is seen near  $3300\text{ cm}^{-1}$ . The band from  $1550\text{ cm}^{-1}$  involves both C-N stretch and C-N-H in-plane bend in the stretch-bend mode. All the characteristic bands due to the silica support have been previously described in the nucleotide imprinting section (section 4.1.2) and can also be seen here.

The coupling steps could also be visualised using fluorescence microscopy. Thus, coupling of the *Fmoc* protected peptides was accompanied by a strong fluorescence which disappeared completely upon deprotection, as illustrated in Figure 4-30.

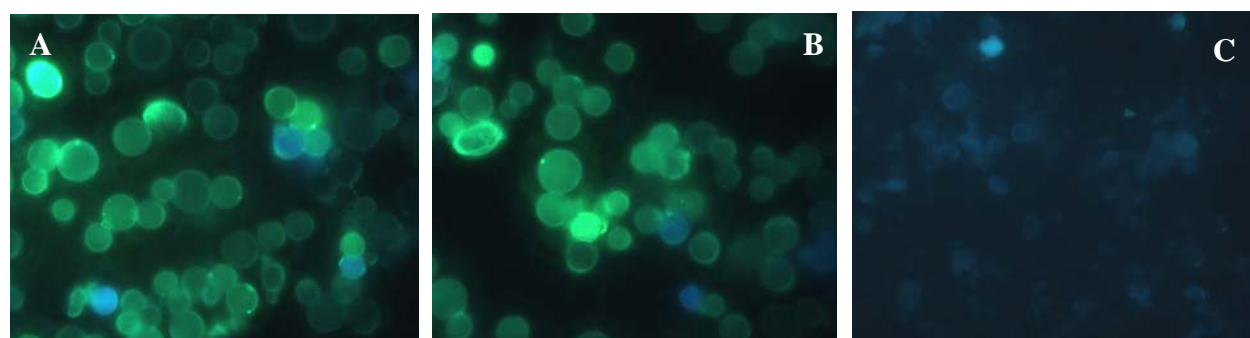


**Figure 4-30:** Fluorescence micrographs (100x magnification) of (A) *Fmoc*-Phe-Gly-Si, (B) *Fmoc*-Phe-Gly-Gly-Si and (C) H-Phe-Gly-Gly-Si.

### 4.2.3 Preparation of the Imprinted Polymers

The crude products resulting from solid phase synthesis were subsequently used for the generation of hierarchically imprinted materials. Thus, the silica pores containing the immobilised peptidic templates were filled with a mixture of MAA, EDMA and azo-initiator (AIBN) (Figure 4-31). This mixture was thereafter thermally cured at  $60^\circ\text{C}$  according to the previously reported procedure (section 4.1.3). Dissolution of the silica mold by treatment with a solution of  $\text{NH}_4\text{HF}_2$  (aq.) resulted in organic polymer beads with a size and morphology reflecting those of the original silica

mold, as proven by SEM, TEM and nitrogen sorption experiments. In addition, the immobilised amino acids and peptides should leave behind surface imprints, leading to preferential retention of the template peptide and the heptadecapeptide Nociceptin when assessing the materials as stationary phases in chromatography.

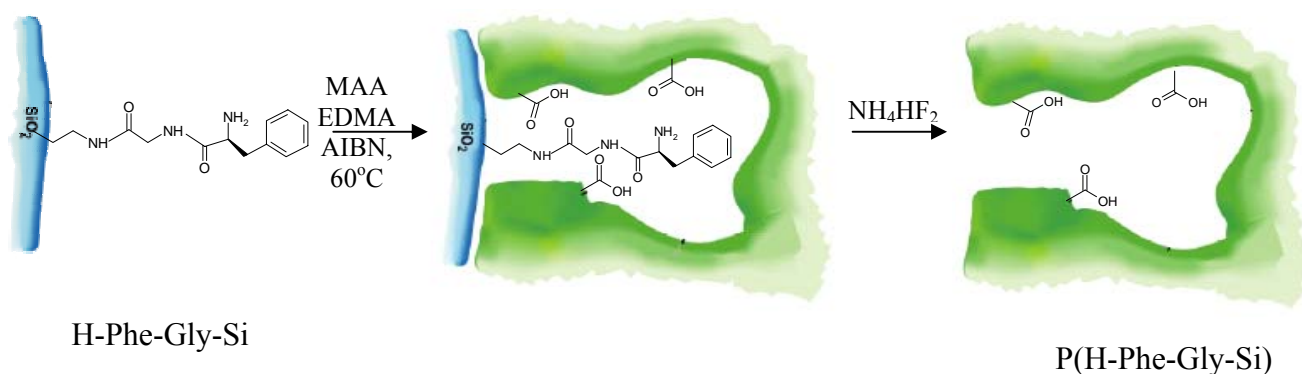


**Figure 4-31:** Generation of an epitope hierarchical imprinted polymer using immobilised dipeptide.

The following polymers were generated from the immobilised epitopes:

**“Protected”**

P(*FMOC*-Phe-Si)  
 P(*FMOC*-Phe-Gly-Si)  
 P(*FMOC*-Phe-Gly-Gly-Si)  
 P(*FMOC*-Phe-Gly-Gly-Phe-Si)

**“Deprotected”**

P(H-Phe-Si)  
 P(H-Phe-Gly-Si)  
 P(H-Phe-Gly-Gly-Si)  
 P(H-Phe-Gly-Gly-Phe-Si)

Control polymers were prepared using the reverse sequence of Nociceptin N-terminus:

P(*FMOC*-Gly-Si)  
 P(*FMOC*-Gly-Phe-Si)

P(H-Gly-Si)  
 P(H-Gly-Phe-Si)

In order to investigate the effect of template immobilisation, another material was prepared using free *FMOC*-Phe-OH (*FMOC*-Phe//Si). This polymer was produced by simply dissolving *FMOC*-Phe-OH in the pre-polymerisation mixture containing the monomers and initiator. The silica pores were completely filled with this pre-polymerisation mixture, followed by polymerisation and silica removal under the



conditions described above. Before the silica dissolution the template was extracted from the composites with methanol using a Soxhlet apparatus.

#### 4.2.4 Characterisation of the Imprinted Polymers

The extent of removal of the silica and peptide template was revealed by elemental microanalysis of the final polymer products (Table 4-10).

**Table 4-10:** *Polymers obtained after dissolution of the silica template and results from nitrogen sorption isotherms.*

Imprinted polymer	% C	% N	$a_s$ (m <sup>2</sup> /g)	$V_p$ (mL/g)	$d_p$ (nm)
P(APS-Si)	57.5	0.25	250	0.62	7.5
P(FMOC-Phe-Si)	56.3	0.23	149	0.58	7.4
P(H-Phe-Si)	55.3	0.15	200	0.53	8.2
FMOC-Phe//Si	56.7	0.50	205	0.37	5.1
P(FMOC-Gly-Phe-Si)	56.4	0.33	210	0.45	5.5
P(H-Gly-Phe-Si)	54.3	0.29	180	0.30	6.2
P(FMOC-Gly-Si)	53.2	0.20	132	0.24	4.0
P(H-Gly-Si)	51.5	0.24	145	0.41	7.4
P(FMOC-Phe-Gly-Si)	59.3	0.26	166	0.27	4.5
P(H-Phe-Gly-Si)	58.5	0.39	204	0.58	5.4
P(FMOC-Gly-Si)	53.2	0.20	132	0.24	4.0
P(H-Gly-Si)	51.5	0.24	145	0.41	7.4
P(FMOC-Phe-Gly-Gly-Si)	55.5	0.14	220	0.49	7.3
P(H-Phe-Gly-Gly-Si)	57.2	0.23	240	0.82	7.2
P(FMOC-Gly-Phe-Si)	56.4	0.33	210	0.45	5.5
P(H-Gly-Phe-Si)	54.3	0.29	180	0.30	6.2
P(FMOC-Phe-Gly-Gly-Phe-Si)	56.7	0.19	230	0.50	7.2
P(H-Phe-Gly-Gly-Phe-Si)	55.9	0.23	210	0.45	6.8

Note: The elemental composition of the polymers should be compared with the composition of a reference polymer prepared in absence of the silica template (C: 59.9; N: 0.1).  $a_s$ = surface area determined using the BET model,  $V_p$ = the total volume of pores according to Gurvitch and  $d_p$ = the average pore diameter according to the BJH model.

The carbon and nitrogen contents indicated that > 95% of the template was removed after the fluoride treatment. The infrared spectra showed no peaks that could be assigned to remaining silica and were otherwise similar to those of a bulk material prepared under the same conditions (Figure 4-32). The EDX spectra of the hierarchically imprinted polymers no longer contained the peaks corresponding to the silicon atom and contained only peaks corresponding to the carbon and oxygen atoms from the polymer (Figure 4-33).

Additional confirmation for successful silica removal was brought by TG analysis. Thus, in Figure 4-34 are plotted the profiles of the mass loss with temperature for the di- and tripeptide hierarchically imprinted polymers and the corresponding composites. For the hierarchically imprinted polymers it can be observed that upon heating up to 1000°C, almost everything was burned out (< 5% residue). The methacrylate based polymer started decomposing around 200°C and since no or very little amount of silica was present in the sample, almost no sample remained in the crucible when the temperature reached 400°C. In the case of the composites, the polymer present inside the silica pores started also decomposing at 200°C and when the temperature reached 400°C, ~ 40% of the initial sample remained in the crucible. This amount remained constant upon heating up to 1000°C and corresponded to the amount of silica present in the sample. These results were in concordance with those obtained from elemental microanalysis.

The surface areas and mesoporosity of the materials (Table 4-10) were in the same range as those of the precursor particles (350m<sup>2</sup>/g). In agreement with the nucleotide imprinting polymers, there was a decrease in the surface area, pore volume and pore size as compared with the original silica material. This may be again due to shrinkage upon silica removal.

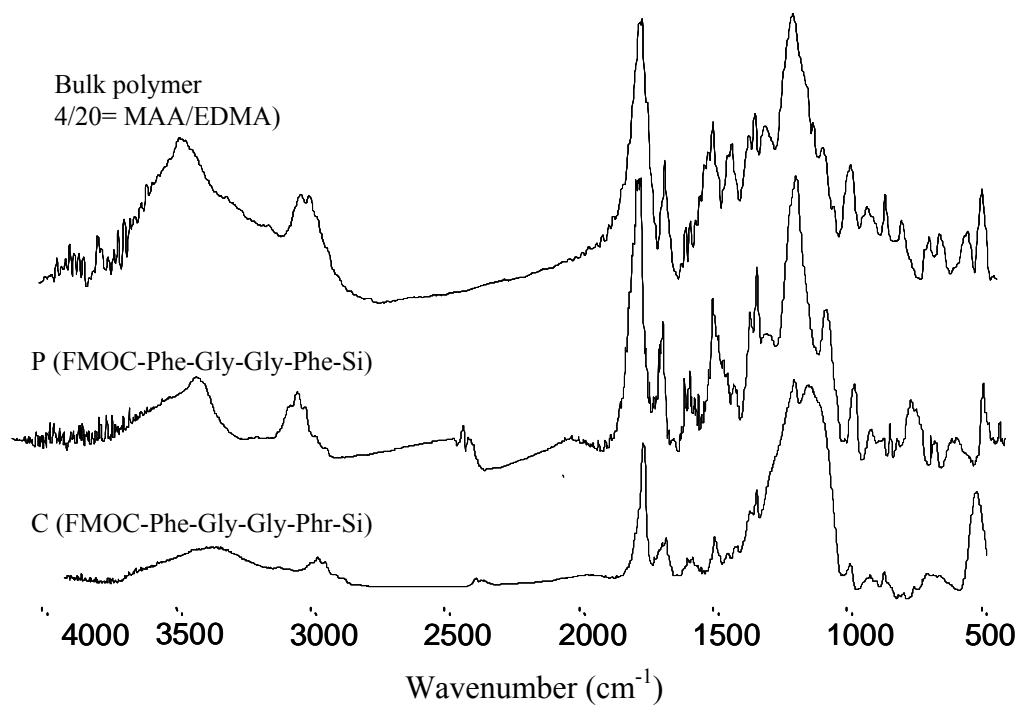


**Figure 4-32:** FT-IR spectra of a bulk polymer, an imprinted composite and the corresponding hierarchical imprinting polymer.

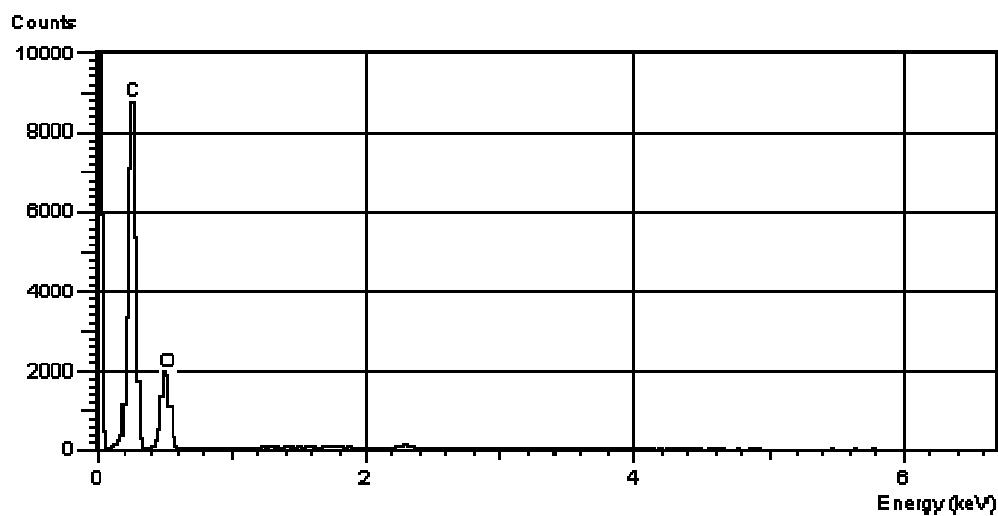


**Figure 4-33:** EDX spectrum of hierarchically imprinted polymer P(Fmoc-Phe-Gly-Si).

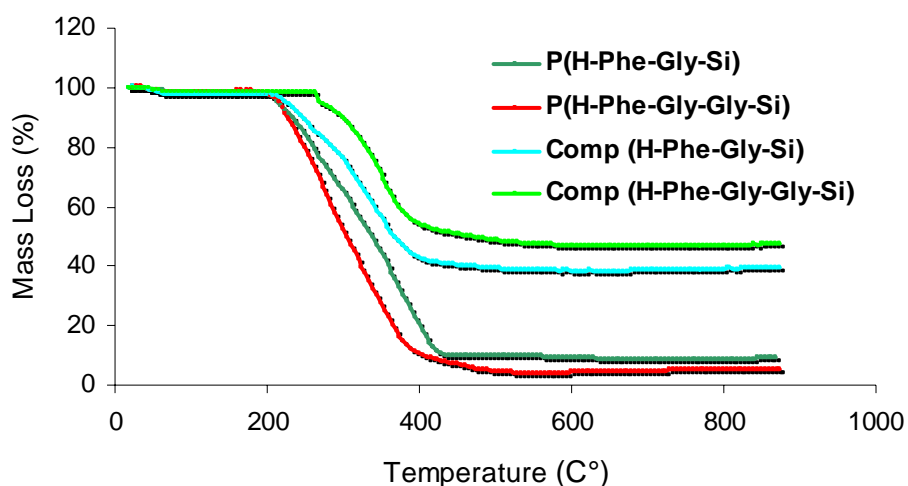


**Figure 4-34:** TGA of the hierarchically imprinted polymers and the corresponding composites.

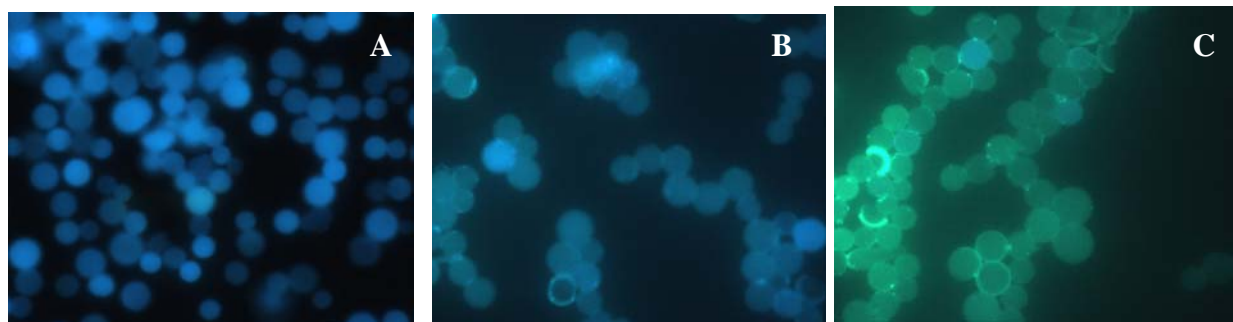


**Figure 4-35:** Fluorescence micrographs at  $\times 100$  magnification of (A)  $P(H\text{-Phe-Gly-Si})$ , (B)  $Comp(H\text{-Phe-Gly--Si})$  and (C)  $Comp(FMOC\text{-Phe-Gly-Si})$ .

Labelling imprinted polymer and composite beads with the fluorescence dye 3-aminoquinoline resulted in enhanced fluorescence intensity for the imprinted polymers (A) in comparison with the composite (B), as a proof of the higher accessibility of the binding sites (Figure 4-35). The successful removal of the template in the dissolution step was visually monitored using the fluorescent microscope, since the composites prepared using the *FMOC* protected amino acids exhibited a strong green fluorescence (Figure 4-35-C) that completely vanished in the corresponding imprinted polymer.

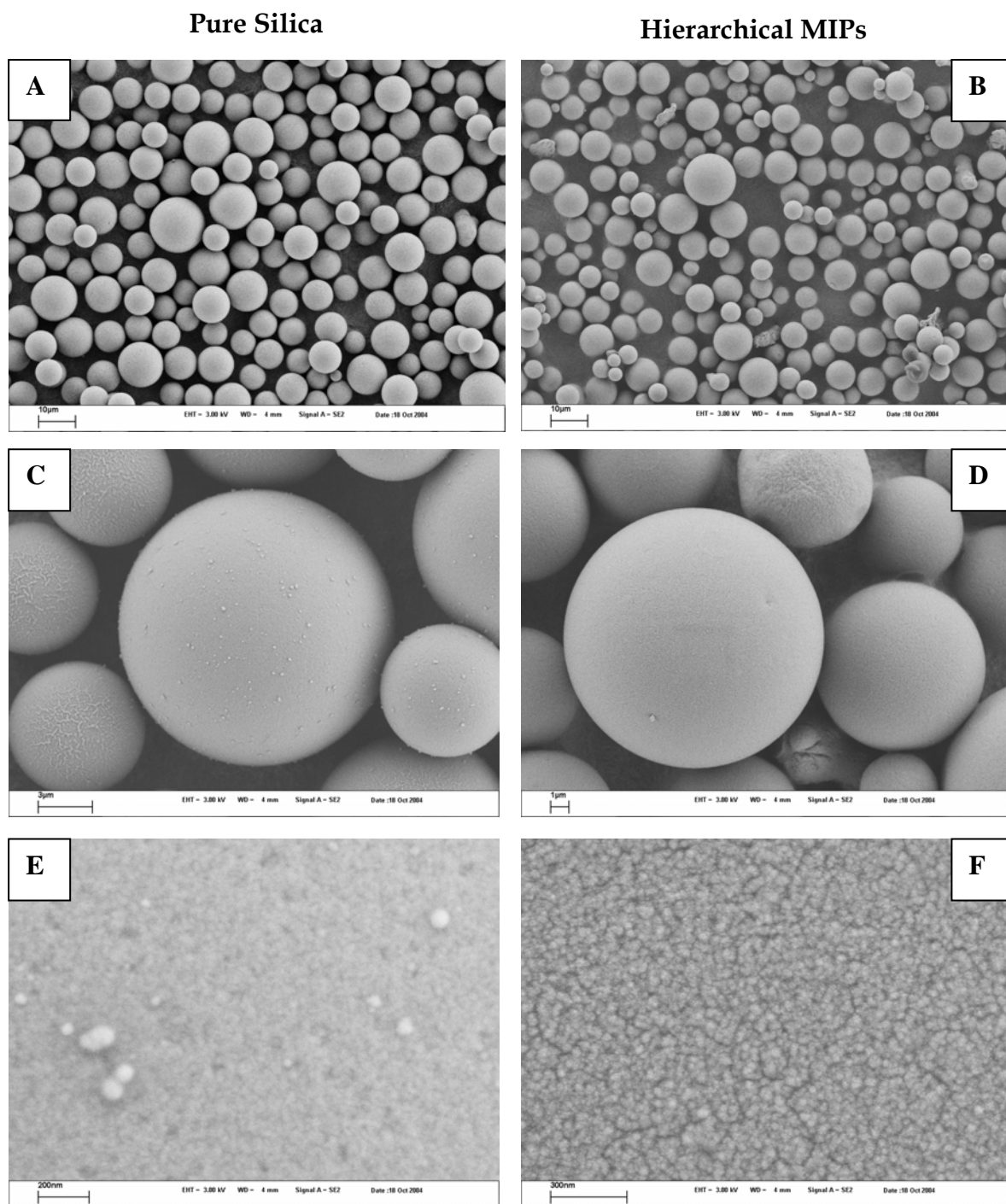


**Figure 4-36:** Scanning electron micrographs of (A, C, E) pure silica at increasing magnifications, (B) P(FMOC-Phe-Gly-Gly-Phe-Si), (D) P(H-Phe-Gly-Si) and (F) P(FMOC-Phe-Si) at the same magnifications as the corresponding silica template on the left side.

The SEM micrographs showed spherical polymer beads with an average particle size of 8  $\mu\text{m}$  and with no agglomeration between particles (Figure 4-36). The particle size of the obtained polymers was slightly smaller than the original silica precursor and they showed the same degree of polydispersity as the pure silica sample. The morphology was very similar with the starting material showing that a successful replicate material had been produced. At higher magnifications (Figure 4-36-E, F) we observed that the surface morphology of the organic hierarchical polymers was different from that of the starting inorganic material. One has also to keep in mind that at very high resolutions the electron beam reacts with the surface of organic polymers.

The internal morphology of these particles was investigated using Transmission Electron Microscopy (TEM). The samples (both the silica precursor and one of the hierarchically imprinted polymers) were incorporated into an epoxy resin, and a cross-section was performed using a diamond cutter. In this way the visualisation of the internal morphology of the particles was possible. Figure 4-37 shows a cross-section inside the silica inorganic template (A) and inside one hierarchical imprinted polymer P(H-Phe-Gly-Si) (B). The morphology inside both materials was to some extent similar, both samples showing pores in the meso range. A clear visualisation of the pores was not possible. Due to the organic nature of the epoxy resin the contrast between the two materials (hierarchical polymer and epoxy resin) was too low for the pores inside the polymer particles to be clearly seen. The pores were observed more clearly in the case of the silica precursor. Overall, the TEM micrographs indicated that the pores in the replicate polymeric material had sizes in the same range as in the inorganic silica with similar shapes. The morphology inside the precursor and final MIP was similar proving once more the successful replication of the inorganic material into a surface imprinted polymer.

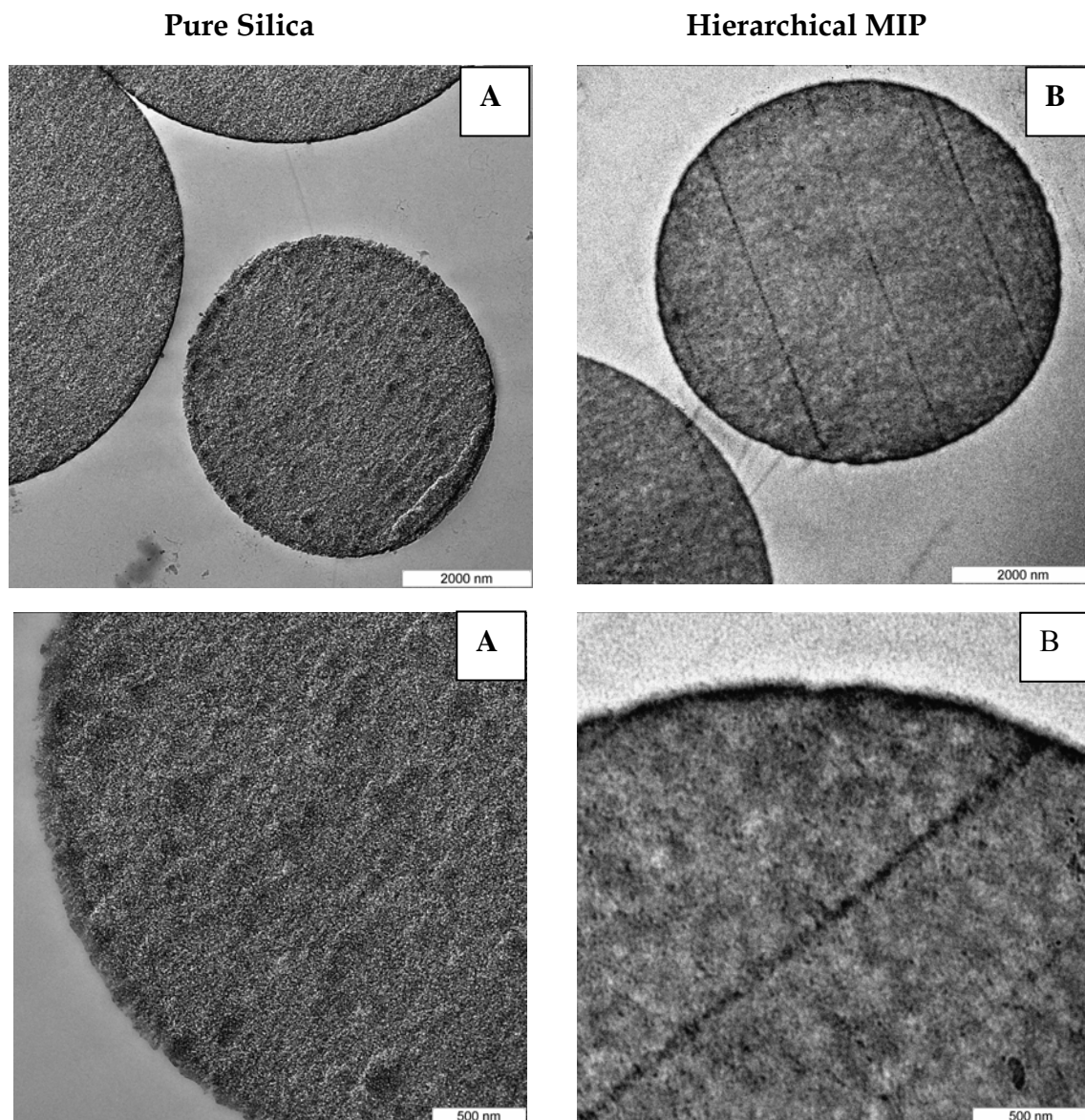


**Figure 4-37:** TEM micrographs of a cross-section inside (A) pure silica particles and (B) P(H-Phe-Gly-Si) hierarchical imprinted polymer particles at two different magnifications.

#### 4.2.5 Assessment of the Imprinted Polymers as Stationary Phases in HPLC

The materials were then assessed as stationary phases in HPLC for their ability to retain the template peptides and larger peptides including the heptadecapeptide Nociceptin, containing the immobilised epitopes.

##### 4.2.5.1 Influence of Covalent Template Immobilisation

My first concern was to investigate the effect of template immobilisation and the extent to which it influences the selectivity and kinetic properties of the formed sites compared to the material prepared from non-immobilised template.

The feasibility of the approach for imprinting of small molecules, *i.e.* nucleotide bases [1] had been demonstrated. However, the benefits of confining the sites to the pore wall surface had not been clearly demonstrated until our second publication on the hierarchical imprinting [2].

For this purpose I compared the two materials prepared using free *FMOC*-Phe-OH (*FMOC*-Phe//Si) and *FMOC*-Phe-OH coupled to APS-Si (*FMOC*-Phe-Si) as templates. As seen in Figure 4-38-A, the polymer obtained using the immobilised template preferentially retained N-protected phenylalanine derivatives, including the dipeptide *FMOC*-Phe-Gly-OH, with *ca.* 5 times larger retention factors (*k*) than those obtained using the polymer imprinted with soluble *FMOC*-Phe-OH as stationary phase. The fact that the dipeptide having the same N-terminal amino acid as the template was more retained than the actual template adds further weight to the idea that the surface-located binding sites can recognise larger molecules containing the imprinted moiety. Meanwhile, phenylalanine derivatives containing free amino groups were retained similarly on both materials. This might be due to the fact that the *FMOC* group also contributes to the recognition process through its carbamate bond. In view of the similar template load used when preparing both materials, the enhanced retention factors seen with the hierarchical materials were likely due to a higher accessibility of the surface-confined binding sites obtained.



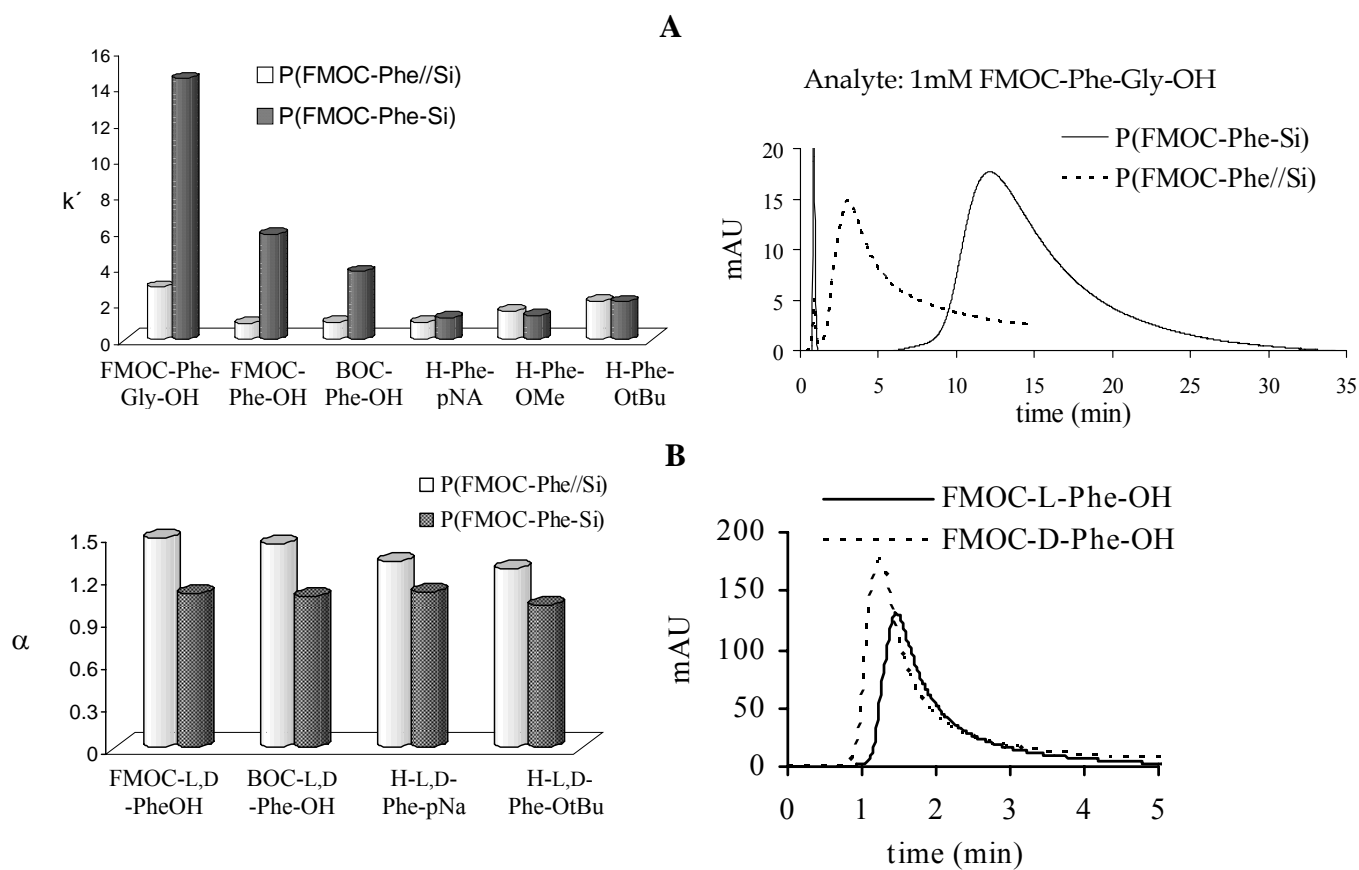


**Figure 4-38:** Retention of amino acid derivatives and peptides injected (10  $\mu$ L of 1mM solutions) on columns (33 x 4 mm i.d.) packed with (A): P(FMOC-Phe-Si) and P(FMOC-Phe//Si) comparing surface and random imprinted polymers; the elution profiles correspond to the dipeptide FMOC-Phe-Gly-OH on the same columns (B): P(FMOC-Phe-Si) and P(FMOC-Phe//Si) comparing the enantioselectivity using acetonitrile as a mobile phase at a flow rate of 0.5 mL/min.

This behaviour contrasted with the observed enantioselectivity of the materials, where P(FMOC-Phe//Si) exhibited a higher enantioselectivity ( $\alpha = k_L/k_D = 1.5$ ) than the surface imprinted material P(FMOC-Phe-Si) ( $\alpha = 1.1$ ) (Figure 3-38-B). Thus the embedded, less accessible sites exhibited higher structural fidelity than surface-exposed sites of higher accessibility. Supporting evidence for such a phenomenon is provided by the work of Gagne [166] on the relationship between site accessibility and fidelity in chiral, bis-naphtol imprinted materials. It should be mentioned that the use of these polymers as CSPs was not the aim of the study. The enantioselectivity of the imprinted polymers was checked only in this particular case for comparison with the “randomly” imprinted one.

The poor enantioselectivity exhibited by the hierarchical imprinted materials may also be due to possible racemisation of the template during the immobilisation step. If one wishes to apply hierarchical imprinting for chiral separations, a possible modification to the present method could be the use of a different coupling agent (*e.g.* PyCloP, PyBroP, PyBOP, PyPOP *etc.* [167]). These coupling agents are known to better solve the problems associated with racemisation during peptide synthesis. After demonstrating the substantial enhancement in retentivity due to the surface confinement, we focused only on the hierarchically imprinted materials.

#### 4.2.5.2 Selectivity of Mono- and Di-Amino Acid Epitope Imprinted Polymers towards Small Amino Acid Derivatives

The dipeptide imprinted materials exhibited interesting retention behaviours. As seen in Figure 4-39, *FMOC*-Phe-Gly-OH is *ca.* two times stronger retained on P(*FMOC*-Phe-Gly-Si) than on P(*FMOC*-Phe-Si) and *ca.* 15 times stronger than on P(*FMOC*-Gly-Si). However, since similar relative retentions were seen for *FMOC*-Phe-OH on the three materials this indicated that the main contribution to the affinity is a different surface density of templated sites. Such a difference can be expected from the different template coverages on the surface of the silica mold. Retention of a possible solute correlates with the amount of accessible sites and their affinity for the solute. In view of *ca.* 6 times higher ligand coverage of *FMOC*-Phe-Gly-Si (1.81  $\mu\text{mol}/\text{m}^2$ ) as compared with *FMOC*-Phe-Si (0.27  $\mu\text{mol}/\text{m}^2$ ) (Table 4-9) and the doubling of the retention of *FMOC*-Phe-Gly-OH substrate, it seemed that the site density was the controlling factor rather than the affinity of those sites towards the target. It was also clear that glycine contributes only weakly to the observed retention. Thus, *BOC*-Gly-OH, H-Gly-OEt and H-Gly-Phe-OH were retained weakly on all the above materials, but still  $\sim 2$  times more retained on the polymers imprinted with the Gly motif P(*FMOC*-Gly-Si) and P(*FMOC*-Gly-Phe-Si) than on P(*FMOC*-Phe-Gly-Si) and P(*FMOC*-Phe-Si). A similar trend was observed on the imprinted polymers prepared using the corresponding deprotected epitopes (Figure 4-39). Overall the retention factors were lower since the *FMOC* group is probably also taking part in the recognition process through its carbamate bond.

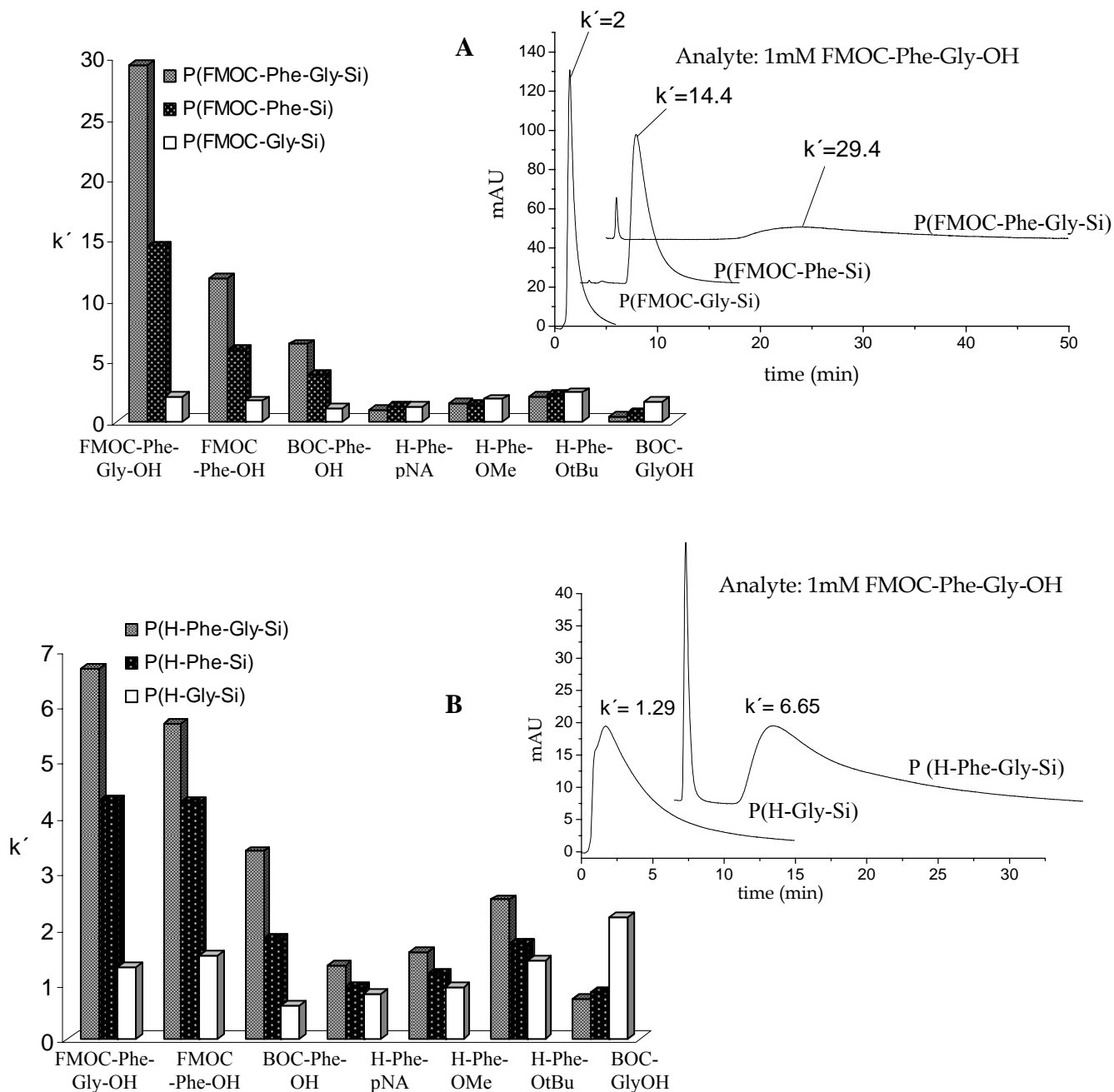


**Figure 4-39:** Retention of amino acid derivatives and peptides injected (10  $\mu$ L of 1mM solutions) on columns (33 x 4. mm i.d) packed with (A): P(FMOC-Phe-Gly-Si), P(FMOC-Phe-Si), and P(FMOC-Gly-Si) using acetonitrile as a mobile phase at a flow rate of 0.5 mL/min; (B): P(H-Phe-Gly-Si), P(H-Phe-Si), and P(H-Gly-Si) using acetonitrile as a mobile phase at a flow rate of 0.5 mL/min; The elution profiles correspond to FMOC-Phe-Gly-OH according to the data shown in the diagrams.

FMOC-Phe-Gly-H was more retained on the polymer imprinted with P(H-Phe-Si) than the direct complement P(H-Phe-Gly-Si). The explanation was found again in the density of imprinted sites (Table 4-9).

As expected, there was a slight increase in the retention of the free N-terminal analogues in comparison with the *FMOC* protected polymers. The resulting binding sites were then more favourable in terms of shape and functionality for the free N-terminus amino acids. The same weak retention was registered for all the analytes on the glycine imprinted polymer, except for its direct complement, which is retained with  $k= 2.2$ .

#### 4.2.5.3 Selectivity of Mono- and Di-Amino Acids Epitope Imprinted Polymers towards Larger Peptides

For biological applications, the retention behaviour in aqueous mobile phases is important. With 5% water (Figure 4-40) a pronounced selectivity for peptides containing the imprinted dipeptide motif was seen. This included also larger peptides containing the H-Phe-Gly motif as N-terminus. Thus, H-Phe-Gly-Gly-Phe-OH was similarly retained to H-Phe-Gly-CONH<sub>2</sub>, with a retention factor of almost 6 on P(*FMOC*-Phe-Gly-Si). This exceeded the retention observed on the exact complement P(H-Phe-Gly-Si). A plausible explanation for this behaviour was found in the amount of immobilised ligands and how they were presented at the surface. The free amino groups resulting from the deprotection may have interacted with neighbouring silanol groups, leading to a poor orientation of the ligand for the creation of high fidelity templated sites; this would have not occurred for the protected counterpart. Further evidence for the presence of peptide discriminating sites was provided by the retention behaviour of dipeptide H-Gly-Phe-OH with the inverse amino acid sequence. Opposite to the other dipeptides this was most strongly retained on the materials imprinted with the structurally closest complements used in this study, namely H-Gly-Si, *FMOC*-Gly-Si and *FMOC*-Gly-Phe-Si. Finally, the heptadecapeptide Nociceptin was *ca.* 2 times more strongly retained on the dipeptide N-terminus complement P(H-Phe-Gly-Si) than on P(H-Gly-Si) and 1.2 times more retained on the P(*FMOC*-Phe-Gly-Si) than on P(*FMOC*-Gly-Si).

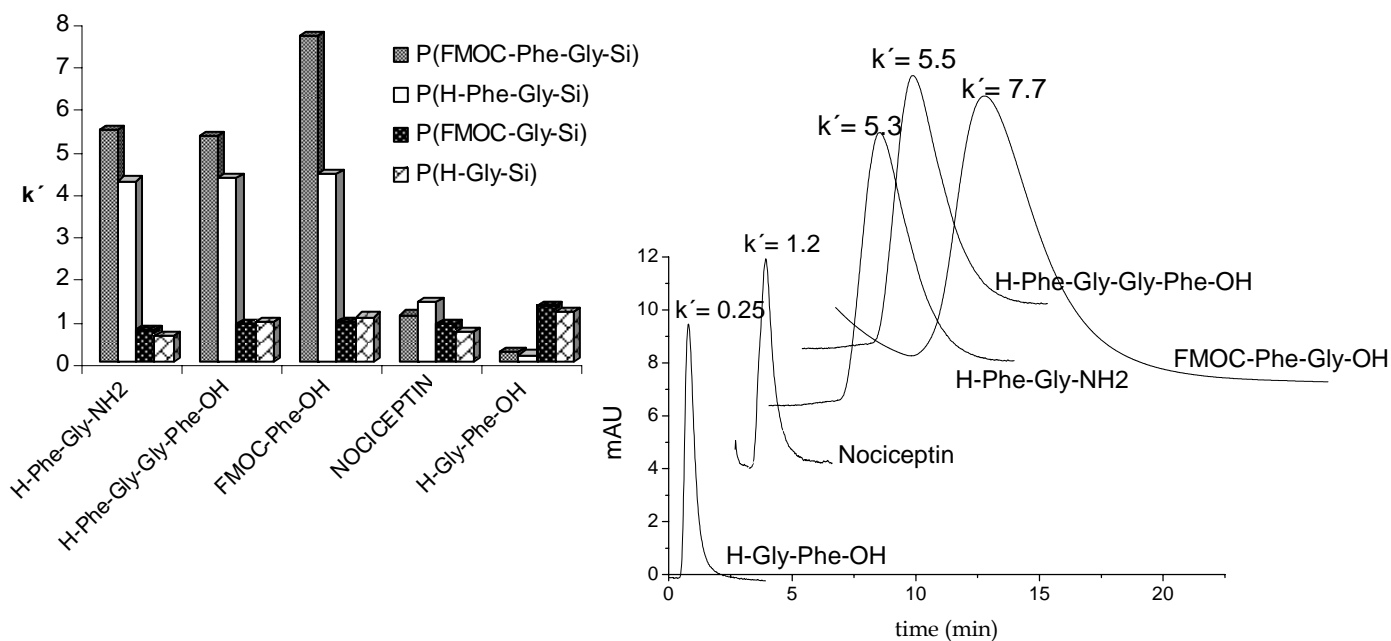


**Figure 4-40:** Retention of amino acid derivatives and peptides injected in a mobile phase containing 5% water in acetonitrile buffered with 1% acetic acid at a flow rate of 0.5 ml/min. on the following columns: P(FMOC-Phe-Gly-Si), P(H-Phe-Gly-Si), P(FMOC-Gly-Si) and P(H-Gly-Si). The elution profiles correspond to the data presented in the diagram on the column packed with P (FMOC-Phe-Gly-Si).

Upon increasing the content of water in the mobile phase to 10 and 20 %, a dramatic decrease in the retention factors was observed (Figure 4-41). We hoped to overcome this problem and be able to recognise larger molecules in more competitive mobile phase by increasing the size of the immobilised epitope.

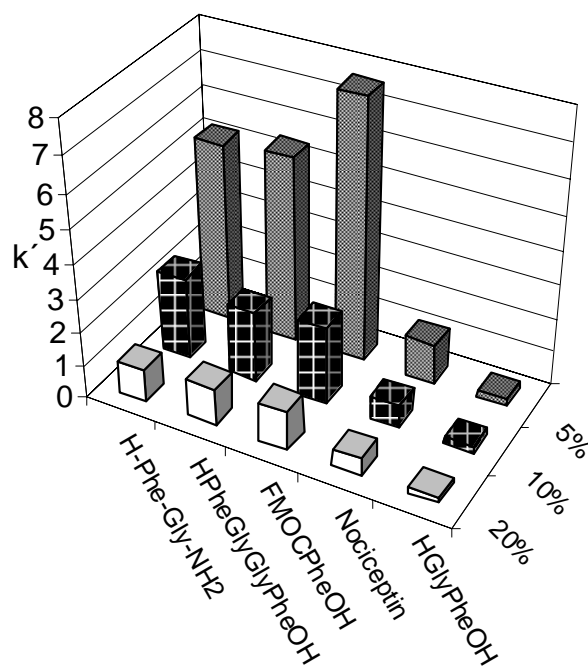


**Figure 4-41:** Decrease of retention factors with increasing water content in the mobile phase on the column packed with P(FMOC-Phe-Gly-Si).

#### 4.2.5.4 The Effect of Epitope Size on Retention of Larger Peptides

After evaluating the mono- and dipeptide materials, we investigated the effect of the immobilised epitope size on the retention behaviour of the imprinted polymers. Thus, we compared the selectivity against larger peptides, including Nociceptin, on the polymers prepared from tri- and tetrapeptides. Fortunately, our expectations were fulfilled and the retention increased with the size of the template (Figure 4-42). As shown before, the *FMOC* protected mono- and dipeptide imprinted materials showed high affinity for the corresponding dipeptide *FMOC-Phe-Gly-OH*. The retention of this dipeptide decreased on the tri- and tetrapeptide imprinted materials possibly due to the fact that the resulting binding sites exhibited less structural fidelity for this smaller analyte. The retention of the larger tri- and tetrapeptides increased as we moved to larger epitope imprinted polymers. Thus, H-Phe-Gly-Gly-Phe-OH was retained 3.5 times more on the tri- and tetrapeptide imprinted materials than on the mono amino acid imprinted analogue and 1.4 times more than on the dipeptide material (Figure 4-42-A). A clear increase in the selectivity towards Nociceptin was also observed on the larger epitope imprinted materials.

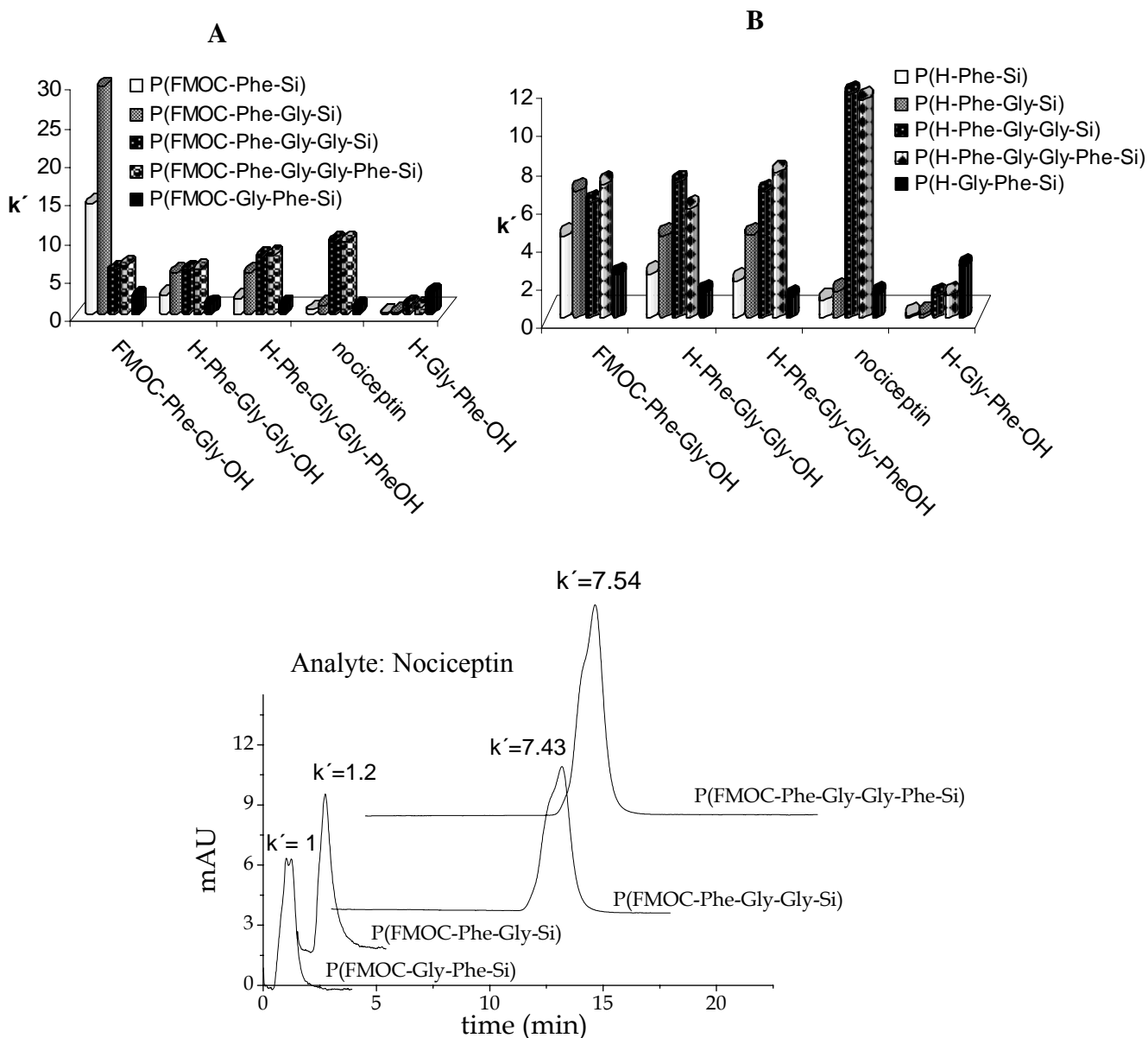


**Figure 4-42:** Retention of peptides injected in a mobile phase containing 5% water in acetonitrile buffered with 1% acetic acid at a flow rate of 0.5 ml/min on the following columns: (A)-P(FMOC-Phe-Gly-Si), P(FMOC-Phe-Gly-Gly-Si), P(FMOC-Phe-Gly-Gly-Phe-Si) and P(FMOC-Gly-Phe-Si). (B)- P(H-Phe-Gly-Si), P(H-Phe-Gly-Gly-Si), P(H-Phe-Gly-Gly-Phe-Si) and P(H-Gly-Phe-Si). The elution profiles correspond to Nociceptin according to the data presented in (A).

It was 8.5 times more retained on the tri- and tetrapeptide imprinted materials than on the one prepared with the immobilised dipeptide. From this observation we concluded that the size of the immobilised epitope plays an essential role in the recognition process and that even only one or two amino acids in the immobilised sequence can play a very important role in the recognition process towards larger targets. The critical epitope size in this case was three amino acids. The inverse

---

sequence H-Gly-Phe-OH was weakly retained on all the imprinted materials except its direct analogue P(FMOC-Gly-Phe-OH). Also, there was a very poor retention of all the other analytes on the polymer prepared with this inverse sequence P(FMOC-Gly-Phe-OH). Similar behaviour was also exhibited by the materials prepared using the deprotected templates (Figure 4-42-B). In this case, Nociceptin was also more strongly retained on the materials imprinted with the tri- and tetrapeptide epitope materials, 8.5 times more retained on the tetra-imprinted material than on the corresponding dipeptide, an observation in perfect agreement with the previous case.

As shown in section 4.2.5.2 for the dipeptide imprinted polymers, the retention decreased once we moved to more aqueous mobile phases. Given the dramatic increase of the retention factors for the tri- and tetrapeptide imprinted materials using an organic based mobile phase, we investigated the behaviour of these materials in water-containing mobile phases.

Using a mobile phase containing 30 % water in acetonitrile, lead to the results shown in Figure 4-43. When comparing these results with those obtained in the mobile phase containing only 5 % water, little difference was seen in the retention factors (Figure 4-43). With increasing the epitope size, not only was the retention against larger peptides containing the immobilised epitope considerably increased, but it was maintained in more aqueous environments. This observation makes the method suitable for biological applications where the recognition of large biomolecules in aqueous media is required.



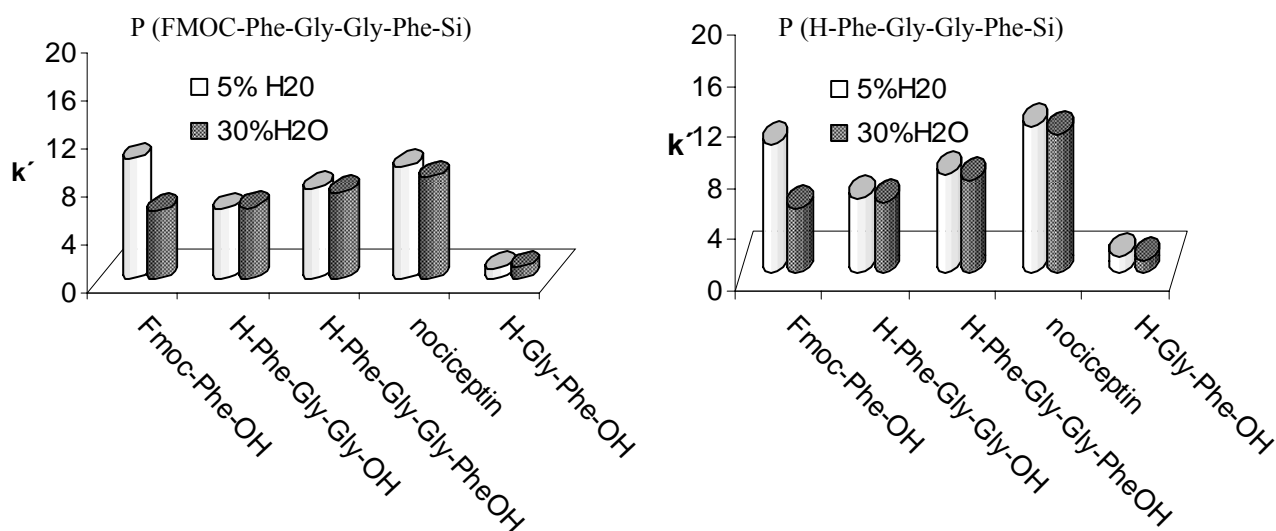


**Figure 4-43:** Comparison between the retention factors on the tetrapeptide imprinted materials in two different mobile phases containing 5% or 30% water in acetonitrile buffered with 1% acetic at a flow of 0.5 ml/min.

#### 4.2.6 Conclusions

In order to create synthetic receptors for larger biomolecules inspiration was taken from nature. In recognising an antigen, an antibody interacts only with a small part of it, the epitope. Hence, I applied the developed hierarchical technology and used shorter immobilised peptides representing only a small exposed fragment of a larger peptide structure. In this way the resulting mesoporous MIP was able to retain the whole peptidic structure. This has led to new recognition elements for biological macromolecules that may include, apart from the here described peptide phases, nucleic acids and oligosaccharides.

The advantages of confining the binding sites to the surface of the polymers through covalent immobilisation was clearly demonstrated. Furthermore, the importance of immobilised epitope size was revealed. It should be noted that epitopes are described as surface domains composed of three to six amino acid residues. A clear increase in the retention of a heptadecapeptide was observed on the polymers prepared using three and four amino acid residues. The retention behaviour was maintained also in aqueous environments, proving the general applicability of this method for biological applications.

### 4.3 IMPORTANCE AND OUTLOOK

A specific application of hierarchical epitope imprinting could, for example, consist in the generation of artificial receptors for Alzheimer's disease.

Alzheimer's disease (AD) is the most common cause of late life dementia and the fourth leading cause of death in the developed world. Although the cause of the disease is not fully understood, recent research suggest that deposition of cerebral amyloid plaques is central to the disease process. Therefore an attractive therapeutic strategy is to prevent, reduce or reverse the formation of amyloid plaques. Amyloid deposits mainly comprise aggregates of a 39-42 residue protein called  $\beta$ -amyloid ( $\beta$ -A). The peptide is derived by proteolytic cleavage of Amyloid Precursor Protein (APP), a transmembrane protein. The larger peptides (42-43 residues) are theorised to be more potent for aggregation and thus, plaque formation and neuronal death (Figure 4-44).

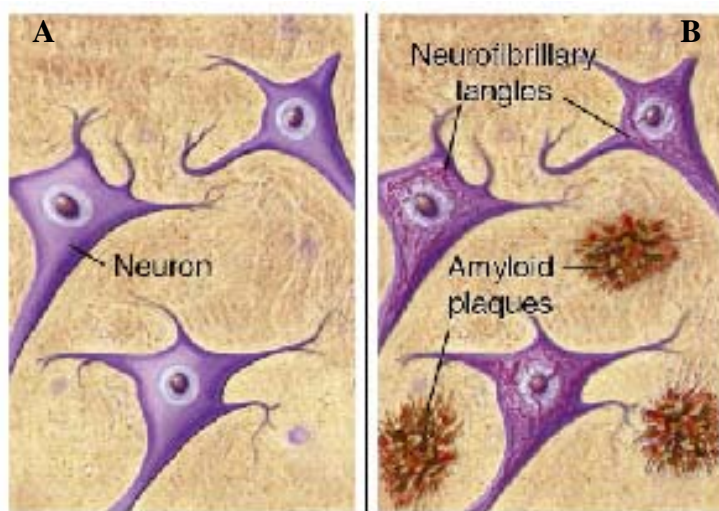


**Figure 4-44:** (A) Healthy neurons; (B) Alzheimer's disease.

Therefore, there is an increased interest on the separation and differentiation between the several amyloid forms. Applying "hierarchical imprinting", shorter peptide sequences (3-7 residues of both termini of the suspect peptides) could be used as "epitopes" for the generation of binding sites.

Different epitopes could be used corresponding to the different peptides (A1-40 peptide, A1-41 peptide, A1-42 peptide, A1-43 peptide):

1-40: DAEFRHDSGYEVHHQKLVFFAEDVGSNKGAIIGLMVGGVV

1-41: DAEFRHDSGYEVHHQKLVFFAEDVGSNKGAIIGLMVGGVVI

1-42: DAEFRHDSGYEVHHQKLVFFAEDVGSNKGAIIGLMVGGVVIA

1-43: DAEFRHDSGYEVHHQKLVFFAEDVGSNKGAIIGLMVGGVVIAT

To distinguish between these peptides, epitopes corresponding to the C-termini (underlined above) could be immobilised to a silica surface, as described herein, and the crude products used for the generation of hierarchically imprinted polymeric receptors against each peptide. Thus, a series of MIPs, each capable of selective and preferential binding to a particular peptide could be prepared, *i.e.* a “plastic antibody” for each of these peptides. These may ultimately substitute the more labile biological receptors (antibodies) and develop new assays or biosensors. A potential strategy for epitope immobilisation to generate these plastic antibodies against amyloid peptides is shown in Figure 4-45. Immobilisation of the identical N-terminus of these peptides could serve for peptide pre-concentration and sample enrichment of all the amyloid peptides.

For this particular potential application of “hierarchical imprinting”, studies of peptide conformation in various environments are necessary in order to obtain information concerning peptide folding and 3-D structure. Another parameter will be the selection of appropriate functional monomer(s) and cross-linker(s). Molecular interactions of novel monomer(s) with the epitope templates have to be studied in order to achieve the highest affinity in monomer-template complex. These studies can be performed using binding experiments and affinity measurements with techniques such as NMR titration.

It has been reported that fibril formation may precede any clinical symptom by decades. The development of such advanced materials, which will provide and promote diagnostic tools, may contribute to early stage diagnosis of the disease. Early awareness will facilitate therapeutic intervention and follow-up treatment.

Additionally, recent clinical reports in the USA and Europe claim that early diagnosis may greatly reduce treatment costs, which reach up to 30,000 euro for a six month treatment.

This is but one example of a potential application of hierarchical imprinting. The principle can be extended to other target peptides or biomolecules associated with early diagnosis or to sample pre-concentrations in the field of proteomics.

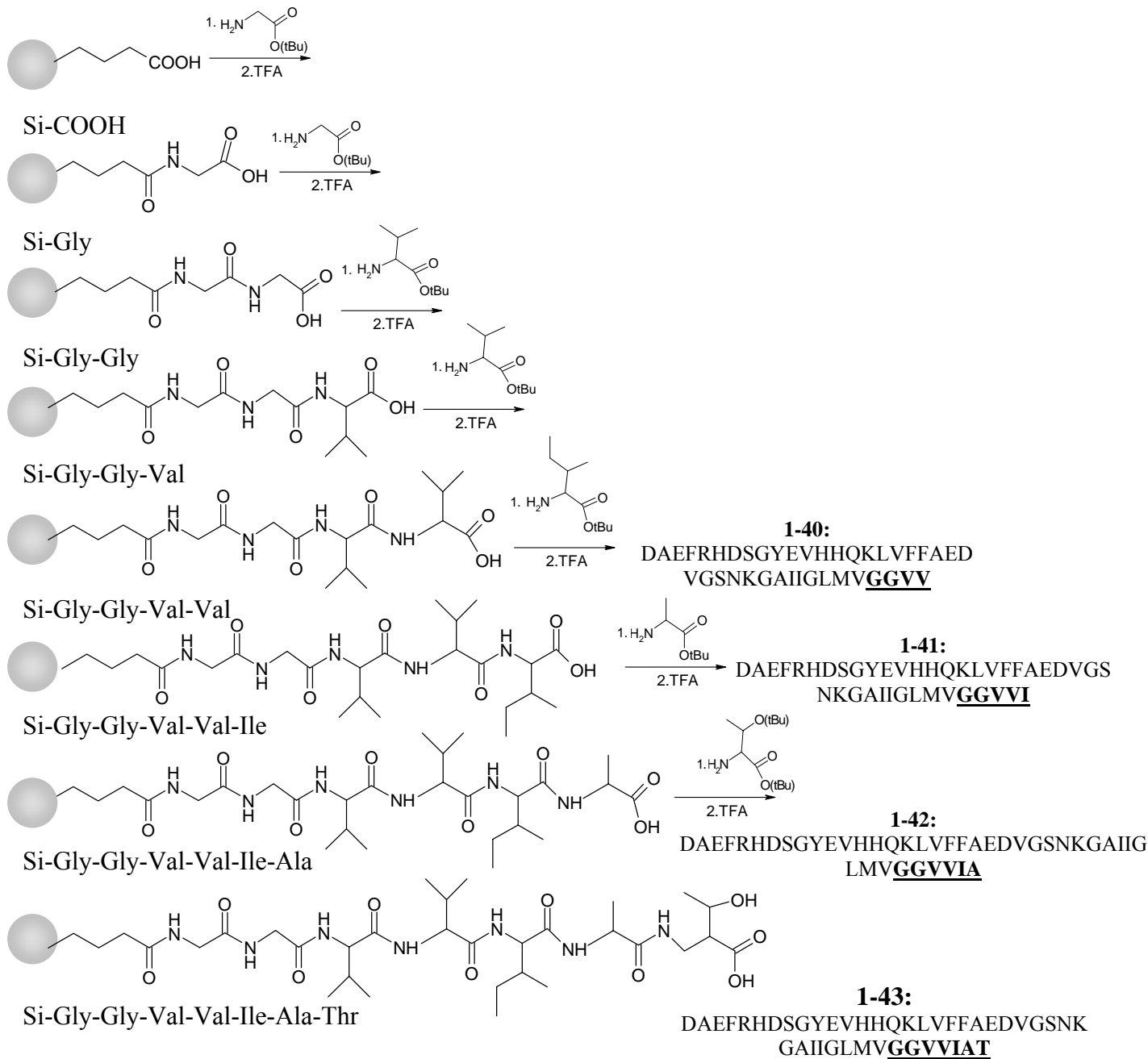


**Figure 4-45:** Strategy for solid phase synthesis of epitopes corresponding to amyloid peptides.

## 5 RESULTS AND DISCUSSION (II): THIN FILM MIP-COMPOSITES

Starting from an inorganic support of known morphology, composites can be synthesised by grafting of an organic polymer film onto its surface. As described in section 3.5, grafting can be performed following essentially two different methods, namely “grafting to” or “grafting from”. In the first method, the polymerisation is initiated in solution and the growing radicals attach to the surface by addition to surface-pendant double bonds. This implies that the polymer is coupled to the surface through reactions involving oligomers or polymers, which can limit the density of grafted polymer. However, in the latter approach the polymerisation is started at the surface by surface-immobilised initiator species or *in situ* generated radicals. This leads to reactions mainly between monomers and surface confined radicals, resulting in a higher density of grafted chains.

When performing the grafting under conventional polymerisation conditions, the thickness of the layers is difficult to control and significant propagation occurs in solution. Controlled radical polymerisation (CRP) offers benefits in this regard. CRP techniques distinguish themselves from conventional radical polymerisations in the lifetime of the growing radical, which can be extended to hours, thus allowing the preparation of polymers with pre-defined molecular weights, low polydispersity, controlled composition and functionality. By performing “grafting from” under CRP conditions, polymer films with controllable thickness, composition and structure can thus be prepared. Furthermore, CRP with living character allows layer-by-layer grafting of different polymers with different functions or characteristics (e.g. polarity, molecular recognition or catalytic properties).

## 5.1 LIVING RADICAL POLYMERISATION

Living Radical Polymerisation was first discovered by Szwarc [168,169] who stated that for a polymerisation to be considered “living” it should meet the following requirements:

- The polymerisation proceeds to full conversion; further addition of monomer leads to continued polymerisation.
- The number average molar mass is linearly dependent on conversion.
- The number of polymer chains is constant during polymerisation.
- The molar mass can be controlled by the reaction stoichiometry.
- The polydispersity of the polymer molar mass distribution is low.
- Chain-end functionalised polymers can be obtained quantitatively.
- In radical polymerisation, the number of active end groups should be two; one for each chain end.

Therefore, by definition, living polymerisations allow the preparation of complex macromolecular architectures in a controlled manner.

During the last decade of the past millennium, living polymerisations underwent a revival by the application of radical chemistry. The onset of this revival can be traced back to the early 1980s, when Otsu discovered that the addition of certain compounds (*e.g.* dithiocarbamates, disulfides) to a radical polymerisation resulted in a system that exhibited some living characteristics [170]. Otsu introduced the term *iniferter* for this technique because the dithiocarbamates acted as initiators as well as transfer and termination agents (reaction a-d in Figure 5-1).

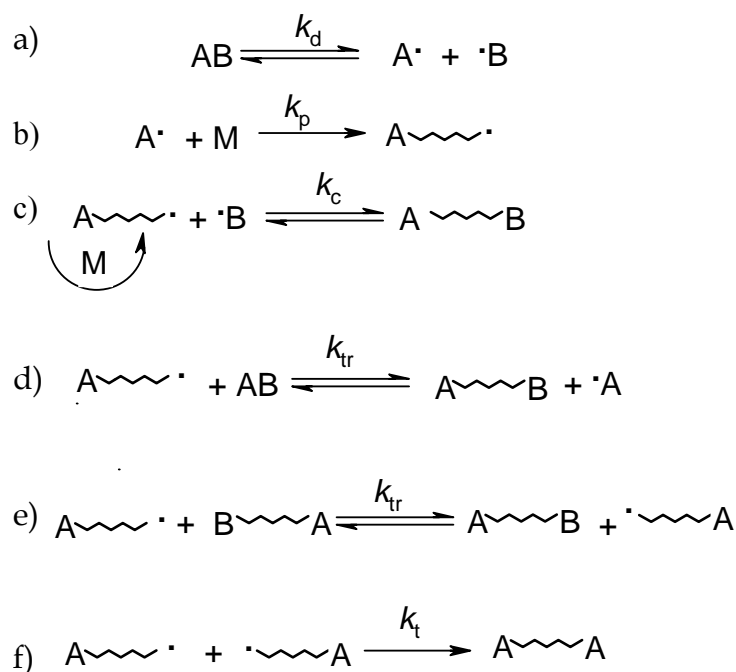
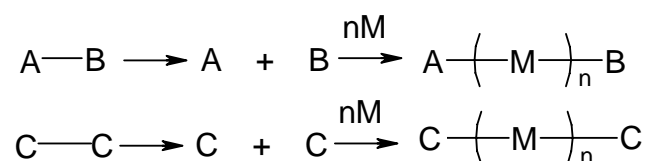


**Figure 5-1:** General mechanism of living radical polymerisation with iniferters.

Iniferter AB dissociates thermally or photochemically, forming a reactive radical A and a stable radical B (a). A initiates polymerisation (b) and can be deactivated by coupling with B (c). This is a reversible process. Transfer to iniferter (d) and transfer to dormant polymer (e) are other possible reactions that may occur depending on the structure of the iniferter. Besides, as in any free radical process, bimolecular termination takes place (f) by combination or disproportionation. The number of monomer units taken up during each cycle in the iniferter process was estimated to be around 30 resulting in high polydispersities. This was caused by the relative low activity of B as a deactivator. The iniferter dissociates into two different radical species (reaction a). One of these species is able to add to monomer and form a growing polymer chain (reaction b). The other radical should be inactive in this respect and serves only to terminate the growing polymer chain (reaction c). The species generated in this process is a dormant polymer chain, which can be reactivated photochemically or by thermal energy, allowing gradual growth through polymerisation.

Several iniferters include sulfides, phenylazo compounds, amines, alkoxyamines, halides and thiols. These are examples of A-B type iniferters. Peroxides, disulfides, and tetraphenylethanes are C-C type of iniferters. Iniferters divide further into thermal- or photo-iniferters, monomeric or polymeric iniferters and single or two-component (redox) iniferters. The two main types of iniferter act as shown in Scheme 5-1.

Scheme 5-1



A· is a reactive radical that participates in initiation and B· is a less reactive or non-reactive radical having the main function of entering into primary termination (PR) to give the polymer. The iniferter used in this thesis to perform grafting under controlled radical conditions is benzyl-*N,N*-diethyldithiocarbamate and belongs to the A-B category. Because one of the radicals formed upon its decomposition is a poor initiator, through immobilisation, the active radical will be covalently attached to the support and the inactive radical will be present in solution (Figure 5-17).

In the case of C-C-type iniferters, the two C· are less reactive radicals that participate in both initiation and PR termination, leading to a final polymer in which n is the total number of inserted molecules. The C-C type iniferters have several disadvantages when compared with A-B type, including the inability to control the reactivity of C· towards initiation or PR and the risk of the iniferter function changing from C-C type to A-B type during the polymerisation.

In 1984, LRP was reported by Rizzardo *et al.* [171,172]. These authors reported the application of stable nitroxide radicals as deactivators. The activation and deactivation rate constants resulted in rapid deactivation of propagating radicals and an equilibrium which was shifted strongly to the dormant side.

Referring to Figure 5-1, reactions d) and e) do not take place in nitroxide mediated polymerisation, and the system relies exclusively on reversible termination.

Once the initiator has been converted to dormant species an equilibrium is



established between the active chains and dormant species. Propagating species and deactivating persistent radicals (*i.e.* nitroxides) are generated in equimolar amounts. Propagating species are slowly taken out of this equilibrium via bimolecular termination resulting in an excess of nitroxide that shifts the equilibrium to the left, increasing the level of control over the reaction, but also decelerating polymerisation (Figure 5-2).

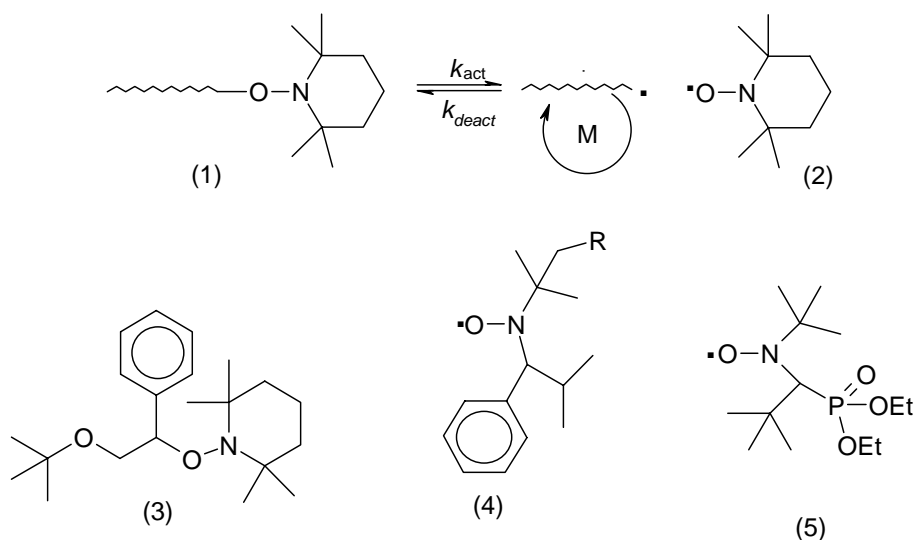


**Figure 5-2:** The activation-deactivation equilibrium in nitroxide mediated polymerisation.

An alkoxyamine (1) dissociates reversibly to produce a radical, which can add monomer, and the persistent 2,2,6,6-tetramethylpiperidine-N-oxyl (2, TEMPO) radical. A typical example of an initial alkoxyamine structure (3) that is applied as initiator for *e.g.* polymerisation of styrene- 2,2,5-trimethyl-3-(1'-phenylethoxy)-4-phenyl-3-azahexane (4) and N-tert-butyl-N-[1-diethylphosphono-(2,2-dimethylpropyl) nitroxide (5), are two examples of more versatile nitroxides applicable to *e.g.* acrylates and conjugated dienes as well.

Another living radical polymerisation technique based on reversible deactivation is atom transfer radical polymerisation (ATRP) [173,174]. This system utilizes a transition metal complex to deactivate a propagating radical by transfer of a halogen atom to the polymer chain-end, thereby reducing the oxidation state of the metal ion complex (Figure 5-3). A halide atom X (*e.g.* Br, Cl) is transferred from the alkyl halide initiator to a transition metal complex M (*e.g.* Cu, Fe) upon which a radical is formed

that initiates polymerisation. The same type of equilibrium is established between propagating radicals and dormant, halogen end-capped polymer chains.

A widely investigated system is based on copper (with a transition of Cu(II) into Cu(I)), but also nickel, palladium, ruthenium and iron qualify as suitable candidates. The halogen is usually bromine or chloride. The process can be applied to a wide range of monomers and at mild reaction, though it must be said that traces of oxygen can have a much dramatic effect on the reaction rate than in a conventional radical polymerisation. A further drawback, restricting industrial application, is the presence of considerable amounts of metal in the product. Nonetheless, numerous well-defined complex polymer architectures have been prepared with ATRP [175,176].

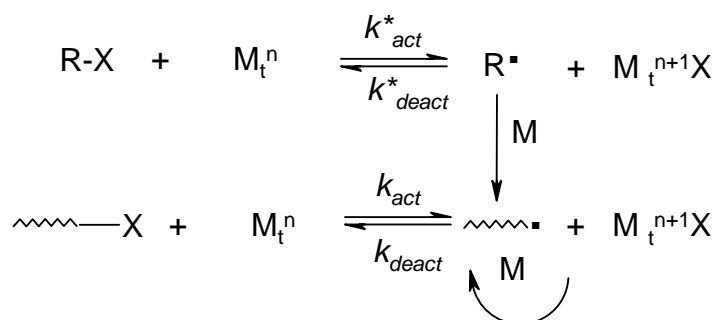


**Figure 5-3:** General scheme of reversible deactivation in Atom Transfer Radical Polymerisation.

Much more dynamic by nature are living radical polymerisations based on degenerative transfer reaction schemes (Figure 5-4). In contrast with the above mentioned living polymerisation techniques, here radicals are generated by a conventional initiator. Transfer takes place to an alkyl iodide (e.g. 1-phenylethyl iodide), end-capping the propagating chain with an iodine atom. Equilibrium is established between propagating chains and dormant iodine-ended chains. The disadvantage with this technique is that the rate coefficient is relatively low (e.g. for 1-phenylethyl iodide  $k_{tr} = 2400 \text{ dm}^3 \text{ mol}^{-1} \text{ s}^{-1}$  for styrene at  $80^\circ\text{C}$  [177]) such that starved conditions have to be used in order to obtain low polydispersities.

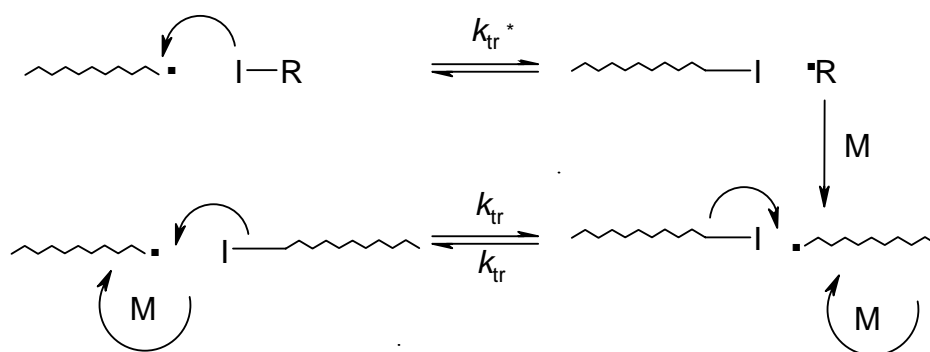


**Figure 5-4:** General scheme of degenerative transfer.

The most recent technique to achieve controlled polymerisation is Reversible Addition Fragmentation chain Transfer Polymerisation (RAFT) [6,178].

Methacrylate monomers were the first species used as RAFT agents. The discovery of cobalt complexes that acted as catalytic chain transfer agents allowed the facile preparation of short methacrylate oligomers with a terminal carbon-carbon double bond (Figure 5-5). It was found that these macromonomers could be applied as chain transfer agents, operating *via* the so-called addition-fragmentation process [179]. When applied in the polymerisation of the same or another methacrylate monomer, the process is reversible (Figure 5-5).

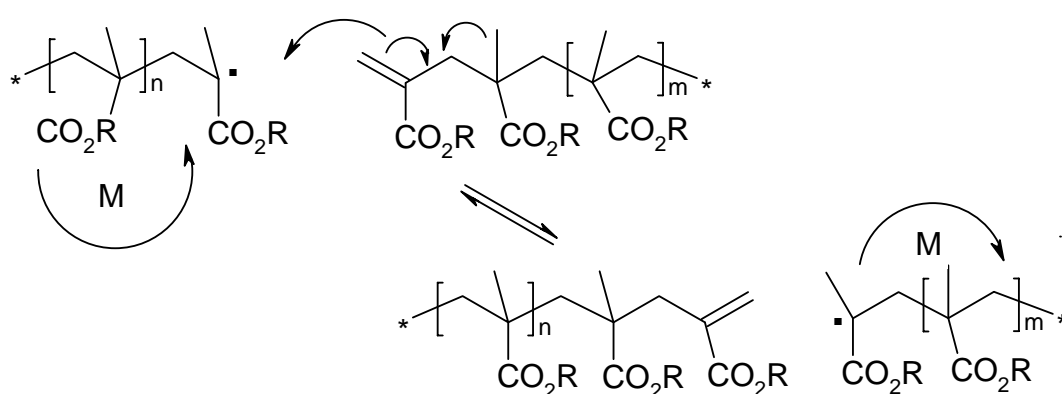


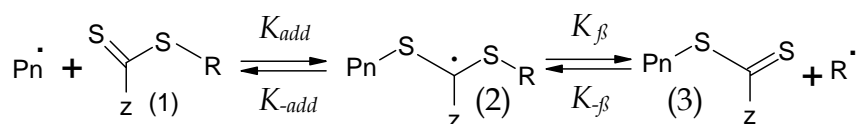
**Figure 5-5:** Reversible addition-fragmentation chain transfer using methacrylic macromonomers.

Due to the high reactivity of these macromolecules a high monomer concentration would lead to the transfer reaction being unable to compete with propagation.

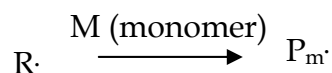
Obviously, for such a process to be generally applicable in batch reactions, more reactive transfer agents would be required. These were found in the form of dithioesters [6,180], selected dithiocarbamates [181,182], xanthates [181] and trithiocarbonates [181]. These molecular structures were remarkably similar to the original iniferters, but were optimised for more efficient transfer reactions.

These RAFT agents function by establishing a dynamic equilibrium between propagating radicals ( $P_n\cdot$ ) and dormant chains by a mechanism of reversible addition-fragmentation chain transfer, as shown in Figure 5-6. Propagating radicals are generated as in a conventional radical polymerisation, *i.e.* thermally, photochemically. The RAFT agent (1) is transformed into a polymeric RAFT agent (3) through reaction with a propagating radical ( $P_n\cdot$ ) *via* an addition-fragmentation process. The radical liberated ( $R\cdot$ ) then reacts with monomer to form a new propagating radical ( $P_m\cdot$ ). Chain extension of the polymeric RAFT agent (3) involves essentially the same process. The reversible addition-fragmentation steps transfer the  $S=C(Z)S$  moiety between active and dormant chains and provide a mechanism for all chains to grow with similar rate and uniformity.

#### Addition-Fragmentation Chain Transfer



#### Re-initiation



#### Chain Equilibration

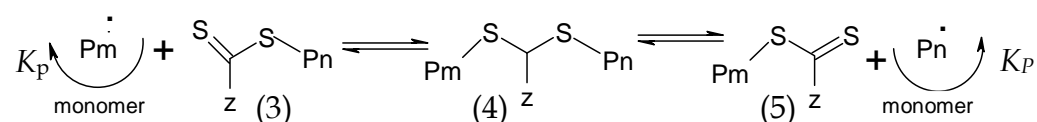


**Figure 5-6:** Schematic representation of RAFT polymerisation using a dithioester.

To achieve control, a delicate balance of the forward and reverse rates of addition ( $K_{add}$  and  $K_{-add}$ ) and fragmentation ( $K_{\beta}$  and  $K_{-\beta}$ ), together with the rates of re-initiation ( $K_i$ ) and propagation ( $K_p$ ), is required.

The approach utilises readily available thiocarbonylthio compounds as chain transfer agents (RAFT agents) to confer living character to the polymerisation. The RAFT agents correspond to the general structure (1) from Figure 5-6 and function efficiently only when R is a good homolytic leaving group when compared to the polymer chain  $P_n$ . On the basis of the addition-fragmentation mechanism, at least four factors are expected to influence the effectivity of thiocarbonylthio compounds (1): (i) the rate constant of reaction of (1) with the propagating (or initiating) radicals ( $k_{add}$ ); (ii) the partitioning of the adduct (2) between starting materials and products (determined by the relative magnitude of  $(K_{-add}$  and  $K_{\beta})$ ); (iii) the absolute rate constant for fragmentation of the intermediate radicals (2) ( $K_{\beta}$ ); (iv) the rate and efficiency at which the expelled radicals ( $R\cdot$ ) re-initiate polymerisation. Factors (i) and (ii) should be directly reflected in the magnitude of the transfer coefficient of 1. If fragmentation is slow, *i.e.* both  $K_{-add}$  and  $K_{\beta}$  are small, or re-initiation of polymerisation is slow with respect to propagation, then polymerisation may be retarded and the probability of the radicals (2) and/or  $R\cdot$  undergoing side reactions leading to some degree of inhibition is increased. If re-addition to reform the adduct radical (2) becomes a significant pathway, the situation may arise where the transfer coefficient for chain transfer is dependent on the concentration of the RAFT agent. The relative effectivity of the RAFT agents is rationalised in terms of interaction of the Z substituent with the C=S double bond to activate or deactivate that group towards free radical addition. In general, the transfer coefficients of RAFT agents decrease in the order: dithiobenzoates > dithiocarbonates > dithioalkanoates > dithiocarbamates. S-Benzyl-N,N'-diethyldithiocarbamate, used as a photoiniferter as will be described in section 5.2, together with other similar dithiocarbamates are not effective RAFT agents [183]. It has been shown that propagating radicals formed under thermal conditions undergo neither RAFT with "iniferters", nor the reversible termination observed under photochemical conditions. The observation also confirms that chain transfer to iniferter type dithiocarbamates is low, despite having

excellent homolytic leaving groups attached to the sulphur atom. The incapability of these types of compounds to undergo reversible addition fragmentation was attributed to a less reactive double bond caused by the delocalisation of the non-bonded electron pair on the nitrogen with the thiocarbonyl group. This lowers the rate of addition at the sulphur and, consequently, the overall rate of chain transfer. Dithiocarbamate derivatives, which have the non-bonded electron pair on the nitrogen atom included as part of an aromatic system, *e.g.* derivatives from pyrrole and imidazole, are effective RAFT agents. In these dithiocarbamates, the non-bonded electron pair on nitrogen is involved in the aromatic system and thus less available for conjugation with the thiocarbonyl group. As a result, reversible radical addition-fragmentation, similar to that observed with dithioesters, becomes more favourable. One of the more versatile RAFT agents is 2-phenylprop-2-yl-dithiobenzoate and was used in my experiments. This RAFT agent satisfies all the criteria mentioned above for functioning as an efficient CTA and has been used previously to graft polymer brushes on silica substrates [184]. The polymers prepared by RAFT polymerisation can be reactivated for chain extension or for use as precursors to produce block polymer, star polymers or polymers of more complex architectures. The active functionality, the thiocarbonylthio group(s), is retained, as has been determined by NMR and mass spectroscopy [182]. However, RAFT polymerisation involves free radical intermediates. Thus, some radical-radical termination, a complication in all forms of living radical polymerisations, cannot be avoided and an amount of dead polymer, determined by the number of chains initiated by initiator-derived radicals, will unfortunately be formed. In order to achieve a high degree of “livingness” in RAFT polymerisation, it is clearly desirable to minimise the number of initiator-derived chains. Thus, RAFT polymerisation could be used to graft several imprinted layers with different properties. The major benefit of the RAFT process over other forms of living radical polymerisation is that the reaction conditions usually employed are typical of those used for conventional free radical polymerisation. Therefore we used this technique in order to graft thin film MIP layers in a controlled manner, using immobilised initiators onto the silica surface.

## 5.2 GRAFTING OF MIPs VIA A SURFACE BOND AZO-INITIATOR USING RAFT POLYMERISATION

Recently, our group proposed a technique for the synthesis of MIP composite materials, with improved kinetic properties involving polymer grafting using immobilised azo-initiators [5]. However, due to only single point attachment of the initiators to the surface, solution polymerisation and resulting gelation is difficult to avoid. Therefore, the method is poorly reproducible and excludes the possibility of up-scaling or of working with a high concentration of immobilised initiator. In order to overcome these problems, in addition to our developed “grafting from” technique, RAFT agents were used to obtain a better control of the polymerisation process.

Using RAFT, the method allows one to work with higher concentration of initiators, leading to thicker and more uniform polymer layers.

### 5.2.1 Surface attachment of free radical initiator

Prior to the first modification step, the silica surface was rehydroxylated according to standard procedures described previously (see section 4.1.1.), resulting in a maximum density of free silanol groups of *ca.*  $8\mu\text{mol}/\text{m}^2$ . The yield of coupling in each step was calculated based on results obtained from elemental microanalysis (see section 4.1.2). A maximum of half the silanol groups reacted with (3-aminopropyl)triethoxysilane (APS) in the first silanisation step. The subsequent step was the attachment of the initiator azobis(cyanopentanoic acid) ACPA (Figure 5-7). On the basis of the increase in nitrogen content, a maximum area density of  $1.5\mu\text{mol}/\text{m}^2$  coupled initiator was calculated. This corresponded to *ca.* 40% conversion of the surface amino groups and on overall conversion of silanol groups of *ca.* 20%.

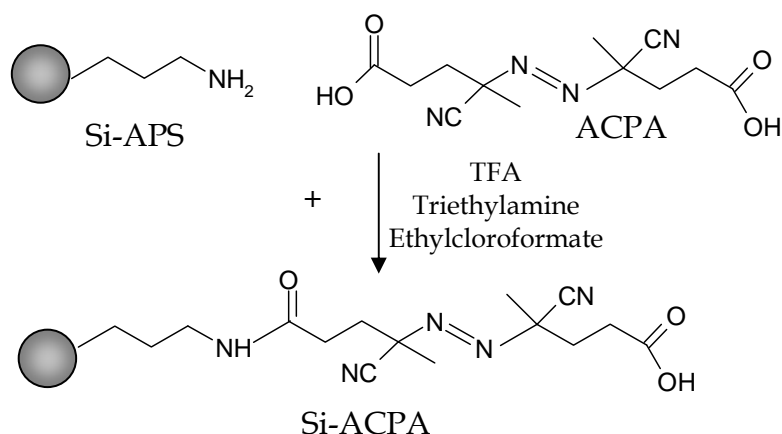


**Figure 5-7:** Covalent immobilisation of an azo-type initiator onto silica surface.

The presence of initiator on the silica surface was also indicated by FT-IR spectroscopy. Thus, bands corresponding to the stretching vibration of the amide and carboxylic acid groups of the initiator were seen in the spectrum of the initiator-modified silica (Figure 5-11).

### 5.2.2 Grafting Step

To allow a straightforward comparison with previously L-phenylalanine anylide (L-PA) model system described in section 3.2.2 [31,32,36], we also chose L-PA as a template for the grafting process, along with EDMA as cross-linker and MAA as functional monomer using toluene as a porogenic solvent. The use of a single enantiomer as template allows assessment of the molecular recognition properties by comparing the retention of the two enantiomers, cancelling non-specific binding.

The RAFT agent, 2-phenylprop-2-yl-dithiobenzoate was synthesised through the reaction of benzoic acid with 2-phenyl-2-propanol in the presence of phosphorous pentasulphide as described in the literature [185].

Photoinitiation was used throughout the experiments, since this is known to lead rapidly to high conversions and to result in MIPs with an enhanced performance in chromatography. The careful removal of oxygen is crucial in this type of experiments



due to the low concentration of generated radicals and dilute conditions. Thus, after the removal of oxygen from the slurry of initiator-modified particles in the monomer mixture, the samples were immersed in a thermostated water bath and irradiated with a high pressure Hg lamp under continuous purging with nitrogen (Figure 5-8). Without a continuous flow of nitrogen during the entire polymerisation process, the yield of grafted polymers on the silica particles was too low for efficient enantioseparation when assessing the materials in HPLC.

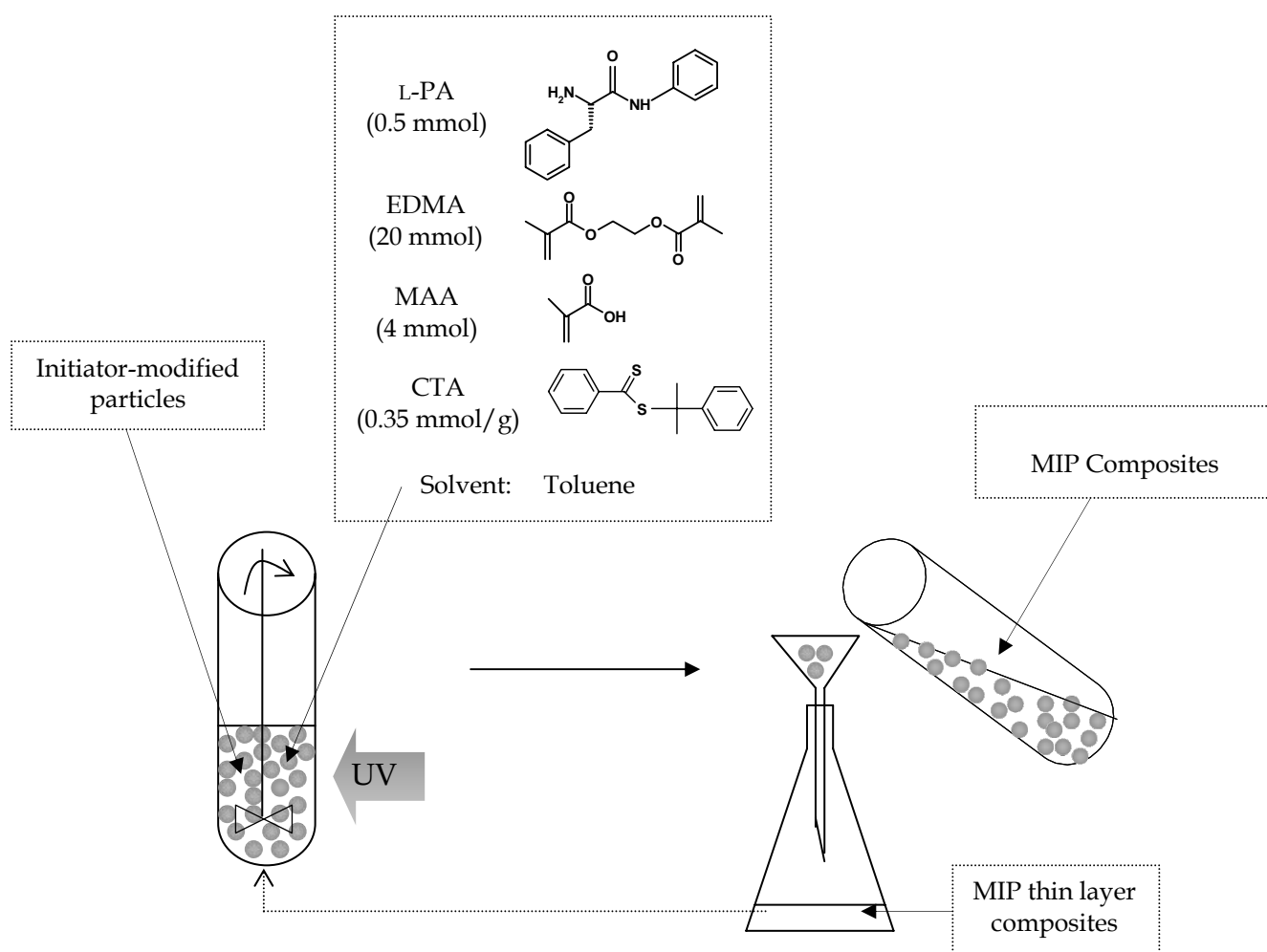


**Figure 5-8:** Protocol for grafting of imprinted polymer layers on support materials with recycling of monomer solution.

Reactions were performed for 60, 90, 120 and 240 minutes, respectively. After these times, the particles were filtered from the monomer solutions, washed, Soxhlet extracted, dried and analysed by elemental microanalysis and FT-IR spectroscopy.

The reactions were reproducible when using the same concentration of coupled initiator (1.5 mmol/m<sup>2</sup>) and an equimolar amount of CTA. The percentage of carbon and the weight of polymer/g silica increased, as expected, with progressing polymerisation time. From this value (g grafted polymer/g silica) and from the carbon content, we estimated the thickness of the polymer layer grafted on the silica particles assuming a homogeneous grafted layer (Table 5-1). The layer thickness was also estimated from the decrease in pore diameter in the resulting composites as compared with the starting silica material. The values obtained using these three independent methods showed a very good agreement (Table 5-1). The layer thickness is a crucial parameter for the future efficiency of the materials as stationary phases in HPLC. A minimum average thickness, of roughly 0.8 nm was found to be required for the materials to exhibit enantioselectivity. Below this value, the enantioseparation and HPLC efficiency were non-existent. Values above this limit were then readily obtained using RAFT polymerisation and working at higher concentrations of immobilised initiator. However, thicker films resulted in poor chromatographical efficiency due to pore blockage.

Another problem that could be overcome using RAFT was up-scaling. Without RAFT agent, due to a single-point attachment of the initiator, the scale of the reaction must be kept low in order to prevent solution polymerisation. Thus, working at the same initiator concentration (1.5 μmol/m<sup>2</sup>) and under the exact same conditions, but in the absence of the CTA, gelation and agglomeration between particles was observed (Figure 5-10-D). In order to obtain useful composites as CSPs without using a CTA, the initiator concentration had to be much lower (0.2 μmol/m<sup>2</sup>) and a maximum amount of initial initiator-modified silica of 0.5 g had to be used. A SEM micrograph of these composite particles is shown in Figure 5-10-D. These particles, prepared after a polymerisation time of 90 minutes, were able to separate L- and D-phenylalanine anilide, but the chromatographic efficiency was much lower than that of the RAFT composites.

### 5.2.3 Characterisation of Grafted Polymer Layers

After polymerisation, the particles were subjected to extensive extraction with methanol in a Soxhlet apparatus, dried and subsequently characterised by elemental microanalysis, FT-IR, SEM, N<sub>2</sub> sorption and fluorescence microscopy.

The average thickness of the grafted MIP layers was calculated from the elemental analysis data, the weight increase and the pore diameters, assuming a homogeneous grafted layer according to the equations below Table 5-1. The obtained values were consistent with each other. The composites prepared without CTA, although obtained from a lower initiator density (0.2  $\mu\text{mol}/\text{m}^2$ ), had a slightly higher layer thickness than those prepared using RAFT due to the lack of control during the polymerisation process.

The composite materials prepared using RAFT contained sulphur in their composition, supporting the RAFT mechanism described in section 5.1.1. Thus, dithioester molecules are attached at the end of the polymer chain and confer living properties to the system to further construct block copolymers.

Figure 5-9-A summarises the most important results from Table 5-1. The layer thickness of the polymer composites increased with the polymerisation time, reaching a value of  $\sim 1.3$  nm for the RAFT composites after 240 minutes and  $\sim 2$  nm for the conventional composites after only 120 min. These higher values for the conventional composites could also be due to the fact that gelation still occurred in solution (Figure 5-10-C) leading to agglomeration and the presence of bulk polymer in-between the particles and not only at the surface.

The close correlation between the values calculated from three independent experimental methods and the narrow pore size distributions in the composites, comparable with the original silica precursor are further in agreement with the presence of a homogeneously grafted polymer film on the silica surface.

**Table 5-1:** Characterisation of molecularly imprinted composites using immobilised ACPs prepared with or without a CTA.

Initiator	Polym. time (min)	%C	%S	$\Delta m$ (g/g)	$a_s$ (m <sup>2</sup> /g)	$d_p$ (nm)	$V_p$ (mL/g)	From N <sub>2</sub> d (nm)	From $\Delta m$ d(nm)	From %C d(nm)
ACPA+ RAFT (CTA)	0	11.76	0	0	360.0	13.30	1.39	0	0	0
	60	15.62	0.32	0.32	191.8	11.50	0.66	0.90	0.97	0.94
	90	17.45	0.31	0.31	192.2	11.50	0.69	0.90	1.16	1.07
	120	18.74	0.29	0.29	193.0	11.40	0.63	0.95	1.41	1.18
	240	19.86	0.30	0.30	181.0	9.94	0.59	1.68	1.61	1.29
ACPA (no CTA)	0	5.98	-	0	360	13.3	1.39	0	0	0
	60	16	-	0.39	285.0	10.60	0.70	1.35	1.08	0.9
	90	21	-	0.52	280.0	10.20	0.63	1.55	1.44	1.47
	120	23	-	0.97	265.0	9.00	0.60	2.15	2.69	1.87

Where:

$\Delta m$  = weight of grafted polymer/ g silica support

$a_s$  = BET specific surface area

$d_p$  = average pore diameter

$V_p$  = specific pore volume

The calculated average thickness assuming a homogeneous grafted layer ( $d$ ) was calculated as follows:

From N<sub>2</sub> sorption:

$$d = \frac{d_{pi} - d_{pf}}{2}$$

Where :

$d_{pi}$  = pore diameter of the original starting material

$d_{pf}$  = pore diameter in the resulting composite

From % C:

$$d = \frac{m_c \times M_w}{M_c \times D \times a_s} \times 10^4 \quad \text{and} \quad m_c = \frac{\%C}{100 - \left( \frac{\%C \times M_w}{M_c} \right)}$$

Where:

- $m_c$  = weight of carbon of the grafted polymer per gram of bare silica support,
- $M_w$  = weighted average molecular weight of the grafted polymer assuming stoichiometric incorporation of reactive monomers,
- $M_c$  = weighted average molecular weight of the carbon fraction of the grafted polymer,
- $D$  = weighted average density of monomers (g mL<sup>-1</sup>)
- $a_s$  = specific surface area of the bare silica support (m<sup>2</sup>g<sup>-1</sup>)

The value used for the % C in these calculations took in account the incorporation of half of the initiator in the grafted polymer layer.

From Δm:

$$d = \frac{\Delta m \times D}{a_s} \times 10^3$$

Where:

- $\Delta m$  = g grafted polymer/ g starting material
- $a_s$  = specific surface area of the bare silica support (m<sup>2</sup>g<sup>-1</sup>)
- $D$  = weighted average density of monomers (g mL<sup>-1</sup>)

It has to be stressed that from this point on, when correlating various parameters with the layer thickness, the utilised value will be the one calculated from the % C contained in the composites.

The nitrogen sorption experiments showed, as expected, an overall decrease in all the pore structural parameters when compared with the starting silica support ( $a_s=360\text{m}^2/\text{g}$ ,  $V_p=1.39\text{ mL/g}$ ,  $d_p=13.3\text{ nm}$ ). This decrease was proportional to the increase in polymerisation time and graft density. For the composites prepared in the absence of the RAFT agent, the decrease in the pore volume was more pronounced, due to the lack of control and possible pore blocking during polymerisation. The pore volumes decreased to around  $0.6\text{ ml/g}$  in both types of composites. After the grafting process, the RAFT composites possessed permanent porosity and high surface areas, characteristics that made them suitable for chromatographical applications. As can be seen in Figure 5-9-B, the pore size distributions and the adsorption isotherms are similar with the starting material.

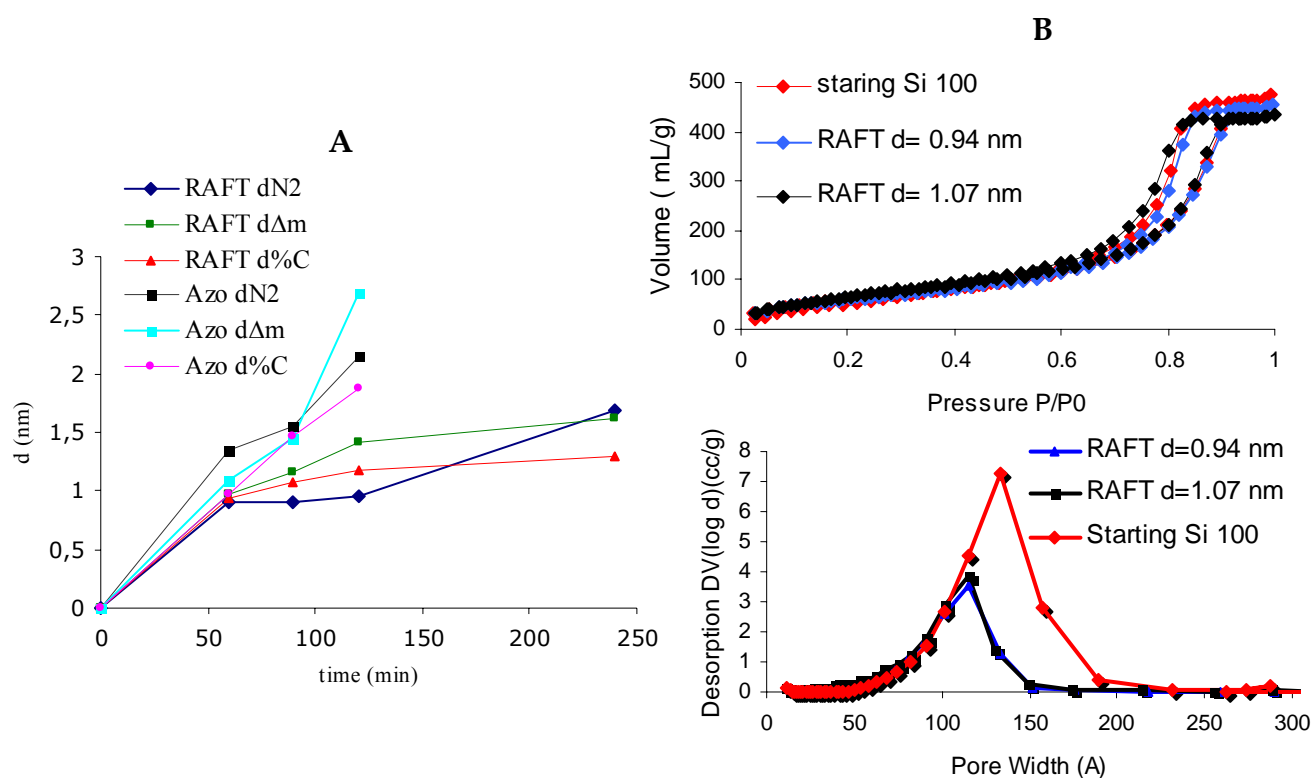


**Figure 5-9:** (A)-Dependence of the average layer thickness of the molecularly imprinted composites with the polymerisation time. (B)-Two examples of pore size distribution and adsorption isotherms in the RAFT composites compared with the starting silica material.

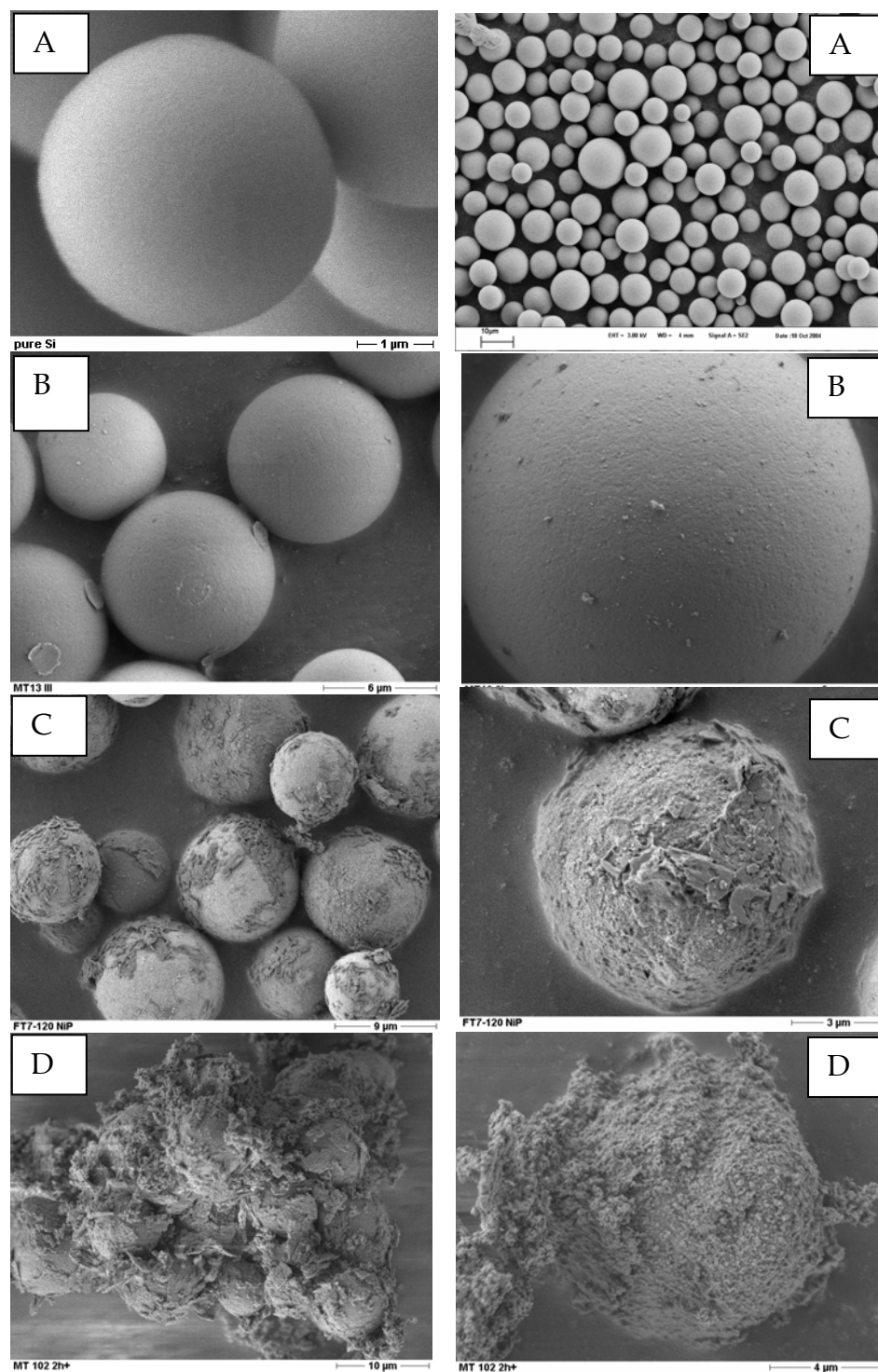


**Figure 5-10:** (A) Native silica gel support; (B) MIP-composites prepared using RAFT at a  $D_s = 1.5 \mu\text{mol}/\text{m}^2 \text{ACPS}$ ; (C) MIP-composites prepared using no CTA at a  $D_s = 0.2 \mu\text{mol}/\text{m}^2 \text{ACPS}$ ; (D) MIP composites prepared using no CTA at a  $D_s = 1.5 \mu\text{mol}/\text{m}^2 \text{ACPS}$ .

The scanning electron micrographs for the composites prepared using RAFT polymerisation showed non-agglomerated particles with uniform grafted layers (Figure 5-10-B). There was a difference in surface morphology when comparing the native (A) and the polymer modified particles (B). It was clear that no solution growth has occurred when comparing with a sample prepared under identical condition and at the same initiator loading but without RAFT (D). Working at even lower concentration of initiator ( $D_s=0.2 \mu\text{mol}/\text{m}^2$ ) revealed that polymerisation between particles was still observed (C).

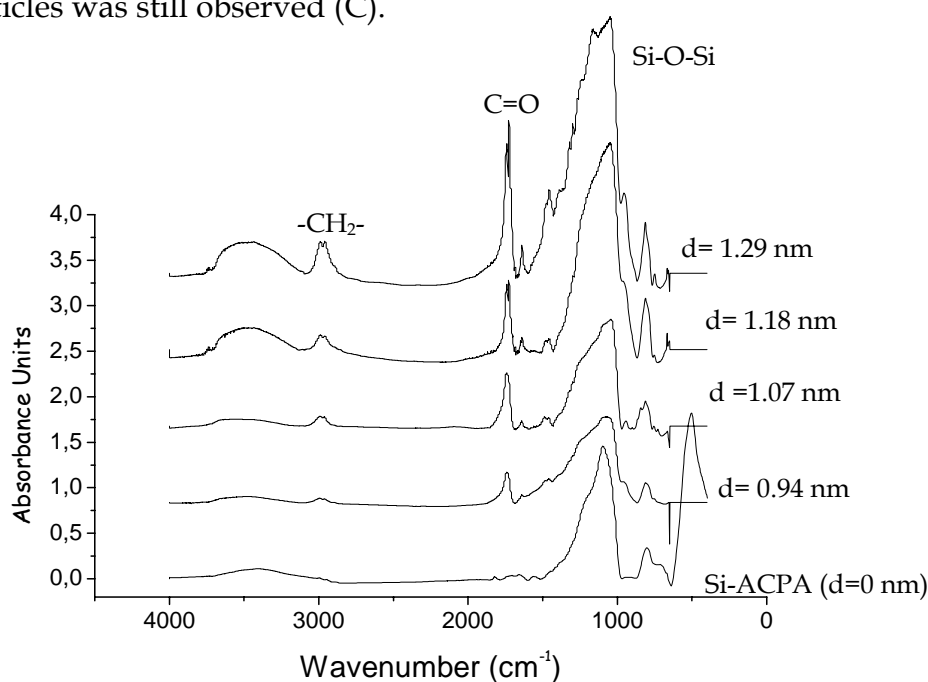


**Figure 5-11:** FT-IR spectra of the ACPA-Si ( $D_s=1.5 \mu\text{mol}/\text{m}^2$ ) and the corresponding composites prepared using a CTA.

In the FT-IR spectra, an increase in the intensity of the carbonyl stretching vibration at  $\sim 1730 \text{ cm}^{-1}$  was observed for all the materials with increasing polymerisation time, indicating an increase of the amount of polymer (Figure 5-11). In the spectra of the silica containing only the immobilised initiator we observed a band at  $\sim 1700 \text{ cm}^{-1}$  corresponding to the amide bond formed by coupling ACPA to the amino modified silica.

Additional evidence for the quality and homogeneity of the grafted polymer films was obtained by fluorescence microscopy of particles labelled with the fluorescent dye 3-aminoquinoline.



Particles prepared via RAFT polymerisation, with layer thicknesses of 0.9 nm (Figure 5-12-A) and 1.3 nm (Figure 5-12-B) respectively, were reacted under amine coupling conditions with 3-aminoquinoline (3-AQ). Samples with the same layer thickness prepared without the RAFT at initiator concentration of  $0.2 \mu\text{mol}/\text{m}^2$  were also labelled under the same conditions.

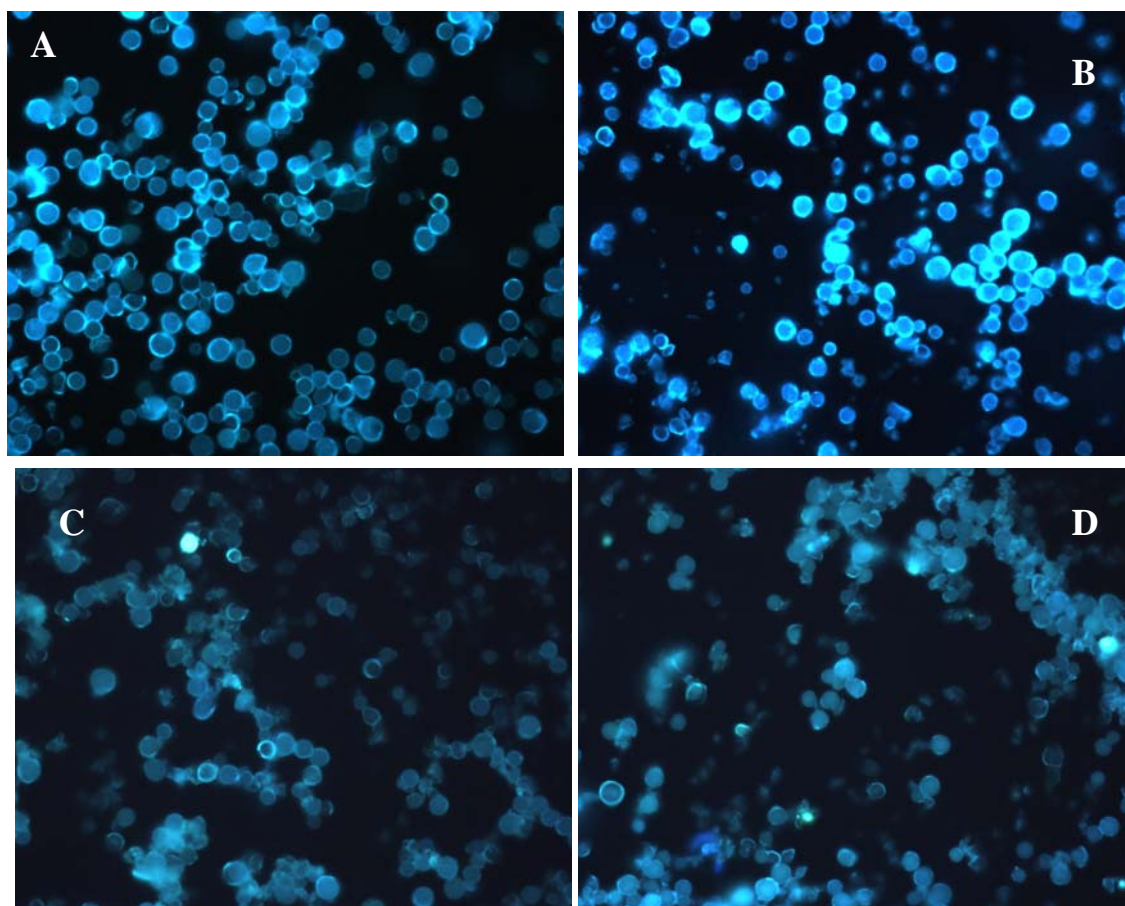


**Figure 5-12:** Fluorescence micrographs of (A, B) imprinted composites ( $d=0.9 \text{ nm}$  and  $1.3 \text{ nm}$  respectively) prepared using RAFT agent and (C, D) imprinted composites ( $d=0.9 \text{ nm}$  and  $1.4 \text{ nm}$ , respectively) prepared without RAFT agent taken at  $\times 40$  magnification

The particles were studied with respect to the intensity of fluorescence, allowing to draw some conclusions about the homogeneity of the grafted layer. For the samples prepared using RAFT, the intensity of fluorescence increased slightly with an increase of the layer thickness, suggesting a uniform distribution of the polymer layer. The particles prepared without RAFT, at a lower initiator concentration, showed a inter- and intraparticle variation in fluorescence intensity (Figure 5-12-

C,D). For the higher density particles prepared without RAFT (Figure 5-12-D), the fluorescence intensity also increased. The silica particles containing only immobilised initiator and no grafted polymer exhibited very weak fluorescence. In conclusion, the particles prepared by RAFT exhibited homogeneous films and the most accessible binding sites.

#### 5.2.4 Characterisation of the Materials in the Chromatographic Mode

The particles were slurry packed into HPLC columns and first evaluated in a water poor mobile phase (ACN/H<sub>2</sub>O/AcOH: 92.5/5/2.5 (v/v/v)), for their ability to resolve and separate the enantiomers of the racemate of the template (L/D-PA). The same studies were later performed in a mobile phase with a higher water content ACN/ sodium acetate buffer, 0.01M, pH 4.8: 70/30 (v/v). The resulting elution profiles were evaluated with respect to the retention of the two enantiomers, determined as the retention factor ( $k$ ) and the enantioselectivity, determined as the separation factor ( $\alpha=k_L/k_D$ ). The enantioseparation of a fluorescent template analogue L/D-phenylalanine p-nitroanilide (L-PA-pNa) was as well investigated.

The chromatographic efficiency and separation factors obtained using the composite particles prepared with or without RAFT were compared. One has to keep in mind that the composites prepared without RAFT had a lower initiator density (0.2  $\mu\text{mol}/\text{m}^2$ ) and were prepared on a smaller scale (0.3g silica) in order to avoid polymerisation in solution. Still, this was inevitable and, therefore, the theoretical layer thickness calculated for the conventional composites had slightly higher values than those of the RAFT-composites, even though the polymerisation time had been the same (Table 5-1).

All the columns packed with the RAFT imprinted materials showed resolution of the template racemate and the p-nitroanilide analogue in both mobile phases. In Figure 5-13-A,B are presented the elution profiles for the racemic mixtures of the template on the columns packed with the RAFT imprinted composites in both mobile phases, together with the corresponding layer thickness. An optimum separation was obtained with the column packed with particles possessing a 1 nm thick imprinted layer. An increase in the retention time in the more aqueous environment at pH= 4.8

was also observed (Figure 4-13-B). This was due to the fact that, at acidic pH, the amino group of L-PA is protonated, the MIPs are partially negatively charged and the recognition mechanism takes place *via* additional electrostatic interactions. The best separation was recorded again for the column packed with 1 nm thick imprinted polymer composites.

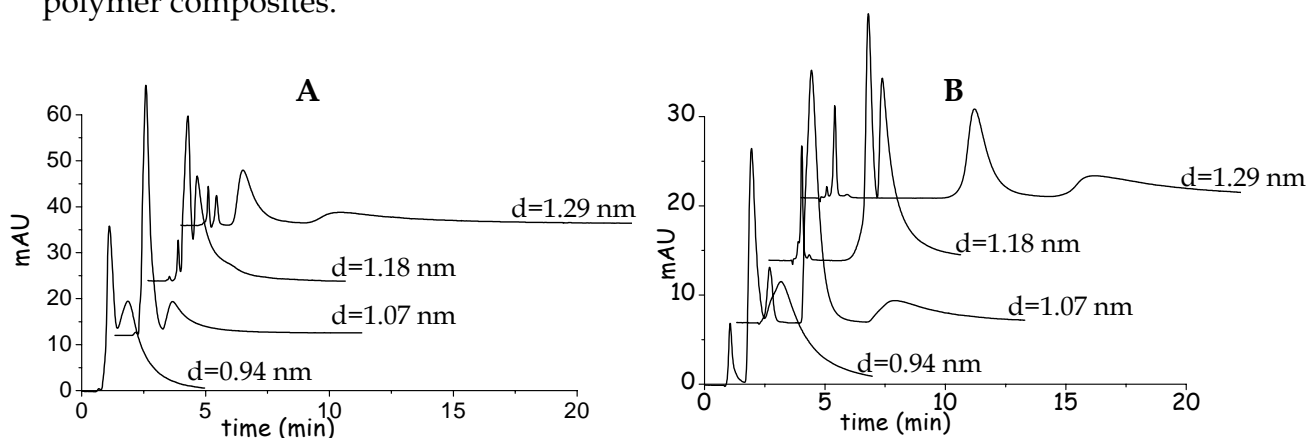


**Figure 5-13:** Racemic resolution of phenylalanine anilide (1mM solution) on the columns packed with the imprinted polymers prepared using RAFT agents in a mobile phase (A) ACN/H<sub>2</sub>O/AcOH: 92.5/5/2.5 (v/v/v) and (B) ACN/ sodium acetate buffer, 0.01M, pH 4.8: 70/30 (v/v).

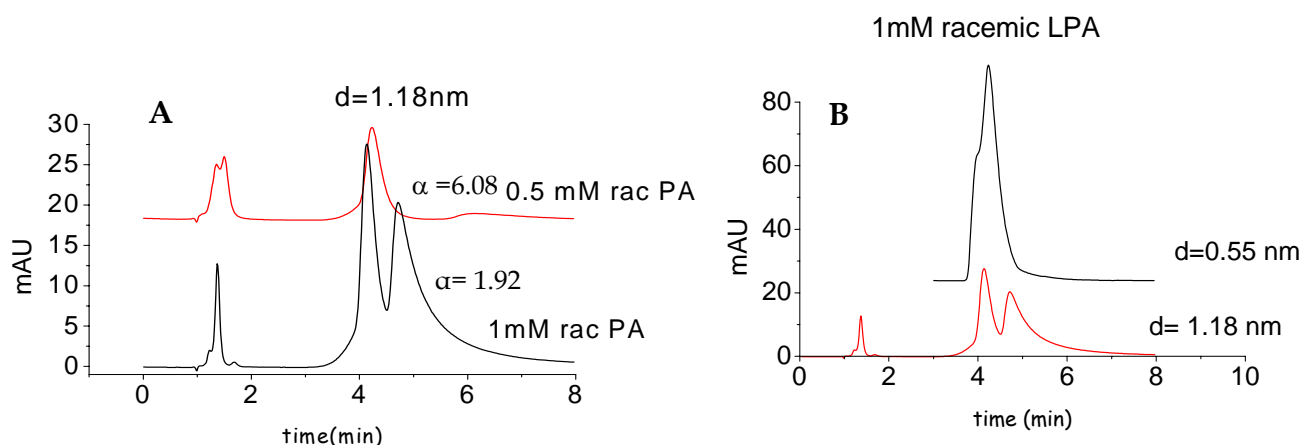


**Figure 5-14:** (A) Dependence of the composite prepared using RAFT ( $d=1.8$  nm) on analyte concentration in ACN/H<sub>2</sub>O/AcOH: 92.5/5/2.5 (v/v/v). (B) Selectivity dependence of the composites prepared using RAFT on grafted polymer layer thickness in ACN/H<sub>2</sub>O/AcOH: 92.5/5/2.5 (v/v/v).

Decreasing the concentration of the racemic mixture from 1 mM to 0.5 mM lead to increased retention times of the L-enantiomer. The case of the composites possessing a layer thickness of 1.18 nm (Figure 5-14-A) was interesting. By decreasing the

template concentration, the racemic mixture was then separated with a clear baseline. Like this, some of the non-specific interactions between functional monomer and high concentration of template were suppressed. This composite had probably a poorer yield of binding sites resulting in a strong dependence of selectivity and binding on sample load, at least within the low sample load regime.

As mentioned before, there was a minimum layer thickness of  $\sim 0.8$  nm after which the composites exhibited selectivity (an example is given in Figure 5-14-B). When the polymerisation was performed at the same initiator concentration, under the same conditions except for the continuous purge of an inert gas ( $N_2$ ) during the entire process, the obtained layer thickness (0.5 nm) was too low to generate enantioseparation.

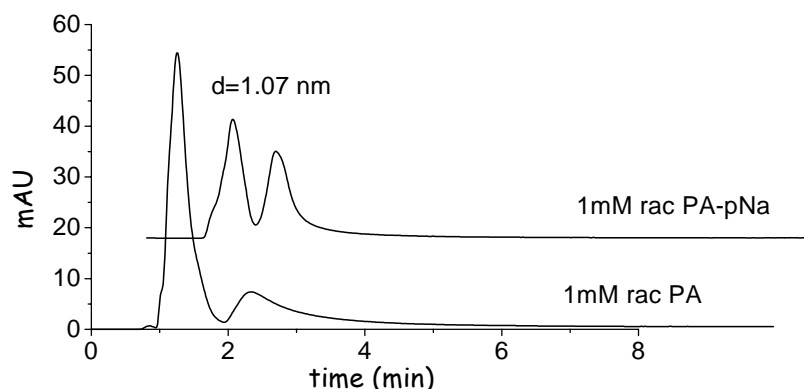


**Figure 5-15:** Racemic resolution of PA and *p*-nitro analogue on the composite prepared using RAFT ( $d=1.07$ nm) in ACN/ $H_2O$ /AcOH: 92.5/5/2.5 (v/v/v).

The racemic mixtures of the template analogue containing the *p*-nitro group could also be resolved with very good separation factors and efficiencies (Figure 5-15). Substituent groups were not involved in the potential binding interactions and lead only to a small decrease in enantioselectivity. In contrast to the template racemate, in the *p*-nitro analogue, the *D*-enantiomer resolved with a larger plate number (*N*) as well as the more retained *L*-enantiomer.

Although the composites prepared with and without CTA did not have exactly the same layer thickness, and the concentration of immobilised initiator was much lower when preparing the azo-based composites, a comparison between the composites containing roughly the same grafted polymer thickness is given in Figure 5-16 -A, B.

The separation factors on the columns packed with the RAFT composites were higher than on the ones prepared using only the immobilised initiator, especially in the low layer thickness range. This was due to a better control of the polymerisation conditions through RAFT, resulting in more homogeneous grafted layers with a better morphology.

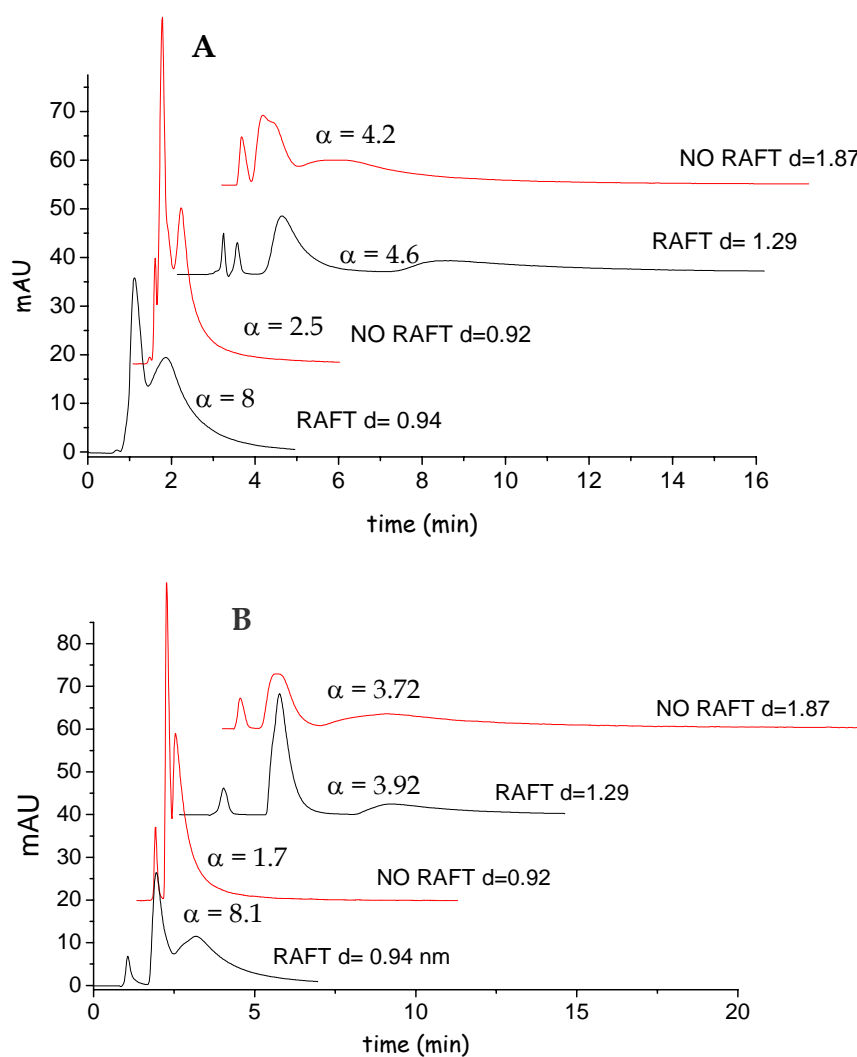


**Figure 5-16:** (A) Comparison between the composites prepared using RAFT and those prepared in the absence of RAFT agent in ACN/H<sub>2</sub>O/AcOH: 92.5/5/2.5 (v/v/v); (B) Comparison between the composites prepared using RAFT and those prepared in the absence of RAFT agent in ACN/ sodium acetate buffer, 0.01M, pH 4.8: 70/30 (v/v); Column size in all experiments was 12 x 4.5 mm. i.d. at a flow rate of 1mL/min with an analyte injection volume of 10  $\mu$ L. Detection DAD, 260 nm.

### 5.2.5 Conclusions and Outlook

A new approach to prepare thin films of imprinted polymers combining covalent immobilisation of azo-initiators with RAFT-based living radical polymerisation on preformed support materials has been described. The method should be adaptable to supports with different morphologies, giving access to imprinted composites with different pore sizes, particle sizes and morphologies. Furthermore, it should be possible to prepare the MIP films using a variety of combination solvents-functional monomers libraries. The technique can potentially be applied to different templates and exhibited distinct advantages over the conventional traditional monolith imprinting procedure. Thus, the materials were obtained in a short period of time (1-4h) and minimal work-up was required.

The method proved to be superior to our previous method when only azo-initiators were used to “graft from” various supports. The synthesis was reproducible, and could use higher densities of immobilised initiators, leading to more homogeneous imprinted polymer layers. The thickness of the films was tuneable, potentially allowing the materials to be optimised for high efficiency analytical or even preparative separation.

### 5.3 GRAFTING OF MOLECULARLY IMPRINTED POLYMERS VIA A SURFACE BONDED INIFERTER INITIATOR

One of the first examples of controlled polymerisation is offered by iniferter type initiators as already described in section 5.1. The photoiniferter technique was explored by Otsu *et al.* in the early 1980s [170]. Living radical polymerisation, using benzyl-*N,N*-diethyldithiocarbamate iniferter species, has found important applications in the manufacturing of micropatterned or bio-compatible surfaces [186,187]. The first association of iniferters with MIPs consists in the use of an iniferter-modified membrane surface to graft a molecularly imprinted polymer layer [67]. However, the use of this concept for preparation of porous composite beads was first reported by our group [7,8]. Some other reports have since appeared, for example, Yoshimi *et al.* used iniferters to perform grafting of theophylline-imprinted polymers onto a cellulose membrane [188].

My contribution to the field consists in the further development of the initial work started in our group. A covalently bound iniferter was used to produce CSPs for chromatography using the conventional *p*(MAA-*co*-EDMA) system and one more hydrophilic system based on *p*(MAA-*co*-HEMA-*co*-EDMA). Simple dissolution of the silica support from the obtained composites resulted in a new type of thin walled MIP with thin (nanometre size) walls possessing a gel-like structure, homogeneous binding sites and an unprecedented enantioselectivity as will be shown in section 5.4.

#### 5.3.1 Iniferter Coupling and Characterisation

The iniferter benzyl-*N,N*-diethyldithiocarbamate was covalently immobilised onto the surface of the same porous silica gel used previously ( $a_s=360\text{m}^2/\text{g}$ ,  $V_p=1.39\text{mL}/\text{g}$ ,  $d_p=13.3\text{ nm}$ ) in two steps as shown in Figure 5-17. After activation, the silanol groups were reacted with *p*-(chloromethyl)phenyl trimethoxysilane. The resulting intermediate was then reacted with sodium *N,N*-diethyldithiocarbamate trihydrate in order to obtain the surface-coupled iniferter. The substitution of the chloromethyl group with *N,N*-diethyldithiocarbamate could be precisely controlled through stoichiometry.

In order to have similar conditions with the grafting from azoinitiator-modified silica supports, we chose the supports containing a density of dithiocarbamate groups of  $1.2 \mu\text{mol}/\text{m}^2$  for the grafting experiments.

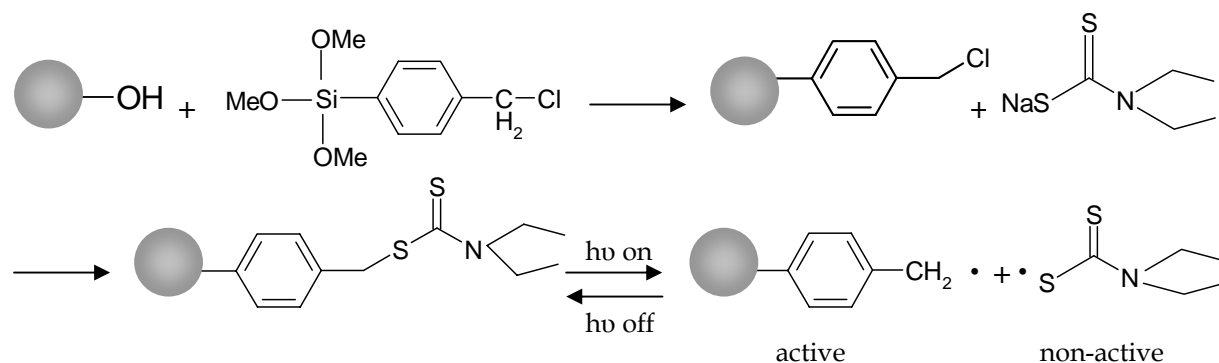


**Figure 5-17:** Modification of silica-based supports with a dithiocarbamate iniferter.

### 5.3.2 Polymer Grafting and Composite Characterisation

As for the AZO/RAFT composites, in order to allow a direct comparison with the L-PA model system described in section 3.2.2., the same p(MAA-co-EDMA) system was employed in the grafting process using the same model template L-PA. In addition, a second system was used, involving the hydrophilic functional monomer 2-hydroxyethylmethacrylate HEMA, used in combination with MAA, EDMA as cross-linker, 1,1,1-trichloroethane as porogen and also L-PA as template. The porogen 1,1,1-trichloroethane was chosen based on previous work, where using a combinatorial method this solvent gave best results associated with HEMA monomer in the imprinting of Bupivacaine [38]. After sealing, mixing and purging the mixtures with nitrogen, polymerisation was initiated by UV-irradiation at 15°C and allowed to continue for either 30, 60, 120, 240, 360 or 480 minutes, respectively, with continuous nitrogen purging. As described in section 5.1, the benzyl-*N,N*-diethyldithiocarbamate iniferter decompose upon UV irradiation in two radicals; an active one present onto the silica surface and a non-active radical present in solution that can terminate the polymerisation (Figure 5-17). Therefore, no solution polymerisation can occur during the grafting process. After polymerisation, the samples were extracted with methanol using a Soxhlet apparatus for 24h. Non-imprinted control polymer composites (NIP)



were prepared as described above but without addition of the template.

The layer thickness was again estimated using the three methods described in the previous section: carbon percentage in the obtained composites, increase in weight related to the starting material and decrease in the pore diameter as compared to the starting material. The obtained values are given in Table 4-2 and showed poor agreement when compared with the azo-initiator system.

**Table 5-2:** Characterisation of molecularly imprinted composites using immobilised iniferters.

System	Polym. time (min)	%C	%N	%S	$\Delta m$ (g/g)	$a_s$ (m <sup>2</sup> /g)	$d_p$ (nm)	$V_p$ (mL/g)	From N <sub>2</sub> d (nm)	From $\Delta m$ d(nm)	From %C d(nm)
MAA EDMA	0	5.98	0.25	1.70	0	360	13.0	1.4	0	0	0
	30	10.24	0.19	0.82	0.42	221.7	9.2	0.73	1.90	1.16	0.73
	60	16.56	0.14	0.70	0.58	209.0	7.1	0.64	2.95	1.61	0.95
	120	17.20	0.15	0.69	0.64	142.0	3.8	0.14	4.75	1.77	1.05
	240	19.95	0.16	0.75	0.72	257.0	3.9	0.30	4.70	2	1.30
	360	23.40	0.15	0.77	0.97	197.0	3.7	0.36	4.80	2.69	1.90
	480	24.57	0.17	0.81	0.99	194.9	3.9	0.22	4.50	2.75	2.01
MAA HEMA EDMA	0	5.98	0.25	1.72	0	360.0	13.0	1.40	0	0	0
	30	9.12	0.18	0.71	0.45	239.8	5.7	0.45	3.65	1.25	1.13
	60	13.50	0.16	0.75	0.51	223.0	5.2	0.41	3.90	1.41	1.30
	120	14.80	0.14	0.72	0.58	226.8	4.8	0.39	4.10	1.61	1.43
	240	16.95	0.17	0.81	0.61	223.0	5.3	0.40	3.85	1.69	1.64
	360	18.80	0.16	0.78	0.67	220.0	5.1	0.39	3.95	1.86	1.86
	480	20.01	0.15	0.79	0.72	221.4	4.1	0.37	4.45	2.05	2.48

A possible explanation can be the fact that the polymerisation occurred more at the outer surface of the silica bead and not so much in the interior. This theory is supported by nitrogen sorption experiments and SEM and TEM measurements.

Looking at Figure 5-18, the difference seems to have something to do with the pore filling, and which pores are the most reactive in the grafting process. The values for the layer thickness calculated from the carbon content and weight increase were in good enough agreement. However, the pore size distributions of the iniferter composites showed a sharp peak around 4 nm. This was not present for the azo-type composites, which had a broader pore size distribution with a maximum around 11

nm (Figure 5-9-B) similar to the silica precursor.

The iniferter composites exhibited also a decrease in the surface area and pore volume; all the pore structural parameters seemed to be affected by the apparently low value of the pore size.

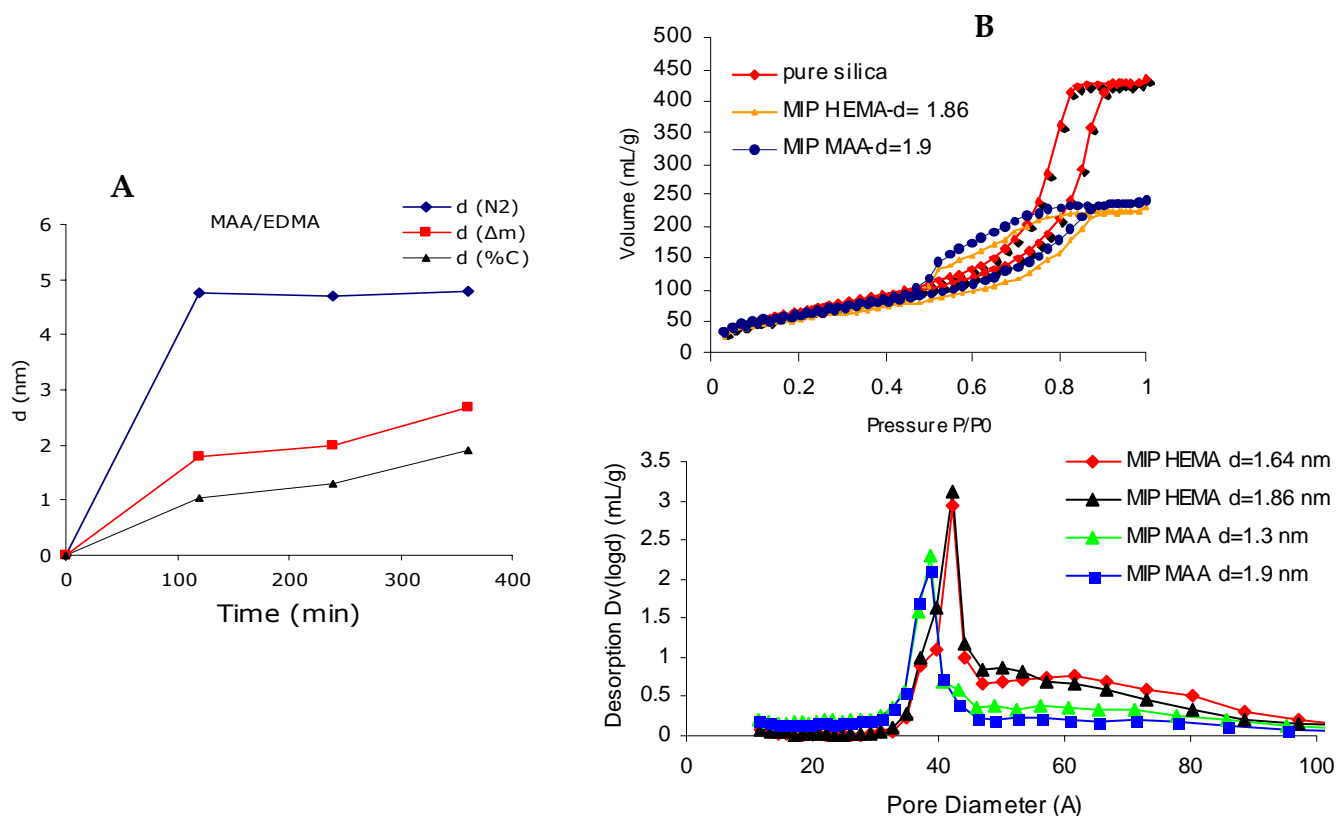


**Figure 5-18:** (A) Dependence of the average layer thickness of iniferter based molecularly imprinted composites with the polymerisation time; (B) Adsorption and desorption isotherms and pore size distributions.

The scanning electron micrographs in Figure 5-19 clearly revealed that a polymer layer covers the particle surfaces, for both the HEMA and MAA systems. As expected, no agglomeration between particles took place during the polymerisation process. For the HEMA system (B), looking at a higher magnification we clearly observed the polymer layer coating the silica surface. When comparing the outer surface of the iniferter composite (B) with a composite prepared using AZO/RAFT (D) in a micrograph taken at the same magnification, different surface morphologies were observed. It seemed that in the case of the iniferter composite the polymerisation occurred more on the outer surface than inside the silica bead.

This might be one possible explanation for the different pore structural parameters of the iniferter based composites when compared with the azo-based analogues.

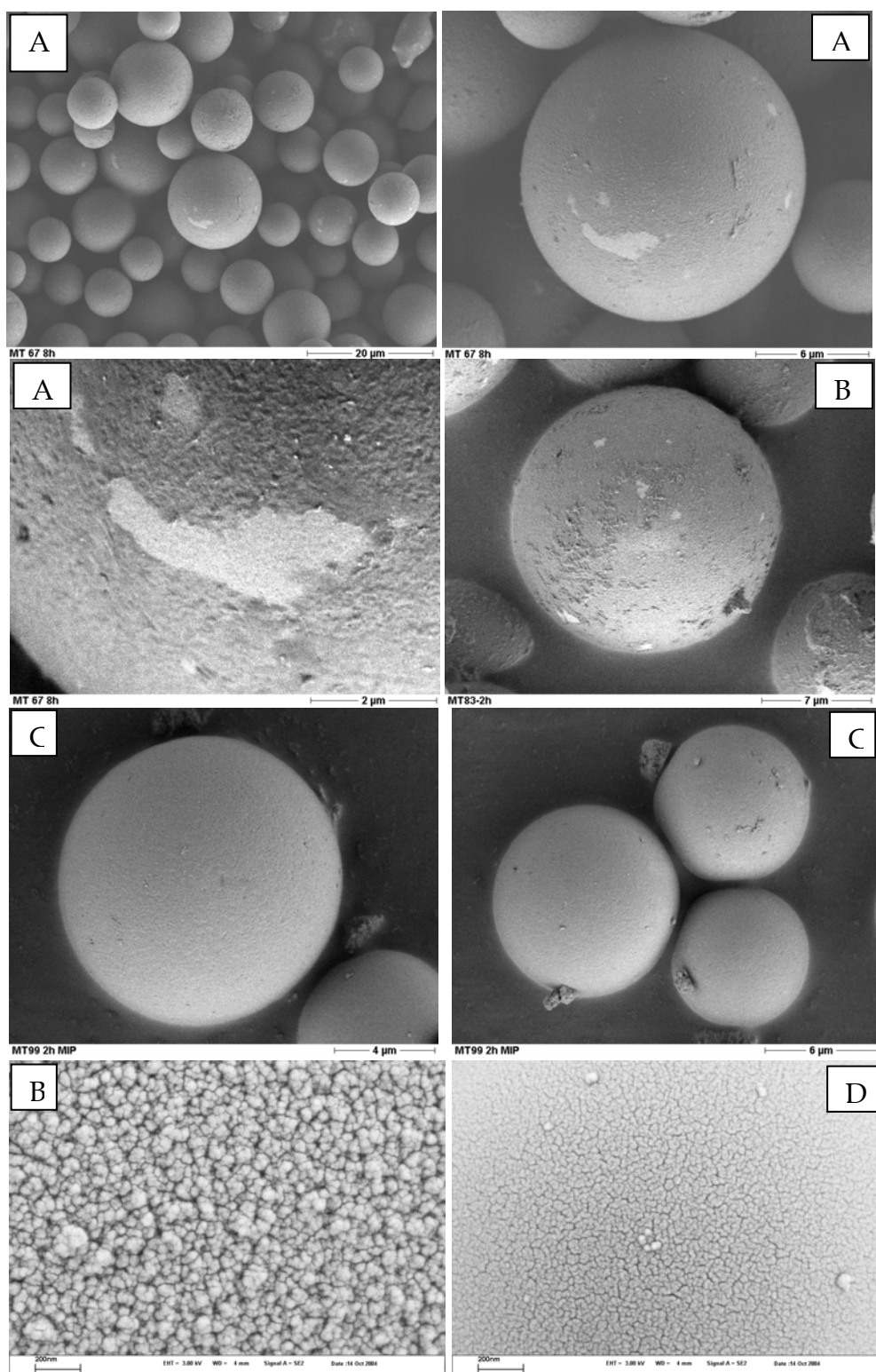


**Figure 5-19:** SEM of iniferter based composites: (A) MAA/HEMA/EDMA composites ( $d=1.43\text{nm}$ ); (B) MAA/HEMA/EDMA composites ( $d=1.64\text{ nm}$ ); (C) MAA/EDMA composites ( $d=1.3\text{ nm}$ ); (D)AZO/RAFT composite ( $d= 1.29\text{ nm}$ ).

The porous structure inside the composites was confirmed also by TEM. The particles (starting silica and HEMA composites) were incorporated in an epoxy resin and a cross-section was performed. When comparing the transmission electron micrographs of the starting silica beads and the composite beads obtained after grafting (Figure 5-20) a similar morphology in the interior of the beads was observed. The iniferter composites exhibited permanent porosity in the interior of the particles.

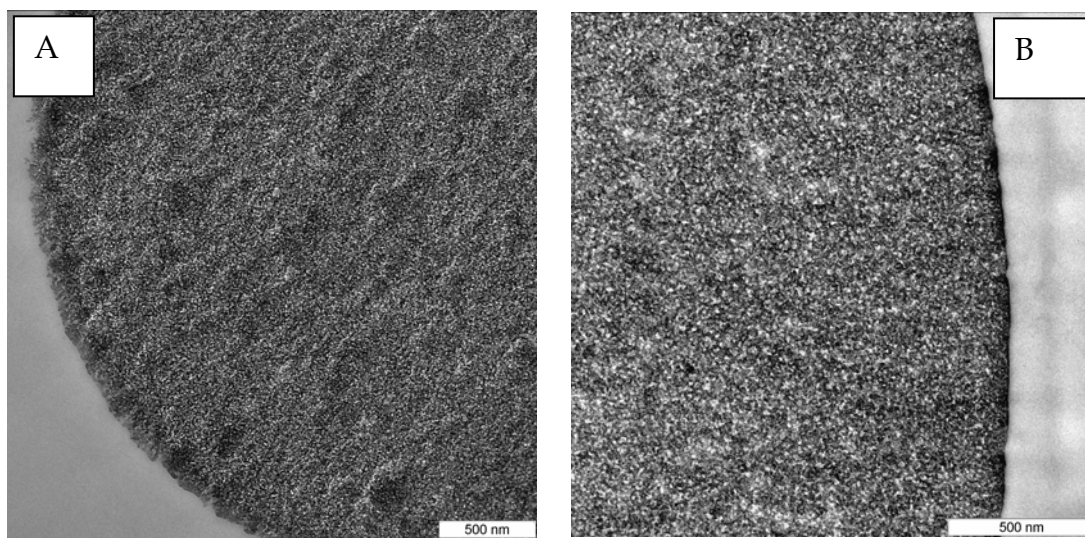


**Figure 5-20:** TEM of (A) starting silica material and (B) iniferter composite MAA/HEMA/EDMA ( $d=1.64$  nm).

However, the absorption band corresponding to the C-C stretch from the unconverted double bonds was clearly seen in the iniferter composite FT-IR spectra and seemed to be no different in intensity from the one present in the azo-composites (Figure 5-21-C). No obvious difference between the amount of unconverted double bonds in the iniferter and azo-based composites was also indicated by  $^{13}\text{C}$ -NMR in solid state (Figure 5-22). This may imply that both, azo and iniferter based composites, had overall a similar cross-linking level and the difference between them lay in how the polymer layer was distributed inside the silica particles. The azo case seemed to form a homogeneous distribution of grafted layer, while the iniferter-based composites had a higher density of graft at the outer surface than in the interior.

The IR spectra showed all absorption bands characteristic also for azo-composites. The intensity of the peak due to the carbonyl absorption band increased with polymerisation time for both the MAA and HEMA systems.

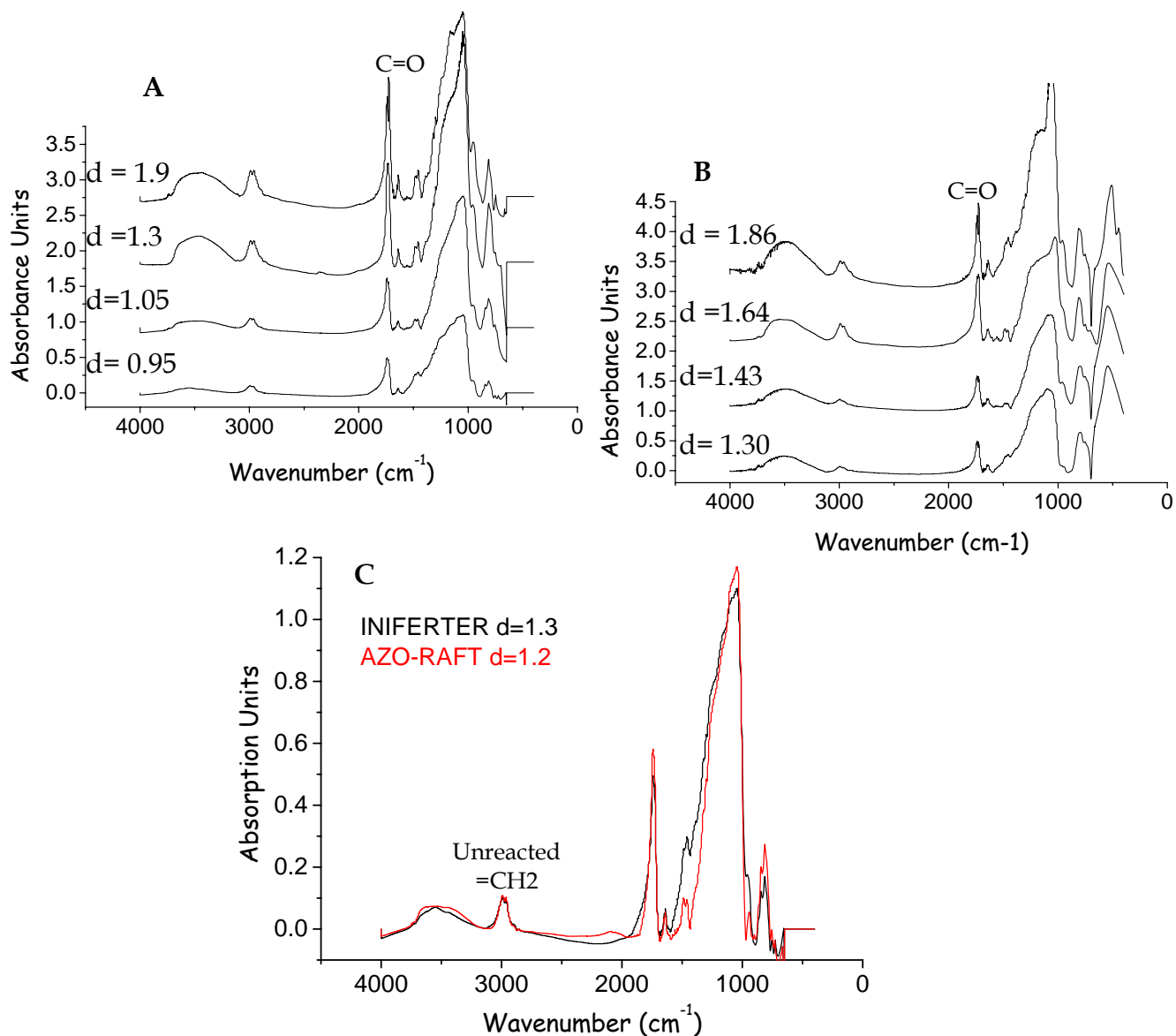


**Figure 5-21:** IR spectra of thin film molecularly imprinted composites; (A) Iniferter based composites prepared using MAA/EDMA; (B) Iniferter based composites prepared using HEMA/MAA/EDMA; (C) Comparison between the MAA/EDMA AZO-RAFT-composites and MAA/EDMA iniferter-composites.

In the solid state  $^{13}\text{C}$ - NMR of the azo and iniferter composites we can observe similar signals for both composites. Thus, the signals corresponding to the unconverted double bonds appear between 120-140 ppm and they have the same intensity for both composites. The signal corresponding to the carbonyl group in EDMA appears around 180 ppm while the one corresponding to the carboxylic groups in MAA located around 170 ppm.

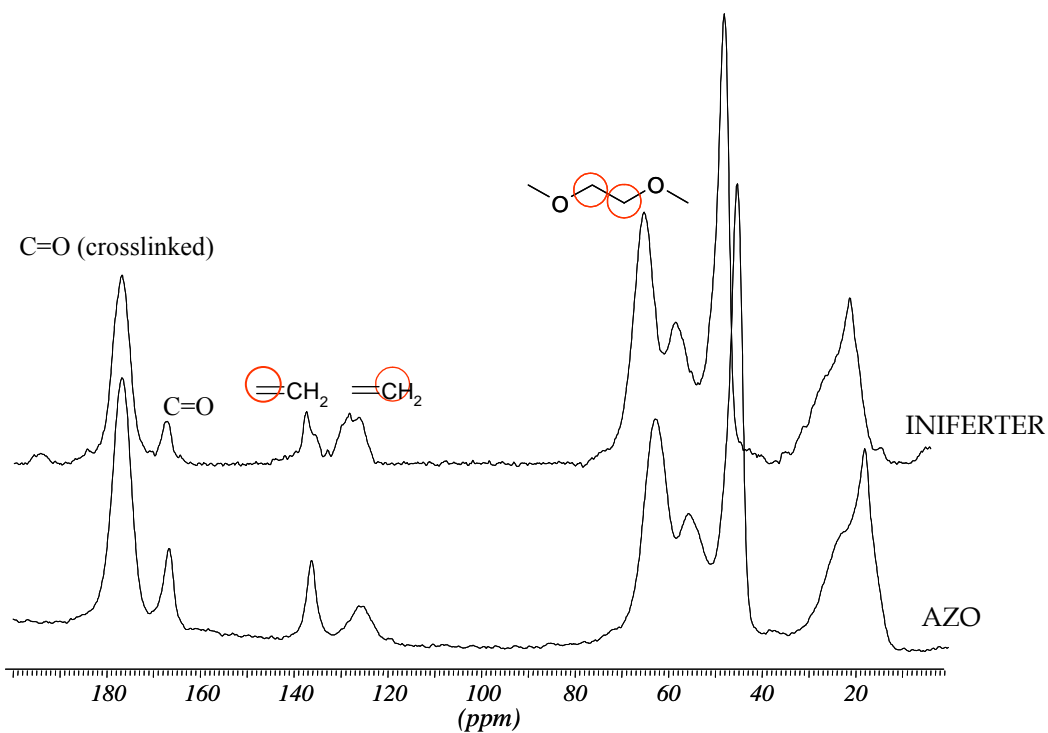


**Figure 5-22:**  $^{13}\text{C}$ -solid state NMR of the azo and iniferter based composites.

### 5.3.3 Evaluation of the Composites as Stationary Phases in HPLC

The HEMA-based composites were evaluated in an organic mobile phase consisting of MeCN/AcOH/H<sub>2</sub>O=92.5/2.5/5 (v/v/v) and an aqueous mobile phase consisting of sodium acetate buffer, 0.01M, pH 4.8. The MAA-based composites were evaluated only in the organic-based mobile phase. In both cases, the ability of the composites to function as CSPs was studied by injecting the individual enantiomers and the racemic mixture of PA and the corresponding p-nitro analogues. The resulting elution profiles were evaluated with respect to the retention of the two enantiomers, determined as the retention factor ( $k$ ), the enantioselectivity, determined as the separation factor ( $\alpha=k_L/k_D$ ). Also the imprinting factor (IF) of these composites was determined ( $IF= k_{L-MIP}/k_{L-NIP}$ ).

None of the iniferter-based composite materials exhibited racemic resolution in the LC mode. However, there was an obvious difference between the L- and D-enantiomers when the two antipodes were injected separately. Again this behaviour might be due to a different distribution of grafted polymer in these composites. Even though the materials clearly possessed enantioselective sites, as demonstrated in the batch rebinding experiments (see section 5.4), they were unable to resolve the racemic mixture of PA or its p-nitro analogue PA-pNa and could discriminate between the two enantiomers only when they were injected separately. In chromatographic mode, the analyte could not find its path to the enantioselective binding probably due the fast dynamic equilibrium process.

First, we evaluated the dependence of the retention factors with polymerisation time. The retention time and retention factors increased with the polymerisation time (layer thickness) showing a maximum value for the 240 min (~1.69 nm) polymerisation time. After this, the retention factors decreased probably due to some pore blockage in the composites. The dependence of the retention factors with the layer thickness for the MAA/HEMA/EDMA composites together with the elution profiles are shown in Figure 5-23. As solutes, both the template L-PA and the p-nitro analogue were used.

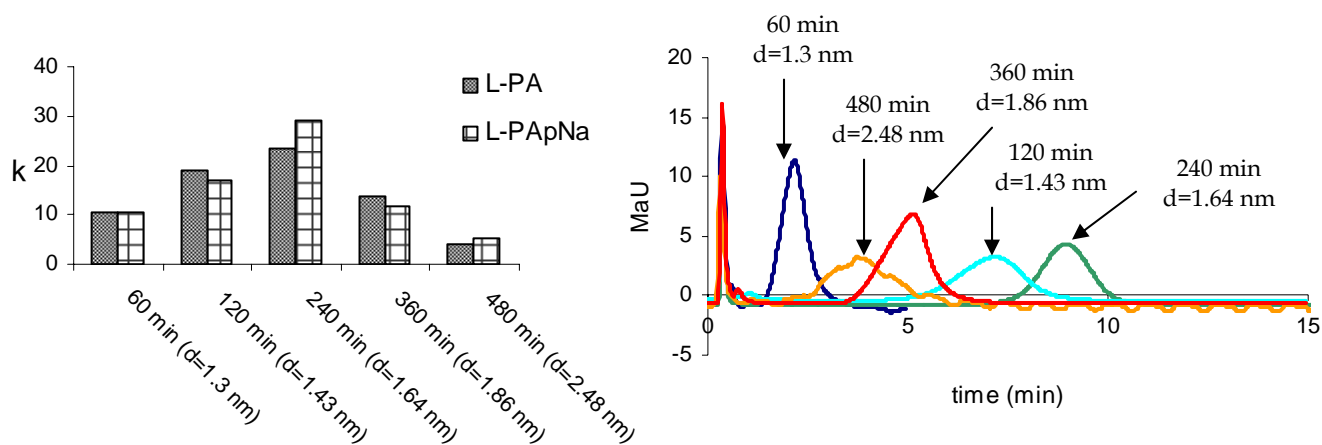


**Figure 5-23:** Dependence of retention factor with layer thickness. The elution profiles correspond to the L-PA (10  $\mu$ L of 1 mM solutions), flow: 1 mL/min, columns 50 x 5 mm. i.d.) in ACN/H<sub>2</sub>O/AcOH: 92.5/5/2.5 (v/v/v).

After the study of the retention factors with the polymerisation time, we also studied the dependence of the enantioselectivity of the HEMA based composites with the layer thickness. As it can be observed in Figure 5-24, the separation factors decreased also with increasing the layer thickness, most probably due to the same pore blocking and poorer accessibility of the solute in thicker films composites.

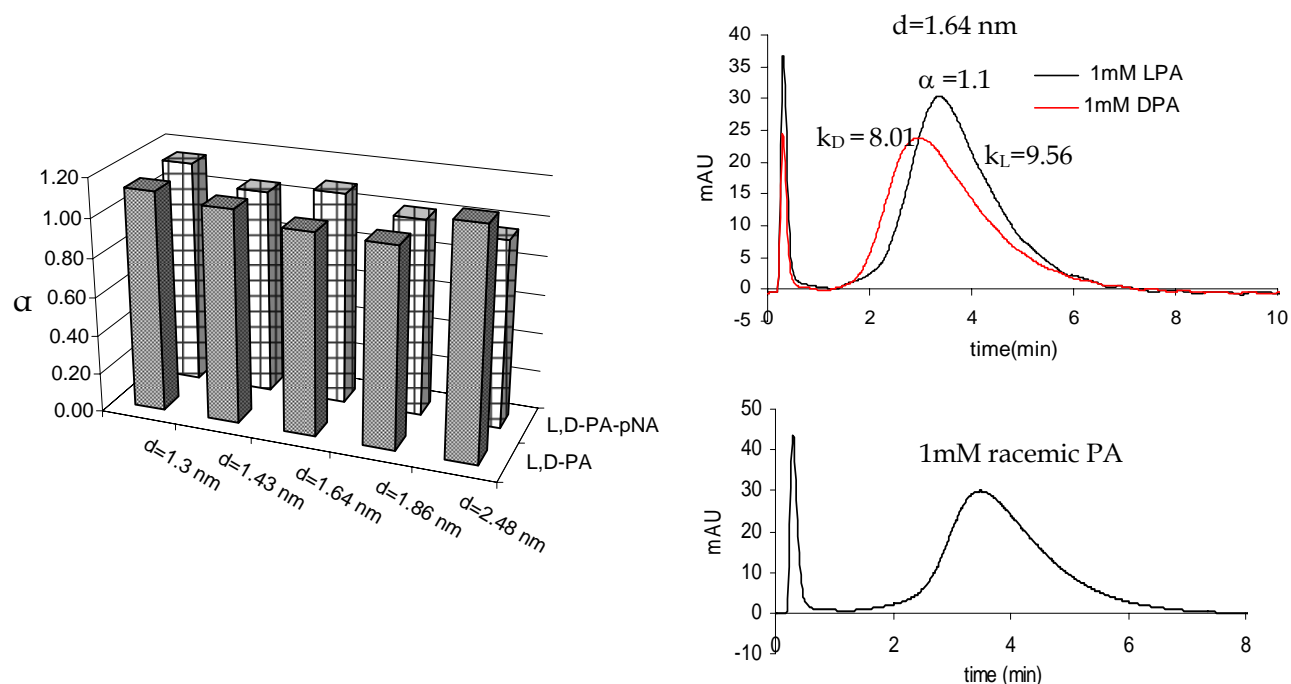


**Figure 5-24:** Enantioselectivity of HEMA based composites (10  $\mu$ L of 1 mM solutions, flow: 1 mL/min, columns 50 x 5 mm. i.d.) in ACN/H<sub>2</sub>O/AcOH: 92.5/5/2.5 (v/v/v). The elution profiles were obtained using a column packed with composites with d=1.64 nm.



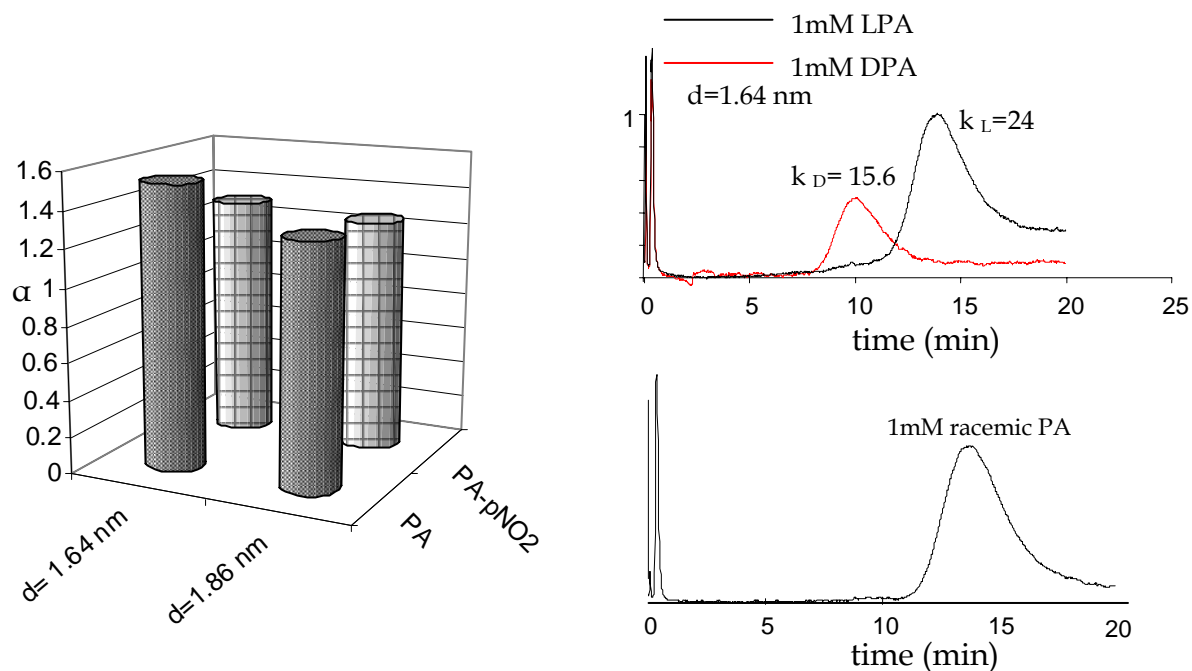


**Figure 5-25:** Enantioselectivity of HEMA based composites (10  $\mu$ L of 1mM solutions, flow: 1mL/min, columns 50 x 5 mm. i.d.) in 100% sodium acetate buffer, 0.01M, pH 4.8. The elution profiles were obtained using a column packed with composites with  $d=1.64$  nm.

HEMA/MAA/EDMA composites exhibited a maximum separation factor of 1.2 for both PA and PA-pNa in the organic mobile phase when the two antipodes were injected separately (Figure 5-24). The separation factor increased in the aqueous media, probably due to the hydrophilic monomer HEMA (Figure 5-25).

As the composites with a layer thickness of 1.43 nm and 1.64 nm respectively, showed a maximum in retention factors the corresponding blank polymers were also prepared in exactly the same conditions but in the absence of the template. The imprinting effects are shown in Figure 5-26. In the organic based-mobile phase, after 240 min of polymerisation for the composite with  $d=1.64$  nm, the template analogue L-PA was 1.36 times more retained on the corresponding imprinted polymer than on the blank, while the p-nitro analogue was also 1.26 times more retained on the MIP than on the blank. Moving to an aqueous mobile phase the imprinting factors increased to 3.25 for the template and to 4.25 for L-PA-pNa. The increase in selectivity was probably, on one hand due to the hydrophilic monomer HEMA and on the other hand due to the protonation of the amino group from L-PA at an acidic pH and the involvement of ionic interactions.

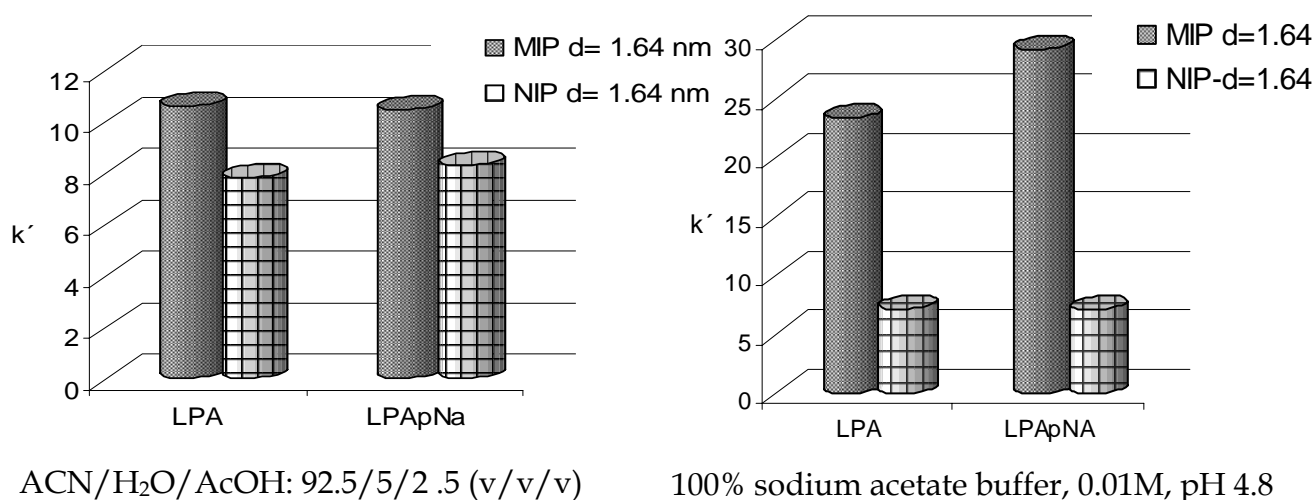


**Figure 5-26:** *Imprinting effects in the HEMA-based composites.*

The MAA based composites also exhibited weak enantioselectivity in the organic mobile phase, with separation factors below 2 (Figure 5-27). The highest separation factor was obtained for the composites possessing layer thicknesses of 1.9 nm. In this case, the separation factors were higher for the p-nitro derivative than for the actual template. Due to the electron withdrawing effect of the nitro group the amide became more acidic. This is an important interaction group in the recognition process and therefore this compound was slightly more retained than the actual template (although still no racemic resolution was possible).

These thin film polymers also exhibited an imprinting effect (Figure 5-28). When comparing the selectivities of blank and imprinted polymers with 1.3 nm, the template L-PA was 3.7 times more retained on the MIP than on the blank. The fluorescent p-nitro analogue was again retained more than the actual template on the MIP (5.8 times more than on the blank).

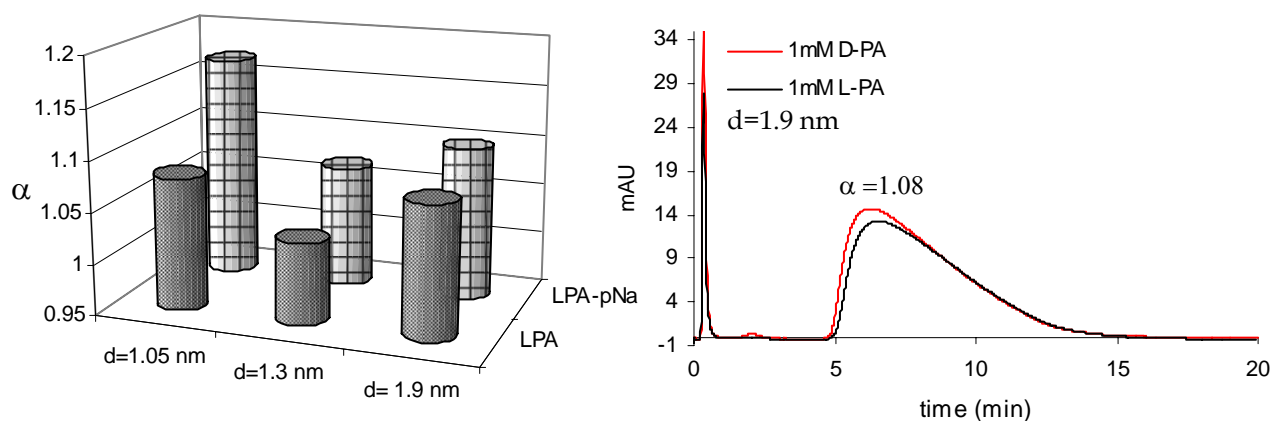


**Figure 5-27:** Enantioselectivity of MAA based composites (10  $\mu$ L of 1mM solutions, flow: 1mL/min, columns 50 x 5 mm. i.d.) in ACN/H<sub>2</sub>O/AcOH: 92.5/5/2.5 (v/v/v). The elution profiles were obtained using a column packed with the composites with  $d=1.9$  nm.

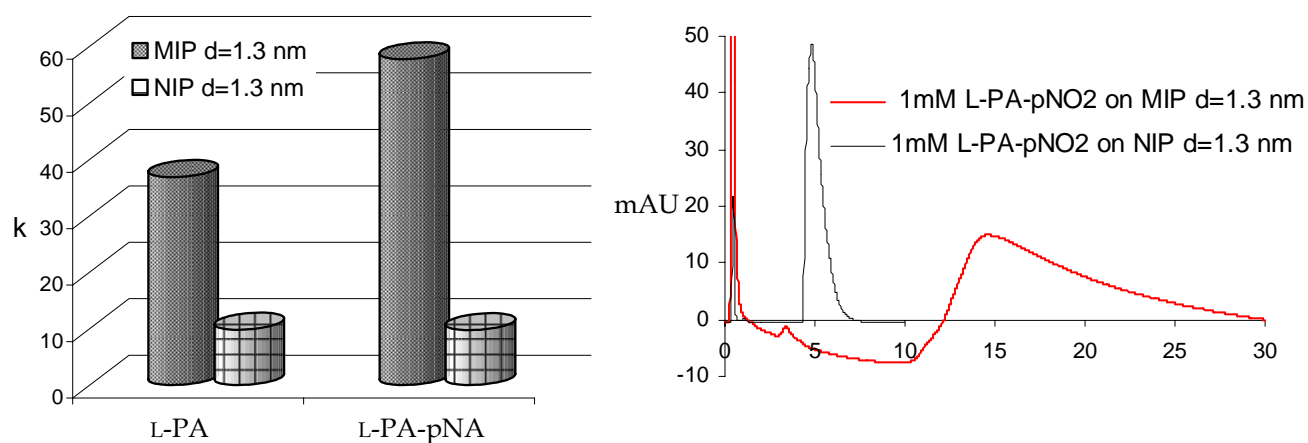


**Figure 5-28:** Imprinting effects in MAA-based composites.

### 5.3.4 Conclusions

The last subchapter confirmed that CRP using iniferters is an attractive way to produce thin film molecularly imprinted composites. The method is very easy and has the advantage of completely avoiding polymerisation in solution due to the non-active radical formed upon iniferter decomposition. The materials can be prepared very quickly, and the method should be compatible with a variety of monomers/solvents combination.

The system confers living radical properties to the resulting composites, therefore several layers of polymers with different structures and properties can be grafted.

Benzyl-*N,N*-diethyldithiocarbamate iniferters have been previously used for micropatterning of polymer regions by lithography techniques [167,168]. Associating this concept with molecular imprinting and transferring the iniferter principle described so far to 2-D micropatterning by lithography may assist in the development of chip-based sensor arrays (Figure 5-29).

The composites prepared using iniferters showed a lower stability in HPLC than those prepared using azo-initiators, but still exhibited significant enantioselectivity in equilibrium batch rebinding experiments.

Using HEMA it was possible to graft a hydrophilic imprinted polymer layer showing higher affinity for its template in an aqueous medium than in an organic-based environment.

The efficiency of the separation could be tuned by changing the polymerisation time, a maximum in selectivity being recorded for 240 min corresponding to a grafted density of *ca.*1.6 nm.

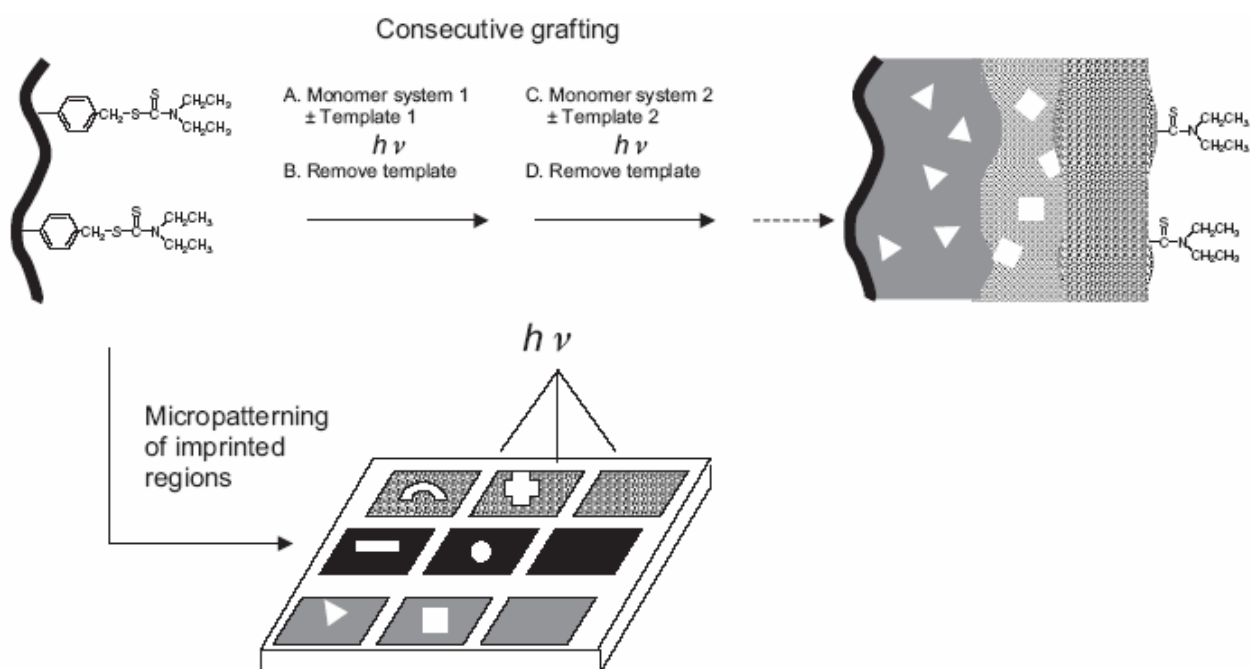


**Figure 5-29:** Scheme showing the possible use of iniferter modified surfaces to prepare nano- or micro-structured molecularly imprinted surfaces or materials. The consecutive grafting can yield two layers imprinted with two different templates or one imprinted layer and one non-imprinted layer. Different monomer systems can be used in each step (Adapted with permission from [8]).

#### 5.4 THIN-WALLED IMPRINTED POLYMERS GENERATED FROM INIFERTER-BASED COMPOSITES

Concepts that have become particularly important in the field of material design with superior level of structural control are grafting and controlled radical polymerisation (CRP) on one side and templated synthesis of materials on the other. Combining these two concepts an unprecedented class of nanostructured materials was generated. This refers to MIPs with very thin walls (1-10 nm), exhibiting a gel-like behaviour.

The concept of CRP grafting on an inorganic support of known morphology was described earlier in this chapter (section 5.1), while chapter 4 dealt with the subject of template synthesis. As a brief reminder template synthesis allows porous materials with morphologies controlled by the solid template to be prepared. Here, either an organic polymer may serve as a shape template for the synthesis of an inorganic porous network [189,190]) or, alternatively, an inorganic material may serve as template for the synthesis of organic materials of defined morphology [101,1,2].

After grafting a thin molecularly imprinted polymer layer on the silica support using iniferters, the silica was etched away, resulting in beads with about half the size compared with the original material (Figure 5-30). The properties of these materials are distinct from those of the materials obtained using “hierarchical imprinting”, where complete pore filling took place before the dissolution process. These are generated from iniferter-based composites, where the pores are not completely filled during the polymerisation process. Therefore, silica dissolution should leave behind a polymer structure with very thin, nanometre walls.

So far in the literature, there are few examples of the combination of CRP and template synthesis. Walt *et al.* used ATRP to graft thick polymer layers on porous silica [191]. Etching away the silica template, hollow spheres remained with a relatively thick shell with thickness larger than 175 nm. Thinner grafts would offer more interesting possibilities, but have so far not been disclosed in the literature.

Polymeric materials with nano-walls would potentially exhibit good high capacity and site accessibility.

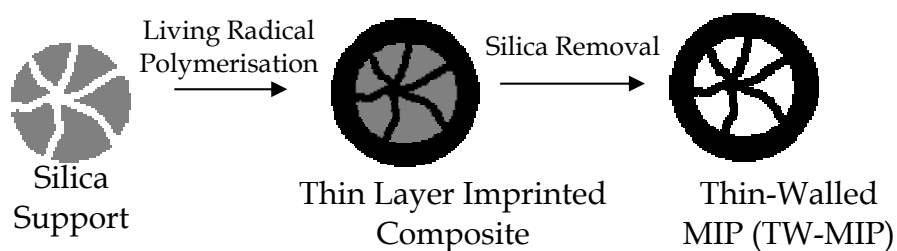


**Figure 5-30:** Schematic representation of thin-walled MIPs synthesis.

#### 5.4.1 Synthesis and Characterisation

According to HPLC experiments, the composites obtained after 120 and 240 min polymerisation times respectively, showed the highest affinity for the template and an analogue. Therefore, we focused on these materials and generated polymers with nanometre thin walls as shown in Figure 5-30. The corresponding non-imprinted thin layer composites were used for the generation of non-imprinted thin-walled materials. Both HEMA and MAA based composites were subjected to the dissolution process.

The extent of silica removal was monitored using microelemental analysis, EDX, TG and FT-IR spectroscopy. The percentage of carbon in the resulting polymers was very close to the theoretical value calculated considering the stoichiometry of the monomers used in the grafting step (59.2 for MAA/EDMA and 58.3 for HEMA/MAA/EDMA). The exact values of the carbon, nitrogen and sulphur content in the thin walled MIPs are given in Table 5-3.

**Table 5-3:** Elemental microanalysis of the generated thin-walled MIPs and NIPs.

TW-Materials	%C	%N	%S
MIP-MAA-2h	59.27	0.18	0.62
NIP-MAA-2h	58.87	0.16	0.61
MIP-MAA-4h	59.52	0.15	0.73
NIP-MAA-4h	59.24	0.17	0.72
MIP-HEMA-2h	55.97	0.05	0.71
NIP-HEMA-2h	55.43	0.15	0.72
MIP-HEMA-4h	56.27	0.15	0.79
NIP-HEMA-4h	56.65	0.13	0.76

As can be observed, the thin-walled MIPs contained a high content of sulphur in their composition. Given that the mass loss during the dissolution process was ~60% this value is lower than the one corresponding to the same amount of coupled iniferter as before dissolution (see Table 5-2). This might be to the fact that, not all the iniferter groups took part in the polymerisation process and some of them remained intact on the silica surface. Therefore, during the dissolution step, some of this iniferter groups were lost, explaining thus the lower sulphur content in the thin-walled materials than the expected value. In order to check the origin of the sulphur in the thin-walled polymers we first investigated the stability of the iniferter molecule in the ammonium hydrogen difluoride solution. For this purpose, we synthesised the iniferter initiator in solution reacting benzyl chloride with sodium, *N,N*-diethyldithiocarbamate trihydrate according to a literature procedure [192]. This iniferter was subjected to the same conditions used for the removal of silica from the composites. After 24h, the aqueous solution of  $\text{NH}_4\text{HF}_2$  containing the iniferter was neutralised and extracted with chloroform. After removing the solvent, a yellow oil with the same appearance as the original iniferter was obtained.  $^1\text{H-NMR}$  and elemental analysis confirmed that the iniferter *N,N*-diethyl-*S*-benzyl-dithiocarbamate did not suffer any structural change during the dissolution process (see section 6.4.5-6).

After this experiment we could conclude that our thin-walled polymers still contained the iniferter in their composition. The iniferter did not suffer any

decomposition or structural modification during the rather harsh dissolution process. This explained the high content of sulphur in the polymers composition. Under these conditions, we may assume that the thin-walled MIPs could still exhibit living properties.

The SEM picture in Figure 5-31 shows the silica elemental mapping of the thin walled MIP obtained from the HEMA composite after 240 min polymerisation time ( $d = 1.64$  nm). The picture represents a cross-section through the polymeric material after it was incorporated in an epoxy resin and cut with a diamond cutter. Looking at the elemental mapping for Si one can see that only a very small percentage of the material still contains silica. More precisely, from all the particles present in the SEM picture only one still had non-dissolved silica. The rest of particles were only polymer beads with no silica trapped inside.

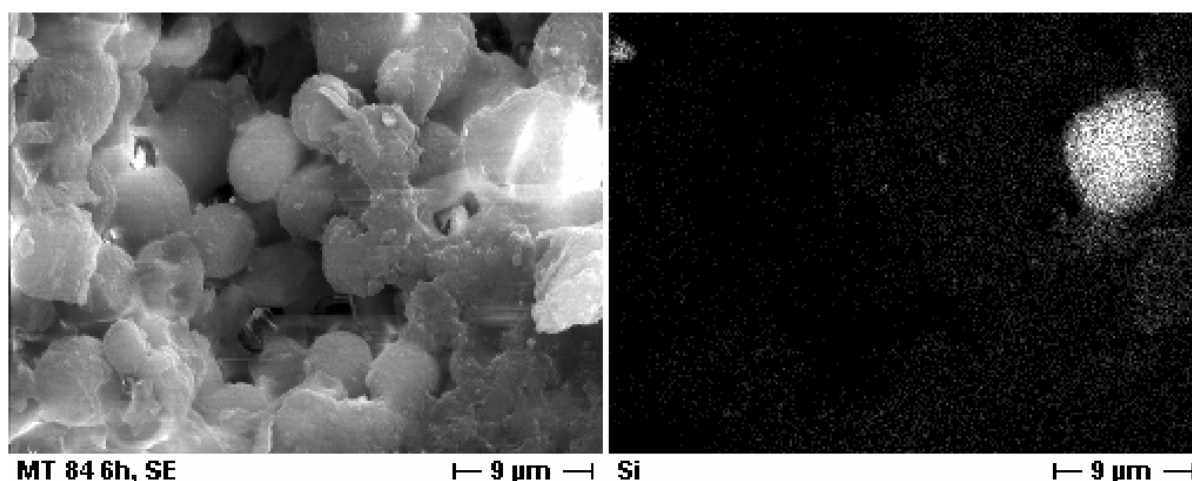


**Figure 5-31:** Silica elemental mapping of HEMA thin-walled MIP.

Figure 4-32 shows the comparison between the IR spectra of the iniferter composites and of the newly generated thin-walled MIPs. No peaks that could be assigned to the silica absorption bands were present in the spectrum of the thin-walled polymers. Both the absorption band at  $450\text{ cm}^{-1}$  corresponding to the Si-O-Si stretching mode and that at from  $1100\text{ cm}^{-1}$ , belonging to Si-O-Si stretching frequencies of siloxanes, were no longer present in the thin-walled MIP spectrum. The intensity of the peak corresponding to the C=O group increased as compared to the one in the composite spectrum.



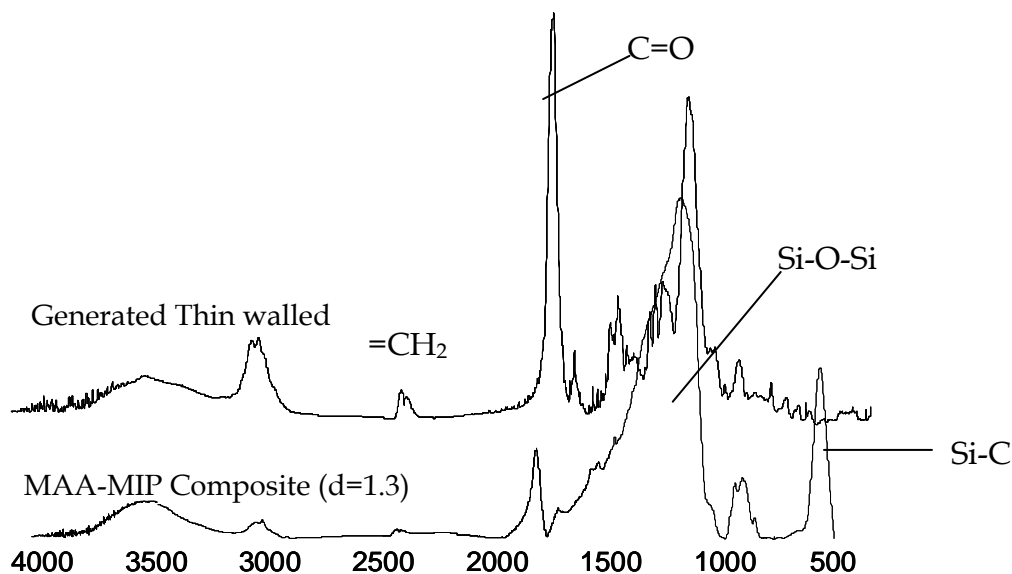


**Figure 5-32:** FT-IR of the iniferter composite and the corresponding thin-walled MIP.

The successful removal of the silica from the composites was also monitored using TGA.

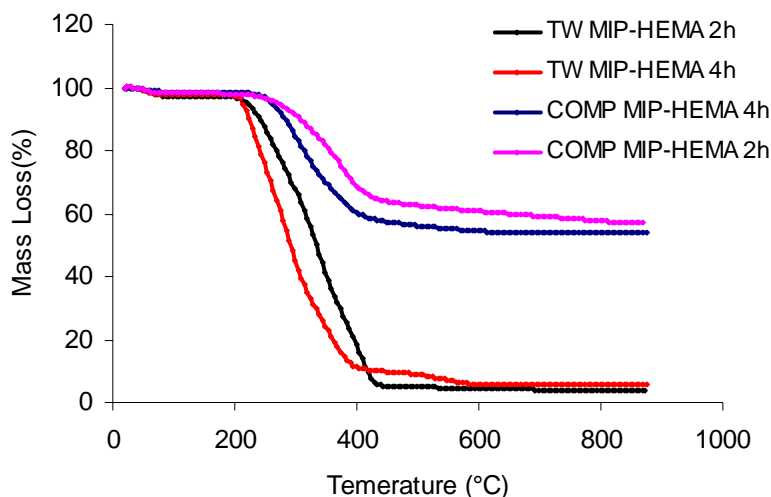
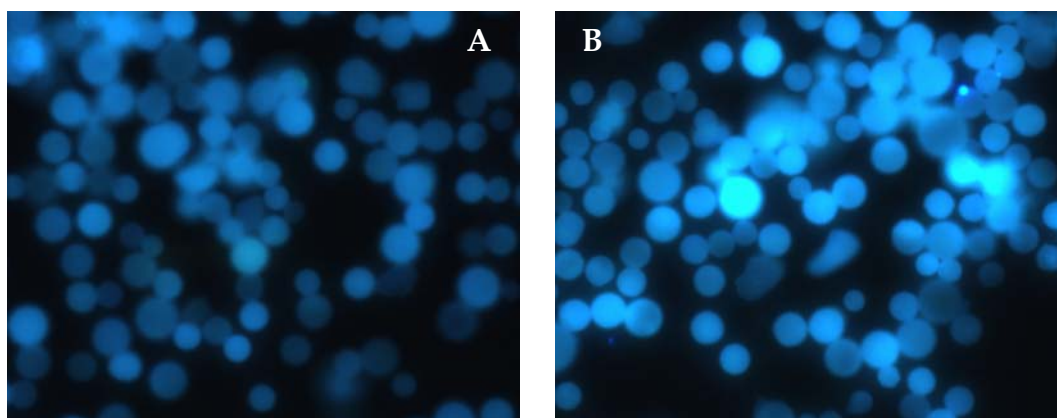


**Figure 5-33:** TGA of the thin-walled imprinted polymers and the corresponding composites.

Thus, the TW-polymers exhibited a similar behaviour with the hierarchically imprinted polymers described in section 4.2.4. Increasing gradually the temperature up to 1000°C, the samples started decomposing. At ~400°C insignificant amount of sample was left in the crucible for both HEMA and MAA based TW-polymers,

whereas for the corresponding composite ~60-70% of the sample was still present (Figure 5-33). The remaining residue corresponded to the silica contained in the sample, proving that for the TW-material the silica was successfully removed.

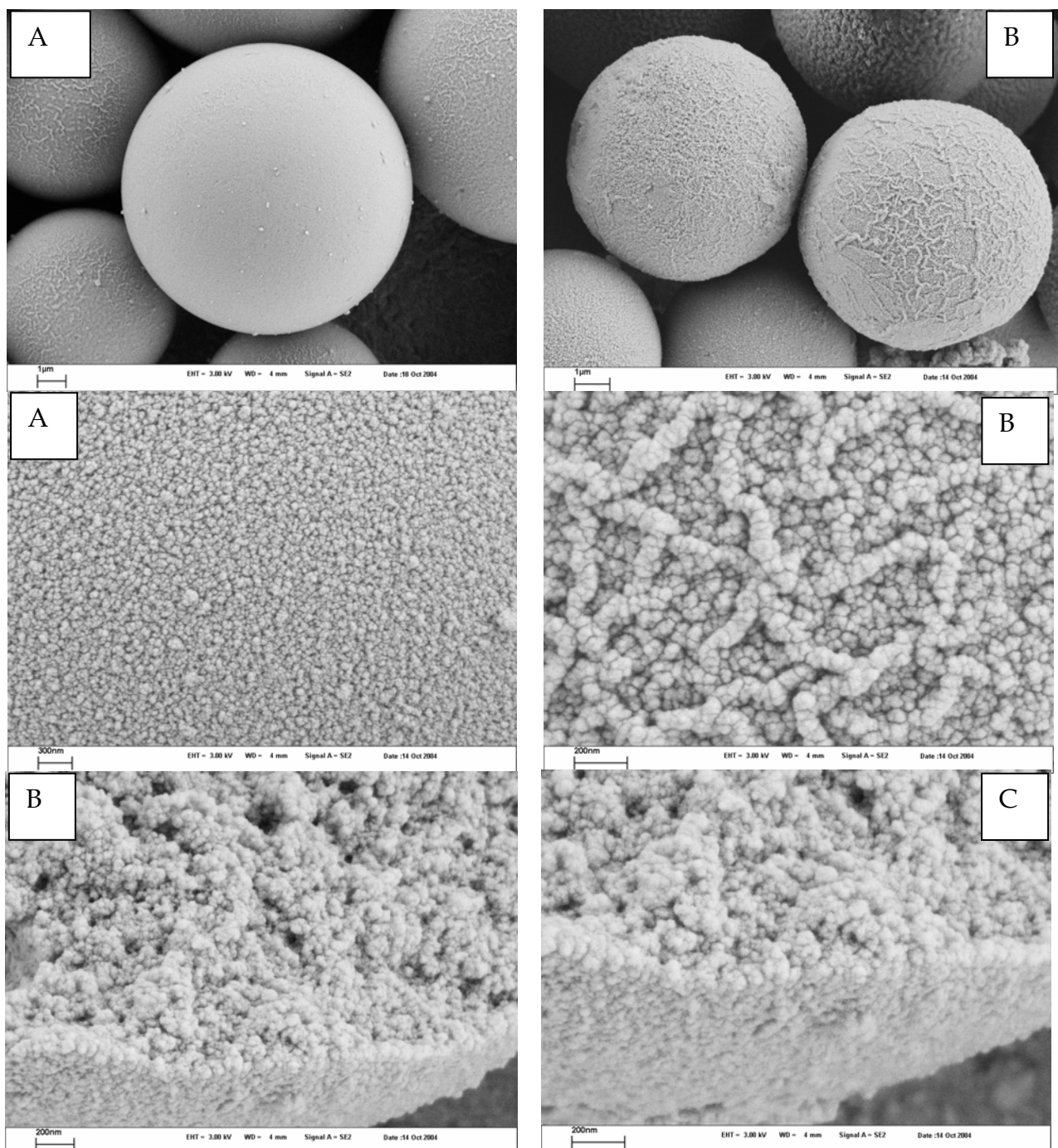
The accessibility of the MIP binding sites was then assessed via fluorescence spectroscopy. Composite and thin-walled MIP samples were labelled under the same conditions with the fluorescent dye 3-aminoquinoline and investigated with respect to the intensity of fluorescence within and between particles. Clearly, the nanometre-walled materials exhibited a stronger fluorescence than the corresponding composites, indicating a higher amount of coupled 3AQ than the composite materials (Figure 5-34).

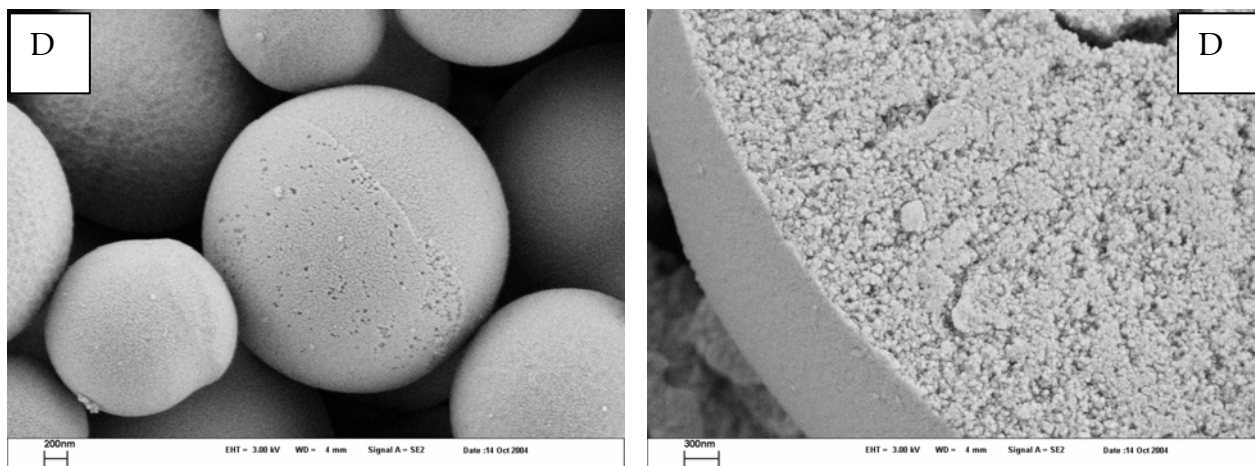


**Figure 5-34:** Fluorescence micrographs; (A) MAA iniferter based composites after 240 min polymerisation time ( $d= 1.3$  nm); (B) Thin-Walled MIP obtained after dissolution of silica from A after labelling with 3AQ. Pictures were taken at  $x$  100 magnification.

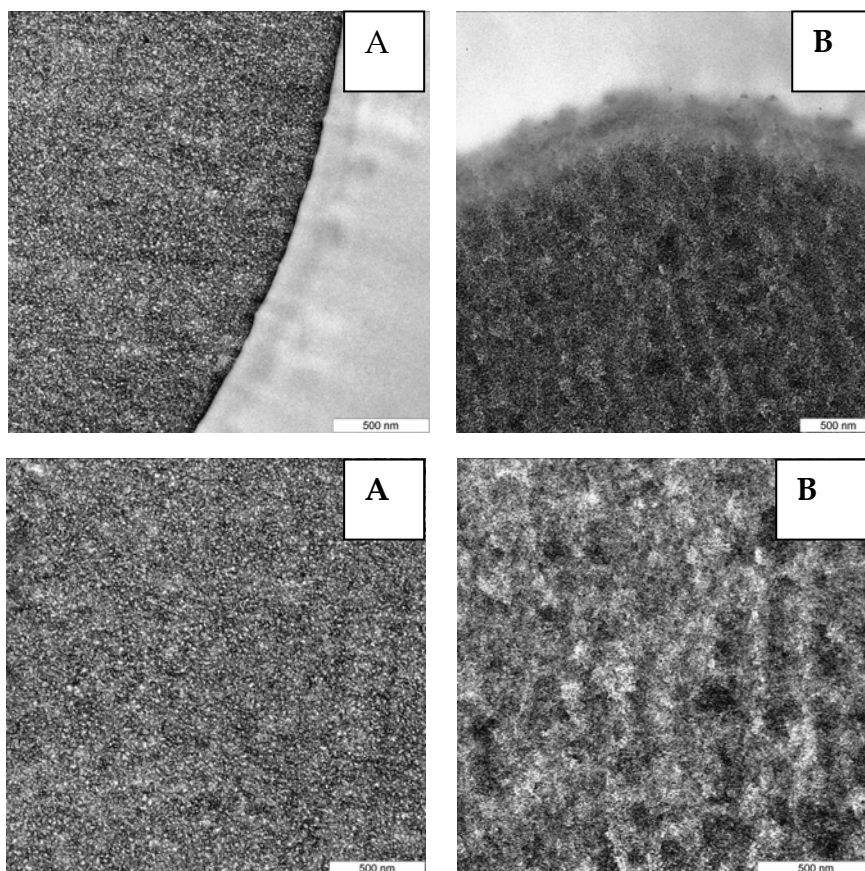
Scanning electron micrographs revealed spherical and non-agglomerated particles with a size around 7  $\mu\text{m}$ , smaller than the original silica (Figure 5-35-A,B). The surface was not as smooth as for the composite particles being probably due to shrinking of the particles during the dissolution step, as was also reflected by the smaller particle sizes of the new polymers as compared to the composites. In order to better elucidate the morphology of these materials, a cross section was made using a cutter. This method allowed us to visualise the internal morphology of these polymers. The particles were not hollow inside and a different morphology between the outer surface and the interior could be observed.

The outer surface appeared somehow denser in the outer shell than the interior. This was in agreement with the morphology of the iniferter composites. TEM confirmed also the different internal morphology and showed a porous texture in the interior of these polymers (Figure 5-36). Nevertheless, this internal morphology differed from the starting silica and from the composites, since the particles no longer contained silica in their composition. Also, due to the incorporation in epoxy resin, the contrast between the resin and the polymeric thin-walls was poorer compared to composites or silica.





**Figure 5-35:** SEM of thin-walled MIPs and cross-sections generated from iniferter composites: (A) MAA/HEMA/EDMA composites ( $d = 1.64$  nm) (B) HEMA/MAA/EDMA thin-walled MIP obtained from the composite with  $d = 1.64$  nm; (C) HEMA/MAA/EDMA thin-walled MIP obtained from the composite with  $d = 1.43$  nm; (D) MAA/EDMA thin-walled MIP obtained from the composite with  $d = 1.3$  nm.



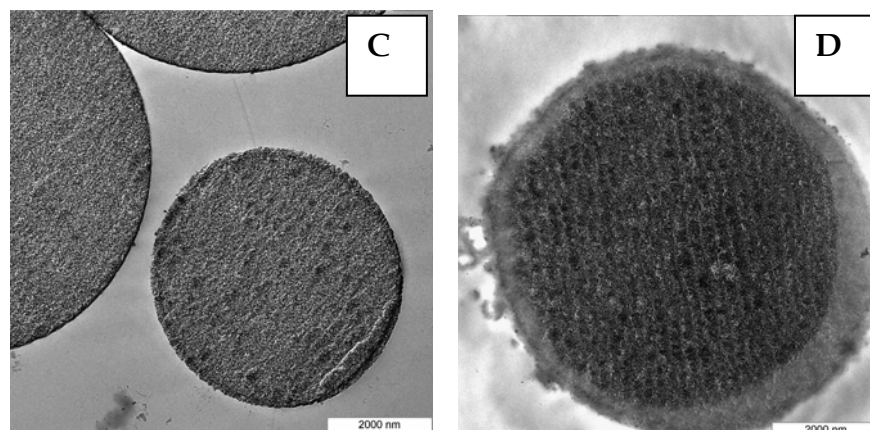


**Figure 5-36:** TEM of thin-walled MIPs and cross-sections generated from iniferter composites; (A) MAA/HEMA/EDMA composites ( $d = 1.64 \text{ nm}$ ) (B) HEMA/MAA/EDMA thin-walled MIP obtained from the composite with  $d = 1.64 \text{ nm}$ ; (C) starting silica template; (D) MAA/EDMA thin-walled MIP obtained from the composite with  $d = 1.3 \text{ nm}$ .

In the dry state, the materials exhibited no porosity as proven by nitrogen sorption experiments. Swelling experiments were performed in the following solvents: ACN, toluene, and 0.01 M sodium acetate buffer pH= 4.8 and cyclohexane. The volume swelling ratio was calculated as:  $V_s \text{ ratio} = \text{bed volume swollen particles } (V_s) / \text{bed volume dry particles } (V_d)$ . Pronounced swelling up to the original composite size was observed in all ACN, DCM and toluene (Table 5-4). The non-imprinted counterparts exhibited lower swelling volume ratios (1-1.1 mL/mL). The presence of the templated binding sites strongly influenced the swelling of the polymers. A similar effect was also observed by Piletsky *et al.* on (+)-ephedrine imprinted polymers [193]. The high swelling and the lack of porosity in the dry state confirmed once more the fact that they acted like gels. Their properties contrasted with those of the hierarchically imprinted polymers, where mesoporous materials with high surface areas were obtained and almost no swelling was observed (see section 4.1.4). The difference came from the fact that in the hierarchical imprinting the pores were completely filled with the monomers, therefore, upon dissolution, a stable mesoporous polymer was obtained with mesopores around 6-8 nm. These values represented the thickness of the initial pore walls in the original silica. In the case of iniferter composites, the polymerisation took place *via* initiator groups on the silica surface forming a thin imprinted layer around and inside the silica bead.

Therefore, after removing of the silica matrix, a free-standing thin-walled polymeric structure should be obtained.

**Table 5-4:** Volume swelling ratios of the thin walled MIPs and NIPs.

Solvent	$V_s$ MAA-TW-MIP4h	$V_s$ MAA-TW-NIP4h	$V_s$ HEMA-TW-MIP4h	$V_s$ HEMA-TW-NIP4h
ACN	1.6	1.0	1.9	1.1
Toluene	1.6	1.0	1.9	1.0
Buffer (pH= 4.8)	1.1	1.0	1.1	1.0
Cyclohexane	1.2	1.0	1.3	1.0

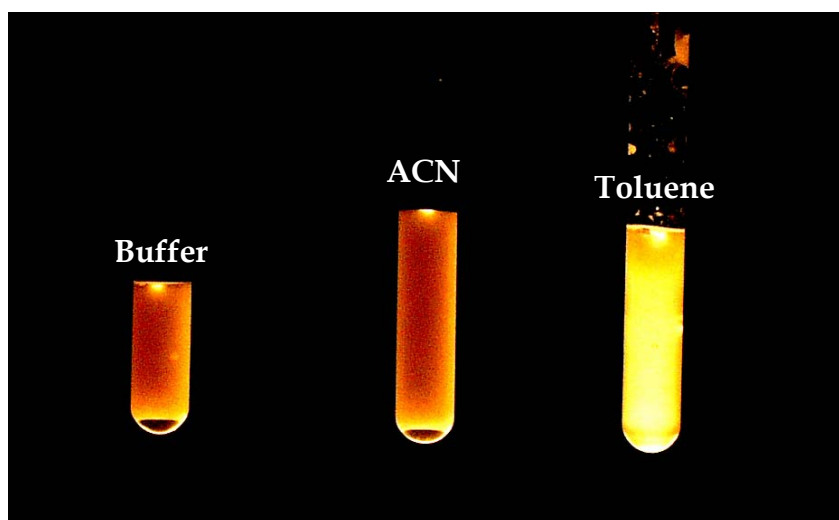


**Figure 3-37:** Visualisation of the swelling and change in colour upon swelling of the HEMA 4h TW-MIPs in toluene, ACN and Buffer (pH=4.8).

In contrast with the traditional bulk polymers and with the hierarchically imprinted polymers the thin-walled MIPs became almost transparent in toluene (Figure 3-37). This property was most likely due to the thin-walled structure of these materials.

In order to obtain information about the total pore volume in the non-swollen state, a non-swelling is generally used to measure the solvent uptake of the polymer. Thus, after the swelling experiments, the excess of cyclohexane was carefully removed and allowed to evaporate until the particles were freely flowing and separate. At this stage, only the pores were assumed to be filled with solvent and the volume uptake was calculated as:

$$\text{Solvent uptake} = ((\text{Weight filled particles} - \text{Weight dry particles}) / d_{\text{solvent}}) / \text{Weight dry particles})$$

MAA-TW-MIP4h: Solvent uptake (Cy)= 1.173 mL / g

HEMA-TW-MIP4h: Solvent uptake (Cy)= 1.672 mL / g

#### 5.4.2 Enantioselectivity of Thin-Walled MIPs and Corresponding Composites

Due to the very pronounced swelling in all the employed mobile phases, these particles were not suitable for chromatographic applications. Therefore, their ability to discriminate between the template and its antipode was investigated in a static equilibrium mode, through batch rebinding experiments.

Adsorption isotherms for the thin-walled MIPs and iniferter composites were obtained by adding incremental amounts of each enantiomer to a given amount of polymer. After equilibration, the concentrations of free enantiomer in the supernatant solutions were measured using HPLC. The concentration of the adsorbed enantiomer was then obtained by subtraction. Figure 5-38 shows the adsorption isotherms of D- and L-PA that were obtained for the adsorption on an L-PA imprinted thin-walled HEMA-MIP and a corresponding non-imprinted material generated from the non-imprinted HEMA composites. The adsorption isotherms for the MAA-based thin-walled MIPs and corresponding composites are shown in Figure 5-39.

For the MAA/EDMA system the solvent used in these experiments was 100% ACN, while for the MAA/HEMA/EDMA system ACN/phosphate buffer (pH=4.8) =30/70(v/v) was used. The adsorption isotherms for the thin-walled MIPs were obtained and compared with those of the corresponding composites.

The iniferter composites exhibited a pronounced enantioselectivity when assessed in batch rebinding experiments, when compared to the HPLC data. This may be due to a low mass transfer process and the shortage of time to equilibrate in the

HPLC mode. The interactions between the template and the binding sites had more time to develop under static conditions equilibrium (batch rebinding).

The binding capacity, affinity and enantioselectivity in the thin-walled MIPs were high for both the HEMA and MAA systems, and clearly enhanced as compared with the corresponding composites. This was probably due to the better accessibility at the imprinted sites upon removal of the silica template. Some previously inaccessible enantioselective binding sites were freed-up and could take part in the recognition process. The uptake of the template increased with the polymerisation time for the composites as well as for the thin walled-materials, this behaviour being more pronounced for HEMA-based materials.

At low concentrations, the template uptake was high and the binding sites were saturated at a concentration of  $\sim 1.5$  mM for the HEMA and 3 mM for MAA composites, respectively.

Experimental details about the conditions under which the rebinding experiments were performed are given in section 6.5.8.



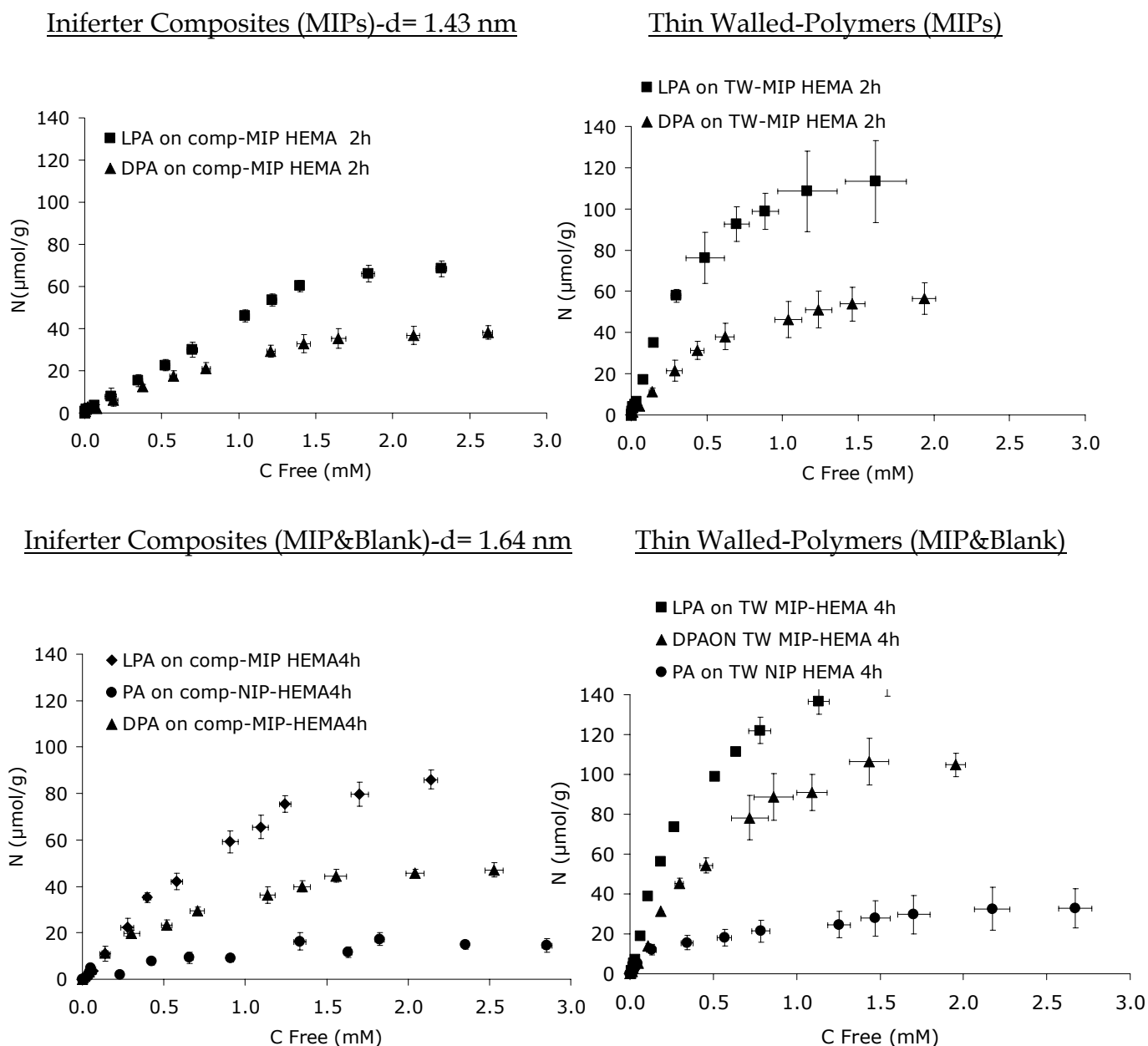
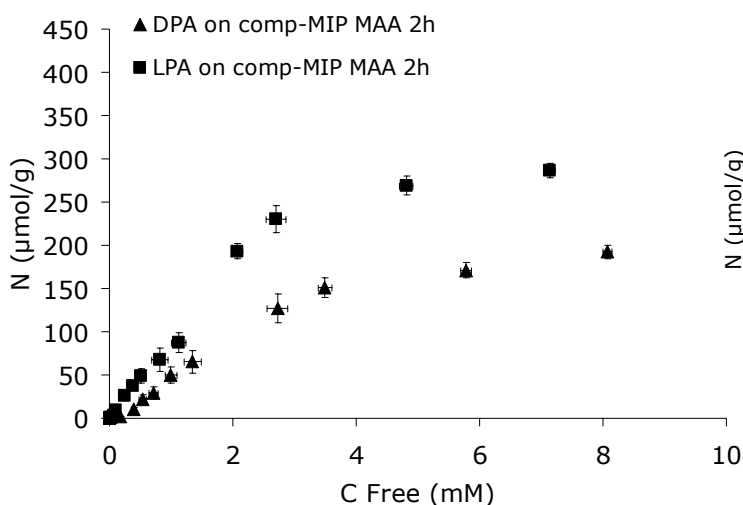
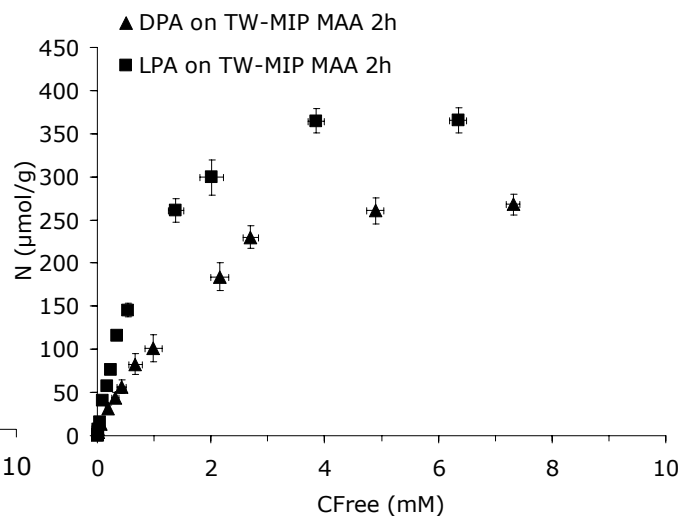


**Figure 5-38:** Adsorption isotherms of D- and L-PA obtained for the adsorption on L-PA imprinted and blank HEMA-based composites and the generated thin-walled MIP and blank polymers. Mobile Phase: ACN/phosphate buffer (pH=4.8) =30/70(v/v); Column: Phenomenex Luna C-18 (125 x 4.6 mm); Flow 1mL/min; Detection: UV 260 nm.

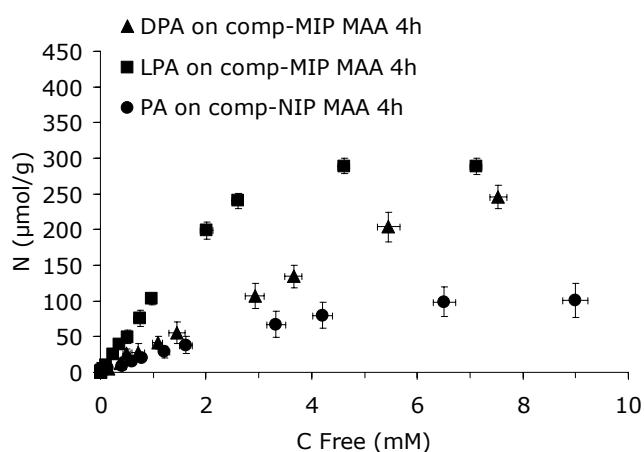
Iniferter Composites (MIP) d= 1.05



Thin-Walled Polymers (MIP& Blank)



Iniferter Composites (MIP&Blank)-d=1.3



Thin-Walled Polymers (MIP& Blank)

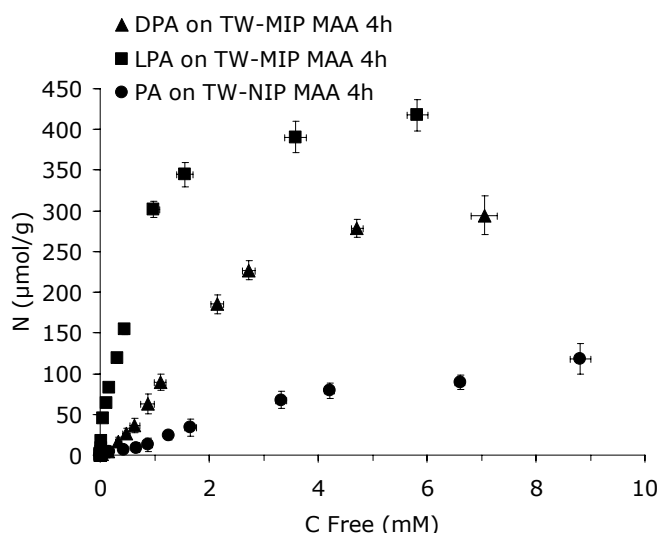


**Figure 5-39:** Adsorption isotherms of D- and L-PA obtained for the adsorption on L-PA imprinted and blank MAA-based composites and the generated thin-walled MIP and blank polymers. Mobile Phase: 100% ACN; Column: Phenomenex Luna C-18 (125 x 4.6 mm); Flow 1mL/min; Detection: UV 260 nm.

For isotherms adhering to the Langmuir isotherms, the binding constant and saturation capacity can be estimated graphically from a linearised version of the isotherm. This is done by plotting the isotherm in a Scatchard format (or x reciprocal format), where each linear region of the isotherm is fitted with a straight line by linear regression. The binding constant is calculated from the slopes and the saturation capacity from the y-intercepts

$\frac{N}{C_{\text{Free}}} = bq_s - bN$	Where:	
	N =	amount of adsorbate bound on polymer
	$C_{\text{Free}}$ =	concentration left in solution
	b =	binding constant
	$q_s$ =	saturation capacity

The binding constant is related to the association constant:  $K_a = b M_w$

where  $M_w$  = molecular weight of the adsorbate

Figure 5-40 shows one example of Scatchard plots of the isotherms data for the batch rebinding of L-PA to the HEMA based composites and the corresponding thin walled MIPs.

The Scatchard plots indicated homogeneous binding sites for both, the composites and the thin-walled materials. However, the binding sites became more homogeneous and accessible upon removal of the silica matrix. On the thin walled MIP generated from the composite with 1.64 nm layer thickness these sites amounted ~160  $\mu\text{mol/g}$ . This corresponded to a quantitative yield of imprinted sites based on the amount of template added to the monomer mixture and is unprecedented for MIPs prepared using conventional monomer systems. The 100% uptake of the template was likely due to the fact that the binding sites are confined to the very thin nanometre wall. In traditional MIPs, saturation capacities in the range of 1  $\mu\text{mol/g}$  or even lower are seen. This corresponds to a yield of binding sites of less than 1%.

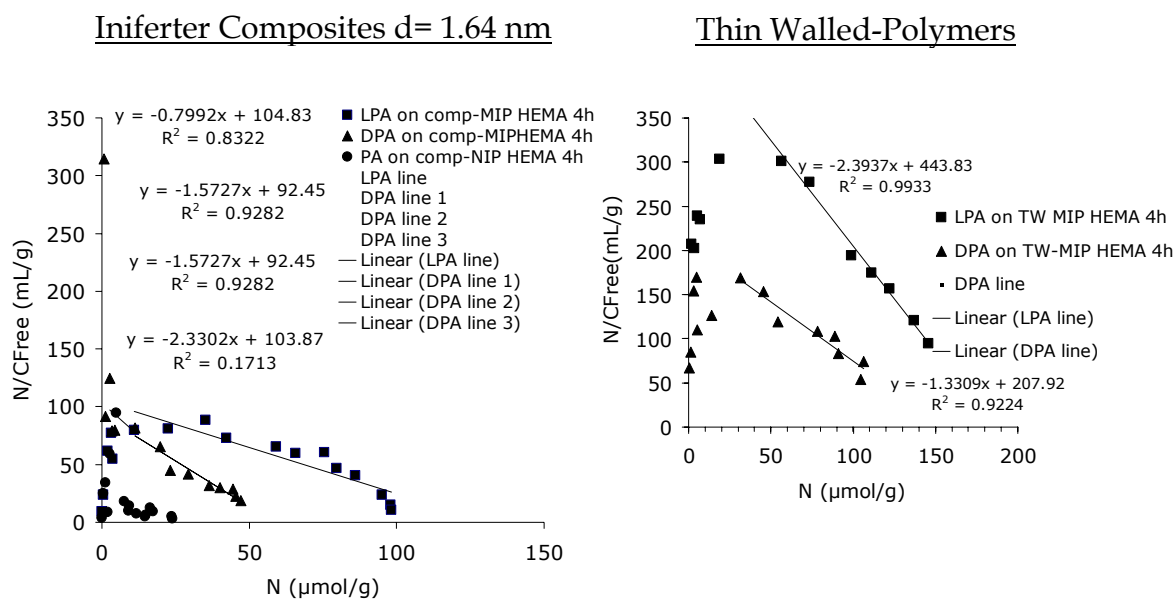


**Figure 5-40:** Scatchard plots of the adsorption isotherms of HEMA-based composites and TW-polymers represented in Figure 5-38.

It also has to be stressed that the recognition and binding experiments were performed in a water-based mobile phase (70 % buffer pH= 4.8). Generally so far, considerably lower binding constants were observed in more polar protic solvents. The good compatibility with the aqueous environments is most likely due to the presence of the hydrophilic co-monomer HEMA. The association constants determined from the linear region of the Scatchard plots are  $K_a = 2185 \text{ M}^{-1}$  for the thin-walled MIP generated from the composite polymerised for 2h and  $K_a = 2393 \text{ M}^{-1}$  for the thin-walled MIP generated from the composite polymerised for 4h, respectively.

The MAA-based thin-walled MIPs showed also a homogeneous distribution of binding sites. Also in this case there was an increase in the homogeneity and accessibility of the binding sites as compared to the composite. The sites amounted to *ca.*  $400 \mu\text{mol/g}$ , corresponding to a yield of imprinted sites of 80% and an association constant,  $K_a = 2166 \text{ M}^{-1}$ .

The results from batch-rebinding experiments were sustained by fluorescence microscopy (Figure 5-41, Figure 4-42). For this, the fluorescent p-nitro analytes L- and D-PA-pNa were employed. Thus, solutions of 1 mM D- and L-PA-pNa were prepared in 100 % ACN for the MAA/EDMA system and in ACN/phosphate buffer (pH=4.8) =30/70(v/v) for the HEMA/MAA/EDMA. A given amount (10mg) of blank and imprinted polymers (comp. and TW) was allowed to equilibrate in 1mL of these solutions. After equilibration the solvent was removed and the particles containing the bound template analogue were investigated with respect to the fluorescence intensity. In agreement with the binding experiments, the imprinted polymers equilibrated with L-PA-pNa exhibited a stronger fluorescence than those equilibrated with the solution of the antipode. The blank polymers exhibited no fluorescence after equilibration with either L-or D-PA-pNa. The TW-MIPs equilibrated with L-PA-pNa exhibited a stronger fluorescence than the corresponding composites equilibrated with the same solution. This behaviour was observed for both the HEMA- and MAA-systems for both polymerisation times.

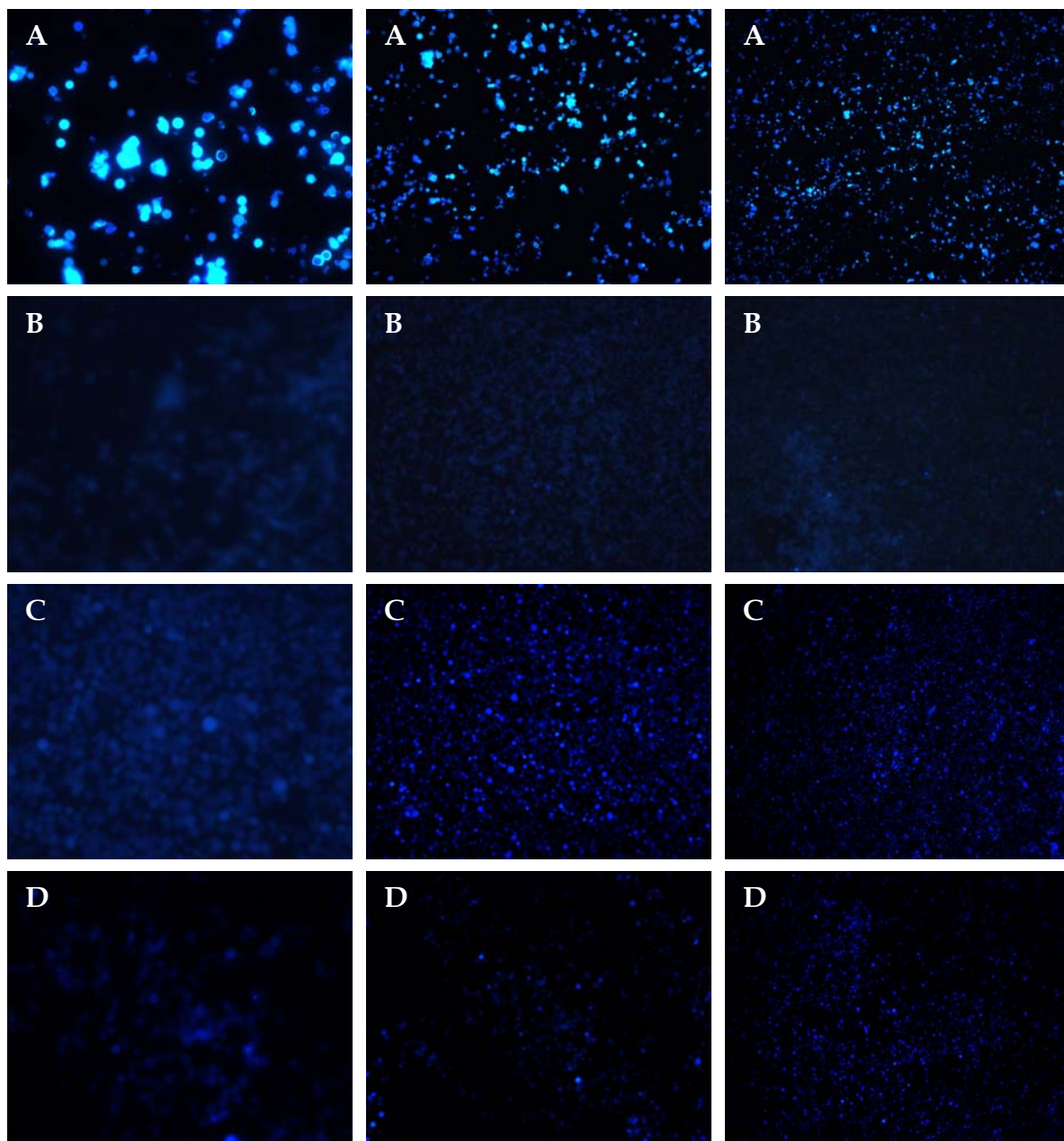


**Figure 5-41:** Fluorescence micrographs of the HEMA 4h based composites and TW- MIPs after equilibration in a 1mM solution of L/D -PA-pNa: (A) TW + L-PA-pNa, (B) TW + D-PA-pNa, (C) Comp.+ L-PA-pNa, (D) Comp. + D-PA-pNa. The pictures were taken at a magnification of x 40, x 20 and x10, respectively.

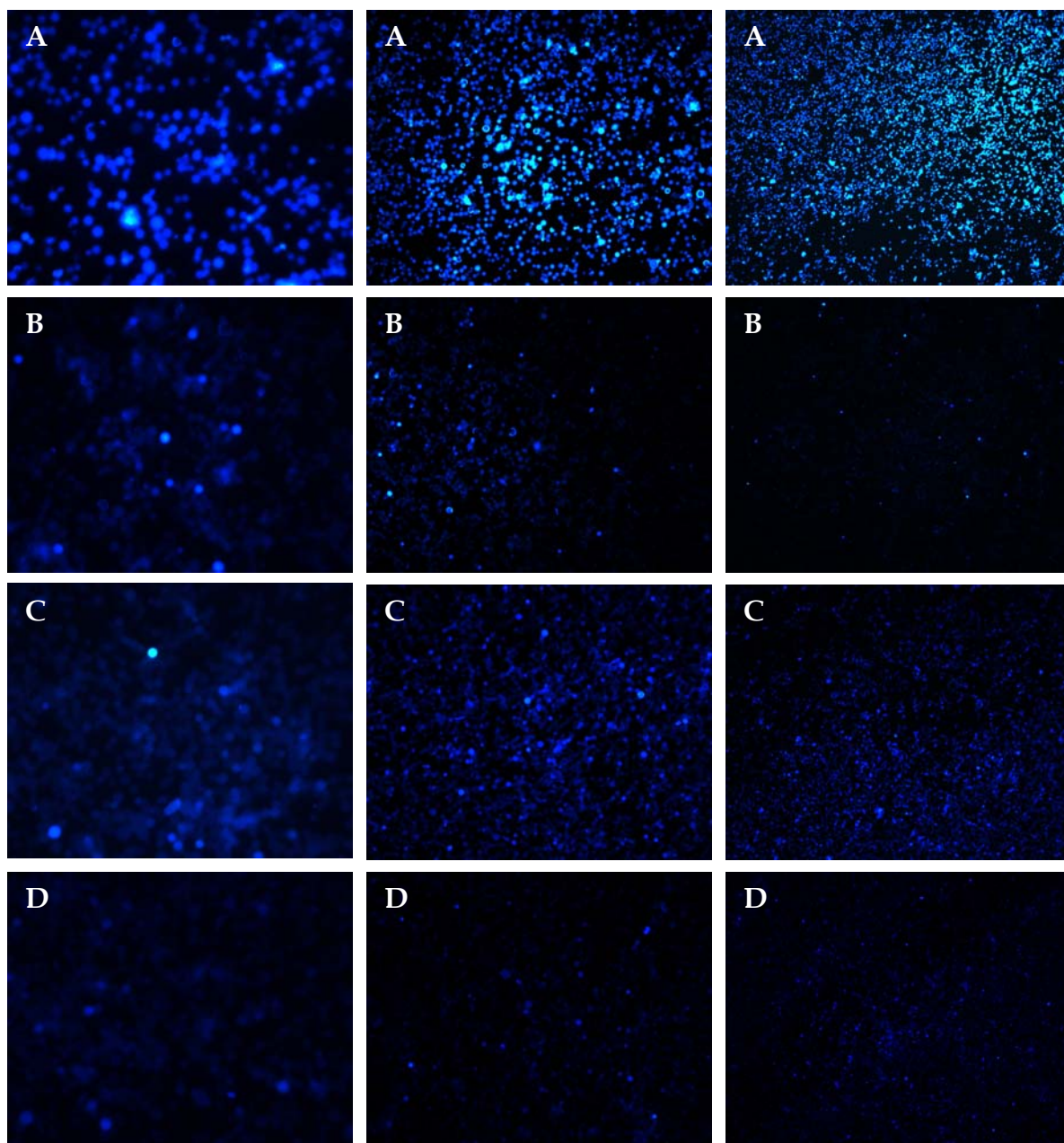


**Figure 5-42:** Fluorescence micrographs of the MAA 4h based composites and TW-MIPs after equilibration in a 1mM solution of L/D -PA-pNa: (A) TW + L-PA-pNa, (B) TW + D-PA-pNa, (C) Comp.+ L-PA-pNa, (D) Comp. + D-PA-pNa. The pictures were taken at a magnification of x 40, x 20 and x10, respectively.

In order to better elucidate the binding events that take place in the thin-walled polymers and composites adsorption kinetic measurements on the MAA/HEMA/EDMA-4h system were performed.

For most applications of specific molecular recognition elements, fast association kinetics in the host-guest interactions are important. For example, in chemical sensors, the response time depends on the association rate between the sensor bound receptor and the target analyte. The kinetics thus influences the sample throughput of analysis, *i.e.* how many samples can be analysed in a certain time interval. Furthermore, in catalysis, the binding kinetics, if being the rate limiting step, determine the rate of chemical transformation and, in chromatographic separations, it will influence the spreading of the chromatographic peaks.

So far, the MIPs prepared via conventional monolith procedure have very slow association-dissociation kinetics due to a heterogeneous population of binding sites and a poor mass transfer.

In the TW-polymers the binding events take place in very thin walls, and as concluded from batch rebinding experiments the binding sites in these materials were homogeneous. Therefore, a fast adsorption kinetic should be expected for such materials.

Kinetic experiments were performed by adding 1mM solution the template L-PA and its optical antipode D-PA to a known amount of HEMA-TW polymer (MIP and NIP) and the corresponding composites. After the addition of the solute, the binding events were recorded by measuring the concentration in the supernatant solution using an HP 1050 instrument each minute. The concentration was monitored till it remained constant, meaning that no more template was bound in the binding sites. The results obtained are shown in Figure 5-43. For the thin-walled materials the adsorption kinetics were very fast. It appeared that most binding took place in the first two minutes after the addition of the template. This was the necessary time for the particles to sediment in order to measure the concentration of the supernatant solution. After 2 minutes, 0.7 mM L-PA and 0.58 mM D-PA have been already bound to the TW-MIP. The concentration of bound L-PA increases in the next 17 min up to 0.79 mM, meanwhile the amount of bound D-PA remained almost constant (0.59



mM). The little binding that occurred on the NIP was also fast and had the same value for both enantiomers. Thus, 0.16 mM of L- and D-PA were bound to the TW-NIP after 2 min and the amount of bound template reached only 0.2 mM after 20 min. The adsorption kinetics were slower on the composite materials than on the TW-polymers. This was most likely due to the fact that not all the sites were fully accessible because of the silica matrix. Thus, after 2 min, 0.37 mM L-PA and 0.1 mM D-PA are bound to the MIP-Comp. After 20 min the bound template reached its maximum concentration of 0.58 mM L-PA and 0.29 mM D-PA. Again, little binding occurred on the NIP composite (0.13 mM after 13 min). For the composite materials, the adsorption kinetics were slower for the binding of D-PA than for L-PA on the MIP. The results obtained from the kinetics experiments were in good agreement with the results obtained from batch rebinding (Figure 5-38).

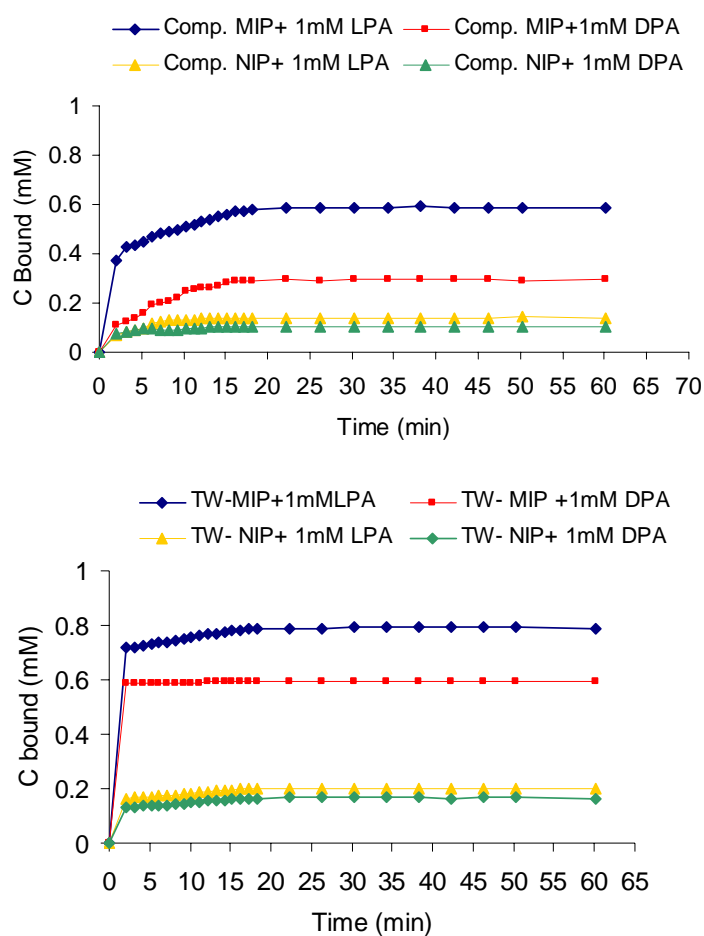


**Figure 4-44:** Adsorption kinetics for the 4h HEMA/MAA/EDMA system.

### 5.4.3 Conclusions and Outlook

The work on molecularly imprinted thin-walled materials is in its incipient stage. It was only demonstrated the principle that, by combining template synthesis with CRP, it is possible to design well-defined nanometre structures. The tailored properties that were applied for this system (enantioseparation of L and D-PA, fast adsorption kinetics) were an improvement in comparison with the composite materials from which this new generation of MIPs were produced.

The applications of this type of materials can be numerous, some examples being their use as adsorbents, in sensors or actuators, to facilitate transfer of a given compound from one phase to another (liquid, solid or gas), to catalyse chemical reactions, as drug delivery vehicles and as screening elements in drug discovery or other therapeutic applications. They could be further designed to exhibit stimuli-responsive functions for use in drug delivery, responsive valves or in artificial muscles.

In the next few lines I would like to discuss some ideas associated with the production and possible applications of this new type of materials.

Because the grafting is performed under CRP conditions, multiple layers may be grafted exhibiting different compositions, structures and functions. After removing the support, the innermost layer (the first grafted layer) would be exposed to give a material with containing two non-equivalent surfaces. In the simplest case, the polarity of the layers could be different; one layer can be composed of a hydrophilic polymer whereas the other layer can be composed of a hydrophobic polymer. After the support removal, a porous material with walls containing one hydrophobic and one hydrophilic surface would be obtained. Depending on the support material morphology, these thin-walled materials could be further designed to exhibit a high surface area. This could be used to enhance the efficiency in liquid-liquid extractions where the hydrophobic pores would be filled with the organic phase and the hydrophilic with the aqueous phase.

Another possibility using this "layer by layer" approach would be to facilitate or catalyse chemical reactions within the film layer.

This can occur either through reactions that happen at the oil/water interface, combined with facilitated transport of the reactants or products, and/or incorporation of catalytically active groups within the thin walls. Both of these approaches would benefit from the potentially high surface area of the thin walls, the short diffusion paths through the walls and the polarity difference between the surfaces. Thus, in the case of one non-polar surface exposed to an organic solvent and one polar exposed to water, interfacial reactions could be performed with a higher efficiency than is possible using classical two phase reactions in liquid-liquid two phase systems. This could, for instance, be the hydrolysis of a lipophilic ester (or amide) to hydrophilic products (the corresponding alcohol (or amine) and acid). The reactants easily adsorb at the non-polar surface, while the products will be released from the polar surface into the aqueous phase. The catalysis of the inverse condensation reaction should be also possible.

These are just a few ideas that can be associated with this type of materials, where a polymer thin film is obtainable by initiating the polymerisation of one or several monomers at an inter-phase, whereafter one of the phases is removed or replaced.

---

## 6 EXPERIMENTAL SECTION

### 6.1 HIERARCHICAL IMPRINTING USING IMMOBILISED NUCLEOTIDES

#### 6.1.1 Silica Surface Activation

300 mL of 17 % HCl were poured into a 500 mL three-necked round bottom flask, using a funnel. The round bottom flask was equipped with a condenser and an overhead stirrer. The calcined silica (20 g) was added in small portions while stirring. The flask was placed in an oil-bath (electronic-thermometer; 150°C; heater: 200°C) and the suspension was subsequently refluxed for 24h. The silica was filtered through a glass filter funnel and washed twice with 150 mL aliquots methanol. Finally, the silica was dried in a vacuum oven at 80°C for 4h and at 150°C for 12h.

#### 6.1.2 Silica Surface Silanisation

In 250 mL three-necked round-bottom flasks equipped with a condenser, an overhead stirrer and a dropping funnel, 6g batches of rehydroxylated silica were suspended in 80 mL dry toluene. The whole system was flushed with N<sub>2</sub>. According to the number of silanol groups on the silica surface (8 μmol/m<sup>2</sup>) the appropriate amounts of GPS (16.8 mmol, 3.96 g), CPS (16.8 mmol, 3.33 g) and APS (16.8 mmol, 3.73 g), respectively, were added to the mixture and refluxed overnight at 110°C. The products were filtered through glass funnels and washed with 2x 50 mL of toluene and 2x 50 mL of MeOH. The products were dried in a vacuum oven at 40°C for 24h. 6.1 g each of GPS, CPS and APS modified silica have been obtained. The products were characterised using elemental microanalysis and FT-IR spectroscopy and the amount of coupled ligands was estimated (see section 4.1.2).

### 6.1.3 End-Capping using Hexamethyldisilazane (HMDS)

In 250 mL three-necked round bottom flasks equipped with a condenser, an overhead stirrer and a dropping funnel, 5 g of the silanised silica gels obtained in the previous step were suspended in 60 mL DCM. 1 mL of HMDS in 20 mL dry DCM was added drop-wise to the suspension under N<sub>2</sub> flow and the whole mixture was stirred at room temperature under nitrogen for 24h and then refluxed for a further 3h. The products were filtered through glass funnels, washed with 50 mL MeOH to remove traces of unreacted HMDS and dried in a vacuum oven at 40°C for 24h. The products were characterised through elemental analysis and FT-IR (see section 4.1.2).

### 6.1.4 Immobilisation of Adenine onto the GPS-Modified Silica Surface

In a 250 mL two-necked round bottom flask equipped with an overhead stirrer and a dropping funnel, 5 g of GPS-modified silica were suspended in 60 mL DMF. The flask was flushed with N<sub>2</sub> and then 2 mL BF<sub>3</sub> were added drop-wise to the mixture and allowed to react for 10 min. After, 2.27 g (16.8 mmol) adenine in 20 mL DMF were added drop-wise to the reaction mixture and the suspension was left to react at room temperature, under stirring and N<sub>2</sub>, for 24 h. The product was then filtered and washed successively with 100 mL DMF, to remove the unreacted adenine, and 100 mL MeOH. The product was dried in a vacuum oven for 24h at 40°C and characterised using elemental analysis and FT-IR spectroscopy (see chapter 4.1.2).

### 6.1.5 Immobilisation of Adenine onto the CPS-Modified Silica Surface

In a 250 mL two-necked round bottom-flask, equipped with an overhead stirrer and a dropping funnel, were introduced 2.27 g (16.8 mmol) adenine and an equimolar quantity of K<sub>2</sub>CO<sub>3</sub> in 80 mL DMF. The components were allowed to react at room temperature under N<sub>2</sub> flow and stirring for 4h, before 5 g of CPS-modified silica were introduced to the flask and the whole mixture was stirred under N<sub>2</sub> for another 24h

at room temperature. The product was then filtered and washed with 100 mL of DMF to remove unreacted adenine and 100 mL MeOH. After drying at 40°C in a vacuum oven for 24h the product was characterised using elemental analysis and FT-IR (see section 4.1.2).

#### **6.1.6 Immobilisation of Adenine onto the APS-Modified Silica Surface**

In a 250 mL three-necked round bottom flask, equipped with a condenser, an overhead stirrer and a dropping funnel, 5 g of APS-modified silica were suspended in 60 mL ethanol. 4.06 g (16.8 mmol) 9-(2-bromoethyl)adenine in 20 mL ethanol were added drop-wise in to the mixture and refluxed under stirring and N<sub>2</sub> flush at 78°C for 24h. The product was filtered, washed with 50 mL DMSO, to remove unreacted 9-(2-bromoethyl) adenine, with 100 mL acetone, to remove the DMSO and with 100 mL MeOH and dried in a vacuum oven at 40°C for 24h. The product was characterised using elemental microanalysis and FT-IR (see section 4.1.2).

#### **6.1.7 Immobilisation of Pyrimidine onto the APS-Modified Silica Surface**

In a 250 mL three-necked round bottom flask, equipped with a condenser, an overhead stirrer and a dropping funnel, 5 g of APS-modified silica were suspended in 60 mL ethanol. 2.42 g (16.8 mmol) 2-chloro-4,6-diaminopyrimidine in 20 mL ethanol were added drop-wise in to the mixture and refluxed under stirring and N<sub>2</sub> flush for 24h. The product was filtered washed with 100 mL ethanol, dried in a vacuum oven at 40°C for 24h and characterised using elemental analysis and FT-IR (see section 4.1.2).

### 6.1.8 Polymerisation in the Template-Modified Silica Pores

A pre-polymerisation solution consisting of 12 mmol (1.04 g, 1.02 mL) methacrylic acid (MAA), 60 mmol (11.8 g, 11.31 mL) EDMA and 0.129 g AIBN was prepared in a glass vial. According to the pore volume of silica (1.083 mL/g), the appropriate amount of the pre-polymerisation mixture (4.33 mL) was added to 4 g of adenine-or pyrimidine-modified silica in a 25 mL one-necked round bottom-flask and then gently stirred with a steel spatula. Four repeated nitrogen-vacuum cycles were applied in order to force the monomer mixture to enter into the silica pores. Each cycle lasted 30 min. The flask was then placed in a thermostatted water bath, where the polymerisation was thermally initiated at 60°C and allowed to continue for 48h. For comparison a blank polymer was prepared under the same conditions, but the procedure was applied to the end-capped silica without template connected to the surface. The products were removed and dried in a vacuum oven for 24h at 40°C.

~7.8 g of composites were obtained in all cases from 4 g of template modified silica and 4.33 mL polymerisation mixture.

The resulting composites were all characterised using elemental analysis and FT-IR spectroscopy (see section 4.1.4.).

### 6.1.9 Silica Dissolution from the Resulting Composites

The silica/polymer composites (4 g MIP and 4 g NIP) were introduced to 100 mL teflon flasks and 60 mL aliquots of a 3M aqueous solution of ammonium hydrogen difluoride ( $\text{NH}_4\text{HF}_2$ ) were added to each. The suspensions were shaken at room temperature for 48h and then filtered through glass funnels. The resulting polymers were washed first with 150 mL water, to remove unreacted  $\text{NH}_4\text{HF}_2$  and other salts formed during the dissolution process, then with 100 mL DMSO to remove any traces of adenine and with 100 mL acetone to remove DMSO. The polymers were dried in a vacuum oven at 40°C for 24h. In all cases, the weight loss following this treatment was around 50%. The polymers were characterised using elemental analysis, FT-IR, TGA, EDX, SEM, TEM, fluorescence microscopy and nitrogen adsorption (see section 4.1.4.).

### 6.1.10 Coupling of Fluorescent Label

The obtained polymers (50 mg), 1-hydroxybenzotriazole (HOBt) (8 mg, 1.08 mmol) and 1,3-dicyclohexylcarbodiimide (DCC) (12.3 mg, 2.53 mmol) were mixed in dry DCM (10 mL) and stirred for 0.5h before a solution of 3-aminoquinoline (3-AQ) (8.5 mg, 1.22 mmol) in 0.5 mL DCM was added dropwise. The solution was stirred for several hours and the modified polymer was washed with 50 mL DMF and with 50 mL MeOH and dried under vacuum at 40°C. Composites and rehydroxylated silica-gel samples were treated under the same conditions.

## 6.2 HIERARCHICAL IMPRINTING USING IMMOBILISED PEPTIDES

Prior to solid-phase peptide synthesis, the silica surface was activated, modified with APS and end-capped as described in the previous section (6.1.1-3). The peptides were then synthesised using standard Merrifield chemistry. In this section I will give the experimental details for the synthesis of a di-peptide onto the silica surface (H-Phe-Gly-Si) only. All other peptides were synthesised following the same experimental procedure, according to the reactions given in Figure 4-28. The polymers were prepared according to the recipe described in 6.1.8 and 6.1.9 and labelled with the fluorescence dye 3-AQ as described in 6.1.10.

### 6.2.1 Immobilisation of Fmoc-Gly-OH onto the APS-Modified Silica Surface

To a two necked 250 mL round bottom flask equipped with an overhead stirrer and connected to a continuous N<sub>2</sub> flux, were added, according to the coverage of the silica surface with amino groups (1.3 mmol/g Si) , 1.75 g (13 mmol) HOBt, 2.68 g ( 13 mmol) DCC and 3.86 g (13 mmol) Fmoc-Gly-OH in 150 mL dry DMF. The reaction mixture was stirred at room temperature for 30 min, before 10 g of APS-modified silica were added into the mixture. The whole suspension was stirred for 24h at room temperature under a gentle flow of N<sub>2</sub>. The product was filtered, suspended in 250 mL DMF and shaken for 35 min to remove formed dicyclohexylurea, washed with



100 mL DCM and 100 mL MeOH and dried in a vacuum oven at 40°C for 12h. The product, *FMOC-Gly-Si*, was characterised using elemental microanalysis (see Table 4-9) and FT-IR spectroscopy (see Figure 4-29).

### 6.2.2 Deprotection of *FMOC-Gly-Si*

In a single-necked 250 mL round-bottom flask equipped with an overhead stirrer, 5 g of *FMOC-glycine* modified silica were suspended in 80 mL solution of 20% piperidine in DMF and stirred at room temperature for 5h. After, the product was washed with 200 mL DMF and 200 mL DCM to remove the base and the dibenzofulvene-piperidine adduct resulting from deprotection and at the end with another 100 mL DCM. The product, *H-Gly-Si*, was dried in a vacuum oven at 40°C for 12h and characterised through elemental analysis (see Table 4-9) and FT-IR spectroscopy (see Figure 4-29).

### 6.2.3 Coupling reaction between *FMOC-Phe-OH* and *H-Gly-Si*

To a 250 mL round bottom flask equipped with an overhead stirrer were introduced 100 mL of dry DMF, 2.26 g (5.85 mmol) *FMOC-Phe-OH*, 1.2 g (5.85 mmol) DCC and 0.79 g (5.85 mmol) 1-HOBT. The mixture was allowed to react under stirring and a gentle nitrogen flow at room temperature. After 30 min, 4.5 g of the *H-Gly-Si* were added to the reaction mixture and the reaction was allowed to continue overnight. The product was filtered, suspended in 250 mL DMF and shaken for 35 min to remove the formed dicyclohexylurea, filtered again, washed with 50 mL DCM and 50 mL MeOH and dried in a vacuum oven at 40°C for 12h. The product *FMOC-Phe-Gly-Si* was characterised using elemental analysis (see Table 4-9) and FT-IR spectroscopy (see Figure 4-29).

#### 6.2.4 Deprotection of Fmoc-Phe-Gly-Si

Into a 100 mL round bottom flask equipped with an overhead stirrer, 2.5 g of Fmoc-Phe-Gly-Si were suspended in a 50 mL solution of 20% piperidine in DMF and stirred at room temperature for 6h. The product was thereafter washed with 50 mL aliquots of DMF and DCM and dried in a vacuum oven at 40°C for 6h. H-Phe-Gly-Si were obtained and characterised according to Table 4-9 and Figure 4-29.

### 6.3 THIN LAYER MIP-COMPOSITES VIA A SURFACE BOUND AZO-INITIATOR AND RAFT POLYMERISATION

After the activation of the silica surface and modification with ACPA according to examples 6.1.1 and 6.1.2, the azo initiator was covalently attached to the silica surface.

#### 6.3.1 Attachment of Azo-bis(cyanopentanoic acid) onto the Silica Surface

The silica gel used for this experiment had a 3.4  $\mu\text{mol}/\text{m}^2$  surface coverage of amino groups, meaning that  $\sim 43\%$  of the initial silanol groups had been converted into amino groups. The amino groups were reacted with the diacid azo-initiator (ACPA) in order to obtain one material with a high initiator coverage, used for the RAFT polymerisation, and another one with lower initiator coverage, useful for the conventional grafting in order to minimise solution polymerisation. Based on our previous experience, 100% conversion of the amino groups into initiator groups (3.4  $\mu\text{mol}/\text{m}^2$ ) will lead to a complete pore blockage in the resulting composites and a low efficiency in HPLC. Therefore, the reaction conditions were designed to favour a maximum 50% conversion of the existing amino groups for the highest initiator coverage.

In the literature, there are two different methods reported for the immobilisation of the azo-initiator ACPA onto the silica surfaces. One is in the immobilisation to a GPS-modified silica surface, as reported by Tsubokawa *et al.* [81], and the other using

APS-modified silica, according to Revillon *et al.* [82](Figure 6-1). The chances that the azo-initiator is coupled through both carboxy groups to the amino silica are very low due to steric hindrance. Since APS-modified silica proved to be more straightforward to use in the hierarchical imprinting, as well as in the previous studies concerning the azo-initiator [5], we chose only this route for our azo-based imprinted composites.

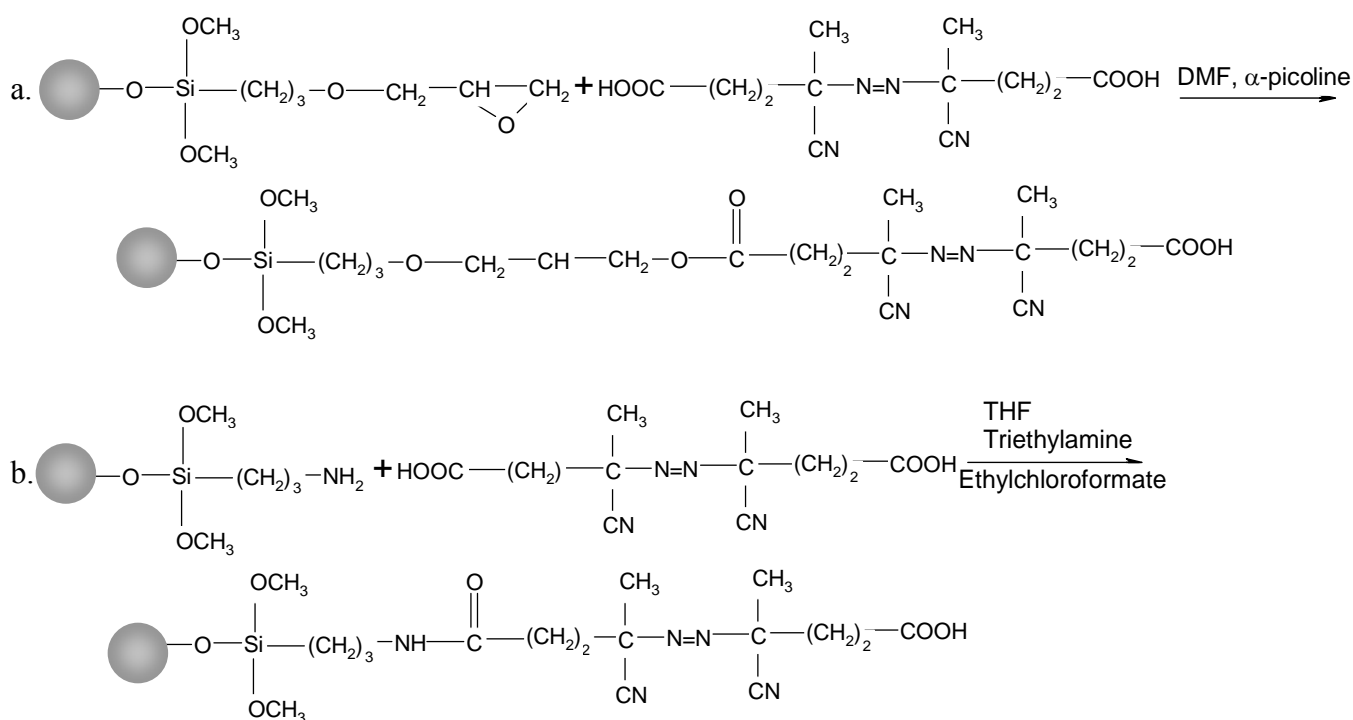


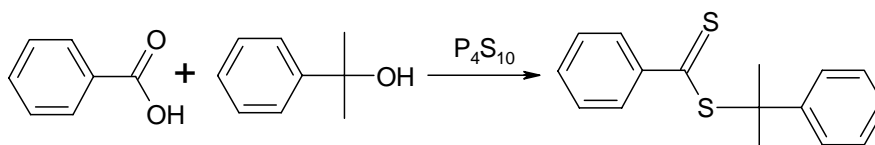
**Figure 6-1:** Possible means of covalently coupling ACPA to the silica surface a).via GPS-modified silica (Tsubokawa); b) via APS-modified silica (Revillon)

Thus, for the high density ACPA-Si ( $1.5 \mu\text{mol}/\text{m}^2$ ), to a 500 mL three-necked round bottom flask, equipped with a dropping funnel, on overhead stirrer and a ethanol thermometer, were introduced 250 mL dry THF. The mixture was then cooled at  $-78^\circ\text{C}$  using a liquid-nitrogen-ethanol bath. Under continuous  $\text{N}_2$  flow were added 5.04 g (18 mmol) azo-initiator (ACPA), 1.95 g (18 mmol) ethylchloroformate and 1.82 g (18 mmol) triethylamine. After stirring for 30 min at  $-78^\circ\text{C}$ , 25 g of amino-modified silica were added to the mixture and the suspension was stirred for 3h at  $-78^\circ\text{C}$  and then for 4 h at  $-10^\circ\text{C}$ . The product was filtered, washed with THF and MeOH and dried under vacuum at room temperature.

Elemental Microanalysis: %C=11.76; %H=1.87; %N=3.93; ( $D_s=1.57 \mu\text{mol}/\text{m}^2$ )

### 6.3.2 RAFT Agent Synthesis

The RAFT agent, 2-phenylprop-2-yl-dithiobenzoate, was synthesised according to the method of by Benicewicz [185] according to the following reaction:



Thus, a mixture of benzoic acid (2.442 g, 20 mmol), 2-phenyl 2-propanol (2.738 g, 20 mmol) and phosphorous pentasulphide 1.78 g (40 mmol) was refluxed in benzene (80 mL) for 12h. The initial colour of the reaction was yellow and after the mixture began to reflux, it turned first into light red and, over time into a dark red colour. After 12h, the reaction was allowed to cool to room temperature and the product purified by column chromatography packed with neutral alumina eluting with toluene. Removal of the solvent by distillation gave the final product as a red-coloured oil.

Reaction yield ( $\eta=30\%$ ).

Elemental analysis: %C= 79.08; %H= 6.58; %S= 13.28

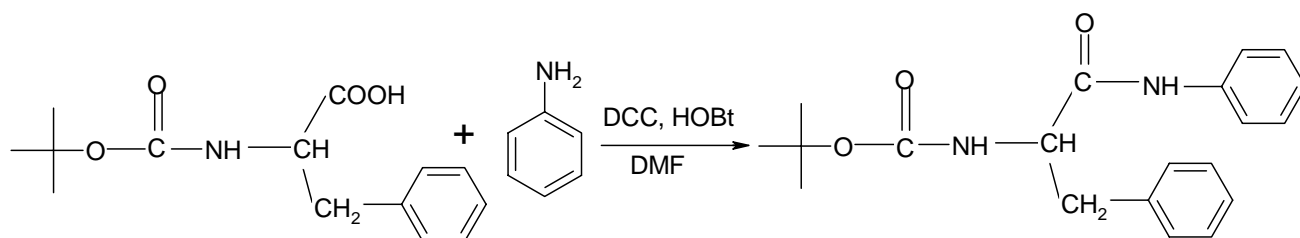
<sup>1</sup>H-NMR: (CDCl<sub>3</sub>)  $\delta= 7.3-7.5$  (m, 10H, 2x -C<sub>6</sub>H<sub>5</sub>),  $\delta=4.6$  (s, 6H, -H<sub>3</sub>C-C-CH<sub>3</sub>)

<sup>13</sup>C-NMR (CDCl<sub>3</sub>)  $\delta=13.9, 21.1, 39.4, 127.0, 128.5, 132.4, 145.6, 229.0$  (C=S)

### 6.3.3 Template Synthesis

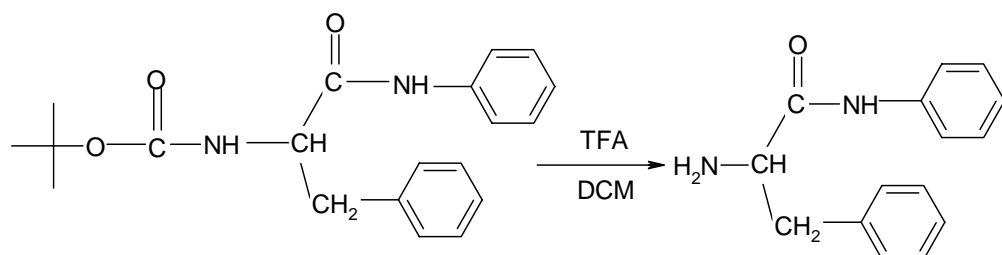
The synthesis of L/D-phenylalanine anilide is reported in the literature [194] and consists of two different steps: synthesis of BOC-L/D-phenylalanine anilide followed by deprotection.

## 6.3.3.1 Synthesis of BOC-L/D-Phenylalanine anylide



BOC-L-phenylalanineanilide was prepared by condensation of BOC-L-phenylalanine and aniline in DMF using DCC and HOBT as condensation agents. 0.05 mol (4.5 mL) of freshly distilled aniline were added under stirring to a solution of 0.06 mol (15.7 g) BOC-L/D-Phe-OH, 0.06 mol (8.1 g) HOBT and 0.08 mol (16.5 g) DCC in 200 mL dry DMF. After stirring for a few hours, the mixture was filtered, the filtrate dried over MgSO<sub>4</sub> and filtered. The filtrate was then reduced to dryness under reduced pressure. The solid residue was dissolved in DCM and washed with 300 mL each of 1M NaHCO<sub>3</sub>, 0.5 M HCl and water. The product obtained after evaporation of DCM was recrystallised from ethanol. Reaction yield ( $\eta=52\%$ ).

## 6.3.3.2 Synthesis of L/D-Phenylalanine anylide



Removal of the BOC-protecting group was performed by treatment with trifluoroacetic acid. To a solution of 0.03 mol BOC-L/D-phenylalanine anilide in 30 mL DCM were added 30 mL TFA under cooling with an ice/salt mixture. The mixture was stirred for 2h and reduced to dryness under reduced pressure. The solid residue was dissolved in 100 mL toluene and the same amount of 1M HCl was added. After stirring for a short time, the phases were separated and the toluene phase was washed again with 1M HCl. The combined aqueous phases were basified

with 5M NaOH and extracted with DCM. After drying over MgSO<sub>4</sub>, filtration and evaporation of the solvent, the residue is recrystallised from tert butylmethyl ether.

Reaction yield ( $\eta$ = 48%).

Elemental Analysis: %C= 75.06; %H=6.71; %N=11.6

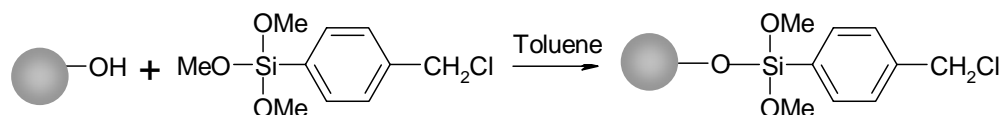
<sup>1</sup>H-NMR (CDCl<sub>3</sub>):  $\delta$ =1.4 (s, 2H, -NH<sub>2</sub>),  $\delta$ =2.76 (m, 1H, -CH<sub>2</sub> <sup>$\beta$</sup> ),  $\delta$ =3.3 (m, 1H, -CH<sub>2</sub> <sup>$\beta$</sup> ),  $\delta$ =3.7 (m, 1H, -CH)  $\delta$ =7.05 (m, 2H, m- NH-C<sub>6</sub>H<sub>5</sub>);  $\delta$ =7.3 (m, 5H, -C<sub>6</sub>H<sub>5</sub>),  $\delta$ = 7.5(m, 3H, o- and p- in NH-C<sub>6</sub>H<sub>5</sub>),  $\delta$ =9.37(s, 1H, NH)

### 6.3.4 Polymerisation

Grafting was performed in specially designed tubes containing 1 g of azo-modified silica particles suspended in a polymerisation mixture containing L-PA (0.240 g, 1 mmol), RAFT agent (0.2 g, 1.5 mmol), MAA (0.68 mL, 8 mmol) and EDMA (7.6 mL, 40 mmol) dissolved in 11.2 mL of dry toluene. After sealing, mixing and purging the mixture with nitrogen, polymerisation was initiated by UV-irradiation, using a high-pressure mercury vapor lamp, at 15°C and allowed to continue for 60, 90, 120 or 240 min, respectively, with continuous nitrogen purging. After polymerisation, the samples were filtered and washed with 50 mL toluene, extracted with methanol using a Soxhlet apparatus for 24h and dried overnight in a vacuum oven at 40°C. Non-imprinted control polymer composites (NIP) were prepared as described above but without addition of the template. "Conventional" grafting was performed using the same procedure with the exception of the RAFT agent and reducing to half the quantities of other reagents. The composites were characterised as described in section 5.1.4.

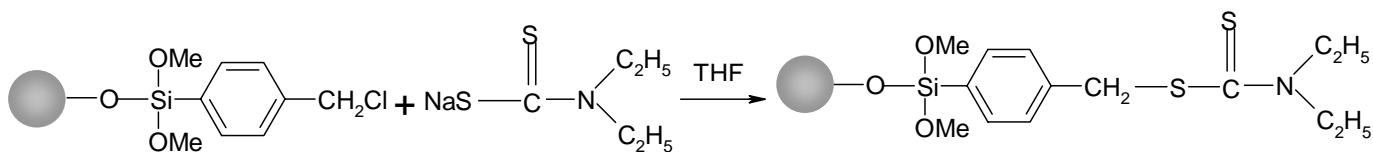
## 6.4 THIN LAYER MIP-COMPOSITES VIA A SURFACE BOUND INIFERTER-INITIATOR

### 6.4.1 Silanisation of silica surface with p-(chloromethyl)-phenyl trimethoxysilane



In a three-necked 250 mL round bottom flask equipped with an overhead stirrer, a condenser and a dropping funnel, 15 g of previously rehydroxylised silica were suspended in 150 mL dry toluene and the flask was connected to a N<sub>2</sub> stream. Then, 10.3 g (42 mmol) of p-(chloromethyl phenyl trimethoxysilane) were added drop-wise to the suspension and the mixture was refluxed with stirring for 24h. The modified silica was filtered, washed with 100 mL toluene and 100 mL MeOH and dried in a vacuum oven at 60°C. Elemental microanalysis: %C=5.57; %H=0.69 (D<sub>s</sub>=1.44 μmol/m<sup>2</sup>)

### 6.4.2 Immobilisation of benzyl N, N-diethyldithiocarbamate iniferter



The previously modified silica was suspended in 100 mL dry THF. To this mixture, 7.76 mmol (1.75 g) sodium *N,N*-diethyldithiocarbamate trihydrate dissolved in 50 mL THF were added drop-wise with stirring.

The suspension was stirred for another 12h at room temperature, filtered, washed with 100 mL THF and 100 mL MeOH and dried at room temperature under vacuum. Elemental microanalysis: %C= 5.98; %H=1.67; %N=0.18; %S=1,71 (D<sub>s</sub>=1.26 μmol/m<sup>2</sup>)

### 6.4.3 Polymerisation

1 g of iniferter-modified silica particles was suspended in a polymerisation solution containing L-PA (0.240 g, 8mmol), MAA (0.68 mL, 8 mmol) and EDMA (7.6 mL, 40 mmol) dissolved in 11.2 mL of dry toluene. Another batch of 1 g iniferter-modified silica particles was suspended in a different polymerisation mixture consisting of L-PA (0.04 g, 0.2 mmol), MAA (0.172 mL, 2mmol), HEMA (0.49 mL 4 mmol) and EDMA (1.26mL, 6 mmol) dissolved in 3 mL of dry 1,1,1-trichloroethan. After sealing with a rubber septum and mixing, the solutions were purged with N<sub>2</sub> for 15 min. The flasks were then placed in a thermostated bath set at 15°C, at 5 cm distance from a high pressure mercury vapour lamp (Philips, HPK, 125 W). The subsequent grafting polymerisation was performed for 30, 60, 120, 240, 360 or 480 min, respectively. Thereafter, the beads were filtered off, washed with 50 mL of the polymerisation solvent, extracted with methanol in a Soxhlet apparatus and dried overnight under vacuum at 40°C. The composite`s fully characterisation is described in section 5.2.2.

### 6.4.4 Generation of Thin-Walled MIPs

Portions of the composite materials prepared using iniferter initiators (1g) were suspended in 10 mL of 3M NH<sub>4</sub>HF<sub>2</sub> (aq.) in Teflon flasks. The suspensions were shaken at room temperature for 2 days resulting in the removal of the silica. A weight loss of 70% was monitored for all the materials.

### 6.4.5 Synthesis of benzyl *N,N*-diethyldithiocarbamate iniferter in solution.

A 100 mL, three-neck round bottom flask was equipped with a magnetic stirrer, condenser and dropping funnel. Sodium *N,N*-diethyldithiocarbamate trihydrate (8.20 g, 3.6 mmol) was dissolved in ethanol (40 mL, 99%) and added to the reaction flask under nitrogen atmosphere at 0°C. A solution of benzyl chloride (5.10 g, 4.1 mmol) in etanol (10 mL) was added dropwise over 30 min. The reaction was gradually warmed to room temperature, and stirring was continued for a further



65h. The precipitate (sodium chloride) was filtered off and the filtrate concentrated under vacuum. Vacuum distillation gave 6.18 g of a pale yellow liquid.

Reaction yield ( $\eta$ = 64.5%).

Elemental Analysis: %C= 60.16; %H=7.09; %N=5.86; %S=26.69

$^1\text{H-NMR}$  ( $\text{CDCl}_3$ ):  $\delta$ =1.3 (t, 6H,  $\text{NCH}_2\text{-CH}_3$ ),  $\delta$ =3.7 (q 2H,  $\text{NCH}_2\text{-CH}_3$ ),  $\delta$ = 4.05 (q, 2H,  $\text{N-CH}_2\text{-CH}_3$ );  $\delta$ = 4.57 (s, 2H,  $\text{SCH}_2\text{-C}_6\text{H}_5$ );  $\delta$ =7.2-7.5(m, 5H,  $\text{-C}_6\text{H}_5$ )

#### **6.4.6 Treatment of benzyl *N, N*-diethyldithiocarbamate iniferter with ammonium hydrogen difluoride**

2 g of benzyl *N, N*-diethyldithiocarbamate iniferter, synthesised in solution as described previously, were treated with 30 mL of 3M  $\text{NH}_4\text{HF}_2$  (aq.) in a Teflon round bottom flask. The mixture was shaken at room temperature for 2 days, neutralised with 3M NaOH and extracted with DCM. After drying over  $\text{MgSO}_4$ , filtration and evaporation of the solvent, 1.9 g of pale yellow oil obtained.

Elemental analysis and  $^1\text{H-NMR}$  were identical with the ones given in section 6.4.5. proving that the iniferter benzyl *N, N*-diethyldithiocarbamate did not suffer any structural modification upon difluoride treatment.

### **6.5 CHARACTERISATION TECHNIQUES AND THEORY**

#### **6.5.1 Elemental Analysis**

Carbon, nitrogen and sulphur contents were determined at the "Institut für Organische Chemie", Johannes Guttenberg Universität Mainz using a Heraeus CHN-rapid analyser (Hanau, Germany).

#### **6.5.2 FT-IR Spectroscopy**

FT-IR spectra were recorded initially using a MATTSON 2030 Galaxy Serie FT-IR Speckrometer (Madison, WI, USA). After moving to the University of Dortmund (work concerning tri- and tetra-peptide hierarchically imprinted materials, polymer

composites and thin walled MIPs) the spectra were recorded using a NEXUS FT-IR spectrometer (Thermo Electron Corporation, Dreieich, Germany).

### 6.5.3 Fluorescence Microscopy

The accessibility of the binding sites and the homogeneity of the grafted polymer films on the samples labelled with the fluorescence dye 3-AQ were investigated using a LEICA DM R fluorescence microscope HC (Bensheim, Germany).

### 6.5.4 Thermogravimetric Analysis

Thermogravimetric analysis was carried out using a NETZSCH TG 209 at the MPI für Kolloid-und Grenzflächenforschung, Golm. The samples (~ 3 mg) were placed on a heating block, which was heated with a heating rate of 20 K/min together, under N<sub>2</sub> atmosphere.

### 6.5.5 Scanning Electron Microscopy

In the first stage of my work, the particle size and morphology was visualised using a Zeiss DSM 962 instrument (Carl Zeiss Oberkochen, Germany) at the Universitätsklinikum Mainz and a LEO 1530 "Gemini" Electronic Microscope (LEO Elektronenmikroskopie GmbH, Oberkochen, Germany) at the MPI für Polymerforschung in Mainz. Later, samples were measured using an SEM Hitachi S 4500 at the Fachbereich Technische Chemie, Universität Dortmund and with a 1550 "Gemini" Electronic Microscope (Carl Zeiss, Oberkochen, Germany) at the MPI für Kolloid-und Grenzflächenforschung, Golm.

The samples were deposited on holders with a carbon foil and no gold sputtering was necessary except for the hierarchically imprinted polymers against nucleotides when the measurements were taken with the Zeiss DSM 962.

### 6.5.6 Transmission Electron Microscopy

The transmission electron micrographs were recorded using a energy filter transmission electron microscope Omega 912 (Carl Zeiss, Germany) at the MPI für Kolloid-und Grenzflächenforschung, Golm.

The samples were suspended in a liquid embedding medium (L. R. White Arylic Resin, London Resin Company Ltd.). The resin was allowed to solidify at 60°C for 3 days and the embedded particles were cut with a diamond knife of the ultramicrotome (Leica Ultracut UCT).

### 6.5.7 Energy Dispersive X-ray analysis

EDX is a technique often implemented in scanning electron micrographs. This was performed using a Zeiss DSM 962 (Zeiss Oberkochen, Germany) at the Universität Klinikum Mainz and at the at the MPI für Kolloid-und Grenzflächenforschung, Golm for the research concerning hierarchical imprinting and using a SEM Hitachi S 4500 at the Fachbereich, Technische Chemie, Universität Dortmund, for the characterisation of the thin walled materials. It is an inelastic emission process and the mechanism of signal generation is the decay of excited states by photons. Each atom emits X-ray photons with specific/characteristic energy and the technique is used for qualitative analysis.

### 6.5.8 Swelling Experiments

NMR tubes were filled up to 1 cm with dry polymer particles (MIPs and NIPs) with a known weight. 1 mL of solvent was added into the NMR tubes and the particles were allowed to equilibrate in the solvent for 24h, whereafter the volume of the swollen particles was measure. The volume swelling ration was calculated as:  $V_s$  ratio = bed volume swollen particles ( $V_s$ )/bed volume dry particles ( $V_d$ ).

### 6.5.9 Nitrogen Sorption Measurements

Nitrogen sorption measurements were performed on a Quantachrome Autosorb 6B (Quantachrome Corporation, Boynton Beach, FL) automatic adsorption instrument at the Institut für Anorganische und Analytische Chemie, Johannes Gutenberg Universität Mainz. Before measurements, 100-150 mg of the samples were heated at 60°C under high vacuum ( $10^{-5}$  Pa) for at least 12 h.

The pore structure of a solid is generally characterised by its porosity, pore diameter, pore shape, pore connectivity, pore size distribution, specific pore volume and specific surface area. These parameters are obtained from sorption measurements with nitrogen or by intrusion techniques. The calculation methods are based on certain assumptions regarding the pore shape and the mechanism of pore filling.

The term porosity refers to an open pore network being accessible to molecules in the gas or liquid phase. According to the IUPAC classification, porous materials are divided into: (i) microporous ( $pd < 2$  nm), (ii) mesoporous ( $2 < pd < 50$  nm) and (iii) macroporous ( $pd > 50$  nm) according to the value of pore diameter.

The Brunauer-Emmett-Teller (BET) [195,196] method is applied to derive the surface area from physisorption isotherm data. For this purpose it is convenient to apply the BET equation in the following form:

$$\frac{p}{n^a(p_0 - p)} = \frac{1}{n_m^a \times C} + \frac{(C - 1)}{n_m^a} \times \frac{p}{p_0}$$

where:  $n^a$  = the amount adsorbed at the relative pressure  $p/p_0$

$n_m^a$  = the monolayer capacity

C = constant dependent on the isotherm shape

According to the BET equation, a linear relation is given if  $p/[n^a (p_0 - p)]^{-1}$  is plotted against  $p/p_0$  (BET plot). From the BET plot it is possible to obtain  $n_m^a$ .

It has to be mentioned that the range of linearity of the BET plot is always restricted to a limited part of the isotherm, usually not above  $p/p_0 \sim 0.3$ .

The second stage in the application of the BET method is the calculation of  $a_s$  from  $n_m^a$ . This requires the knowledge of the average area,  $a_m$  (molecular cross-sectional area), occupied by each adsorbed molecule in the complete monolayer.

$$a_s = n_m^a \times L \times a_m$$

where:  $L$  = Avogadro constant.

Usually it is assumed that the BET nitrogen monolayer is closed-packed, giving  $a_m(\text{N}_2) = 0.162 \text{ nm}^2$  at 77K.

The determination of the specific pore volume, according to Gurvich [197], is as follows: at a high relative pressure ratio of  $p/p_o > 0.95$  the isotherm specific for mesoporous materials shows a plateau, indicating complete filling of the mesopores with adsorbate liquid. The amount of adsorbed nitrogen at the relative pressure  $0.95 < p/p_o < 1$  is converted into the volume of liquid nitrogen using the normal liquid density.

The pore volume distribution according to Barrett, Joyner and Halenda [198] is calculated from the desorption branch of the nitrogen adsorption isotherm at 77K in the relative pressure range between  $0.3 < p/p_o < 0.99$ . The calculation starts at the highest  $p/p_o$  value where saturation is obtained and the isotherm is parallel to the relative pressure abscissa. In each desorption step the pore radius is calculated using the Kelvin equation ( $r_k$ ). The value  $r_k$  is corrected by the thickness of the adsorbed multilayer at the respective  $p/p_o$  range using the  $t$ -plot.

For the correct pore radius it follows that:  $r_{\text{corrected}} = r_k + t$

The pore diameter is calculated by:  $p_d = 2 r_k + 2 t$

The differential pore volume is obtained by plotting  $\Delta V / \Delta p_d$  against  $\log p_d$ . The average pore diameter  $p_d$  is the median of the differential pore volume distribution curve for example the maximum of the curve.

### 6.5.10 HPLC Measurements

The obtained polymers and polymer composites, with 8-10  $\mu\text{m}$  grain size, were slurry packed into stainless steel columns (Merck, Darmstadt, Germany) using MeOH/H<sub>2</sub>O : 80/20(v/v) as the mobile phase. The column, filed with solvent, was attached below a stainless steel reservoir of about 50 mL volume. Before adding the polymer slurry, it was verified that the particles sediment giving a clear supernatant. As all the particles had the same size, further sedimentations and decantations were not necessary.

The polymer particles were added and the packing started by pumping the solvent at a maximum pressure of 300 bar using an air driven pump (Haskel DSTV-122). After having passed at least 50 mL of the pushing solvent, the column was disconnected, the end-fitting attached and the packing and flow direction clearly labelled. The ends of columns were sealed in order to avoid the column drying out.

After packing, HPLC measurements were carried out on Hewlett-Packard HP 1050 instruments (Agilent Technologies, Waldbronn, Germany) equipped with a UV-DAD detector and an autosampler.

Upon a change in the mobile phase, the column was washed with the new mobile phase until a stable base line was reached. The elution was monitored using a DAD dectector at 260 nm. The retention factors ( $k_{\text{MIP}}$ ,  $k_{\text{NIP}}$ ,  $k_{\text{L}}$  or  $k_{\text{D}}$ ) and the imprinting factors (IF) or separation factors ( $\alpha$ ) were calculated as follows:

$$k_{\text{MIP}} = (t_{\text{MIP}} - t_0) / t_0$$

$$k_{\text{NIP}} = (t_{\text{NIP}} - t_0) / t_0$$

$$\text{IF} = k_{\text{MIP}} / k_{\text{NIP}}$$

Where:  $k_{\text{MIP}}$  = retention factor of the MIP

$k_{\text{NIP}}$  = retention factor of the NIP

$t_{\text{MIP}}$  = retention time of the MIP

$t_{\text{NIP}}$  = retention time of the NIP

$t_0$  = retention time of the void marker (acetone)

And for CSPs:

$$k_L = (t_L - t_0) / t_0$$

$$k_D = (t_D - t_0) / t_0$$

$$\alpha = k_L / k_D$$

Where:  $k_L$  = retention factor of the L-enantiomer  
 $k_D$  = retention factor of the D-enantiomer  
 $t_L$  = retention time of the L-enantiomer  
 $t_D$  = retention time of the D-enantiomer  
 $t_0$  = retention time of the void marker

When the analyte travels through the column, the peak width increases proportionally to the time spend in the column. The increase in peak width is expressed by the theoretical plate height:

$$H = (\sigma_L)^2 / L$$

Where:  
 $\sigma_L$  = standard deviation of a Gaussian peak in units of length,  
 $(\sigma_L)^2$  = variance of the peak in units of length  
 $L$  = length of the analytical column.

Instead of the theoretical plate height  $H$ , the theoretical plate number  $N$  is often used.

Both parameters are related as follows:

$$H N = L$$

$$N = 5.54 (t_r / w_{t0.5})^2$$

Where:  
 $t_r$  = the retention time ;  
 $w_{t0.5}$  = peak width at half height.

For a given column, the number of theoretical plates is a measure of its separation efficiency. The higher the plate number, the higher the separation efficiency and the narrower the peaks.

### 6.5.11 Rebinding Tests

10 mg each of the HEMA/MAA/EDMA imprinted and non-imprinted iniferter composites obtained after 120 and 240 min polymerisation, respectively ,and MAA/EDMA imprinted and non-imprinted iniferter composites obtained after the same polymerisation times, together with their corresponding generated thin-walled MIPs were weighed into separate HPLC vials. To these materials, incremental

amounts of L/D-PA were added. For the HEMA-based polymers, the solutions were prepared in ACN/phosphate buffer (pH=4.8) =30/70(v/v) while for the MAA materials the solution were prepared in 100% ACN. 1 mL of increasing L/D-PA concentrations was added to the 10 mg of polymers. The HPLC vials were then sealed and their contents allowed to equilibrate overnight at room temperature with gentle shaking.

After 12h, the polymer particles were sedimented at the bottom of the vials allowing analysis of the supernatant solutions using a Hewlett-Packard HP 1050 instrument. For the HPLC tests, a commercially available HPLC column, Phenomenex Luna C-18 (125 × 4.6 mm<sup>2</sup>) was used. A mobile phase of 100% ACN was used for the MAA-based materials, while ACN/phosphate buffer (pH=4.8) =30/70(v/v) was used for the HEMA-based materials. The supernatant solutions were injected in the order of increasing concentrations at 1mL/min and the concentration of free (unbound) L/D-PA was determined at a wavelength of 260 nm. The adsorption isotherms were thereafter obtained by plotting the free concentration of L/D-PA over the concentration bound to the polymers using calibration curves for L/D-PA.

Adsorption isotherms yield important information concerning binding energies, modes of binding and site distributions in the interaction of template molecules with binding sites in a solid adsorbant. The isotherms can be fitted using various models where different assumptions are made. The most simple is the Langmuir adsorption isotherm (eq 1), where the adsorbant is assumed to contain only one type of site; adsorbate-adsorbate interactions are assumed not to occur and the system is assumed ideal. The isotherm depends on two parameters: the saturation capacity (site density),  $q_{s1}$  (eq 2), and the binding constant,  $b_1$ , related to  $K_a$  as shown in eq (3), with  $M_w$  being the molecular weight of the adsorbate.

$$q = \frac{a_1 C}{1 + b_1 C} \quad (1)$$

$$q_{s1} = \frac{a_1}{b_1} \left( \frac{g}{l} \right) \quad (2)$$

$$Ka = b_1 M_w (/M) \quad (3)$$



### 6.5.12 Kinetic Experiments

10 mg of the HEMA based MIP and NIP composites and the corresponding thin walled MIP and NIP were allowed to equilibrate over night in 0.5 mL of 0.01 M Sodium Acetate Buffer (pH =4.8)/ACN=70/30 while shaking. After equilibration, the vials were centrifuged so that the particles sediment at the bottom of the vial, and the supernatant solutions could be analysed for leakages using a Hewlett-Packard HP 1050 instrument in the flow injection mode detection 240 nm, Flow 1mL/min, Inj. Vol: 0.5  $\mu$ L.

After, to the first vial containing the thin-walled MIP (TW-MIP) in buffer/ACN, 0.5 mL of 2 mM D-PA in buffer/ACN=70/30 was added and the time was recorded. The vial was manually shaken to allow equilibration, and centrifuged for particle sedimentation. After exactly 2 min from adding the D-PA solution, the supernatant was measured using the HP 1050 in the same conditions as described above every 1.2 minutes for the first 22 minutes and every 4.2 minutes for another 34 minutes. In order to check that no more analyte is bound to the polymers, the supernatant was measured again after 12h. The same procedure was repeated to the second vial containing again the TW- MIP in buffer/ACN, but this time using 0.5 mL of 2 mM L-PA in buffer/ACN=70/30.

After analysing the TW-MIP, the procedure was applied successively in the following order: D-PA on TW-NIP; L-PA on TW-NIP; D-PA on MIP-Comp., L-PA on MIP-Comp, D-PA on NIP Comp, L-PA on NIP-Comp.

The measured areas were converted into concentration, by measuring the areas of the pure 1mM solution of L and D-PA which was the final concentration formed in the vial during measurements.

## 6.6 CHEMICALS

### 6.6.1 Chemicals for Synthesis

1,1,1-trichloroethane (dry)	Merck KGaA, Darmstadt, Germany
1-Hydroxybenzotriazole	Across, Geel, Belgium
2-chloro-4, 6-diaminopyrimidine	Across, Geel, Belgium
2-hydroxyethyl methacrylate	Aldrich, Steinheim, Germany
2-phenyl-2-propanol	Lancaster, Frankfurt am Main, Germany
3-Aminoquinoline	Fluka, Deisenhofen, Germany
4,4'-azo bis (cyanopentanoic acid)	Fluka, Deisenhofen, Germany
Acetone (for synthesis)	Merck KGaA, Darmstadt, Germany
Adenine	Across, Geel, Belgium
Aminopropyltriethoxysilane	Aldrich, Steinheim, Germany
Ammonium hydrogen difluoride	Across, Geel, Belgium
Aniline	Aldrich, Steinheim, Germany
Azo-N,N'-bis-isobutyronitrile	Across, Geel, Belgium
Benzene	Merck KGaA, Darmstadt, Germany
Benzoic acid	Across, Geel, Belgium
BOC-D-Phe-OH	Bachem, Heidelberg, Germany
BOC-Phe-OH	Aldrich, Steinheim, Germany
Boron trifluoride	Aldrich, Steinheim, Germany
Chloropropyltrimethoxysilane	Aldrich, Steinheim, Germany
Dichloromethane (dry)	Fluka, Deisenhofen, Germany
Dimethylsulphoxide (p.a.)	Merck KGaA, Darmstadt, Germany
Dimethylformamide (dry)	Fluka, Deisenhofen, Germany
Toluene (dry)	Fluka, Deisenhofen, Germany
Dicyclohexyl carbodiimide	Aldrich, Steinheim, Germany
Ethanol (dry)	Fluka, Deisenhofen, Germany
Ethanol( p.a.)	Merck KGaA, Darmstadt, Germany
Ethyl chloroformate	Aldrich, Steinheim, Germany
Ethyleneglycol dimethacrylate	Aldrich, Steinheim, Germany
FMOC-Gly-OH	Bachem, Heidelberg, Germany
FMOC-Gly-Phe-OH	Bachem, Heidelberg, Germany
FMOC-Phe-Gly-OH	Bachem, Heidelberg, Germany
FMOC-Phe-OH	Bachem, Heidelberg, Germany
Glycidoxypropyltrimethoxysilane	Aldrich, Steinheim, Germany
Hexamethyldisilazane	Merck KGaA, Darmstadt, Germany

---

Hydrochloric Acid (conc.)	Merck KGaA, Darmstadt, Germany
Magnesium sulphate	Across, Geel, Belgium
Methacrylic Acid	Aldrich, Steinheim, Germany
Methanol (p.a.)	Merck KGaA, Darmstadt, Germany
Neutral alumina	Across, Geel, Belgium
p-(chloromethyl)-phenyl-trimethoxysilane	Lancaster, Frankfurt am Main, Germany
Phosphorous pentasulphide	Across, Geel, Belgium
Potassium carbonate	Merck KGaA, Darmstadt, Germany
Pyrimidine	Aldrich, Steinheim, Germany
Si-100	Merck KGaA, Darmstadt, Germany
Sodium hydrogen carbonate	Merck KGaA, Darmstadt, Germany
Sodium hydroxide	Merck KGaA, Darmstadt, Germany
Sodium diethyldithiocarbamate	Fluka, Deisenhofen, Germany
tert-Butylmethylether	Fluka, Deisenhofen, Germany
Tetrahydrofuran (dry)	Fluka, Deisenhofen, Germany
Tetrahydrofurane( p.a)	Merck KGaA, Darmstadt, Germany
Triethylamine	Aldrich, Steinheim, Germany
Trifluoroacetic acid	Aldrich, Steinheim, Germany

Ethyleneglycol dimethacrylate was purified by extraction with 10% NaOH, washing with brine, drying over magnesium sulphate and subsequent distillation under reduced pressure. Methacrylic acid and 2-hydroxyethyl methacrylate were distilled under reduced pressure prior to use. Azo-*N,N'*-bisisobutyronitrile was recrystallised from methanol before use. Aniline was distilled under reduced pressure before use. All other reagents were used as received.

### 6.6.2 Chemicals for Analysis

2,4,6-triaminopyrimidine	Across, Geel, Belgium
Adenine	Across, Geel, Belgium
BOC-L/D-Phe-OH	Bachem, Heidelberg, Germany
Cytosine	Aldrich, Steinheim, Germany
D/L-phenylalanine anilide	own synthesis
D/L-phenylalanine p-nitroanilide	Bachem, Heidelberg, Germany
FMOC-L/D-Phe-Gly-OH	Bachem, Heidelberg, Germany
FMOC-L/D-Phe-OH	Bachem, Heidelberg, Germany
Folic acid	Aldrich, Steinheim, Germany
H-Gly-Gly-Phe-OH	Bachem, Heidelberg, Germany
H-Gly-OH	Bachem, Heidelberg, Germany
H-Gly-Phe-OH	Bachem, Heidelberg, Germany
H-Phe-Gly-Gly-Phe-OH	Bachem, Heidelberg, Germany
L/D-phenylalanine methylester	Bachem, Heidelberg, Germany
L/D-phenylalanine tertbutylester	Bachem, Heidelberg, Germany
Methotrexate	Aldrich, Steinheim, Germany
Nociceptin	Bachem, Heidelberg, Germany
Phenylalanine-glycineamide	Bachem, Heidelberg, Germany
Thymine	Aldrich, Steinheim, Germany
Uracil	Aldrich, Steinheim, Germany

### 6.6.3 HPLC Solvents and Chemicals

Acetic acid (biochemical grade)	Fluka, Deisenhofen, Germany
Acetonitrile (HPLC grade)	Merck KGaA, Darmstadt, Germany
Methanol (HPLC grade)	Merck KGaA, Darmstadt, Germany
Potassiumhydrogen diphosphate	Merck KGaA, Darmstadt, Germany
Sodium acetate	Merck KGaA, Darmstadt, Germany
Sodium hydrogen diphosphate	Merck KGaA, Darmstadt, Germany
Water (HPLC grade)	Merck KGaA, Darmstadt, Germany

---

## 7 REFERENCES

1. M. M. Titirici, A. J. Hall, B. Sellergren, *Chem. Mater.*, **2002**, *14*, 21
2. M. M. Titirici, A. J. Hall, B. Sellergren, *Chem. Mater.*, **2003**, *15*, 822
3. M. M. Titirici, B. Sellergren, *Anal. Bioanal. Chem.*, **2004**, *378*, 1913
4. A. Rachkov, N. Minoura, *J. Chromatogr. A*, **2000**, *889*, 111
5. C. Sulitzky, B. Rückert, A. J. Hall, F. Lanza, K. Unger, B. Sellergren, *Macromolecules*, **2002**, *35*, 79
6. J. Chiefari, Y. K. Chong, F. Ercole, J. Kristina, J. Jeffrey, P. T. Le, R. T. A. Mayadunne, C. F. Meijs, C. L. Moad, G. Moad, E. Rizzardo, S. H. Thang, *Macromolecules*, **1998**, *31*, 5559.
7. B. Ruckert, A. J. Hall, B. Sellergren, *J. Mater. Chem.*, **2002**, *12*, 2275
8. B. Sellergren, B. Ruckert, A. J. Hall, *Adv. Mater.*, **2002**, *14*, 17.
9. G. M. Whitesides, J. P. Mathias, C. T. Seto, *Science*, **1991**, *254*, 1312
10. M. Antonietti, C. Göltner, *Angew. Chem.*, **1997**, *109*, 944; *Angew. Chem. Int. Ed. Engl.*, **1997**, *36*, 910
11. C. Sanchez, G. Soler-Illia, F. Ribot, T. Lalot, C. R. Mayer, V. Cabuil, *Chem. Mater.*, **2001**, *13*, 3061
12. B. Sellergren, (Ed), *Molecularly Imprinted Polymers-Man-Made Mimics of Antibodies and Their Application in Analytical Chemistry*, Techniques and Instrumentation in Analytical Chemistry, Vol 23, **2001**, Elsevier Science, Amsterdam, Netherlands
13. B. Sellergren, *Angew. Chem. Int. Ed.*, **2000**, *39*, 1031
14. K. Haupt, *Chem. Comm.*, **2003**, 171
15. H. Kempe, M. Kempe, *Macromol. Rapid. Commun.*, **2004**, *25*, 315
16. N. Pérez, M. J. Whitcombe, E. N. Vulfson, *Macromolecules*, **2001**, *34*, 830
17. N. Pérez, A.G. Mayes, *MRS Symp. Proc.*, **2002**, *723*, 61
18. L. Ye, R. Weiss, K. Mosbach, *Macromolecules*, **2000**, *33*, 8239
19. F. G. Tamayo, J. L. Casillas, A. Martin- Esteban, *Anal. Chim. Acta*, **2003**, *482* (2), 165
20. J. Wang, P. A. G. Cormack, D. Sherrington, E. Khoshdel, *Angew. Chem.*, **2003**, *115*, 5494
21. M. Kempe, K. Mosbach, *J. Chromatogr. A*, **1994**, *644*, 276

22. B. Sellergren, K. Shea, *J. Chromatogr. A*, **1993**, 17, 654
23. M. Kempe, *Anal. Chem.*, **1996**, 68, 1948
24. L. J. Pauling, *J. Am. Chem. Soc.*, **1940**, 62, 2643
25. F. H. Dickey, The preparation of specific sorbents. *Proceedings of the National Academy of Science of the United States of America*, **1949**, 35, 227
26. A. H. Beckett, P. Anderson, *Nature*, **1957**, 179, 1074
27. G. Wulff, A. Sarhan, *Angew. Chem.*, **1972**, 84, 364
28. G. Wulff, *Angew. Chem. Int. Ed.*, **1995**, 34, 1812
29. R. Arshady, K. Mosbach, *Makromol. Chem.*, **1981**, 182, 687
30. L. Andresson, B. Sellergren, K. Mosbach, *Tetrahedron Lett.*, **1984**, 25, 5211
31. B. Sellergren, K. Shea, *J. Chromatogr.*, **1993**, 654, 17
32. B. Sellergren, M. Lepistö, K. Mosbach, *J. Am. Chem. Soc.*, **1988**, 110, 5853
33. B. Sellergren, K. J. Shea, *J. Chromatogr. A*, **1995**, 690, 29
34. A. Zander, P. Findlay, T. Renner, B. Sellergren, *Anal. Chem.*, **1998**, 70, 3304
35. Y. Chen, M. Kele, P. Sajonz, B. Sellergren, G. Guiochon, *Anal. Chem.*, **1999**, 71, 928
36. P. Sajonz, M. Kele, G. Zhong, B. Sellergren, G. Guiochon, *J. Chromatogr.*, **1998**, 810, 1
37. B. Sellergren, *Makromol. Chem.*, **1989**, 190, 2703
38. B. Dirion, Z. Cobb, E. Schillinger, L. I. Anderson, B. Sellergren, *J. Am. Chem. Soc.*, **2003**, 125, 15101
39. S. Piletsky, E. Piletska, K. Karim, G. Foster, C. Legge, A. Turner, *Anal. Chim. Acta*, **2004**, 504, 123
40. A. J. Hall, L. Achilli, P. Manesiotis, M. Quaglia, E. De Lorenzi, B. Sellergren, *J. Org. Chem.*, **2003**, 68, 9132
41. M. J. Whitcombe, M. E. Rodriguez, P. Villar, E. N. Vulfson, *J. Am. Chem. Soc.*, **1995**, 117, 7105
42. Y. N. Belokon, V. I. Tararov, T. F. Savel'eva, M. M. Vorob'ev, S. V. Vitt, V. F. Sizoy, N. A. Sukhacheva, G. V. Vasil'ev, V. M. Belikov, *Makromol. Chem.*, **1983**, 184, 2213
43. P. K. Dahl, F. H. Arnold, *J. Am. Chem. Soc.*, **1991**, 113, 7417
44. J. Damen, D. Neckers, *Tetrahedron Lett.*, **1980**, 21, 1913

45. V. Braun, W. Kuchen, *Chem. Ztg.*, **1984**, *108*, 255
46. M. Whitcombe, C. Alexander, E. Vulfson, *Trends Fd. Sci. Technol.*, **1997**, *8*, 140
47. A. G. Mayes, K. Mosbach, *Anal. Chem.*, **1996**, *68*, 3769
48. K. Hosoya, K. Yoshizako, N. Tanaka, K. Kimata , T. Araki, J. Haginaka, *Chem. Lett.*, **1994**, 1437
49. K. Yu, K. Tsukagoshi, M. Maeda, M. Takagi, *Anal. Sci.*, **1992**, *8*, 701
50. F. Puoci , F. Iemma , R. Muzzalupo, U. G. Spizzirri, S. Trombino, R. Cassano, N. Picci, *Macromol. Biosci.*, **2004**, *4*, 22
51. A. Biffis, N. B. Graham, G. Siedlaczek, S. Stalber, G. Wulff, *Macromol. Chem. Phys.*, **2001**, *202*, 163
52. S. C. Zimmerman , M. S. Wendland, N. A. Rakov, I. Zharov, K. S. Suslik, *Nature*, **2002**, *418*, 399
53. R. H. Schmidt, K. Mosback, K. Haupt, *Adv. Mater.*, **2004**, *16* (8), 7
54. S. Dai, Y. Shin, C. E. Barnes, L. M. Toth, *Chem. Mater.*, **1997**, *9*, 2521
55. S. Fireman-Shoresh, D. Avnir, S. Marx, *Chem. Mater.*, **2003**, 3607
56. A. Katz , M. E. Davis, *Nature*, **2000**, *403*, 286
57. R. Makote, M. M. Collinson, *Chem .Commun.*, **1998**, *3*, 425
58. M. Glad, O. Norrlöw, B. Sellergren, N. Siegbahn, K. Mosbach, *J. Chromatogr.*, **1985**, *347*, 11
59. S. S. Iqbal, M. F. Lulka, J. P. Chambers, R. G. Thomson, J. Valdes, *J. Mater. Sci. Eng. C*, **2000**, *7*, 77
60. M. Lahav, A. B. Kharitonov, O. Katz, T. Kunitake, I. Willner, *Anal. Chem.*, **2001**, *73*, 720
61. S. W. Lee, I. Ichinose, T. Kunitake, *Langmuir*, **1998**, *14*, 2857
62. S. W. Lee, I. Ichinose, T. Kunitake, *Chem. Lett.*, **1998**, *12*, 1193
63. T. Kobayashi, H. Y. Wang, N. Fujii, *Chem. Lett.*, **1995**, *9*, 927
64. S. A. Piletsky, E. V. Piletskaya, T. L. Panasyul, A. V. El'skaya, R. Levi, I. Karube, G. Wulff, *Macromolecules*, **1998**, *31*, 2137
65. M. J. Hong, P. E. Anderson, J. Qian, C. Martin, *Chem. Mater.*, **1998**, *10*, 1029
66. A. Dzgoev, K. Haupt, *Chirality*, **1999**, *11*, 465
67. H. Y. Wang , T. Kobayashi, N. Fujii, *J. Chem. Tech. Biotech.*, **1997**, *70*, 355

68. S. A. Piletsky, H. Matuschewski, U. Schedler, A. Wilpert, E. V. Piletskska, T. A. Thiele, M. Ulbricht, *Macromolecules*, **2000**, *33*, 3092
69. T. A. Sergeyeva, H. Matuschewski, S. A. Piletsky, J. Bending, U. Schedler, M. Ulbricht, *J. Chromatogr. A*, **2001**, *907*, 89
70. V. Kochkodan, W. Weigel, M. Ulbricht, *Analyst*, **2001**, *126*, 803
71. O. Norrlöw, M. Glad, K. Mosbach, *J. Chromatogr.*, **1984**, *299*, 29
72. G. Wulff, D. Oberkobusch, M. Marik, *Reac Polym.*, **1985**, *3*, 261
73. F. H. Arnold, S. Plunkett, P. K. Dahl, S. Vidyasankar, *Polym. Prep.*, **1995**, *36(1)*, 97
74. M. Glad, P. Reinholdsson, K. Mosbach, *React. Polym.*, **1995**, *25*, 47
75. L. Schweitz, L. I. Anderson, S. Nilsson, *Anal. Chem.*, **1997**, *69*, 1179
76. O. Brüggemann, R. Freitag, M. J. Whitecombe, E. N. Vulfson, *J. Chromatogr.*, **1997**, *781*, 43
77. R. Shoji, T. Takeuchi, I. Kubo, *Anal. Chem.*, **2003**, *75*, 4882
78. J. Matsui, K. Akamatsu, S. Nishiguchi, D. Miyoshi, H. Nawafune, K. Tamaki, N. Sugimoto, *Anal. Chem.*, **2004**, *76*, 1310
79. A. Friggeri, H. Kobayashi, S. Shinkai, D. N. Reinhoudt, *Angew. Chem. Int. Ed.*, **2001**, *40*, 4729
80. K. Hirayama, M. Burow, Y. Morikawa, N. Minoura, *Chem. Lett.*, **1998**, 731
81. N. Tsubokawa, A. M. Kogure, Y. Sone, M. Shimomura, *Polym J.*, **1990**, *22 (9)*, 827
82. E. Carlier, A. Guyot, A. Revillon, M-F. Llauro-Darricades, R. Retiaud, *React. Polym.*, **1991/1992**, *16*, 41
83. O. Prucker, J. Rühle, *Langmuir*, **1998**, *14*, 6893
84. J. P. Wittmer, M. E. Cates, A. Johner, M. S. Turner, *Europhys. Lett.*, **1996**, *33*, 397
85. O. Prucker, J. Rühle, *Macromolecules*, **1998**, *31*, 602
86. T. Otsu, *J. Polym. Sci. Part A: Polym Chem.*, **2000**, *38*, 2121
87. X. Huang, M. J. Wirth, *Anal. Chem.*, **1997**, *69*, 4577
88. T. Von Werne, E. T. Patten, *J. Am. Chem. Soc.*, **2001**, *123*, 7497
89. Y. N. Kim, L. N. Jeon, I. S. Choi, S. Takami, Y. Harada, K. R. Finnie, G. S. Girolami, R. G. Nuzzo, G. M. Whitesides, P. E. Laibinis, *Macromolecules*, **2000**, *33*, 2793
90. M. Baum, W. J. Brittain, *Macromolecules*, **2002**, *35*, 610



91. M. Qualia, E. De Lorenzi, C. Sulitzky, G. Massolini, B. Sellergren, *Analyst*, **2001**, 126, 495
92. M. Ulbricht, *React. Fuct. Polym.*, **1996**, 31, 16
93. M. Ulbricht, K. Richau, H. Kamusewitz, *Colloids Surfaces A*, **1998**, 138, 353
94. Y. Xia, G. M. Whitesides, *Angew. Chem. Int. Ed.*, **1998**, 37, 550
95. A. Aherne, C. Alexander, M. J. Payne, N. Perez, E. N. Vulfson, *J. Am. Chem. Soc.*, **1996**, 118, 8771
96. C. Alexander, E. N. Vulfson, *Adv. Mater.*, **1997**, 9, 751
97. F. L. Dickert, O. Hayden, K. P. Halikias, *Analyst*, **2001**, 126, 766
98. H. Shi, W.-B. Tsai, M. D. Garrison, S. Ferrari, B. D. Ratner, *Nature*, **1999**, 398, 593
99. S. M. D' Souza, C. Alexander, S. W. Carr, A. M. Waller, M. J. Whitcombe, E. N. Vulfson, *Nature*, **1999**, 398, 312
100. S. Polarz, M. Antonietti, *Chem. Com.*, **2002**, 2002, 2593
101. S. A. Johnson, E. S. Brigham, P. J. Olivier, T. E. Mallouk, *Chem. Mater.*, **1997**, 9, 2448
102. S. A. Johnson, P. J. Olivier, T. E. Mallouk, *Science*, **1993**, 283, 963
103. G. Vlatakis, I. L. Anderson, R. Muller, K. Mosbach, *Nature*, **1993**, 361, 645
104. B. Sellergren, *Molecular And Ionic Recognition With Imprinted Polymers*, eds A. Bartsch., M. Maeda, American Chemical Society, Washington, **1998**
105. E. Yilmaz, K. Haupt, K. Mosbach, *Angew. Chem. Int. Ed.*, **2000**, 39, 2115
106. S. Dai, M. C. Burleigh, Y. H. Ju, H. J. Gao, J. S. Lin, S. J. Pennycook, C. E. Barnes, L. Xue, *J. Am. Chem. Soc.*, **2000**, 122, 992
107. S. Dai, *Chem. Eur. J.*, **2001**, 7, 763
108. Q. Fu, H. Sanabe, C. Kagawa, K-K, Kunimoto, J. Haginaka, *Anal. Chem.*, **2003**, 75, 191
109. M. S. Vazquez, D. Spivak, *Macromolecules*, **2003**, 36, 5105
110. B. Sellergren, K. Nilsson, *Meth. Mol. Cell. Biol.*, **1989**, 1, 59
111. O. Ramström, L. I. Andersson, K. Mosbach, *J. Org. Chem.*, **1993**, 58, 7562
112. C. Yu, K. Mosbach, *J. Org. Chem.*, **1997**, 62, 4057
113. M. Kempe, K. Mosbach, *Int. J. Peptide Protein Res.*, **1994**, 44, 603
114. M. Kempe, L. Fischer, K. Mosbach, *J. Mol. Recogn.*, **1993**, 6, 25

- 
115. L. I. Anderson, D. J. O'Shannessy, K. Mosbach, *J. Chromatogr.*, **1990**, 513, 167
  116. O. Ramström, L. Ye, P-E. Gustavson, *Chromatographia*, **1998**, 48, 197
  117. L. Fischer, R. Müller, B. Ekberg, K. Mosbach, *J. Am. Chem. Soc.*, **1991**, 113, 9358
  118. O. Ramström, C. Yu, K. Mosbach, *J. Mol. Recogn.*, **1996**, 9, 691
  119. L. Schweitz, L. I. Andersson, S. Nilsson, *Anal. Chem.*, **1997**, 69, 1179
  120. M. J. Lin, T. Nakagama, K. Uchiyama, T. J. Hobo, *Pharm. Biomed. Anal.*, **1997**, 15, 1351
  121. M. J. Lin, T. Nakagama, K. Uchiyama, T. J. Hobo, *Chromatographia*, **1996**, 43, 585
  122. M. Glad, O Norrlov, B. Sellergren, N. Siegbahn, K. Mosbach, *J. Chromatogr.*, **1985**, 11, 347
  123. M. Burow, N. Minoura, *Biochem. Biophys. Res. Commun.*, **1996**, 227, 419
  124. A. Rachkov, N. Minoura, *Biochem. Biophys. Acta*, **2001**, 1544, 255
  125. J. Haginaka, S. Haruyo, *Anal. Chem.*, **2000**, 72, 5206
  126. S. Mallik, S. D. Plunkett, P. K. Dahl, R. D. Johnson, D. Pack, D. Shnek, F. H. Arnold, *New. J. Chem.*, **1994**, 18, 229
  127. F. H. Arnold, *Bio/Technology*, **1991**, 9, 151
  128. B. R. Hart, K. J. Shea, *J. Am. Chem. Soc.*, **2001**, 123, 2072
  129. L. Schweitz, P. Spégel, S. Nilsson, *Analyst*, **2000**, 125, 1899
  130. P. Martin, I. D. Wilson, D. E. Morgan, G. R. Jones, K. Jones, *Anal. Commun.*, **1997**, 34, 45
  131. W. M. Mullett, E. P. C. Lai, *Anal. Chem.*, **1998**, 70, 3636
  132. C. Berggren, S. Bayoudh, D. Sherrington, K. Ensing, *J. Chromatogr. A*, **2000**, 889, 105
  133. M. T. Muldoon, L. H. Stanker, *Anal. Chem.*, **1997**, 69, 803
  134. I. Ferrer, F. Lanza, V. Tolokan, V. Horvath, B. Sellergren, G. Horvai, D. Barceló, *Anal. Chem.*, **2000**, 72, 3934
  135. V. Pichon, M. Bouzige, C. Miege, M-C. Hennion, *Trends Anal. Chem.*, **1999**, 18, 219
  136. F. L. Dickert, O. Hayden, *Anal. Chem.*, **2002**, 74, 1302

- 
137. J. Matsui, M. Higashi, T. Takeuchi, *J. Am. Chem. Soc.*, **2000**, 122, 5218
  138. B. Sellergren, R. N. Karmalkar, K. J. Shea, *J. Org. Chem.*, **2000**, 65, 4009
  139. M. Emgenbroich, G. Wulff, *Chem. Eur. J.*, **2003**, 9(17), 4106
  140. K. Lettau, A. Warsinke, A. Laschewsky, K. Mosbach, E. Yilmaz, F. W. Scheler, *Chem. Mater.*, **2004**, 16, 2745
  141. K. Mosbach, Y. Yu, J. Andersch, L. Ye, *J. Am. Chem. Soc.*, **2001**, 123, 12420
  142. C. Du Fresne von Hohenesche, V. Ehwald, K. K. Unger, *J. Chromatogr. A*, **2004**, 1025, 177
  143. M. M. Conn, G. Deslongchamps, R. de Mendoza, J. Rebeck, *J. Am. Chem. Soc.* **1993**, 115, 3548
  144. S. C. Zimmerman, Z. Zeng, *J. Org. Chem.*, **1990**, 55, 4789
  145. S. C. Zimmerman, W. Wu, Z. Zeng, *J. Am. Chem. Soc.*, **1991**, 113, 196
  146. J. C. Adrian, C. S. Wilcox, *J. Am. Chem. Soc.*, **1989**, 111, 8055
  147. S. M. Barbas, P. Ghanzal, C. F. Barbas, D. R. Burton, *J. Am. Chem. Soc.*, **1994**, 116, 2161
  148. R. E. Nielsen, M. Egholm, R. H. Berg, O. Buchart, *Science*, **1991**, 245, 1497
  149. D. Y. Sasaki, K. Kurihara, T. Kunitake, *J. Am. Chem. Soc.*, **1991**, 113, 9685
  150. D. A. Spivak, K. J. Shea, *Macromolecules*, **1998**, 31, 2160
  151. D. A. Spivak, M. A. Gillmore, K. J. Shea, *J. Am. Chem. Soc.*, **1997**, 119, 4388
  152. K. Shea, D. Spivak, B. Sellergren, *J. Am. Chem. Soc.*, **1993**, 115, 3368
  153. J. Matsui, M. Higashi, T. Takeuchi, *J. Am. Chem. Soc.*, **2000**, 122, 5218
  154. Y. C. Huang, C. C. Lin, C. Y. Liu, *Electrophoresis*, **2004**, 25, 554
  155. G. J. Lancelot, *J. Am. Chem. Soc.*, **1977**, 99, 7037
  156. C. Aureliano, M. M. Titirici, B. Sellergren, *Unpublished Results*, **2004**
  157. M. Quaglia, K. Chenon, A. J. Hall, E. De Lorenzi, B. Sellergren *J. Am. Chem. Soc.*, **2001**, 123, 2146
  158. J. D. Watson, F. H. C. Crick, *Nature (London)*, **1953**, 171, 737
  159. D. A. Spivak, K. Shea, *Analytica Chimica Acta*, **2001**, 435, 65
  160. D. L. Venton, E. Gudipati, *Biochim. Biophys. Res. Commun.*, **1996**, 227, 419
  161. S. Hjerten, J-L. Liao, K. Nakazato, Y. Wang, G. Zamaratskaia, H-Y. Zhang, *Chromatographia*, **1997**, 44, 227

- 
162. K. Hirayama, M. Burow, Y. Morikawa, N. Minoura, *Chem. Lett*, **1998**, 731
163. R. Guerrini, G. Calo, A. Rizzi, R. Bigoni, D. Rizzi, D. Regoli, S. Salvadori, *Peptides*, **2000**, 21, 923
164. R. Guerrini, G. Calo, A. Rizzi, C. Bianchi, L. H. Lazarus, S. Salvadori, P. A. Temussi, D. Regoli, *J. Med. Chem.*, **1997**, 40, 1789
165. A. Rizzi, R. Bigoni, G. Calo, R. Guerrini, S. Salvadori, D. Regoli, *Eur. J. Pharmacol.*, **2000**, 278, 1183
166. M. R. Gagne, J. J. Becker, N. M. Brunkan, *Polym Prepr.*, **2000**, 41, 404
167. S. Y. Han, Y. A. Kim, *Tetrahedron*, **2004**, 60, 2447
168. M. Szwarc, *Nature*, **1956**, 178, 1168
169. M. Szwarc, M. Levy, R.M.Milkovich, *J. Am. Chem. Soc.*, **1956**, 78, 2656
170. Otsu T, Yoshida M, *Makromol. Chem .Rapid Commun.*, **1982**, 3,133
171. D. H. Solomon, E. Rizzardo, P. Cacioli, *European Patent 135280A2*, **1985**; U.S. Patent 4581429 , **1985**
172. E. Rizzardo, *Chem. Aust.*, **1987**, 54,3 2
173. M. Kato, M. Kamigaito, M. Sawamoto, T. Higashimura, *Macromolecules*, **1995**, 28, 1721
174. J. S.Wang, K. Matyjaszewski, *Macromolecules*, **1995**, 28, 7901
175. K. Matyjaszewski, T. E. Patten, J. Xia *J. Am. Chem. Soc.*, **1997**, 119, 674
176. T. E. Pattern, K. Matyjaszewski, *Adv. Mater.*, **1998**, 10, 901
177. A. Goto, K. Ohno, T. Fukuda, *Macromolecules*, **1998**, 31, 2809
178. R. T. A. Mayadunne, E. Rizzardo, J. Chiefari, Y. M. Chong, G. Moad, S. H. Thang, *Macromolecules*, **1999**, 32, 6977
179. J. Krstina, G. Moad, E. Rizzardo, C. L. Winzor, C. T. Berge, M. Fryd, *Macromolecules*, **1995**, 28, 5381
180. T. P. Le, G. Moad, E. Rizzardo, S. H. Thang, *Patent WO 98/01470* **1998** [*Chem. Abstr.* **1998**, 128: 115390]
181. J. Chefari, R. T. A. Mayadune, G. Moad, E. Rizzardo, S. H. Thang, *Patent WO 99/31144*, **1999**
182. R.T.A. Mayadune, E. Rizzardo, J. Chefari, Y. K. Chong, G. Moad, S. H. Thang, *Macromolecules*, **2000**, 33, 243

- 
183. A. Goto, K. Sato, Y. Tsujii, T. Fukuda, G. Moad, E. Rizzardo, S. H. Thang, *Macromolecules*, **2001**, 34, 402
184. M. Baum, W. J. Brittain, *Macromolecules*, **2002**, 35, 610
185. A. Sudalai, S. Kanagasabapathy, B. C. Benicewicz, *Org. Lett.*, **2000**, 20, 3213
186. J. Higashi, N. Y. R. E. Marchant, T. Matsuda, *Langmuir*, **1999**, 15, 2080
187. Y. Nakayama, T. Matsuda, *Langmuir*, **1999**, 15, 5560
188. K. Hattori, M. Hiwatari, C. Iiyama, Y. Yoshimi, F. Kohori, K. Sakai, S. A. Piletsky, *J. Membr. Sci.*, **2004**, 233, 169
189. C. S. Kresge, M. E. Leonowicz, W. J. Roth, J. S. Vartuli, J. S. Beck, *Nature*, **1992**, 359, 710
190. Z. Dai, H. Möhwald, B. Tiersch, L. Dähne, *Langmuir*, **2002**, 18, 9533
191. T. K. Mandal, M. S. Fleming, D. R. Walt, *Chem. Mater.*, **2000**, 12, 3481
192. J. Chefari, R. T. A. Mayadunne, C. L. Moad, G. Moad, E. Rizzardo, A. Postma, M. A. Skidmore, S. H. Thang, *Macromolecules*, **2003**, 36, 2273
193. S. Piletsky, A. Guerreiro, E. V. Piletska, I. Chianella, K. Karim, A. P. F. Turner, *Macromolecules*, **2004**, 37, 5018
194. M. Lepistö, B. Sellergren, *J. Org. Chem.*, **1989**, 54, 6010
195. S. Brunauer, P. Emmett, E. Teller, *J. Am. Chem. Soc.*, **1938**, 309
196. S. J. Gregg, S. W. Sing, *Adsorption Surface Area and Porosity*-Academic Press, London, **1982**
197. L. Gurvich, *J. Phys. Chem. Soc. of Russia*, **1915**, 47, 80
198. E. P. Barrett, L.E. Joyner, P. P. Halenda, *J. Am. Chem. Soc.*, **1951**, 73, 373

## Dipl. Chem. Maria-Magdalena Titirici

---

Date and place of birth: 24.03.1977, Bucharest, Romania

Address: Gabelsbergerstr 8, 44141, Dortmund

Telephone: 0049-179-4568065 (home)

0049-231-7556114 (work)

E-mail: magda @ infu.uni-dortmund.de

## Curriculum Vitae

### University Studies

- |                          |  |
|--------------------------|--|
| January 2001-present     | PhD student at Johannes Gutenberg University Mainz and University of Dortmund under the supervision of P.D. Dr. Börje Sellergren with the topic:<br><i>"Synthesis and Evaluation of Novel Formats in Molecular Imprinting"</i> |
| November 1999-April 2000 | Diploma work at the University of Bucharest under the supervision of Prof. Dr. Anca Nicolae with the topic:<br><i>Arylglyoxals-Synthesis, Characterisation and Applications"</i>   |
| October 1995- June 2000  | Studies at the Faculty of Chemistry from University of Bucharest finalised with a diploma in chemistry.  |

### Education

- |                          |   |
|--------------------------|---|
| June 1995                | Baccalaureate examination in Romanian Language and Literature, Mathematics, Physics, Chemistry and English Language |
| September 1991-June 1995 | Theoretical High School "Horia-Hulubei", Bucharest, Romania   |
| May 1991                 | General Certificate of Education  |
| September 1983- May1991  | Elemental School 137, Bucharest, Romania  |

### Research Stages

July 2000-December 2001

Young Research Assistant at the National Institute for Material Science, Bucharest, Romania under the supervision of Dr. Lucian Pintilie. Research undertaken on a project concerning the preparation of ferroelectric thin films using sol-gel chemistry and spin-coating on silicon wafers.

Visiting Researcher at the Faculty of Physics University of Rostock, in the group of Prof. Dr. Eberhard Burkel. This stage involved the characterisation of the above materials at the Deutsche Elektronen-Synchrotron (DESY), Hamburg, using Small Angle X-Ray Scattering.

### Other Skills

Languages

Romanian	mother tongue
English	fluent (spoken and written)
German	intermediate
French	intermediate
Spanish/Italian	beginner

Computers

Good knowledge and easy handling of the Microsoft Office Package and other programme such as Origin, Adobe Photoshop, Chem. Draw, *etc.*

Hobbies

Music, Literature, Cinema, Theatre, Latin Origin Languages, European History, Mountain Hiking, Swimming, Cycling, Travelling, Social Activities, Fashion.

## **Publications**

1. M. Magdalena Titirici, Andrew J. Hall and Börje Sellergren

*Chemistry of Materials*, **2002**, 14, 21-23

*“Hierarchically Imprinted Stationary Phases: Mesoporous Polymer Beads Containing Surface-Confined Binding Sites for Adenine“*

2. M. Magdalena Titirici, Andrew J. Hall and Börje Sellergren

*Chemistry of Materials*, **2003**, 15, 822-824

*“Hierarchical Imprinting using Crude Peptide Solid Phase Synthesis Products as Templates“*

3. M. Magdalena Titirici and Börje Sellergren:

*Analytical and Bioanalytical Chemistry*, **2004**, 378 (8), 1913-1921

*“Peptide Recognition via Hierarchical Imprinting“*

4. Fernando G. Tamayo, M. Magdalena Titirici, A. Martin Esterban and Börje Sellergren

*Analytica Chimica Acta*, **2005**, ASAP Paper

*“Synthesis and Evaluation of New Propazine-Imprinted Polymer Formats for Use as Stationary Phases in Liquid Chromatography“*

## **Conferences**

1. *New Materials and their Dynamics-Advances through Synchrotron Radiation*

September 2000, Rostock, Warnemünde, Germany

**attendance**

2. *The 10-th Symposium on Handling of Environmental and Biological Samples in Chromatography*

April, 2001, Mainz, Germany

**attendance**

3. *Doktorandenseminar /Chromatographie*

January 2002, Hohenroda, Germany

**oral presentation:** *“Hierarchically Imprinted Stationary Phases: Mesoporous Polymer Beads Containing Surface-Confined Binding Sites for Adenine“*



4. *Second International Workshop on Molecularly Imprinted Polymers*

September, 2002, La Grande Motte, France

**poster presentation:** *"In Situ Imprinting of Peptides Synthesised on Solid Supports"*

5. *International Symposium on the Separation of Proteins, Peptides and Polynucleotides*

November, Heidelberg, Germany

**poster presentation:** *"Hierarchical Imprinting using Crude Peptide Solid Phase Synthesis Products as Templates"*

6. *International Symposium on Separation and Characterization of Natural and Synthetic Macromolecules*

February, Amsterdam, The Netherlands

**oral presentation:** *"Mesoporous Polymer Beads Containing Surface-Confined Binding Sites for Biomolecules"*

7. *27-th Symposium on High Performance Liquid Phase Separations and Related Techniques*

June 2003, Nice, France

**oral presentation:** *"Peptide Recognition via Hierarchical Imprinting"*

8. *1-st Dortmund Graduate Student Symposium on Molecular Imprinting Technology*

October 2003, Dortmund, Germany

**oral presentation:** *"New MIP formats in Molecular Imprinting-The Next Generation"*

9. *Vortragstagung der Fachgruppe Makromolekulare Chemie*

March 2004, Düsseldorf, Germany

**poster presentation:** *"Thin Film Molecularly Imprinted Polymer Composites"*

10. *World Polymer Congress MACRO 2004- 40-th International Symposium on Macromolecules*

July 2004, Paris, France

**poster presentations:**

(i) *"Hierarchically Epitope Mesoporous Polymer Beads"*

(ii) *"Molecularly Imprinted Composites-Preparation, Characterisation and Use in the Generation of Novel Thin Walled MIPs"*

11. *Second International Workshop on Molecularly Imprinted Polymer*  
September, 2004, Cardiff, U.K.

**poster presentations:**

(i) *"Hierarchically Imprinted Mesoporous Polymer Beads Containing Surface Confined Binding Sites for Nociceptin"*

(ii) *"Molecularly Imprinted Composite Materials via Iniferter-Modified Silica Particles: Preparation, Characterisation and Use in the Generation of Novel Thin-Walled MIPs"*

(iii) *"Thin Film Molecularly Imprinted Polymer Composites Prepared via Reversible Addition Fragmentation Chain Transfer Polymerisation"* -**BEST POSTER AWARD**

**Oral presentation**

*"Thin Film Molecularly Imprinted Polymer Composites Prepared via Reversible Addition Fragmentation Chain Transfer Polymerisation"*